Electronic Thesis and Dissertation Repository

4-28-2014 12:00 AM

Elemental Distribution in Bone Impacted by Bacterial Diseases

Steven J. Naftel
The University of Western Ontario

Supervisor
Dr. Eldon Molto
The University of Western Ontario

Graduate Program in Anthropology
A thesis submitted in partial fulfillment of the requirements for the degree in Master of Arts
© Steven J. Naftel 2014

Follow this and additional works at: https://ir.lib.uwo.ca/etd

Part of the Biological and Physical Anthropology Commons

Elemental Distribution in Bone Impacted by Bacterial Diseases

by

Steven J. Naftel

Graduate Program in Anthropology

A Thesis submitted in partial fulfilment
of the requirements for the degree of
Master of Arts

The School of Graduate and Postdoctoral Studies
Western University
London, Ontario, Canada
April, 2014

ABSTRACT

Previous work, by this and other authors, noted several elements in bones and teeth are distributed non-uniformly. It was theorized that elemental distributions may be accentuated in the case of bacterial infections. Regions of bone surrounding Dental Abscess and Tuberculosis lesions were identified from, Varden (AdHa-1) and LeVesconte, Ontario; San Pedro, Belize and Kellis II Cemetery, Egypt. The abscess cavities were excised intact and cross-sectioned through the identified lesion. Elemental distributions in the bones were obtained using Synchrotron X-ray Fluorescence mapping. Maps of Zinc, Copper, Iron and Bromine were collected from the samples. The elements included in this study displayed **no correlation between distribution patterns and the presence of a dental abscess**. This conclusion is limited to the elements studied. Other elements or possible effects on bone structure, crystallinity or elemental chemistry will need to be addressed in future work. However, it was found that **Zinc concentration correlates with active bone formation areas**.

To Connie and the Kids

ACKNOWLEDGEMENTS

TABLE OF CONTENTS

LIST OF TABLES

LIST OF FIGURES

Elemental Distribution in Bone Impacted by Bacterial Diseases

CHAPTER 1: STATEMENT OF PROBLEM

The distribution of elements within the body is a complicated problem which has long fascinated researchers in many disciplines. Elements play key roles in many biological processes, especially in the proper functioning of enzymes, as well as, enzymatic activation and inhibition mechanisms (Berdanier and Zempleni, 2009). Thus a knowledge of the use and function of elements in the biochemistry of the body is vital to medical practice and diagnosis. Even so, our understanding of elemental concentrations within tissues, healthy or diseased, is very limited.

The specific association of some elements with particular tissues and the advantages of this knowledge for medical practice has become so familiar that it is often forgotten. The association of Iodine with the thyroid gland, and the subsequent use of iodized salt is a case in point. Other associations are less well known, for example, Zinc (Zn) is concentrated in the prostate gland (Zaichick and Zaichick, 2009) to levels 10 times those in other soft tissues (A guide to element symbols can be found in appendix A). When affected by malignant tumours the Zn level is seen to drop significantly, thus methods of measuring the Zn content in the prostate are attracting significant attention (Zaichick and Zaichick, 2009).

Malignant cancers are a significant concern worldwide and many people are aware of the connection between pollutant metals and cancer. Even though a causal connection has not been firmly established in all cases, and the metals are possibly just being concentrated or depleted by the altered metabolism of the cancer cells, nonetheless the elements provide a clue to causality and diagnosis (Durham and Snow, 2006). Still, the association between cancer and metals is well established. It is perhaps surprising then, that the analysis of trace metals in cancerous tissues is a relatively new field of enquiry (Reddy *et al.*, 2004).

Recent technological advances such as Synchrotron Radiation X-Ray Fluorescence (SRXRF), and others, now allow researchers the ability to interrogate a wide variety of materials for elemental concentrations as low as parts per million (ppm) with a spatial resolution at the micrometre (μm) scale (see appendix A for a guide to units). Carvalho *et al.* (2007) recently compared some of these new studies noting that the analytical techniques used are receiving increased attention in the medical physics community. Micro-scale trace element analysis techniques, such as SRXRF, Particle Induced X-Ray Emission (PIXE), and Total Reflection X-Ray Fluorescence (TRXRF), have been applied to various cancerous tissues confirming a link between anomalous localized concentrations of elements and cancer. For instance Geraki *et al.* (2008) found Calcium (Ca), Copper (Cu) and Zn to be at higher concentrations in breast cancer tissues. Reddy *et al.* (2004) found that Chromium (Cr), Iron (Fe) and Nickel (Ni) are concentrated in cancerous intestines while Zn was depleted below normal.

The micro-scale spacial variation of element concentrations are not just limited to the cancerous tissues themselves. Bazhanova *et al.* (2007) have demonstrated that the concentrations of Cr, Ni, Cadmium (Cd), and Antimony (Sb) are higher than normal in the cells surrounding tumours. Indeed, micro-scale analysis of several healthy body tissues have revealed interesting localized concentrations of elements. For instance, Zoeger *et al.* (2008) have found that Lead (Pb) and Zn are concentrated in a 70 micrometre wide band at the mineralization front in knee cartilage. Zinc and other elements have been found to be significantly enhanced in the cementum of teeth (Martin *et al.*, 2004). In a recent study of compact bone Swanston *et al.* (2012) observed increased amounts of Pb and Strontium (Sr) around some Haversian canal systems. As well, in a study of periodontal disease Martin *et al.* (2010) found a correlation between Cu and Zn in plaque covering diseased teeth and an associated decrease of Zn in the cementum.

Taken together these brief examples suggest that; **In and/or around tissue areas having altered metabolic needs**, [Cancer, Bacterial Infection (periodontal disease), active growth (mineralization front, Haversian systems, cementum)] as compared to

normal, **unique micro-spacial distributions of elements can occur and may be related to specific diseases or metabolic processes**. If this suggestion is correct then the implications for diagnostic medicine and treatment of diseases are clear. The importance of such elemental associations would not be restricted to clinical medicine but would also greatly enhance the practice of diagnosing ancient diseases in paleopathology and paleoepidemiology. More accurate diagnosis of ancient disease could enhance our understanding of the evolution of disease through time and the impact of such on past populations.

It is with the archaeological/paleopathology perspective in mind that this thesis will make a start at probing the relation between disease and trace element distribution patterns in bone. Specifically, I will examine if the distribution of elements in bone surrounding areas of bacterial infection are unique, making use of samples of archaeological origin. Thus the null hypothesis under investigation is: **There are no elemental distributions in bone that are related to bacterial infections.** An important corollary to this is, of course, that elemental analysis offers no clues to diagnosing diseases in archaeological or modern bones.

CHAPTER 2: BACKGROUND

"The Complexity of things - the things within things - just seems
to be endless. I mean nothing is easy, nothing is simple."
Alice Munro

Doctors, nutritionists, toxicologists and anthropologists have studied the elemental composition of the human body since the emergence of their representative disciplines. So we know that, in general, the body consists, on a dry mass basis, of mainly Carbon (C, 50%), Oxygen (O, 20%), Hydrogen (H, 10%) and Nitrogen (N, 8.5%). These four are closely followed by Calcium (4%), Phosphorous (P, 2.5%) and Potassium (K, 1%) making up 96 % of our bodily elements (Murray *et al.*, 2000; Ochiai, 1977). Approximately 21 additional elements are considered essential for human health including Sulfur (S), Sodium (Na), Chlorine (Cl), Magnesium (Mg), Iron, Nickel, Zinc and Copper (Berdanier and Zempleni, 2009; Ochiai, 1977; Underwood and Mertz, 1987). Many of the physiological roles of these elements have been documented over the years (Berdanier and Zempleni, 2009; Ochiai, 1977, for example). Still, many details of the elements' roles in metabolic processes remain to be understood. This is especially true of the trace elements (Cu, Fe, Zn, Arsenic (As), Cr, Cd, Cobalt (Co), Fluorine (F), Iodine (I), Manganese (Mn), Molybdenum (Mo), Ni, Selenium (Se), Silicon (Si), Vanadium (V), Lithium (Li)) due in large part to their extremely low concentrations in biological tissues.

The results of some recent studies have highlighted a couple of surprising aspects of trace element chemistry in the body. In 2004 we (Martin *et al.*, 2004) reported that Cu, Zn, Pb and Bromine (Br) were significantly concentrated within the cementum of some human teeth. Zn remarkably occurs at over 10 times the concentration in the cementum than in the rest of the tooth. This Zn distribution has so far occurred in all the teeth we have studied (Martin *et al.*, 2004; 2007; 2010; Dolphin *et al.*, 2013). The cementum is an

actively growing calcified tissue that surrounds the roots of mammalian teeth and is typically 100 to 200 micrometres thick (Hillson, 1996). Figure 2.1 shows an example of this remarkable distribution in the case of Zn.
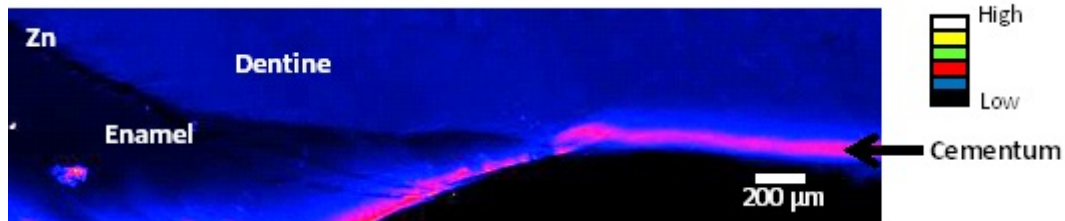
Figure 2.1. X-ray Fluorescence Intensity map for Zn in a healthy tooth. Indicating the typical Zn enhancement in the cementum. (After Martin *et al.*, 2010, Figure 2).

Zoeger and coauthors (2008) reported a similar enhancement of Zn and Pb at the mineralization front in knee cartilage samples from horses. The distinct region of element enhancement in this case was only an average of 70 micrometres wide. In another study we reported on the concentration of Zn and Cu in the cementum of human teeth affected by periodontal disease (Martin *et al.*, 2010). In this instance we noted an increase of Cu and Zn concentrations in the plaque covering the cementum of diseased teeth. We also noted an associated decrease in the Zn concentration within the cementum directly under the covering plaque. In a recent study Swanston *et al.* (2012) report increases in Pb and Sr localized in Haversian systems in cortical bone.

These studies suggest that: 1) distinct localized distributions of elements within the body occur in regions as small as 10's of micrometres across; 2) these distributions can be associated with processes of biological change such as cementum growth, cartilage mineralization and periodontal disease; 3) unique localized distributions of elements can be observed in surrounding tissues as well; and 4) at least some localized elemental concentrations can be preserved in the hard tissues after death.

The four ideas above are in general what this thesis will begin to investigate. Specifically, I want to address the second suggestion; **can localized distributions of elements be associated with processes of biological change?** Biological change may, of course, mean growth/development or disease/decay. The question arises, where would

one expect to see the most clear examples of these localized distributions of elements in tissues?

The elements that enter the body from the diet can be either controlled physiologically or not. Those elements that are not controlled are expected to have tissue concentrations that track with the amount of element in the diet (Burton, 2008). It is also important to note that one of the functions of bones is as element storage for the body, primarily for Ca and K, so it is no surprise that most elements to be found in the body can be found in the bones (Berdanier and Zempleni, 2009).

As an aside, I should note that even though some elements are not controlled physiologically they may mimic those elements that are (such as Sr^{2+}, Ba^{2+}, and Pb^{2+} which mimic Ca^{2+} in charge and ionic size) and thus may enter into controlled mechanisms and appear to be under physiological control even though they are not.

Those elements which are under physiological control will be expected to have tissue concentrations that are maintained in homeostasis and may not follow dietary intake. The concentration of these elements in individual tissues may be remarkably variable and not related to dietary levels (Zn levels in prostate for example (Zaichick and Zaichick, 2010)) except in situations of inadequate intake. Against these normally maintained background concentrations, if homeostasis is disturbed by disease or the presence of different metabolisms (infection by bacteria, rapid growth in cancer) then we could expect abnormal concentrations and spatial patterns to develop that may reflect the modified metabolic needs present. We could also expect unique elements to be present or absent and we could even expect unique chemistry or structures to develop because of the variable physiology. For example, Ca, Cu, Zn, and Fe have been found to concentrate in tissues affected by uterine cancer (Bazhanova *et al.*, 2007). The changes in Zn and Cu concentrations observed by us in periodontal disease may be another example (Martin *et al.,* 2010).

Therefore I would expect the best evidence of localized elemental distributions to be found in cases of disease, so my question becomes; Do diseases affect the trace element distributions and concentrations in bone? Of course there are many elements and

many diseases. I have decided to focus on a comparison of two bacterial diseases, Tuberculosis (TB) and Dental Abscesses (DA). These two pathologies have been chosen because 1) both display distinct skeletal patterns during their normal disease course which can be used for reliable diagnosis in dry bones, and 2) one (TB) is an aerobic bacterial disease while the other (DA) is caused by an anaerobic bacteria. Aerobic bacteria use oxygen in their basic metabolism, especially during cell division, whereas anaerobic bacteria can rely on Sulfur and other elements such as Mn, Fe or N for their energy needs (McInerney and Gieg, 2004).

In the end I have three parallel questions for this thesis;

1) Does TB affect the trace element distribution or concentrations in bone?

2) Do Dental Abscesses affect the trace element distribution or concentrations in bone?

3) Do TB and DA affect the elemental distribution or concentrations the same way?

Or to state the problems using falsifiable statements (Null Hypothesis);

1) There is no difference between the element distributions and concentrations in bone affected by TB and normal bone.

2) There is no difference between the element distributions and concentrations in bone affected by dental abscesses and normal bone.

3) There is no difference between the elemental distributions and concentrations between TB and DA affected bone.

I have tried to describe above the factors that led me to this work and some of the rationale behind the choices which narrowed down the general question to ones that can be tested. But what is the significance of the answers? In the field of biological anthropology there are many bone lesions which are not pathognomonic for any one disease, such as rib lesions (TB, pneumonia etc.)(Waldron, 2009). This situation prevents accurate prevalence numbers for past populations from being obtained. If element distributions are found to be unique they could be used to distinguish specific

diseases. The added diagnostic ability provided will significantly reduce the errors and improve the statistics inherent in the fields of paleodemography and paleoepidemiology. Also, elemental distributions could be another piece of data to study the changes of disease through time or to track treatments through time in the fields of medical anthropology or history.

In the current world the distribution of elements in a diseased tissue will provide new information, or another perspective, for the study of diseases in the body. Such detailed elemental distributions may highlight the role of certain biochemical pathways that use the elements in question and suggest new directions for medical research in current diseases. Understanding the elemental roles in disease better may also provide new directions for diagnostic tests and treatments.

2.1: Biomineralization

Typically bone is presented as a simple binary material made roughly of one third collagen and two thirds inorganic minerals, mainly hydroxyapatite. Bone is, of course, somewhat more complex. Along with other calcified tissues in the body, teeth, mineralized collagen, mineralized tendons and various pathological calcifications, (Dorozhkin and Epple, 2002) bone is the main human manifestation of a fascinating class of mineral materials formed within living organisms. The formation of biologically produced minerals is generally referred to as biomineralization which has recently received much attention (see for example: Dorozhkin and Epple, 2002; Weiner, 2010; Guo and Barnard, 2013).

Many animals and plants display processes of biomineralization, including jellyfish, fish, marine algae, bacteria, limpets, land plants, mollusks and snails (Dorozhkin and Epple, 2002). A total of 60 - 65 different minerals are known to be produced by various organisms (Weiner, 2010), which range from highly disordered (opal) to highly organized materials (magnetite). It is important to note that biogenic minerals often have shapes that are quite distinct from their inorganic mineral counterparts (Weiner *et al.*, 2005; Weiner, 2010). Biogenic minerals are also formed

under controlled conditions (temperature and concentrations) well below those conditions required in laboratories, which would kill any cells (Weiner *et al.*, 2005). Biomineralization, unlike inorganic mineralization, also gives rise to mineral crystals which are of uniform size, orientation and are often intimately associated with organic components (Dorozhkin and Epple, 2002; Weiner, 2010).

2.2: Bone Structure

Bones certainly make up the largest proportion of the vertebrate, including human, manifestation of biomineralization. In general the bones of the skeleton serve as a structural support for the body, protection for several organs and as a major reservoir of calcium, phosphate (Dorozhkin and Epple, 2002) and most other trace elements (Berdanier and Zempleni, 2009) necessary for proper metabolic function. Each bone is uniquely shaped and structured to fulfill its roles within the skeleton. Yet all bones are made of the same complex compound material which varies little in composition from bone to bone.

The two main components of bone are 1) the protein collagen which makes up 90% of the organic content of the bone and 2) calcium phosphate in the mineral form of carbonate hydroxyapatite (CHA). Overall, bone is about 1/3 by weight collagen with the rest mainly CHA. The collagen forms intertwined flexible, slightly elastic fibres. The collagen fibres are intimately associated with crystals of carbonate hydroxyapatite which stiffen the material giving rise to the composite materials amazing properties (Dorozhkin and Epple, 2002; Burton, 2008; White *et al.*, 2012). Bone also contains bone cells (osteoblasts [bone builders], osteoclasts [bone resorption] and osteocytes [bone maintainence]) as well as other physiological fluids and blood which are important for the health and maintenance of the bone. Like any composite material the loss or damage of any component of the system may have significant consequences for the normal functioning of the whole.

However, the detailed structure of bone varies depending on the length scale at which it is examined. Weiner and Wagner (1998) have organized the hierarchical

structures of bone into seven basic levels, the largest three levels are illustrated in figure 2.2. At the largest length scale (Level 7), we see the whole bone. It is at this scale where the shape-function relationship of the bone is most studied. The study of the whole bone is the mainstay of bioarchaeological and zooarchaeolgical research and much still needs to be learned about the shape-function relationship at this level (Weiner, 2010).

A step smaller in length (Level 6), at a scale of centimetres, lies the compact-spongy bone continuum. There is no sharp demarcation between densely packed compact bone and the open pore system in trabecular bone (Weiner, 2010). The obvious difference between these structures is their visible porosity, however, most bones are composed of a dense outer layer of compact bone (cortical bone) surrounding an area of trabecular (spongy or cancellous) bone. To be complete at this stage, the interior of the bone also contains a gel-like tissue called the marrow (Dorozhkin and Epple, 2002).

Porosity is an important property of bone material, and although compact and spongy bone look macroscopically different, the difference between the two in terms of surface area is not significant. The majority of canaliculi in bone are of nanometre size, most less than 6 nanometres (Weiner, 2010) and occur at the level of the mineralized collagen fibre. There are of course larger passages in the bone mainly to allow access for blood vessels, nerves and bone cells (Haversian systems, lacunae, canaliculi) (White *et al.*, 2012). The porosity of bone, besides allowing the collagen/hydroxyapatite matrix to be bathed by body fluids, is a relevant factor in understanding the biomechanics of bone especially as it relates to disease and deterioration of bone after death (Weiner, 2010).

Level 5 in the hierarchical structure (figure 2.2) of bone material is termed the lamellar bone. This refers to the layers of bone first deposited on a surface, the new bone is laid in layers which are more or less parallel to the surface on which the bone is laid. If this surface is a internal one the layers end up arranged cylindrically around one another creating the lamella of the Haversian systems. It is at this length scale where the action of the osteoblasts and osteoclasts is clearly seen. The hormones; parathyroid hormone, thyroid hormone and growth hormone along with many factors termed cytokines coordinate the bone forming action of the osteoblasts and the bone destroying action of

~ 0.3 – 0.5 metres

Level 7: Whole Bone

~ 8 – 10 cm

Level 6: Trabecular-Compact Continuum

Periosteum

Haversian System
(Secondary Osteon)

Blood Vessel

Level 5: Lamellar Bone

Lamellae

Lacunae

Canaliculi

~ 100 - 300 micrometres
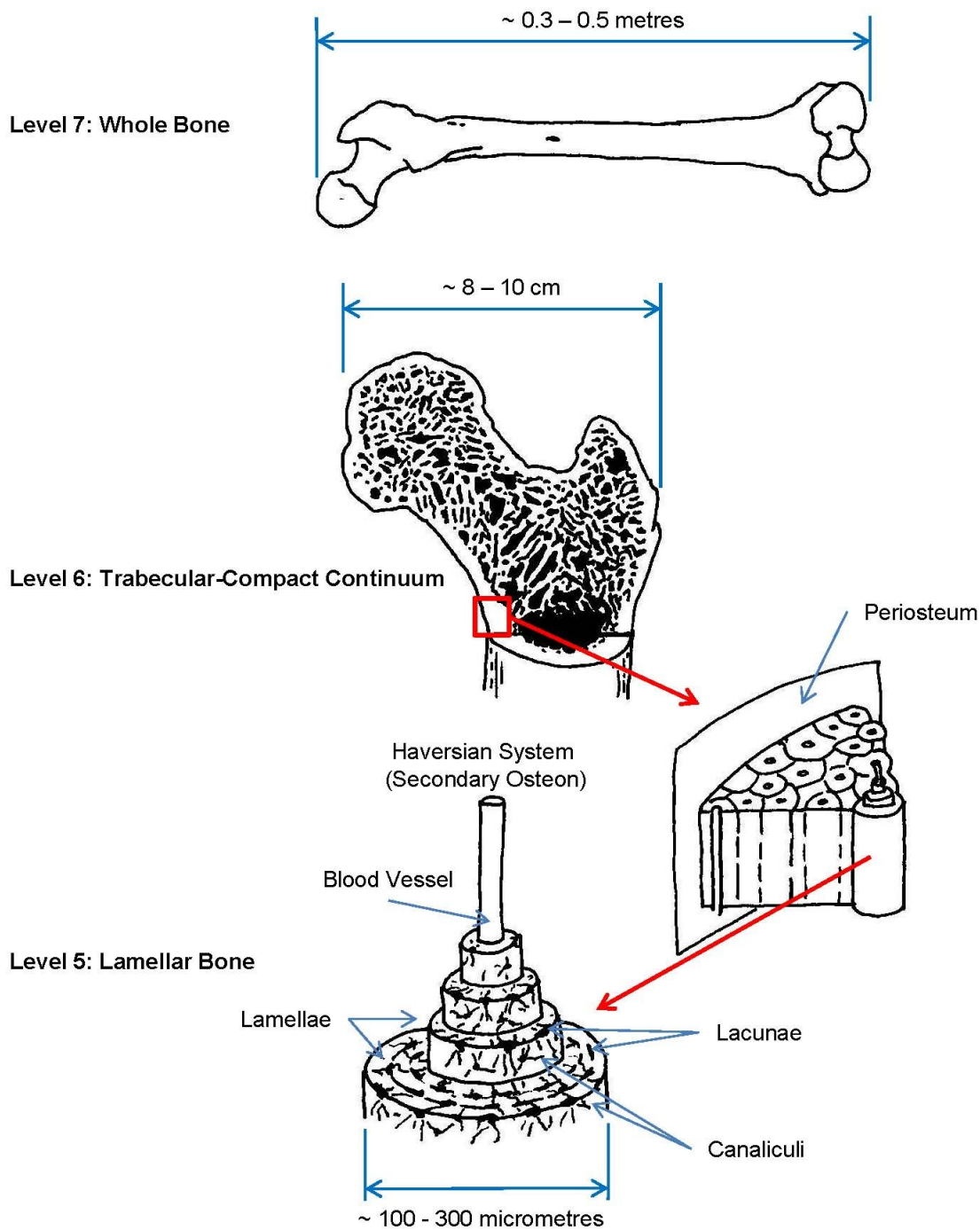
Figure 2.2.   Hierarchical organization of bone from Level 5, lamellar bone, to Level 7, the whole bone.
(After: White *et al.*, 2012, Figure 3.7, p. 34).

the osteoclasts to continually remodel the bone structures for maximum function (Waldron, 2009; White *et al.*, 2012) .

The structures discussed so far can all be seen with the eye or under low magnification. To examine the smaller scales of bone structure it is best to jump to the smallest scale and work our way back up. At the smallest scale, hierarchical level 1, we meet the basic molecular components of bone material. The organic phase, Type I collagen, the inorganic phase, Carbonate Hydroxyapatite and water.

Type I collagen is fibrous in nature and is the type of collagen which also appears in skin and tendon (Weiner and Wagner, 1998). The individual collagen fibres in bone, termed the fibril, are composed of three polypeptide chains wound together in a triple helix. Each peptide is about 1000 amino acids long, the helical molecule is thus cylindrical in shape about 1.5 nanometres in diameter and 300 nanometres long (figure 2.3). The manner in which these fibrils pack in bone is unique (Weiner and Wagner, 1998; Weiner, 2010). In the plane parallel to the fibril axis the individual fibrils are arranged parallel to each other and aligned along their long axes, furthermore, the ends of each fibril are offset by about 68 nanometres from each other, creating a staggered arrangement with a slightly smaller gap between successive helical molecules. Perpendicular to the fibre long axis the gaps align to form a narrow channel (Weiner and Wagner, 1998). It is in these channels where the crystals of carbonate hydroxyapatite fit (Weiner, 2010; Dorozhkin and Epple, 2002).

Although many authors state that the mineral component of bone is hydroxyapatite (or hydroxylapatite, or hydroxy-calcium phosphate), chemical formula $Ca_5(PO_4)_3(OH)$ (Burton, 2008; Waldron, 2009), this has been found to be strictly incorrect (Weiner, 2010; Dorozhkin and Epple, 2002). The mineral component of bone can be termed carbonate hydroxyapatite, that is hydroxyapatite where some of the phosphate (PO_4) groups are replaced by carbonate (CO_3) groups. This material can also be termed dahllite, $Ca_5(PO_4,CO_3)_3(OH)$ (Weiner and Wagner, 1998). Although this may seem like a small point, it is very important and will be discussed later, at this juncture it should be noted that biological carbonate hydroxyapatite is never pure, containing many

impurities like carbonate, fluoride, manganese and strontium (Bigi *et al.*, 1997; Dorozhkin and Epple, 2002).
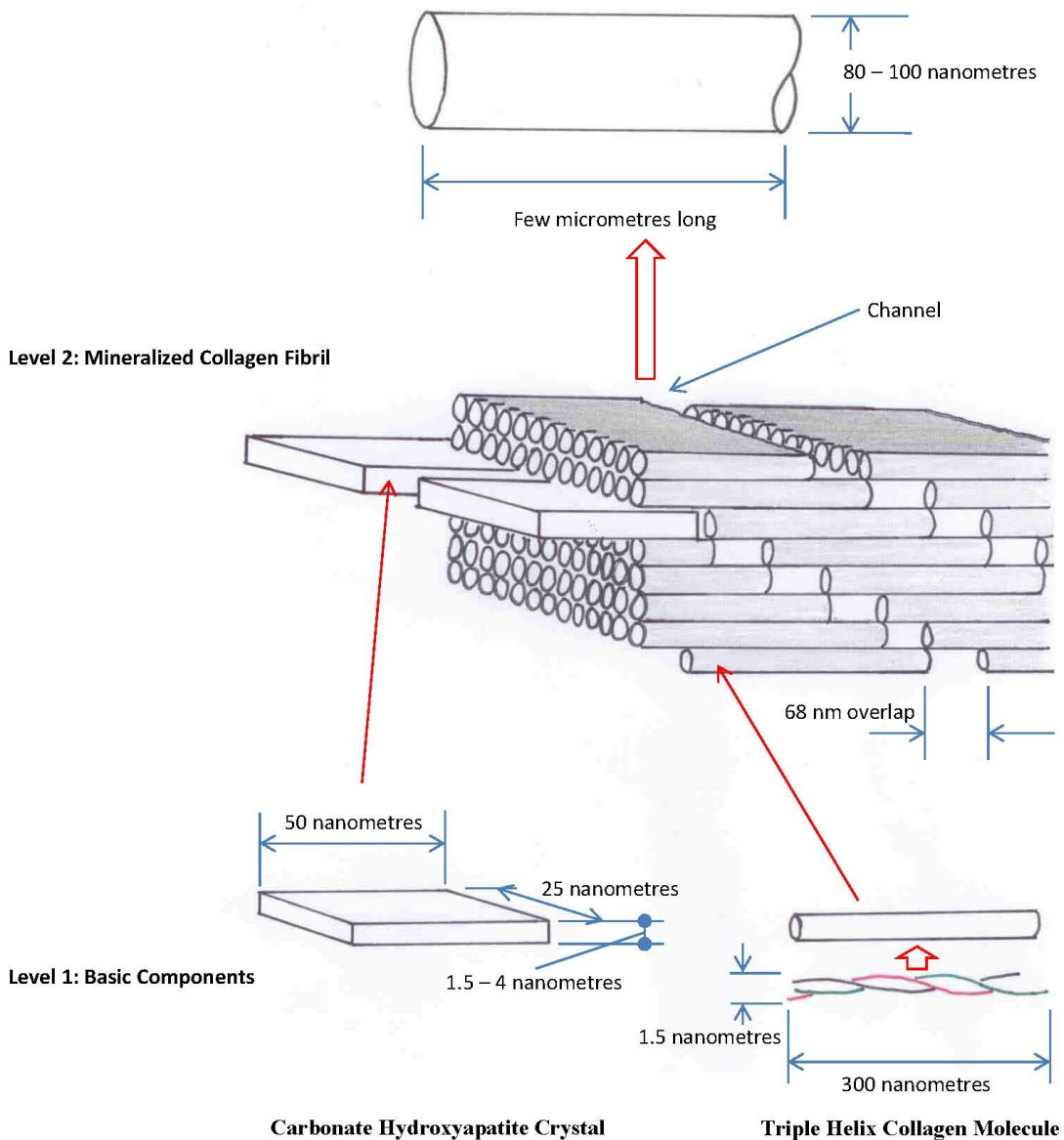
Figure 2.3. Schematic representation of the hierarchical organization of bone from Level 1, the basic components, to Level 2, the mineralized collagen fibril. (After: Weiner and Wagner, 1998, Figure 3).

The crystals of carbonate hydroxyapatite are very small, 50 nanometres long by 25

nanometres wide and only a few (2-4) nanometres thick, this is only a few unit cells wide. Another way to look at this is that the crystals are only about 10 - 15 atomic layers thick (Dorozhkin and Epple, 2002; Weiner and Wagner, 1998; Weiner 2010). Even so the crystals are remarkably uniform, having the bulk atomic structure of carbonate

Level 4: Array Packing Motifs

Type 1
Parallel arrays

Type 3
Plywood like

Type 2
Random 3D

Type 4
Layers of Random 2D

Fibril Bundle

Level 3: Fibril arrays (or bundles)

Mineralized Collagen Fibril
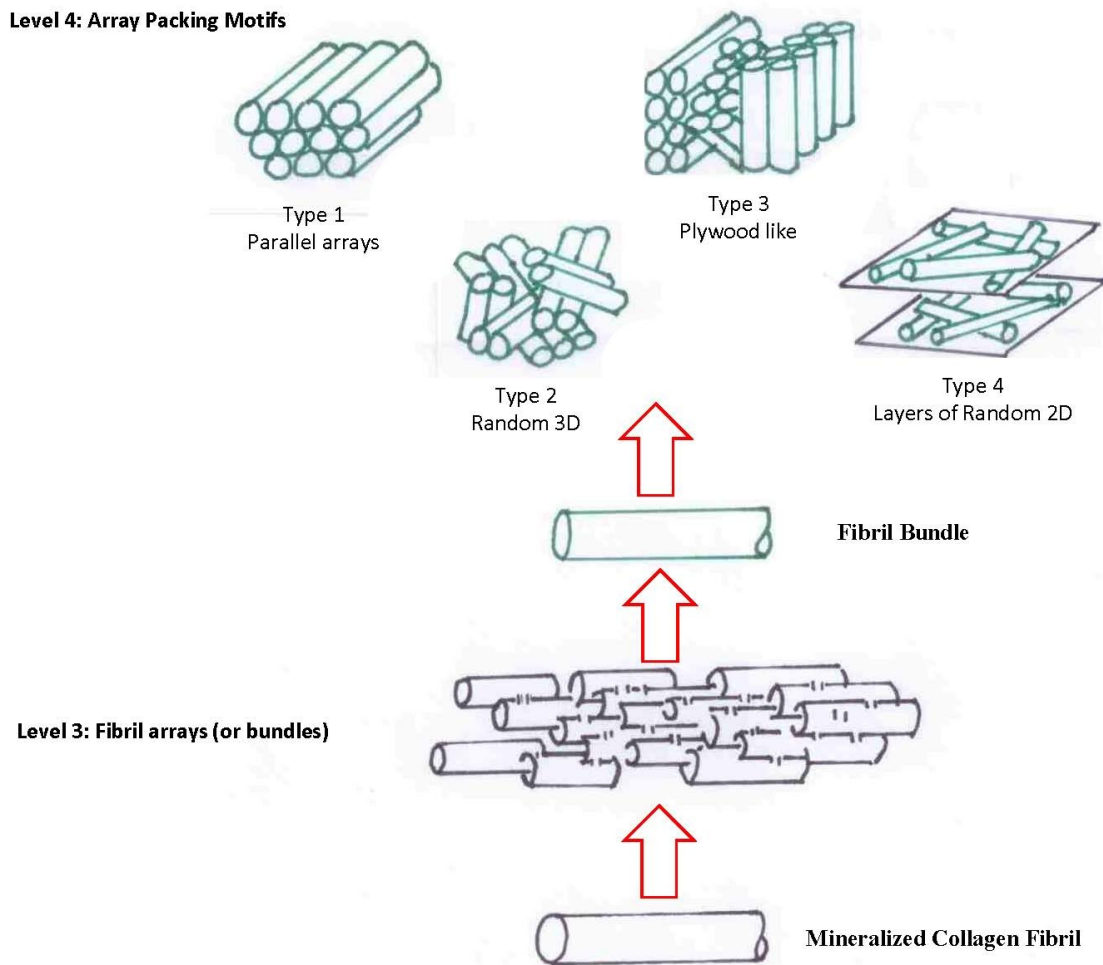
Figure 2.4. Schematic diagram of the hierarchical organization of bone structure from Level 3, Fibril arrays, to Level 4, Array packing motifs. (After Weiner and Wagner, 1998, Figure 6).

hydroxyapatite although not the bulk shape which is hexagonal (Weiner and Wagner, 1998). The reason for the plate shaped crystals is currently unknown, as are the details of the chemical interface between the collagen and these very small crystals.

The collagen fibrils and carbonate hydroxyapatite crystals are arranged together to make the mineralized collagen fibrils, hierarchical level 2 (figure 2.3). The crystals are arranged within the gaps of the collagen molecules in parallel arrays like a pavement.

An important feature of the mineralized collagen fibril is that the c-crystallographic axis of the carbonate hyroxyapatite crystals are aligned parallel to the collagen fibril axis. The mineralized fibrils are the basic building block of all the larger bone structures and are 80 - 100 nanometres in diameter and a few micrometres in length, although their exact length can not be determined.

At organizational level 3 the mineralized fibrils are bundled together in groups or arrays aligned along their long axes (figure 2.4). The arrays are not, however, discrete with fibrils often fusing with one another and with other arrays. The detailed internal structures of these arrays have thus not been documented fully to date (Weiner and Wagner, 1998).

The fourth hierarchical level of organization deals with how the fibril bundles are packed within the mineralized material. There are four common ways, or motifs, in which the arrays pack in bone materials, see figure 2.4. These arrangements give rise to different mechanical properties for the composite material and it is at this level that the material is adapted to a particular mechanical function in a particular tissue (Weiner and Wagner, 1998; Weiner, 2010). It is also at this micrometre to millimetre scale where the common microscopic repeating structures observed in mineralized tissues originate, such as Sharpey's fibers, Enamel prisms, Striae of Retzius, etc.

Type 1 is the simplest arrangement of fibril arrays, it is basically an extension of the parallel packing motif and is common in mineralized tendon and bovine bone (Weiner and Wagner, 1998). Type 2 is the opposite, involving completely unorganized packing of fibrils in three dimensions, this type is important as it is commonly found in newly formed fetal bone, woven bone and during wound repair. The third common motif is the most common structural arrangement found in mature bones. It is characterized by layers of parallel fibril arrays arranged in a plywood-like fashion with their long axes differently oriented in each layer. This arrangement is thought to provide the greatest mechanical

stability in all directions (Weiner, 2010). The fourth common type of fibril arrangement is characteristic of dentin. In this arrangement the fibril arrays are arranged in sheets parallel to the surface of the structure but the axes of the arrays within a sheet are randomly aligned.

Each of these fibril array packing motifs generate layers of mineralized composite material on surfaces giving rise to the bulk lamellar layers of organizational level 5, figure 2.2. Much more could be said about the details of bone structure, function, histology and the roles of the non-collagen proteins and water, but it is clear, that bone is not a simple material structurally. Nor is bone simple chemically, and since this is the organizational level at which the elements are involved we will now look more closely at the inorganic chemistry of bone.

2.3: Inorganic Chemistry

As already mentioned above, the mineral component of the hard tissues in not exactly hydroxyapatite (HA). An examination of the data in table 1 shows that the average physical parameters of the inorganic phases of both teeth and bone do not exactly match hydroxyapatite, or for that matter, other common calcium phosphate compounds. This has led to some disagreement as to which mineral phase is actually present in bone. Weiner and Wagner (1998) suggest that the inorganic phase in bones is best considered carbonated hydroxyapatite (CHA) (or dahllite), while Dorozhkin and Epple (2002) favour the compound calcium deficient hydroxyapatite (CDHA).

In general the inorganic phase in bones and teeth is a calcium phosphate, of which there are many stoichiometric compounds known (some are listed in table 1). The important parameters for bone chemistry are considered the Ca/P ratio and the solubility. For the pure calcium phosphates the Ca/P ratio ranges between 0.5 - 2.0, the lower the ratio the more acidic in solution and the more soluble the compound typically is in water (Bigi *et al.*, 1997; Dorozhkin and Epple, 2002). Of course the biologically produced calcium phosphates are known to be poorly crystalized and non-stoichiometric materials containing significant amounts of Na, Mg, K, Sr, F, Cl and carbonate (CO_3) (Weiner and

Wagner, 1998; Dorozhkin and Epple, 2002; Burton, 2008).

I should note that the Ca/P ratio in the bioanthropological literature is quoted as a mass ratio, whereas, in chemical literature it is given as a molar ratio (as above). Unfortunately both typically have a value around 2 so care must be taken to understand the ratio being used by any particular author. It is easy to convert from one to the other ratio. For example: for hydroxyapatite, formula $Ca_5(PO_4)_3OH$

$$Ca/P = \frac{5 \text{ Ca atoms}}{3 \text{ P atoms}} = 1.67 \text{ (molar)} \text{ or } \frac{5 \text{ Ca atoms x 40 amu/atom}}{3 \text{ P atoms x 30.97 amu/atom}} = \frac{200 \text{ amu}}{92.91 \text{ amu}} = 2.15 \text{ (mass)}$$

where amu refers to atomic mass unit (See appendix A).

To complicate matters further, neither HA, CDHA or CHA precipitates from supersaturated solutions of calcium and phosphate ions, there is always some intermediate phase involved (Weiner and Wagner, 1998; Dorozhkin and Epple, 2002; Burton, 2008). Three possible precursor materials have been suggested, namely DCPD (dicalcium phosphate dihydrate), OCP (octocalcium phosphate) and ACP (amorphous calcium phosphate) (Dorozhkin and Epple, 2002), but at this point it is not clear which material is involved. Whichever material is the precursor it only occurs transiently and as such is very difficult to detect in vivo. Although, the use of a precursor to affect the desired crystallization product under unfavourable thermodynamic conditions has been found to be common in the realm of biomineralization (Weiner *et al.*, 2005).

Regardless of the original material the crystals laid down are quite small and most importantly only about 1.5 - 4 nanometres thick. This thickness represents only about 10 - 15 atomic layers, and yet the crystals are surprisingly uniform in structure adopting the hexagonal structure of HA or CHA (see figure 2.5) although they are plate shaped similar to OCP (Weiner and Wagner, 1998). What this means is that the atomic order of the calcium phosphate crystals is interrupted abruptly leaving what should be a very reactive or disordered surface (Weiner, 2010). In the bulk crystal the hexagonal structure is adopted to reduce the disorder and/or pacify the reactive surface.

For the uninitiated CHA (or HA) is a mineral compound that has a definite

repeated structure or arrangement of atoms in three dimensions, a crystal. In the case of CHA this is a highly symmetric <u>hexagonal structure </u>(Chang *et al.*, 1996; Ulian *et al.*, 2013) that basically has an arrangement of Ca^{2+} ions surrounded by phosphate (PO_4^{3-})

Table 2.1: Some properties of selected calcium phosphate compounds (from Dorozhkin and Epple, 2002).

Compound	Formula	Ca/P (molar)	Ca/P (mass)	Solubility at 37°C, $-log(K_{sp})^b$	pH stability range (aq.) at 25°C	Typical crystal size (nm)
Enamel[a]	-	1.63	2.10	-	-	100 x 50 x 50000
Dentine[a]	-	1.61	2.08	-	-	35 x 25 x 4
Bone	**-**	**1.71[a]**	**2.20[a]**	**47.5[d]**	**+ 8.1[d]**	**50 x 25 x 4[a]**
monocalcium phosphate monohydrate (MCPM)	$Ca(H_2PO_4)_2 \cdot H_2O$	0.5	0.65	-	0.0 - 2.0	-
dicalcium phosphate dihydrate (brushite)(DCPD)	$CaHPO_4 \cdot 2H_2O$	1.0	1.29	6.63	2.0 - 6.0	-
octocalcium phosphate (OCP)	$Ca_8(HPO_4)_2(PO_4)_4 \cdot 5H_2O$	1.33	1.72	95.9	5.5 - 7.0	-
α-tricalcium phosaphate	$Ca_3(PO_4)_2$	1.5	1.94	25.5	no ppt.[c]	-
β-tricalcium phosphate	$Ca_3(PO_4)_2$	1.5	1.94	29.5	no ppt.[c]	-
amorphous calcium phosphate (ACP)	$Ca_x(PO_4)_y \cdot nH_2O$	1.2 - 2.2	1.55 - 2.84	-	-	-
calcium deficient hydroxyapatite (CDHA)	$Ca_{5-x}(HPO_4)_x(PO_4)_{3-x}(OH)_{1-x}$ **(0 < x < 0.5)**	**1.5 - 1.67**	**1.94 - 2.15**	**85.1**	**6.5 - 9.5**	**-**
carbonate hydroxyapatite (dahlite) (CHA)	$Ca_5(PO_4,CO_3)_3(OH)$	**1.67 - 5+**	**2.15 - 6.45+**	**-**	**-**	**-**
hydroxyapatite (HA)	$Ca_5(PO_4)_3(OH)$	**1.67**	**2.15**	**117.2**	**9.5 - 12**	**200 - 600**
tetracalcium phosphate (TTCP)	$Ca_4(PO_4)_2O$	2.0	2.58	37 - 42	-	-

[a]Typical values from Dorozhkin and Epple (2002) other authors present different values.

[b]The smaller the value the more soluble the compound is in water.

[c]Compound does not precipitate from aqueous solution.

[d]These values were calculated from the work of Berna *et al.* (2004). Any misinterpretation of their work is the sole responsibility of the author.

molecular ions (the prizms in figure 2.5). Any hydroxide ions (OH⁻) occupy the edges of

the unit cell parallel to the *c*-crystal axis (which is the main axis of rotational symmetry). Any carbonate molecular ions (CO_3^{2-}) to be found in the structure substitute for a phosphate group. If expanded to a physically visible size the crystals of CHA adopt the hexagonal appearance seen in figure 2.5a. Clearly this is not the shape observed in actual bone where they are flat and plate-like (figure 2.3).

The disordered crystal surfaces, precursor material, and presence of substitutions within the structure, all combine together so that the mineral component of bones and teeth are in a constant state of change, remodelling or changing towards a more stable mineral form, which is often taken to be hydroxyapatite (Dorozhkin and Epple, 2002; Burton, 2008). The process of maturing is a spontaneous chemical process which occurs naturally (Weiner, 2010)
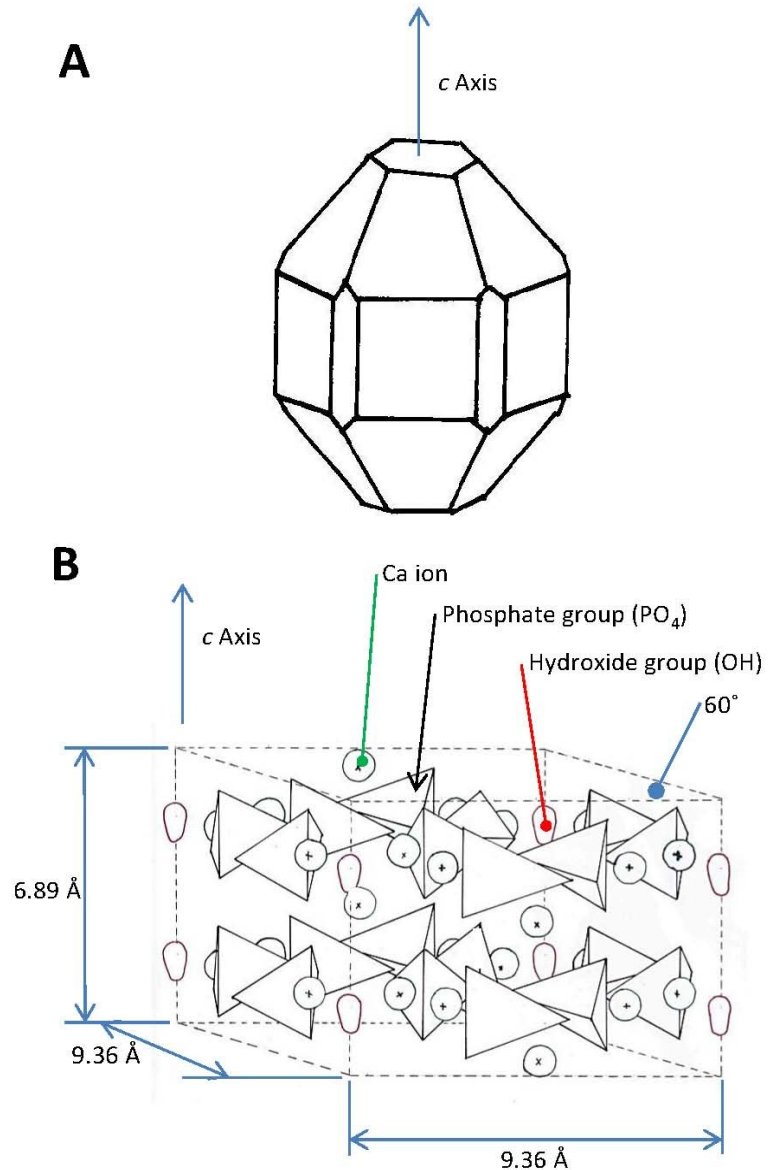
Figure 2.5. A) Bulk crystal habit of carbonate hydroxyapatite. B) Simplified schematic depiction of the unit cell of carbonate hydroxyapatite (not all atoms are shown).

and is distinct from the cell mediated processes of bone remodelling. In general it has been observed that the mineral crystallinity and Ca content increase while the phosphate concentration decreases over time within living bone (Bonar *et al.*, 1983; Weiner and Wagner, 1998; Bigi *et al.*, 1997; Dorozhkin and Epple, 2002; Burton, 2008) leading to an increase in the Ca/P ratio. This fact should be kept in mind as the same process continues to occur after death causing the Ca/P ratio to increase slowly after burial (Price *et al.*, 1992; Burton, 2008; Weiner, 2010).

Although the bone mineral is in a constant state of thermodynamic change, it may not be more soluble than pure CHA or CDHA as some authors suggest (Burton, 2008). It is certainly true that the small size of the crystals in bone material increases their active surface area, however, the crystals are so small that they should probably be considered nanoparticles. When a material decreases in physical size to the point that a significant portion of its atoms occur on the surface (usually in the nanometre range) the chemistry of the compound is no longer dominated by bulk thermodynamic constraints and new behaviours can arise often based on shape or symmetry (Guo and Barnard, 2013; for a simple example see Naftel *et al.*, 1999).   So the actual chemistry of the carbonate hydroxyapatite crystals may be unknown, as are the crystals' interactions with it's surrounding matrix of polypeptide collagen fibrils, water media, cytokines etc. This whole unknown area of chemistry is a huge challenge for future research in bone chemistry. It is also apropos as the topic of nanoparticles and the implications of nanomaterial chemistry has been a topic of intense research in chemistry for the past decade and continues to be so.

Now, how do the mineral crystals in bone form? This is a question of open debate which centres on whether the process is 'active' or 'passive' in nature. What is clear is that the formation happens under the direction of the osteoblasts. In the 'active' process the crystals are formed within a cell in a vesicle designed for the purpose. The crystals then need to be transported outside the cell and assembled with the collagen fibrils. Alternatively, it has been noted that blood serum is supersaturated in Ca and phosphate ions so if a suitable nucleation site were available then crystallization should occur

spontaneously. It is thus suggested in the 'passive' mechanism, that the osteoblasts only form the collagen matrix and the crystals naturally form within the gaps in their structure (figure 2.3) without cellular involvement (Dorozhkin and Epple, 2002; Weiner, 2010).

How about the trace elements which are the centre of this thesis? Beyond the fact that all the elements in the body tend to be found trapped or stored in the matrix of the hard tissues (Berdanier and Zempleni, 2009) little is know about exactly how they get there or how they are incorporated into the material. Certainly some ions such as carbonate (CO_3^{2-}), F^-, Ba^{2+} and Sr^{2+} are known to become incorporated within the crystal structure of calcium phosphate by replacing a Ca^{2+} ion or a phosphate (PO_4^{3-}) in the matrix. Incorporation, however, is just one possible way for elements to be held in the bone material. The elements could be adsorbed to appropriate sites on the crystal surface without being incorporated into the crystal structure. Suitable sites for adsorption could also exist on the surface of the collagen fibrils. Lastly the presence of elements required for metabolic processes such as enzyme centres or co-factors should reside within the bone cells.

Of course any particular element could be distributed between any one or several of these possible sites. Little work has been done to elucidate the exact mechanisms or sites of incorporation for many of the trace elements in bone. In the bioarchaeological literature, it appears assumed, that any element incorporates into the crystal structure or is adsorbed on the mineral phase, rarely both together. This is another area which needs significant attention in the future as the exact incorporation method will have some affect on the distribution of the elements in the bones as well as affecting the fate and stability of the element distributions after death. Although the technique (Synchrotron Radiation X-ray Fluorescence (SRXRF) mapping) I will use to investigate the micro-distribution of elements in bones in this work can be extended via the related techniques of X-ray Absorption Near Edge Structure (XANES) spectroscopy and Extended X-ray Absorption Fine Structure (EXAFS) spectroscopy, to assess the chemical environment of the elements and thus possibly determine the actual incorporation mechanisms, they were not part of the current work.

2.4: Using Elements in Bioarchaeology

There is no doubt that the presence of elements occurring in low concentrations in tissues begs the question; Why are they there? The sheer volume of literature investigating any particular element and offering plausible explanations, hypotheses and guesses both rash and sober speaks to the inherent attraction and/or usefulness of this question to various scientific endeavours. Even more intriguing, perhaps, is the presence of differences in elemental concentrations between sample sets, whether between different tissues in one organism, between organisms or even between individuals in a population and differences within a specific tissue.

Unfortunately, except in rare cases, unequivocal explanations of the variations uncovered by years of studies have defied achievement. Even so the inherent plausibility of the "You are what you eat" idea continues to produce studies attempting to trace ancient diet (Vuorinen *et al.*, 1996; Pinheiro *et al.*, 1999; Carvalho *et al.*, 2000; Carvalho *et al.*, 2004; Qu *et al.*, 2013; Dolphin *et al.*, 2013), migration patterns (Knudson and Price, 2007; Weiner, 2010), pollution and industrial activity (Grattan *et al.*, 2005; Pyatt *et al.*, 2005; Alomary *et al.*, 2006) even age and sex (Vuorinen *et al.*, 1996; Jaouen *et al.*, 2012), social status (Schutkowski *et al.*, 1999) and behaviour (Dolphin *et al.*, 2005; Williams *et al.*, 2005) via analysis of trace elements in bones and teeth. Ezzo (1994) and more recently Burton (2008) have critically evaluated trace element analysis in the field of bioarchaeological studies of past diets. The tone of these reviews is uniformly cautionary.

In bioarchaeology the possibility of using trace elements to determine diet from ancient bone samples came to light in the late 1960's (Ezzo, 1994; Burton and Price, 2000). This idea grew out of the study of radioactive Strontium 90 isotope fallout from nuclear testing in the 1950's. It was realized that Sr is chemically similar to Ca and accumulates in Ca-rich tissues and materials like bones and mother's milk. Fearful of poisoning by radioactive Sr isotopes, copious studies accumulated data on Sr physiology and biochemical behaviour. These studies eventually revealed that Sr levels decrease in organisms as one moves up the food chain. This 'biopurification' occurs because Sr does

not pass through the gut lining as efficiently as Ca, but is otherwise not differentiated biochemically from Ca in other processes. Significantly Sr is incorporated into the crystal structure of bone as a replacement to Ca. The biopurification leads to a trophic level (an organism's position in the food chain) separation which it was realized should reflect diet and be recognizable in bone.

Ezzo (1994) and other reviewers (Burton and Price, 2000; Burton, 2008) point out that decades of intense research went into understanding the physiology and biochemistry of Sr and then again into validating its link to diet and trophic levels. The link between Sr and diet is by no means simple and indeed it has been found that the concentration in tissues is not the analytical value to use but the Sr/Ca ratio (Burton and Price, 2000; Burton, 2008). The Sr/Ca ratio, it turns out, reflects the largest single Ca contributor to the diet not the total Ca or Sr from all sources in the diet (Burton, 2008).

Ba is another element similar to Ca and Sr and also replaces Ca in the bone structure. Again, Ba has similar biochemistry and chemistry and so is not differentiated by physiological processes. Ba has just about as long a history of dietary studies in bioarchaeology as Sr does, thus the reviewers (Ezzo, 1994; Burton, 2008) list Ba as a good indicator of diet again as the Ba/Sr ratio. It is thought that the early success of Sr and Ba studies lead to the suggestion that other elements forming 2+ ions such as Zn and Pb may be indicators of diet as well, but subsequent studies largely overturned these hypotheses (Ezzo, 1994) and current studies continue to challenge their use as dietary indicators (Zapata *et al.*, 2006; Carvalho *et al.*, 2007a; Wittmers Jr. *et al.*, 2008; Dolphin and Goodman, 2009) along with other elements.

Ezzo (1994) also reviewed several other attempts to use such elements as Al, Fe, Mg, Mn, Na, K and P in dietary studies, he found that all these along with Zn and Pb lacked a basic underpinning in the knowledge of the elements' physiological roles and basic biochemistry. When examined, such knowledge as understood at the time could be seen to contradict the diet-bone concentration link. Ezzo also pointed out that significant corroborating studies had not been done at that time, leading Ezzo to suggest that only Sr and Ba should be used as dietary indicators in bioarchaeology. This situation has not

significantly changed according to Burton and Price (2000) and Burton (2008). Burton and Price (2000) sum up the situation nicely:

> Although the chemical analysis of bone has gained widespread recognition as a tool for paleodietary and paleoenvironmental research, the primary focus of such research is now mainly isotopic. Trace-element compositional studies have fallen into disfavor, a consequence of disappointing attempts to deduce prehistoric behavior from such analyses. These disappointments, however, are largely the historical result of applying overly enthusiastic and simplistic ideas when drawing inferences from bone compositions. These ideas, in turn, stem from an accumulation of methodological missteps, individually quite minor but cumulatively significant enough to warrant serious reevaluation of the trace-element approach. (pp. 160).

A little later on they state more bluntly, " ... we have a research method that continues to be applied in a routine, if not appropriate, manner by archaeologists while much of the archaeometric community that created the methodology has abandoned it." (Burton and Price, 2000. p. 161). The continued warnings of these and other authors need to be heeded in any study of trace element chemistry. And of course significant work needs to still be done to elucidate the physiology and biochemistry of any element in bone.

It is interesting to note that the elemental methods (Sr/Ca ratio, Ba/Ca ratio) that have found acceptance in dietary studies are based on ratios. The C, N and O isotopic methods in bioarchaeology involve analysing the concentrations of the carefully controlled biological elements C, N and O and are thus properly thought of as elemental methods although they are, by accepted use, considered as a separate field of study. Since the 1970's stable isotope analysis, based on determining the ratios of the isotopes C^{13}/C^{12}, N^{15}/N^{14} and O^{18}/O^{16} in biological hard tissues, has become a common tool for tracing diet and migration patterns in past populations (Katzenburg, 2008; Weiner, 2010). It should, perhaps, not be surprising that these methods are all based on ratios.

Taking the ratio of two complicated measurements is a common technique in the physical sciences. The ratio has the effect of accounting for significant undetermined (or unknowable) parameters that affect the two measurements equally. This practice saves

the researcher much effort in determining the parameters exactly but still allows accurate and meaningful results to be determined.

In the case of stable isotopes, and element ratios, the unknown parameters affecting the individual measurements that make up the ratio are of course the physiological and biochemical processes that control the elements' concentrations within the hard tissues. It is thus important that the element components of the ratio be dealt with in the body in the same way. To put this differently, the body needs to see no chemical difference between the component elements in the ratio. In the case of the stable isotopes, this is obviously true, as there is no chemical difference, by definition, between isotopes in reactions. The slight ratio arises because of a difference in reaction rates that occurs based on the mass of the atoms. The reaction rate difference (isotope effects, or fractionation) is very small and it is important to note that the effect only becomes measurable after many sequential passages through any particular reaction, indeed this effect has been used to isotopically purify Uranium ores for nuclear fuel (Kotz and Purcell, 1991). It is thus the successive recycling of atoms within the biochemical processes that eventually gives rise to the isotopic ratios.

The same is true of the Sr and Ba ratios, as these elements are not chemically differentiated from Ca (Ezzo, 1994; Burton, 2008), yet because they are distinct in size their reaction rates within the Ca biochemical reactions are very slightly slower. Turnover within the tissues will thus, eventually, generate a slightly different element ratio, just as happens with stable isotope ratios.

My point here is that, in as much as trophic level shifts in isotopic ratios have been validated, the underlying physiological and biochemical processes that govern the concentration of C, N or O do not have to be clearly understood for isotopic analyses to produce meaningful data. However, it is important to point out that any process or factor which could upset the normal balance of the biochemical processes, such as systemic disease, may have an effect on the expected stable isotope ratios. Such situations would confuse the standard interpretations based solely on diet, indeed White and Armelagos (1997) found that nitrogen isotope ratios of osteopenic women are higher than healthy

individuals while, Olsen *et al.* (2008, 2014) have found that isotope ratios from within lesions are higher than normal bone. As such, any interpretations of stable isotope ratios based solely on diet should not be accepted without careful consideration of the disease status of the samples. Just like in the field of elemental analysis, there are no easy answers in stable isotope analysis (or we should not consider that there are).

I mentioned earlier that some element intensities in bone, and other tissues as well, have been used to evaluate pollution both present and past. These types of studies have been typically better received in archaeology as the elements examined (Pb, As etc.) are not typically found in bone or the diet at significant levels. We should not take these studies for granted though, contradictory studies abound in this field as well (Brenn *et al.*, 1999; Martin *et al.*, 2005; Martin *et al.*, 2013, for example). These pollution studies are similar to provenience studies sourcing materials such as metals and ceramics based on elemental or isotopic composition of their raw materials. Of course the inference in this type of work depends on accurately determining or assuming the source of the element, as in Cesium from the 2012 nuclear accident in Japan found in tuna recently (Madigan *et al.*, 2013). Such clear relationships may not be obtainable, especially in the past. Again it is important to consider both the past and present environment in any specific situation.

Rare elements in bones and teeth, such as U, Ti or the rare earth elements (REE), have also been used to infer diagenetic change in samples. This is because these elements are thought to not occur in bone except by leaching in from soils containing these rare elements. No physiological role has yet been found for these elements, however, most like U, are poisonous and as a result some biochemical pathway may yet be found that aims to protect the body from excess amounts. Either way, it is known that a portion of any U that does enter the diet does find its way into the bones (Emsley, 2001). It is important then, that care should be exercised, especially, in areas where these elements are naturally part of the rocks and soils and thus might enter in the diet, to understand how the body deals with these elements physiologically and biochemically.

Overall, one could summarize any aspect of the field of elemental studies in bioarchaeology, as one of confusion, the literature displaying conflicting results and

interpretations. Carbon, N and O stable isotope analysis, is well founded with a large literature, but even in this field of elemental studies new research is beginning to problematize the standard interpretations.

One important parameter that I have not mentioned yet is the actual concentration of any element in bone material. Looking through the nutrition, physiological and bioarchaeological literature one can find a bewildering array of values and ranges for any element. Table 2.2 presents such a brief review for the element Bromine in teeth as a suitable example.

Table 2.2. Brief sample of Br concentration values in teeth and bone from the literature.

Tissue	Br conc. (ppm)	Reference
Enamel	4.6	Soremark and Samsahl, 1961
Crown Dentine	4.2	Soremark and Samsahl, 1962
Crown Dentine	100 - 1000	Hardwick and Martin, 1967
Enamel	10 - 100	
Crown Dentine	114	Retief *et al.*, 1971
Enamel	33.79	
Enamel	1.12 (0.32 - 2.6)	Losee *et al.*, 1974
Enamel	0.87 - 7.3	Rasmussen, 1974
	1 - 4.4	
Enamel	3.4	Curzon *et al.*, 1975
Enamel	4.54 (0 - 33.2)	Curzon and Crocke, 1978
Root Dentine	3.53 ± 2.51	Molokhia and Nixon, 1984
Crown Dentine	2.28 ± 1.91	
Enamel	0.26 ± 0.16	
Root Dentine	5.7 (5 - 7.1)	Pinheiro *et al.*, 1999
Crown Dentine	8.0 (5 - 10)	
Enamel	2.7 (1 - 4.5)	
Root Dentine	30 (13 - 48)	Carvalho *et al.*, 2000
Crown Dentine	15 (7 - 21)	
Enamel	1 (1 - 2)	
Root Dentine	10 ± 3	Carvalho *et al.*, 2004
Crown Dentine	6 ± 3	
Enamel	2.2 ± 0.7	

Clearly, although the ranges overlap and an average value can be obtained its statistical certainty is so broad that comparisons between differing values become meaningless. Hancock *et al.* reviewed this point in their 1989 paper. They found that, because of factors such as diet, storage conditions and contamination from preparation methods, even the analysis of elements in modern clean bones suffer from large anomalies and are thus not very useful reference values for dietary and physiological inferences. Since the same factors are present in archaeological samples with the addition of long burial times their conclusion is that much of the dietary inferences found in the literature are erroneous.

Some of the profound variation in concentration data that exists, may be explained in part, by the simple reality that most studies to date have relied on ground bone and tooth samples with only moderate attention given to the type of bone and location of the bone sample within the skeleton. Both of these factors have been found to affect the concentration of the elements in bone, indeed, as in the example that started this thesis, the variation in elemental concentration occurs at scales smaller than even the region of the bone sampled. I hope that by effecting analysis of bones at micrometre scales, that the concentration of elements measured within localized regions will become more precise and statistical comparisons between regions will become meaningful as will dietary and physiological inferences derived from them.

If all the above issues were not enough, there is still the matter of archaeology's proverbial wrench in the works - diagenesis. To this final complication I will now turn.

2.5: Diagenesis

Diagenesis refers to all processes that modify the bone structure or chemistry from the time of death to the time of analysis. As such, diagenesis covers; cultural practices of body preparation and burial; biological processes of decay; attack by other organisms (pre- or post- burial); mechanical processes such as crushing or breaking (either of cultural or environmental origin); and of course chemical processes such as ion exchange

and recrystallization. Many excellent reviews of diagenesis have been written over the years: Sillen, (1989); Price *et al.*, (1992); Radosevich, (1993); Sandford, (1993); Hedges, (2002) and Weiner, (2010) are some examples.

Obviously, just like the area of bone structure and chemistry diagenetic processes are complicated and intertwined and it would be incorrect to suggest that they are fully understood. Nonetheless, diagenetic processes are vital to bioarchaeological and paleontological analysis and all aspects continue to be intensively studied. In the section that follows I will try to briefly describe the various processes and experimental measures of diagenesis in bone, the review will, of course, reflect my limited understanding in the area and is not intended to be exhaustive.

2.5.1: Processes of Diagenesis:

In general there are three main categories of processes which occur during diagenesis. These are; 1) modification or breakdown of component structures, 2) incorporation/contamination by other materials, and 3) leaching/loss of component materials. All three of these categories of changes have aspects occurring over length scales from the whole bone down to the molecular chemistry scale. Also, they all include processes which occur either fast or slow dependant on the environmental conditions and history of the buried remains.

Living bone is, as many point out (Price *et al.*, 1992; Weiner, 2010), amazingly active both physiologically and chemically. This is so that bone can perform its many biological roles. After death, physiological control within the bone is lost and any changes are then governed by physical laws or the needs of outside microbes.

The first processes of diagenesis, and some argue the most important (Collins *et al.*, 2002) are obvious, cultural preparation of the body (de-fleshing, preserving, disarticulating etc.) and biological degeneration of the soft tissues and living bone cells. What exactly the effects of these processes might be are not clear, but, they may depend on the rapidity of the activity as well as the initial disease ('health') state of the individual. Relatively speaking these initial processes are rapid.

After de-fleshed bones are obtained, physical laws (diffusion, chemical reactivity, crystal structure, etc.) and environmental conditions take over control of the remaining diagenetic processes, which are generally much slower or of longer duration (Collins *et al.*, 2002). Many diagenetic processes occur simultaneously and differently on each element of the skeleton and within each individual soil matrix (Radosevich, 1993; Hedges, 2002). The ultimate outcome of diagenetic processes also depends on the pre-burial condition of the remains after the initially rapid cultural treatments and biological disintegration (Collins *et al.*, 2002; Trueman and Martill, 2002).

It is not surprising then, that contradictory findings abound in the literature of diagenesis studies (Price *et al.*, 1992; Hedges, 2002). Some of this confusion also arises because of various researchers' attitudes, which have ranged from overly optimistic (no diagenesis occurs) to overly pessimistic (every effect seen is diagenetic).

One of the first points to come from diagenetic studies was that bone is very porous, this allows infiltration of the bone structure by other materials. Thus soil/water have been found to penetrate deeply into the structures of bones. This contamination can be both physical (soil/rocks/quartz) and/or chemical in nature. For instance, calcium can be introduced by precipitation of calcium carbonate within the smallest pores of the bone structure (Price et al., 1992; Weiner, 2010).

Obviously more open bone structures such as trabecular bone are more easily infiltrated by large components of the soil matrix as are fractured or broken components of bones. Two conclusions, generally arose from the basic observation of soil inclusions: 1) the more complete/undamaged the remains are visually the less likely that diagenesis would be expected; and 2) compact bone and teeth are considered less susceptible to diagenesis. Although from a chemical point of view these two conclusions may not be generally valid, (Jans *et al.*, 2002; Weiner, 2010) they are still considered basic tenets of the field.

One important instance of a structural breakdown process in diagenesis is the attack of bone by fungal hyphae or soil bacteria. This process, although recognized as important early on (Price *et al.*, 1992), has been extensively studied more recently (see,

Jans *et at.*, 2002; Trueman and Martill, 2002 for reviews). The extent of biologically induced breakdown found in these studies does not correlate with the overall physical appearance of the bones.

2.5.1.1: Microbial Attack and Collagen:

Microbial attack of bone is thought to be the principle agent behind the initial degradation of bone (Trueman and Martill, 2002). Microbes (bacteria, fungi and protozoa) demineralize the bone, producing tunnels or borings. The easiest way to assess these structures is via microscopic analysis of prepared thin sections. The term 'microscopical focal destructions' (MFD) has been used to refer to any microbially produced change in the histomorphology of bone. In order to quantify the destruction seen under the microscope Hedges *et al.* (1995) devised a histological destruction index based on the amount of bone affected by the biological destruction. The Oxford Histology Index (OHI), as the index is now called, ranges from 5 (< 5% affected bone) to 0 (no original histological features visible). The index has been found to have no relation to the age of burial or the burial environment for archaeological samples (Hedges *et al.*, 1995; Trueman and Martill, 2002). Furthermore the histological index has been shown not to correlate with the overall macroscopic appearance of the bone, with small fragile fragments sometimes having higher indices than whole bones (Jans *et al.*, 2002).

The growth of the invading organism depends on access to the bone collagen (Hackett, 1981). This is closely tied to the destruction of the mineral content (Collins *et al.*, 1995; 2002). The apatite mineral protects the collagen both from biological and enzymatic attack but the collagen also protects the mineral from dissolution because the collagen essentially coats the apatite mineral due to their close association in the material. This mutual protection between the collagen and mineral in bone gives bone a surprising longevity after death. However once the mutual protection is broken (presumably by microbial or fungal attack) rapid destruction of the bone results (Trueman and Martill, 2002; Weiner, 2010). The exact factors that lead to this initial breakdown in bone collagen and mineral are not clear (Collins *et al.*, 2002; Trueman and Martill, 2002).

Infrared spectroscopy and X-ray diffraction studies indicate that when collagen is lost from the bone the crystallinity measurably increases (Burton, 2008). The reasons for this change will be discussed below. Just what these biological destruction processes have to do with elemental changes in the bone is unclear but it seems that they are closely tied together, so to fully understand the process of chemical change one must understand biogenic attack and its associated effects on crystallinity.

It is interesting to note that in fossilized bone very little bioerosion is found and as a result the bones, although often chemically altered, have maintained their histological structures. Destruction of the collagen in fossil bone is thought to occur via an abiological hydrolysis to gelatin (Collins *et al.*, 1995; 2002) which does not require removal of mineral from the bone structure. This process would, however, expose apatite mineral to rapid dissolution, thus, a slow balanced process of collagen degradation and stabilization of apatite crystals must occur for fossilization to be the result. It is thought that such a process may preserve biogenetic elemental signals in fossilized bone (Trueman and Martill, 2002). Such is often assumed in paleontological papers (see Fernández-Jalvo *et al.*, 2002; Lee-Thorp and Sponheimer, 2006; Qu *et al.*, 2013 for example).

2.5.1.2: Chemical Alteration of Bone:

Much work on the chemical diagenesis of bone has gone into elucidating the changes that are seen to occur in the Ca content of bone after death. Calcium ($CaCO_3$) Carbonates are a common component of ground water, the main mineral form is Calcite although other structural forms exist (Weiner, 2010). However, Calcium Carbonate has been found to precipitate in bone from the ground water. Such a process incorporates extra Ca and carbonate ions into the bone structure, the main result of which is a change in the Ca/P ratio (Price et al., 1992) or the CO_3^{2-}/P ratio (Nielsen-Marsh and Hedges, 2000).

The diagenetic calcium carbonate can be found as crystals of Calcite on the surface or within cracks or pore spaces in the bone structure but can also be present

adsorbed on the surface of the bioapatite crystals or incorporated into the crystal lattice of the apatite replacing either normally present CO_3^{2-} or PO_4^{3-} ions (Nielson-Marsh and Hedges, 2000).   With incorporation of calcium carbonate the Ca/P ratio and the CO_3^{2-}/P ratio both increase above that for pure carbonate hydroxyapatite. The presence of diagenetic Calcite can also be seen via the infrared spectrum which displays a peak at 713 cm^{-1} which is not present in the IR spectrum of carbonate hydroxyapatite (Nielson-Marsh and Hedges, 2000; Weiner, 2010).

Although the Ca/P or CO_3^{2-}/P ratio increases may indicate diagenetic carbonates other natural processes work to decrease these same ratios. The carbonate hydroxyapatite crystals in bone can become more crystalline via normal crystal changes (Ostwald Ripening) or via processes of recystallization in which the carbonate hydroxyapatite dissolves in the surrounding ground water but because pure hydroxyaptite is less soluble it then precipitates back into the crystal. The net result is a decrease in the carbonate content and an increase in the crystallinity of the bone mineral that remains (Weiner, 2010). Because of these competing processes the measures of Ca/P and CO_3^{2-}/P ratios and the crystallinity are problematic measures of diagenesis.

It is important to mention that if the pH of the ground water is below 7.2 then in practice all bone will eventually dissolve. Also, in soils with a high Calcite content, bone will not dissolve as the Calcite buffers the soil pH to over 8.2 which prevents the dissolution of all the hydroxyapatites (Weiner, 2010).

In terms of other elements in the bone tissue, diagenesis is typically thought to involve the incorporation or uptake of groundwater solutes or the dissolution or leaching of bone minerals into the groundwater. Exactly how the elements are bound in the bone (Hancock *et al.*, 1989) or for that matter in the soil (Burton, 2008) are important considerations which are not clearly known. From the soil perspective, even if an element is present in the soil in significant concentrations it may not be soluble and thus not be present in the groundwater. Such elements are Ti, Zr, Mn and Hafnium, which can only contaminate bone through physical inclusion into pore spaces (Burton, 2008). Hancock *et al.* (1989) reported that on ashing of bone samples some elements such as Na,

Cl and Br change dramatically. The change with ashing suggests that the elements are associated both with the organic phase and with the inorganic crystals. If such a mixed distribution of elements between the organic and inorganic components in bone is true then the question of which phase of bone the elements are adsorbed to within the burial environment may have significant effects.

Some elements have been used to indicate the presence of diagenetic processes simply by virtue of their presence within the bone. These elements are considered to be much more abundant in certain burial environments than in uncontaminated bone. These elements include Uranium and the rare earth elements (REE), which from a chemistry perspective, are those elements in the lowest two rows of the periodic table, the Lanthanides and the Actinides. If these elements are found in bone then significant diagenesis is assumed (Price *et al.*, 1992; Hedges, 2002; Burton, 2008). Of course, as I already pointed out above, care must be taken because the assumption that these elements do not exist in tissues may be violated in certain environments.

Potassium, Iron, Aluminum, and Manganese are abundant in soil oxides and clays but are considered low in fresh bone and as such are often considered of diagenetic origin in elemental studies when appearing in the bone (Burton, 2008). Some elements are considered to be regularly leached from bone materials into surrounding soils, such as Na and Mg (Price *et al.*, 1992). Unfortunately, any list of elements such as these contradicts other researcher's lists, creating significant confusion for the reader.

In discussing the movement of any element or ion in groundwater into or out of buried bone the concentration gradient that exists between the bone and soil needs to be considered. Elements will not naturally move against the concentration gradient. That being said, the concentrations of the soil and bone elements are not the most important factors in the system. This is because the process is a <u>heterogeneous (two phase - soil solution and solid bone matrix) exchange reaction</u>. Exchange processes are the basis of most separation science, water purifiers and all types of chromatography. The most important factor in these processes is the strength of the ion to solid substrate binding.

If the ion binding is strong then the ion will be concentrated in a narrow band on

the surface of the bone regardless of the soil concentration. Such a situation exists in the instance of Fluorine. When present in the ground water, Fluorine ions form the permanent compound Fluorapatite in which F^- ions replace the PO_4^{3-} ions in the apatite crystal structure (Wrobel, 2007). Whether the ion replaces a component of CHA is not vital. What matters is the strength of the attraction. In the case of F this is essentially irreversible.

On the other end of the ion binding scale, an ion may not have any interaction with the components of bone. In such a case the presence of the bone will have no effect on the solution concentration of the ion in the soil. The concentration of the ion would exist within the bone pore spaces at the same level as the available ion concentration in the soil matrix. Essentially the ion concentration in the bone would be approximately even throughout. Exactly what would happen to this distribution through the drying of the bone may not be clear, it could all evaporate from the bone matrix with the water or remain at some concentration.

Most ions/elements/compounds will display binding properties between these two extremes. Thus most ions would be expected to create some band of elemental concentration (or leaching) which would move through the bone from the exposed surface in the direction of the flow of the ground water (think chromatography). At this point it is important to remember that there are two solid phases in the bone matrix. The collagen and the CHA crystals will behave separately from each other with independent binding coefficients for any one element. As a result for any ion, both components of the bone matrix could bind strongly, both could bind weakly or one could bind strongly while the other binds the ion weakly. The complexity abounds. It is clear that an understanding of the exchange process as chromatography may be necessary to resolve the existing conflicting results and interpretations in the literature.

Focussing on the diagenetic processes of ion exchange in buried bone as a chromatographic process also highlights the need to proceed with the analysis of elements in bone on a smaller length scale than is currently done. Clearly, grinding bone samples, no matter how carefully chosen, will destroy any banding or distributions of elements

within the matrix. Grinding of the bone would be akin to attempting to analyse a chromographic plate by grinding it up first. What the result would be and how it would relate to the original situation is anybody's guess.

Does diagenesis occur throughout the whole bone or only on the exposed surfaces of the bone? It has been generally assumed that the latter is the case and as a result, my discussion above assumes the same. However very few researchers have provided evidence for this behaviour (Brenn *et al.*, 1999) and many suggest that this assumption is false (Price *et al.*, 1992). Even so various mechanical or chemical etching techniques were developed to remove diagenetic elemental changes from bone samples (Price *et al.*, 1992). Whether these methods worked to remove diagenetic effects has been unclear (Price *et al.*, 1992) and very few studies (Burton, 2008) have been done that looked at cross-sections of bone material in an attempt to view such diagenetic profiles.

The majority of studies of diagenesis as well as elemental concentrations and isotope ratios are done on ground bulk bone samples following one of the standard surface cleaning techniques. It would seem clear, at least to this researcher, that enough evidence exists to suggest that elemental concentrations, isotope ratios and diagenesis would best be studied at the microscopic scale not at the current bulk scale. Such a shift in focus may eventually lead to a sorting out of the often conflicting diagenetic studies in the literature. Unfortunately, this is not the focus of the present research, as timely and important such work may be.

2.5.2: Measures of Diagenesis:

In the preceeding section I mentioned several measurements that may be indicative of a diagenetically altered bone. The following table will list these along with several other measures. It should be pointed out that there is generally not a one-to-one relationship between any process of diagenetic change and a specific measure (Hedges, 2002). Coupled with the inherent microscale of the processes, and the understanding that the processes may vary within a site, grave, or even a given bone, the listed measures can only function as a crude guide to the quality of the bone being studied. Many diagenetic

Table 2.3. Measures of bone diagenesis used in element and stable isotope work.

Measure Name	Analytical Technique	Brief Description	Reference
Calcite ($CaCO_3$) Inclusions	Microscope **or** IR	No peak at 713 cm^{-1} in normal bone	Nielsen-Marsh and Hedges, 2000
U and REE Element Inclusions	Mass Spec	U or REE not seen in normal bone	Price *et al.*, 1992 Hedges, 2002
Porosity	Water Uptake **or** Mercury Intrusion	< 5 nm scale pores decrease > 10 nm scale pores increase	Nielsen-Marsh and Hedges, 1999
Oxford Histological Index	Polarizing Microscope	Range 0-5 [Normal bone = 5]	Jans *et al.*, 2002
Birefringence	Polarizing Microscope	Decreases or disappears [Strongly present in normal bone]	Jans *et al.*, 2002; Burton, 2008
Crystallinity Index (IRSF) (CI)	IR	Index increases with crystallinity - PO_4^{3-} IR peak components at 565 and 605 cm^{-1} used in index [Normal range about 2.8-4.0]	Weiner and Bar-Yosef, 1990 Wright and Schwarcz, 1996
Crystallinity	XRD linewidth	FWHM (Full width half maximum) of 002 reflection decreases with time (increased crystallinity)	Sillen, 1989 Reiche *et al.*, 2002
Ca/P Ratio	Mass Spec	About 2.15 by mass	Hancock *et al.*, 1989
Protein Content (%N)	Mass Spec	% N by weight in bone reflects quantity of collagen present **if** > 0.4%	Nielsen-Marsh and Hedges, 2000
C/N ratio (from collagen)	Mass Spec	Ideal 3.2 [Acceptable range 2.9 - 3.6]	DeNiro, 1985
Collagen Yield %	Mass of Hydrolysised protein material	Fresh bone is ~ 22% [Minimum yield 1%: note - much protein is not hydrolysed]	van Klinken, 1999
Amino Acid Ratios	Atomic Absorption spectroscopy on extracted protein	Considered not reliable	van Klinken, 1999
C/P ratio (CO_3/PO_4) ratio in apatite	IR	Ratio increases with included CO_3. Comparison of CO_3 and PO_4 peak heights. [Normal range about 0.15-0.30]	Wright and Schwarcz, 1996
CO_2 gas Yield from apatite	Mass Spec	Normal yield between 0.6% and 1.3%	Ambrose, 1993

measures assess the collagen content of the bone in some way, thus they can be considered reasonable measures of diagenesis because of the close relationship between the collagen preservation and the mineral preservation and hence the microscopic bone preservation.

Many of the parameters listed do not display any linear relationship with time since death, hydrology, soil type, temperature or any other factors (Hedges, 2002). It is my hope that microscopic measures of the crystallinity index via micro-IR spectroscopy coupled with the microscopic measure of the Oxford Histological Index will be able to significantly add to the understanding of diagenetic processes. These techniques should be investigated further and incorporated into any future studies of elemental distributions of the type presented in this work.

2.5.3: Implications:

So what is clear? - 1) the survival of the collagen matrix is tied in some way to the survival of the mineral matrix and vice versa; 2) although some of the parameters used to assess diagenesis do change with diagnetic severity, the direction and magnitude of such changes can not yet be reliably tied to any environmental conditions or specific mechanisms; 3) much work needs to be done on the mechanisms of diagenesis. Unfortunately, untangling such a complicated nest of interrelated processes is not the theme of this thesis, that will have to wait for now. So in the meantime, we must be very cautious with any interpretations of elemental distributions. As Sillen *et al.* (1989) suggested, there are no easy answers in isotopic and elemental analysis of skeletal materials.

Although one could despair of ever overcoming the obviously significant challenges of trace element bone analysis the puzzle is still intriguing and studies continue to abound. What is needed in the field now is not exuberance but sober and careful work, that errs on the side of interpretive caution. The use of collaborative information, such as the Oxford Histological Index and Micro-IR spectroscopy and micro Ca/P ratios, to help assess diagenesis and temper any conclusions about diet should be

encouraged, as should extensive work in the physiology and biochemistry of all the elements.

CHAPTER 3: SAMPLES

3.1: General Selection and Preparation of Samples

The purpose of this project is to examine the distribution of elements in those areas of bone surrounding obvious lesions, which can be reliably associated with the presence of a specific bacterial infection. As I stated in chapter 1, dental abscess and tuberculosis were chosen initially. This was because, both these diseases were either common in past populations (DA) and/or were represented in sufficient numbers within the skeletal collections (TB) currently housed at Western University.

Both DA and TB also result in identifiable pathognomonic lesions in the skeleton and in the case of TB can be confirmed by the use of ancient DNA analysis of skeletal samples (Donoghue *et al.*, 2004). It was also important that the two diseases are caused by different classes of bacteria, either aerobic or anaerobic, so that their effects within the bone lesions could be compared.

The samples for the work were drawn from four skeletal collections currently housed at Western University, Department of Anthropology. These collections were from: San Pedro, Belize; Kellis II cemetery, Dahkleh Oasis, Egypt; LeVesconte Burial Mound, Ontario and the Varden Site, Ontario (see details later). Initially each skeleton in a collection was examined for the presence of the required disease lesions. Where possible the visually best preserved specimens were chosen from the most complete skeletal elements available.

Besides being conveniently located at Western, all the collections used, except for the LeVesconte population, were previously studied by stable isotope analysis and as such, typical measures of diagenetic change are available for each skeleton selected in this study (See table 3.1 for a summary, pg 60). So each of the samples chosen can be considered, by current standards, to be in excellent condition with little diagenetic change expected, keeping in mind the limitations discussed in the preceding chapter.

The individual elements chosen from each population were then carefully

documented including a comprehensive list of both metric and non-metric skeletal traits. For the dental abscess samples the mandible was chosen as it was considerably easier to access the abscess in the mandible versus the maxilla. For tuberculosis samples individual vertebrae were selected. As well several rib sections were also chosen. Once described and measured each element was photographed. All these details were recorded on an individual bone form for each element. The bone form also indicated where on the element the sample was to be removed for this study (these forms can be viewed in Appendix B). In each case the attempt was made to be as complete as possible because the sampling was, of necessity, destructive and it was important to preserve as much data as possible for future researchers who might want to use these collections.

The detailed bone forms were shown to the curator responsible for each of the populations for approval before destructive sampling was undertaken. Once approval for each selection was obtained the sample area was extracted with a rotary tool using a fine ceramic tile bit. After the section was removed it was blown clean of dust and debris with compressed air. No other cleaning or washing was done to the samples before embedding and sectioning.

In removing the dental abscess samples from the mandibles, the tooth involved in the abscess was retained in the section, this was so that the tooth could serve as a reference as to the location and size of the abscess. As well, the tooth served as an important test comparison for the accuracy of the X-ray Fluorescence maps as literature exists on what to expect within teeth.

The samples were blown clean with compressed air then embedded in epoxy resin (Struers, EpoFix) which sets at room temperature. The embedded sample was placed under vacuum for 30 minutes to ensure good resin penetration into the sample. (I should note that one set of samples was left under vacuum too long, this resulted in significant bubbling of the resin. This bubbling made sectioning of the subsequent samples more difficult and the sample more delicate to handle.)

Once embedded the bone sections were cross-sectioned through the middle of the lesion, if present, (see figure 3.1) using a low speed diamond saw (Buehler, Isomet) using

distilled water as a lubricant. The cross-sections were affixed to glass mineralogical slides using Crystalbond™ and polished on one side with successive sizes of diamond paste. The ultimate thickness of the finished cross-sections was approximately 400 micrometres. Once polished the samples were carefully removed by gentle heating on a hot-plate and cleaned of residual Crystalbond™ adhesive using a small amount of acetone. The cross-sections thus obtained were robust enough to be mounted directly in the synchrotron experimental apparatus without further modification.
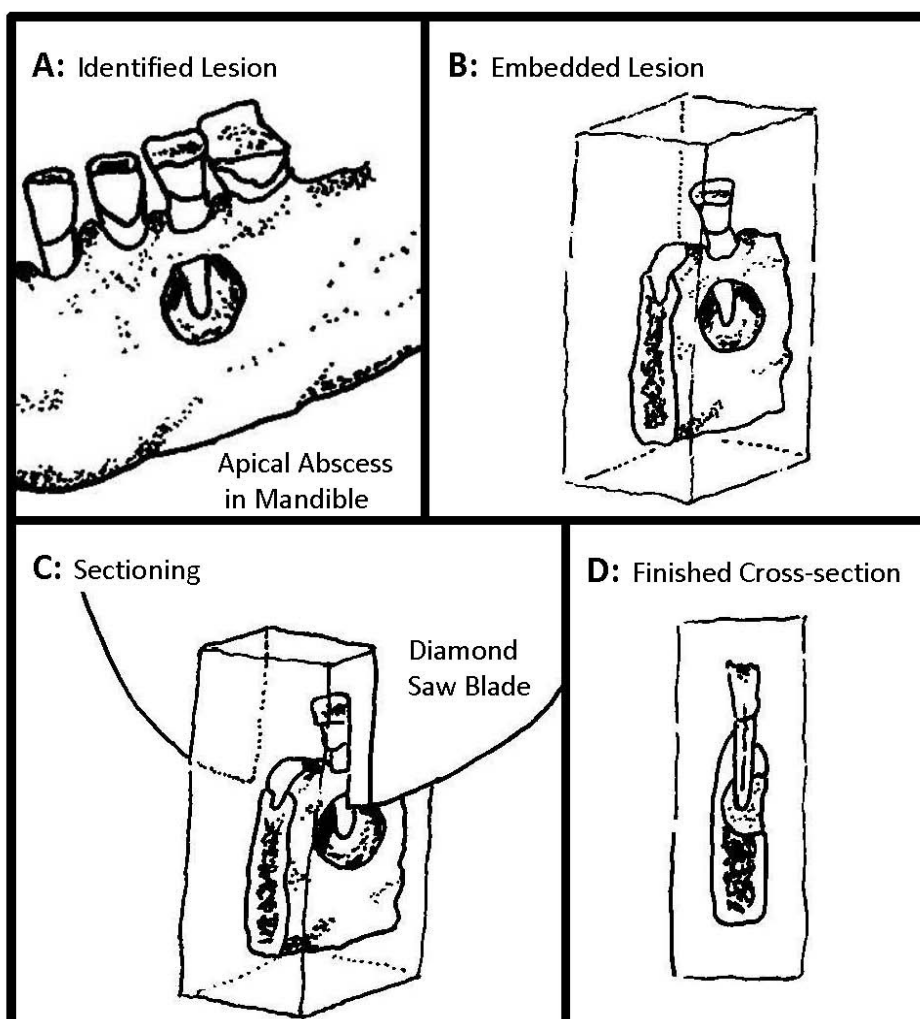
Figure 3.1. Schematic illustrating the process of creating the final cross-sectional samples for use in the synchrotron.

Proceeding without washing or cleaning was done deliberately in this case because it would be expected that the region affected by diagenesis would be the first several micrometres of exposed bone; alternatively, one could say that diagenesis is expected to affect the distribution of elements near the surface of the lesions. Of course, this is exactly the region over which it is expected that the elemental distributions caused by the disease would occur. Also, this thin region of surface bone is the target of most methods of diagentic cleaning. Therefore, in order to avoid obliterating the signal which is expected, no cleaning was done on the samples. This of course means that the signal of interest could be overlayed/obscured or overpowered by diagentic effects which occur at the same scale.

Diagenesis, as stated in background chapter, can be variable even within a specific skeletal element and any bulk measure of the degree of diagenesis may not ensure the absence of diagenesis. Indeed most researchers would say that diagenesis is definitely present at some level in all samples.

How then do I intend to capture or ameliorate the effects of diagenetic elemental changes that may have occurred in my samples? Here I have to rely on a series of comparisons between the distribution patterns in various samples.

3.2: Sample Strategy

In order to try to evaluate both diagenesis or elemental changes due to disease in any particular sample a series of both intra-skeletal, intra-population and inter-population comparisons will be set up for each disease case. These are graphically pictured in figure 3.2 for the ideal case.

Firstly, for a disease affected bone sample, a second sample from the same skeleton which is unaffected by the disease was selected. In this intra-skeletal comparison we would hope to see a difference between the diseased and unaffected bone elemental distributions. To these we need to compare a second 'healthy' sample from a different skeleton drawn from the same population. This second intra-population comparison should show the same differences in elemental distribution, if any, as those

between the 'healthy' and diseased bone samples if the distribution is caused by disease.

Two things should be noted here. Firstly, the 'healthy' samples suffer from the osteological paradox (Wood *et al.*, 1992). In other words they appear to be not affected by the disease of interest but they are drawn from a skeletal population which are of course all dead. Meaning, that the individual was decidedly not healthy, they died of something. Whatever did cause the death of the individual could have had its own affect over the distribution of elements in the region of interest, although hopefully not the same as the other comparison skeleton. The ideal healthy individual would come from a younger individual who, it could be reasonably certain, died as a result of sudden trauma, but these samples are rare in the archaeological record.

Second, it is important to select all samples from the same region or type of bone. Again from the background chapter we know that compact and trabecular bone have different structures, and behave differently in response to diagenetic changes. Thus it is vital that the lesions and 'healthy' samples be drawn from the same kind of bone, at least as near a possible.
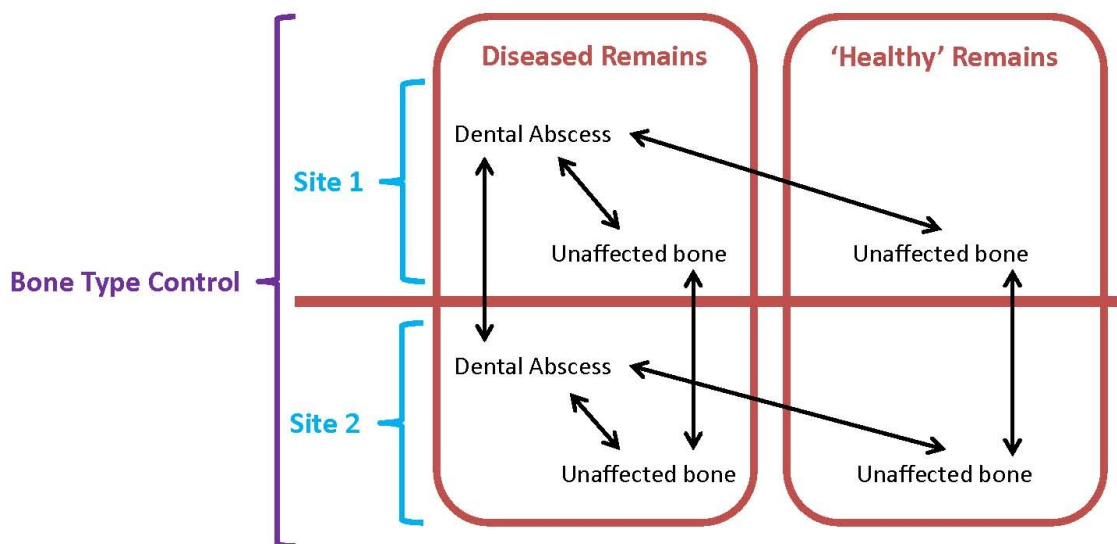
Figure 3.2. Ideal web of sample comparisons for one disease.

All the comparison samples indicated within the one population may still have the same distributions because of diagenesis, if the diagenetic signature within the population's burial site is similar! But if the two 'healthy' samples are the same **but** different from the diseased samples we could say with some confidence that the disease caused the distribution difference. Even so it could be that the diseased portion of bone was more affected by diagenetic affects, so we can not be certain.

In an attempt to clarify the result further, another three samples from a distinct population will be included. In this case if the two diseased distributions are similar then the likelihood of the distribution being related to the disease is increased as it would be unlikely that the diagenetic effects from two distinct sites would be the same.

Two extreme possibilities may occur when comparing the six samples together. Firstly, the distributions could all be the same between the six samples. In this case, we would have to accept the null hypothesis and conclude that the disease had no effect on the elemental distributions within the bone around the lesion, and/or, we would have to state that diagenesis affected each sample (from different sites) in the same way which would seem unlikely.

The second extreme is the opposite, if all the distributions are unique. In this case it is probably the simplest and strongest conclusion to state that diagenesis has affected each sample differently and masked the looked for disease effects, if they existed at all. It could be hoped in either situation that more careful work could eventually allow us to separate the diagenetic distribution fingerprints and obtain a glimpse of any possible disease effects. But it would certainly be premature to accept the null hypothesis in this case.

Of course any pattern in between these two extremes may present itself and I will not attempt to qualify them all at this point.

3.3: The Diseases

A bacterial infection results in an inflammatory reaction in the host tissue. Inflamation consists of increased blood flow, capillary dilation and increased vascular

permeability. These changes allow the immune cellular responders (neutrophils and phagocytes) access to the infected site. The exact changes seen are dependent on the severity of the infection, the causative organism, and the exact tissue involved (Kumar *et al.*, 2007).

Within bone, an unchecked infection typically results in the development of an abscess (Hillson, 2005; Schwartz, 2007). An abscess is a local concentration of pus (consisting of necrotic (dead) cells, neutrophils and fluids) rimmed by a layer of preserved neutrophils and a zone of dilated vessels (Hillson, 2005; Kumar *et al.*, 2007). Abscesses can eventually be completely walled off and be filled with connective tissue, or they can expand past containment in the bone creating a pus drainage hole or cloaca.

3.3.1: Dental Abscess

In the case of dental bacterial infection, the causative bacteria typically enters via the central canal of the tooth eventually infecting the apex of the tooth root. Any oral bacteria can enter the root canal, subsequent to damage of the crown of the tooth caused by a carious lesion (cavity), significant abrasion or trauma (Schwartz, 2007; Waldron, 2009). The actual causative bacteria is difficult to determine. It may be distinct for each abscess although clearly related to the oral flora (Finegold, 1977). Regardless the apical environment is restricted in oxygen and thus the bacteria must be a strict (always anaerobic) or faculative (can change from aerobic to anaerobic, eg. many species of *Streptococci* and *Actinomyces*) anaerobe. Among the possible organisms the *Streptococci* and *Actinomyces* factor prominently in cultures grown from lesions (Finegold, 1977).

The prevalence of caries, abrasion and trauma are influenced by the characteristics of the food and the manner of its preparation and social norms (eg., using teeth as tools, dental care) (Larsen, 1997; Hillson, 2005) and as such vary with population and with type of tooth (Brothwell, 1981; Larsen, 1997). Abscess occurrence is of course closely related to dental disease as it is one of the possible outcomes. Dental care in the past was not as effective as today's and food was unprocessed, caries, abrasion, trauma and as a result, dental abscesses can be found in most ancient populations (Brothwell, 1981; Larsen,

1997).

At an early stage, periapical abscess, can only be recognized radiographically or by pulling out the associated tooth (Brothwell, 1981; Schwartz, 2007). Waldron (2009) cautions that there are actually three types of periapical lesions which may be present: cysts, granulomas and abscesses of which typically a third are actual abscesses. A granuloma (aggregates of macrophages which assume a thin tissue-like structure (Kumar
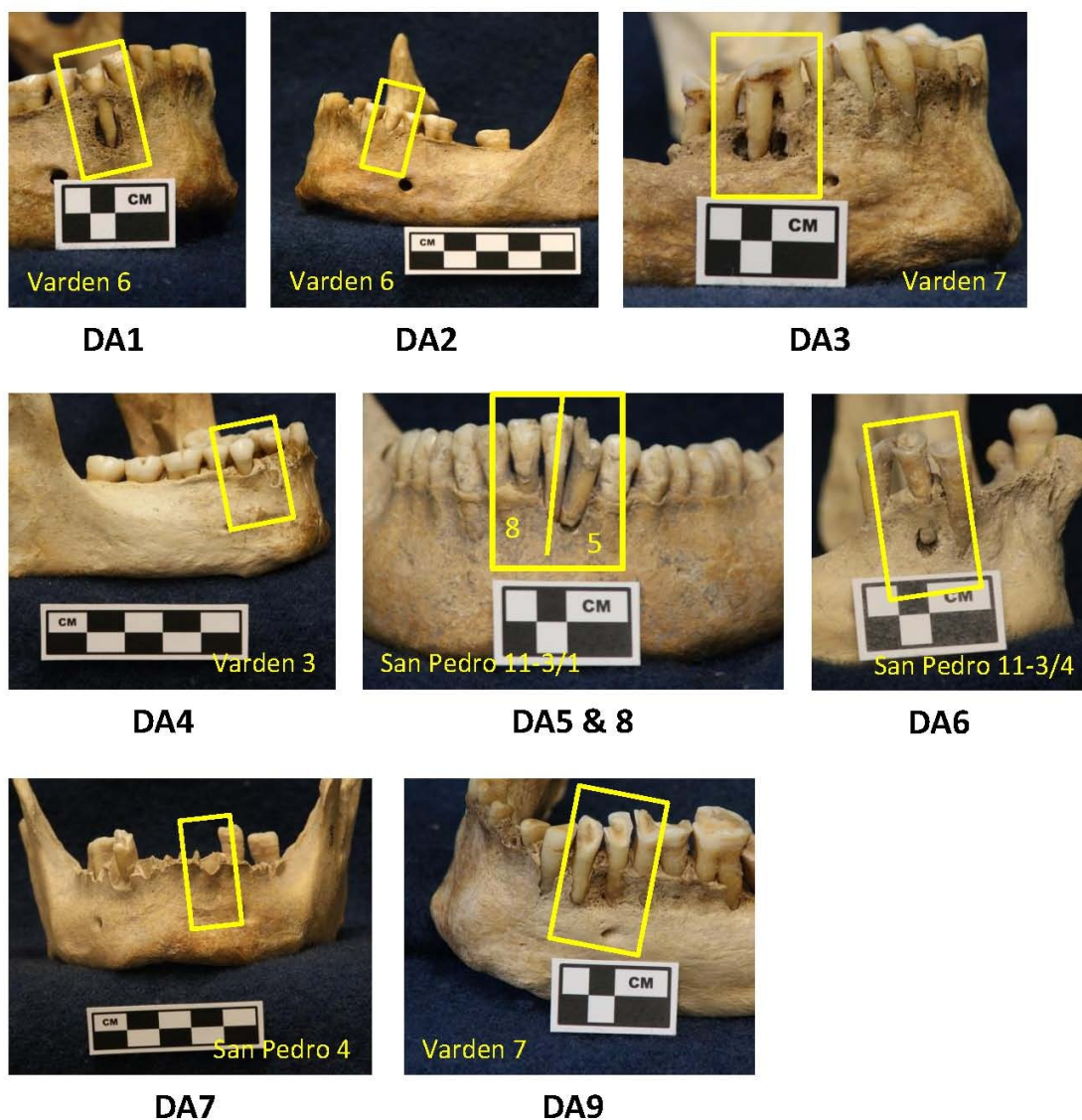
Figure 3.3. Views of the 9 Dental Abscess (DA) samples selected for synchrotron analysis.

et al., 2007)) is chronologically the first lesion to form periapically and typically measures less than 3 mm in diameter. If the tissue in the granuloma develops into a fluid this is termed a cyst; when pus forms it is an abscess. Both granulomas and cysts develop a smooth-walled cavity while an abscess typically has rough-walled cavities (Waldron, 2009).

The fluid or pus in the lesion can drain through the bone spaces and eventually resolve. Alternatively, the abscess can enlarge, eventually producing a drainage hole (Finegold, 1977; Brothwell, 1981; Waldron, 2009) typically on the buccal side (Schwartz, 2007) of the alveolus, although drainage to the lingual side is also possible. In dry bone the classic presentation of a periapical abscess is an ovoid to spherical cavity seen though an oval or circular opening in the alveolus with thin and crisply defined edges. Typically the tip of the tooth root can be seen within the cavity (see figure 3.3 DA1 and DA6 for example) (Brothwell, 1981; Schwartz, 2007).

 All the cases of Dental Abscesses chosen for this project displayed the classical presentation of the condition (Figure 3.3). Comparison samples were taken from two populations, San Pedro, and Varden (see later for details). The San Pedro samples included a lower left second incisor which exhibited an abscess which encompassed the neighbouring root of the first incisor (DA5). Also from this mandible the lower right first incisor (DA8), which was not affected by an abscess, was also sampled as an intra-skeletal control. A second mandible yielded a lower right first premolar with a classic apical abscess (DA6). From a third mandible the lower left canine socket (DA7) was taken as a healthy control. The canine could not be found with the remains and it was assumed that the tooth was lost postmortem as no evidence of healing was visibly evident in the socket.

The Varden samples selected included a lower right first premolar with a periapical abscess (DA1), and the lower left first premolar with no evidence of an abscess (DA2) from the same mandible. From a second mandible the lower right first molar was sampled with an abscess around the distal root (DA3). Also the lower left second premolar from this mandible was sampled (DA9). DA9 displayed a rounded pocket next

to the root on the mesial side indicative of an infection of this particular tooth. As well the lower right premolar from a third mandible from the Varden site with no signs of abscesses was sampled (DA4).

3.3.2: Tuberculosis

Tuberculosis is a disease with considerable history, appearing throughout Europe, as early as 5800 BP, ancient Egypt, as early as 4500 BC and the Americas as early as 700 AD (Roberts and Manchester, 2007). It is an ancient scourge and is a re-emerging global pathogen (Donoghue *et al.*, 2004; Roberts and Manchester, 2007) of significant concern. The causative organism is a *Mycobacterium*, a member the of the *Mycobacteria tuberculosis* complex which includes *M. tuberculosis*, *M. bovis, M. africanum, M. cannetti, M. microti* and *M. avium* (Mays *et al.*, 2001; Donoghue et al., 2004; Roberts and Manchester, 2007).

M. bovis and *M. tuberculosis* are the main causative organisms in human populations and both present similar skeletal manifestations of the disease. The main difference between the two infections being the route of entry into the host. *M. tuberculosis* is typically transmitted via inhalation of infected aspirated droplets from another person, leading initially to lung infection. *M. bovis* is transmitted to humans initially via ingestion of infected milk or milk products producing stomach and intestinal infections initially (Roberts and Manchester, 2007; Waldron, 2009).

It is estimated that about 3-5 % of tuberculosis cases produce skeletal lesions, but when skeletal lesions are present the spine is involved in up to 60 % of cases (Roberts and Manchester, 2007). The classic skeletal presentation of tuberculosis involves one to four vertebrae in the upper lumbar or lower thoracic regions of the spine. The progress of the infection follows a similar course to Dental Abscess formation, that is, it begins with the formation of a local point of infection in the vertebral body followed by abscess formation, eventual penetration of the body wall by the infection and drainage, typically into the chest cavity (Roberts and Manchester, 2007). The destruction of large portions of the anterior vertebral body leads to eventual collapse of the vertebra and subsequent

bony fixation producing a severely anteriorly angled deformity of the spine. The deformed spine is the classic presentation of Pott's disease or skeletal TB (Brothwell, 1981; Roberts and Manchester, 2007; Schwartz, 2007; Waldron, 2009).

It is important to note that in tuberculosis the posterior neural arch is largely unaffected by the infection, as well TB is characterised by very little new bone formation within the lesion (Schwartz, 2007; Waldron, 2009) which helps distinguish TB from other diseases or trauma which can severely angle the spine in a similar fashion.
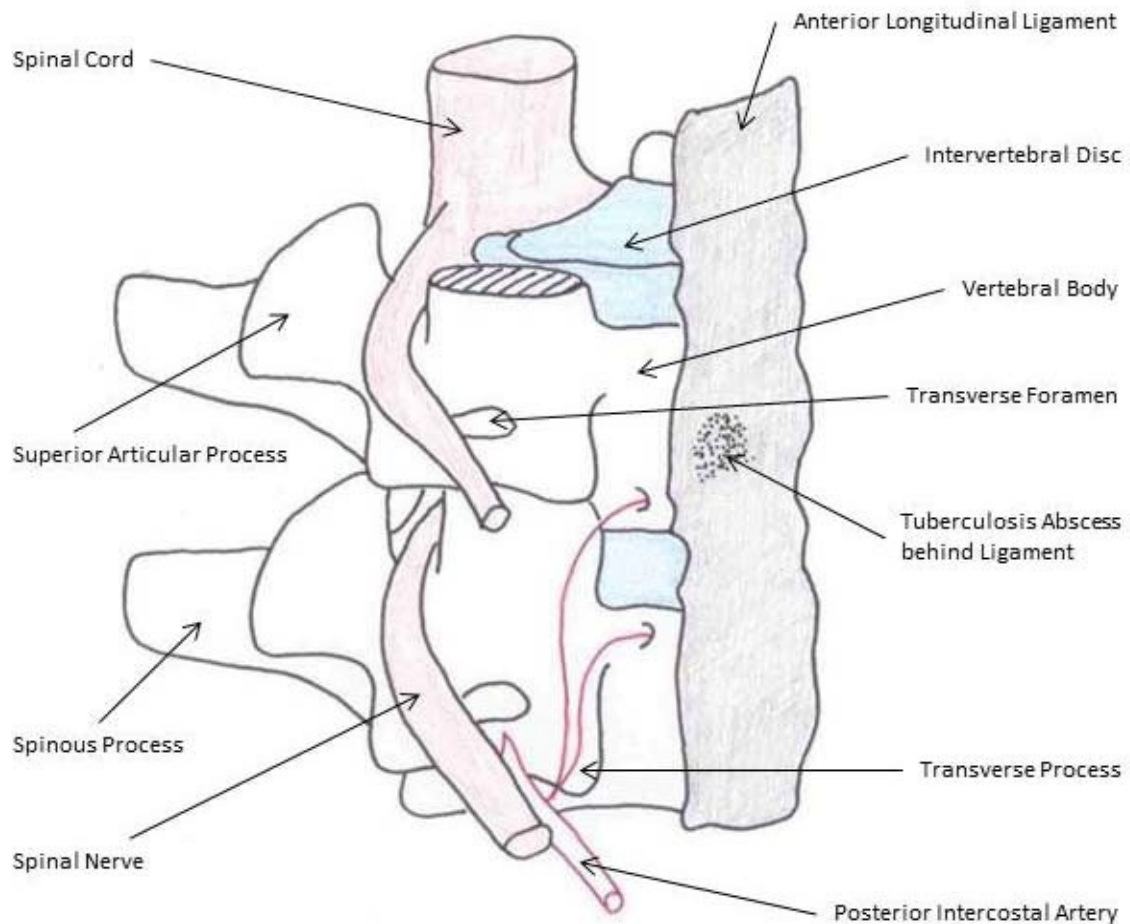
Figure 3.4. Schematic of several vertebrae showing the approximate arrangement of the Intercostal Artery and Anterior Longitudinal Ligament and a TB infection.

Although spinal kyphosis with sparing of the posterior neural arch is considered indicative of TB in paleopathology (Schwartz, 2007; Waldron, 2009), uncertainty can remain, and as a result ancient DNA has been used to confirm diagnoses of TB (Mays *et al.*, 2001; Donoghue *et al.*, 2004; Roberts and Manchester, 2007; Waldron, 2009). The classic presentation of TB is also not appropriate in this work as the extensive destruction of the vertebral bodies leaves little bony material for comparison with unaffected vertebra. As a result, it was necessary to be able to diagnose possible cases of TB in vertebrae early in the disease course before significant destruction occurred.

The route taken for a TB infection to spread from its point of origin in the body to the spine provides a possible unique lesion. The tubercular bacteria travels to the anterior of the vertebral bodies via the lumbar and intercostal arteries (figure 3.4). This leads to the formation of the primary lesion toward the anterior middle of the body. Development of the abscess usually involves the intervertebral disc and/or migration to the anterior longitudinal ligament at the front middle part of the body of the vertebra (Aufderheide and Rodríguez-Martín, 1998). Ultimately, a lesion, which in appearance, is a spherical lytic pocket with a draining cloaca towards the anterior surface of the vertebrae body (Roberts and Manchester, 2007; Waldron, 2009) develops. Such a localized presentation of lesions in isolated vertebra, associated with little or no new bone formation and lack of involvement of the posterior neural arch, has been thought to indicate an early stage TB infection. However, such a lesion could also be caused by other diseases and bacterial infections that affect the spine and are spread via the vascular system (such as rheumatoid arthritis, septic arthritis, sarcoidosis, malignant bone tumours, Paget's disease, actinomycosis, blastomycosis, coccidioidomycosis and osteochondritis (Aufderheide and Rodríguez-Martín, 1998; Schwartz, 2007)). Because of the non-specificity of the lesions, confirmation of the infection needs to be done. Such confirmation is typically done using ancient DNA (Waldron, 2009). This early presentation of TB was what was sought in the samples chosen for this project.

The TB samples (see table 3.1) all arose from the Kellis II cemetery in Dahkleh Oasis, Egypt. The presence of TB in each sample selected was confirmed by aDNA

analysis (Donoghue *et al.*, 2005). In this case four samples were chosen from the available Kellis materials currently housed at Western University.

      The first sample TB1, was found in a second lumbar vertebra. The vertebra displayed a significant abscess pocket and oval cloaca (17 x 8 mm) draining anteriorly. This sample also displayed a parrot beak osteophyte projecting inferiorly from the lower body edge. Both the lesion (TB1-L) and the osteophyte (TB1-O) were sectioned for analysis. The second sample from a different individual in the Kellis population was a second thoracic vertebra, again, with an anterior abscess pocket and anterior cloaca (TB2). As an intra-skeletal comparison an unaffected first lumbar vertebra from the same individual as TB2 was chosen for sectioning (TB3).
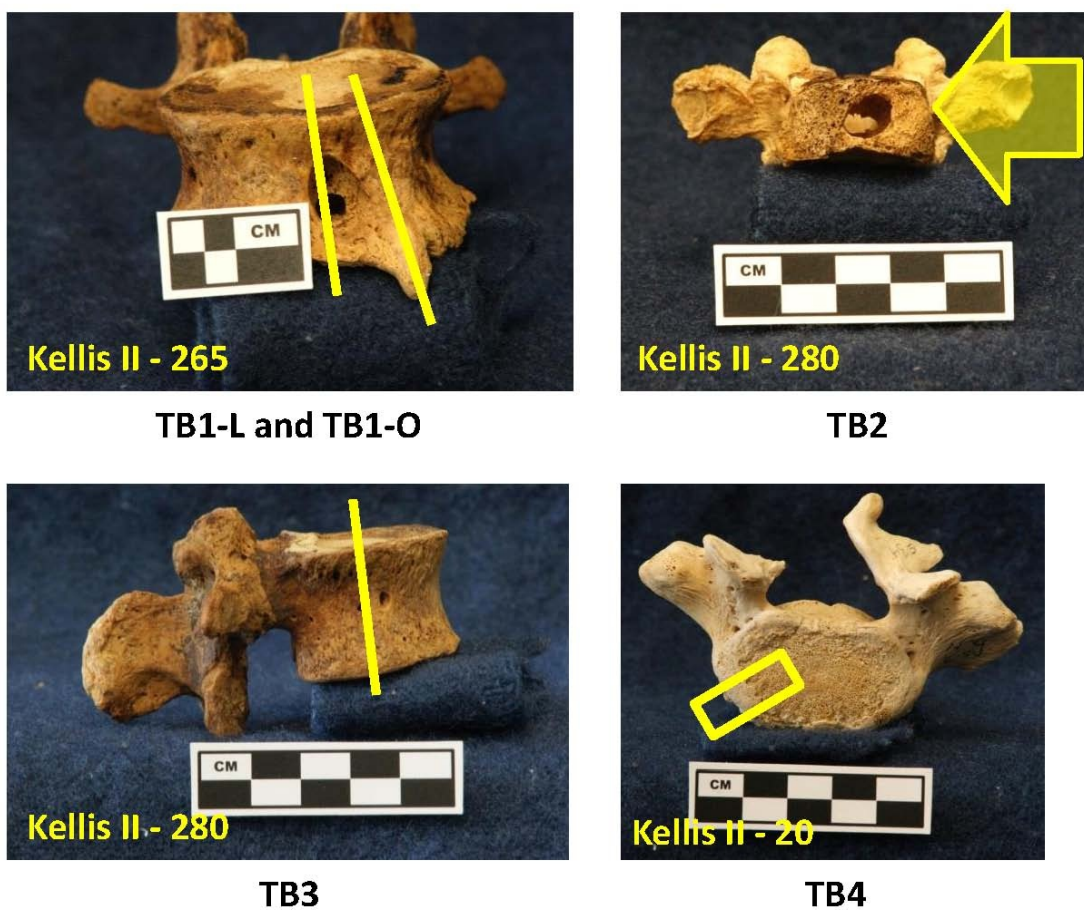
Figure 3.5. Views of the four Tuberculosis samples selected for synchrotron analysis.

Finally an unaffected fifth lumbar vertebra from a third individual was chosen for sectioning as an inter-skeletal control (TB4). This third vertebra was interesting in its own right, as it displayed a congenital afusion of the spinous process as well as trauma to the neural arch (see appendix B-10 for details). All the TB samples from Kellis are pictured above in figure 3.5.

Unfortunately, due to the availability of collections, the rarity of skeletal TB lesions in ancient populations and the destructive nature of the sampling process a second comparison population could not be secured for the work, so only one set of TB samples was studied. However, other samples were available at Western University which displayed interesting pathologies and it was decided to sample several of these to function as possible test cases for any conclusions that might be drawn from the DA and TB work. As they are individual samples no statistically significant conclusions could or should be drawn from their analysis.

3.3.3: Actinomycosis

The first additional sample was a rib (R1) taken from an individual from the LeVesconte Burial Mound site in Ontario. This individual was extensively studied by

R1

Figure 3.6. View of the right rib affected by Actinomycosis (R1) selected for synchrotron analysis.

Molto (1990). After differential diagnosis Molto concluded that the rather unique combined lytic and proliferative lesions giving rise to pleural swelling on the rib (figure 3.6) were indicative of infection by actinomycosis.

Actinomycosis is an infection caused by the bacterium *Actinomyces israelii*. *A. israelii* is an endogenous oral cavity bacterium. An anaerobic bacterium, it is also heavily suspected in cases of dental abscess formation. Pulmonary infections of *A. israelii*, although rare today, were more common in past populations. Rib involvement is prevalent in cases of pulmonary infection, in about 60% of patients. The initial focus of infection is typically seen to be the lower lobes of the lung particularly on the right side. The bony response to seeding, from adjacent infected pleural tissue, is described as a diffuse hypervascular periosteal bone growth progressing to an ossifying periostitis with accompanying lytic lesions. Together these responses produce a thickened rib with mixed osteoblastic and osteolytic lesions. The rib from the right side of individual 18 from the LeVesconte Mound presents this combination of osseous responses (Molto, 1990).

3.3.4: Other Samples

The LeVesconte Mound population also contained a second individual displaying a significant array of pathologies. This individual, burial 8, was an elderly female with significant pathologies throughout the skeleton. Mainly the remains are marked by concentrations of small, oval to round, lytic lesions of about 1 mm diameter. Each lesion is sharp edged with a punched out appearance, ie. sharply sloped or bevelled to the interior of the bone (figure 3.7a, left image). The bones lack any new bone formation near these concentrations of lesions.

The lesions are concentrated in the hematopoietic regions of the skeleton (ends of the long bones, innominate bone, sternal ends of ribs etc.). The type of lesion and their concentration leads us to suggest that this individual suffered from Leukemia (El Molto and Bruce Rothschild, Personal Communication).

As a comparison rib sample a cross-section of rib from the same individual

described above was taken from the mid-shaft which displayed no lesions (sample R2). A section of rib was taken through the sternal end including the leukemia lesions was labeled (R3). A fourth rib cross section was taken from an individual from the Kellis II

Figure 3.7. Views of the two ribs from which samples R2, R3 and R4 were taken.

cemetery population. This individual was already sampled and displayed TB lesions in the spine. The rib sampled had no evidence of any pathology (figure 3.7b), however, the superior margin of the rib had several small sclerotic lumps (only about 1 mm in diameter, indicated by arrow in figure 3.7b). Although these are likely not pathological, but a normal variation in form, a section of rib was taken in an attempt to capture one of these lumps in cross section (R4).

This concludes a brief survey of the skeletal elements selected for synchrotron radiation X-ray fluorescence analysis. More details of each element can be found in appendix B at the end of the thesis. Relevant demographic parameters (age, sex) and diagenetic test results are included in table 3.1 (page 60) where available.

3.4: Sample Sites

The samples were all selected from collections of skeletal elements currently housed at Western University. The collections represent sites from three countries on two continents (figure 3.8). They were collected by many different researchers over many seasons of work and I am grateful that they were all made available to me for sampling. Brief descriptions of the sites are included below.

3.4.1: San Pedro

San Pedro is an ancient Maya site which was occupied from the Terminal Postclassic to Historic times (AD 1400 - 1650). The site is located on Ambergris Cay, the northern most island off the coast of Belize (Williams *et al.*, 2005 and references therein). San Pedro is approximately 8 km north of the southern most tip of the island along the windward side (facing the ocean)(see figure 3.8). The excavations occurred from 1990 through to 1993. Numerous burials were recovered which represented various stages of the Postclassic period. Cultural affiliations of the remains were assigned based on grave goods, construction fill and stratigraphy. Age at death and sex of individuals was assessed using standard bioarhaeological methods.

In the context of other isotopic studies numerous measures of diagenesis have been obtained on each set of remains from ground bone samples (Williams *et al.*, 2005). Relevant parameters for each sample used in this work are indicated in table 3.1. Three mandibles were chosen from the remains held at Western (see Appendix B for detailed osteologies of these elements). The mandibles came from Burial 4, a 30 - 40 year old male, Burial 11/3-1, a 20 - 25 year old female and a 40+ year old female, Burial 11/3-4.

3.4.2: Varden (AdHa-1)

The Varden site is a multicomponent site located on Long Point extending into Lake Erie in South Central Ontario (see figure 3.8). The site is a sand knoll overlooking
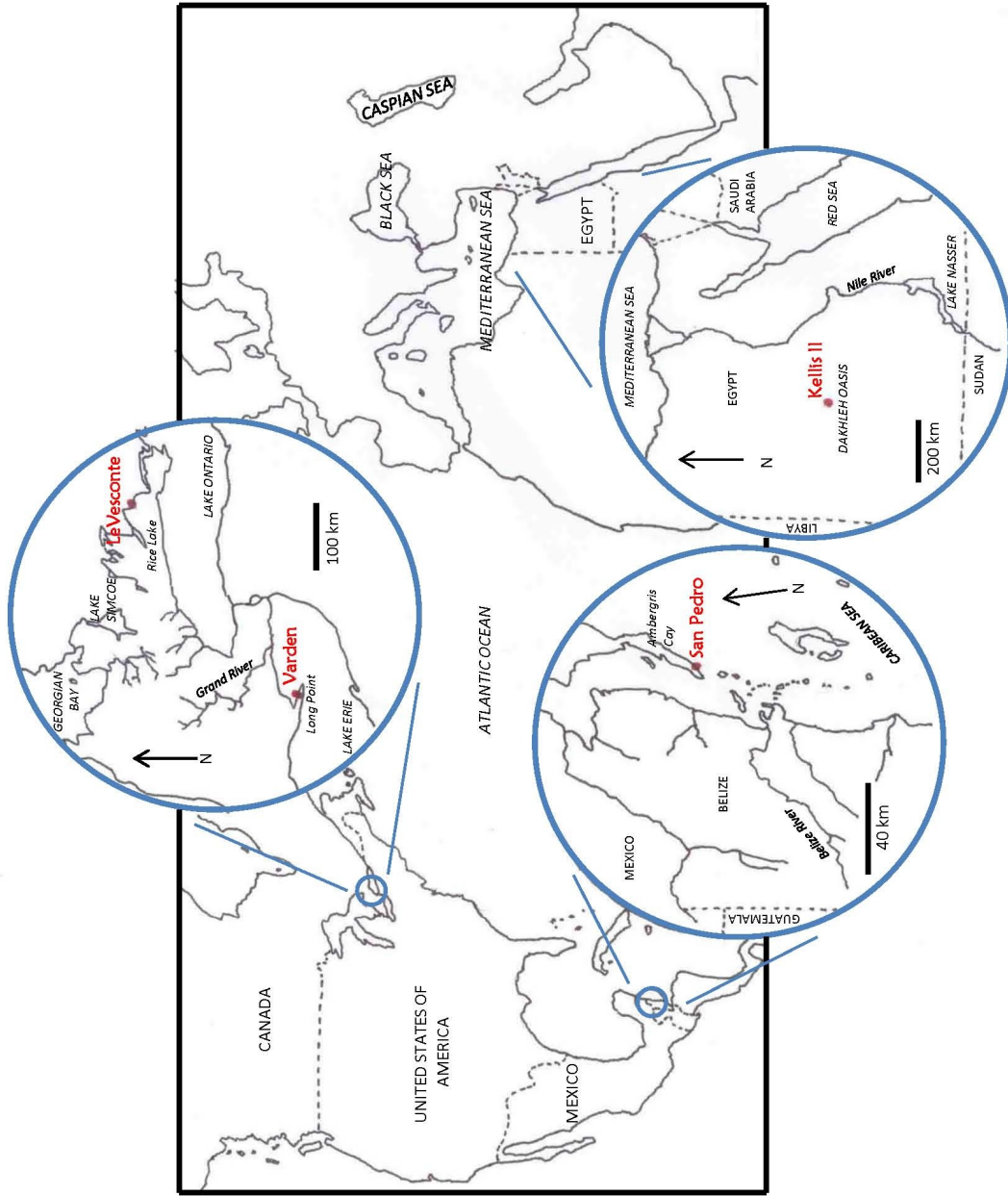
Figure 3.8. Map showing the location of the four Sample Sites: 1) Varden and 2) LeVesconte Burial Mound in Southern Ontario, Canada; 3) San Pedro, Belize and 4) Kellis II, Egypt

Anderson Pond and Gravelly Bay 6 km from the eastern tip of the point. The area is dominated by marshland. The site was first discovered in July of 1981 by recreational boaters. The site was subsequently excavated and mapped by William Fox, the Regional Archaeologist at the Ministry of Citizenship and Culture in London, Dr. Michael Spence of the University of Western Ontario and then graduate student John MacDonald of McMaster University (Foreman and Molto, 2008-2009 and references therein).

Based on stratigraphy, lithic and ceramic artifact analysis four distinct cultural components were identified at the site. Two Transitional Woodland Princess Point components (AD 500 - 1050), a Late Woodland Transitional Princess Point-Glen Mayer component (AD 900 - 1250) and a Late Prehistoric/Early Historic Iroquoian component (AD 1400 - 1500). Although carbon dating of several artifacts from the site confirmed the multicomponent nature of the site, the skeletal remains recovered could not be convincingly associated with any particular component. This was a result of the lake levels raising throughout the 1970's and 80's inundating the site and also the collapse of a large elm tree which scattered the remains throughout the shallows of Gravelly Bay. Subsequent detailed osteological work by Foreman and Molto (2008 - 2009) and others has placed the remains in the Princess Point Culture (AD 500 - 1050).

Three well preserved mandibles were again selected from the remains available at Western University. Burial 3, Burial 6 and Burial 7 (see table 3.1).

3.4.3: Le Vesconte

Le Vesconte Burial Mound is located in southeastern Ontario about 15 km from Rice Lake, along the north branch of the Trent River. The site is about 9.6 km downstream from Campbellford, Ontario and sits on a promontory with steep banks 12.2 m above the river. The mound was excavated in 1962 and the bones are curated at the Royal Ontario Museum in Toronto, Canada. The mortuary complex belongs to the Point Peninsula hunters and gatherers who inhabited the region in the Middle Woodland times (300 BC to 500 AD)(Molto, 1990).

From these well preserved individuals ribs from burial 18 and 8 were selected (see

table 3.1 for more data).

3.4.4: Kellis II

The Kellis II cemetery is located in the Dahkleh Oasis in Egypt's Western Desert. The Oasis is one of five major depressions in the desert and measures about 100 km long from east to west, and 25 km at its widest point (Fairgrieve and Molto, 2000, and references therin). It is about 800 km south-south west of Cairo. The soils in the depression have a high iron oxide content and the climate is extremely arid, water seeps to the surface of the depression from the Nubian Sandstone and Shale series, which contains one of the largest ground water aquifers in the world. This allows the residents of the Oasis to grow a range of fruits, vegetables and grains.

Since 1977 the Oasis has been the focus of the Dahkleh Oasis Project (DOP). The Oasis has been continually occupied from Pharaonic Periods to today. The analysis of the human remains from several ancient cemeteries existing in the oasis focus mainly on the 'Ein Tirghi (31/435-D5-2) and Kellis II (31/420-C5-2) cemeteries. 'Ein Tirghi dates from the Late Period and was used over several hundred years from around 900 BC to Ptolemaic times. Kellis 1 was used from about 60 BC to 100 AD. Kellis II dates from the Christian Period (100 - 400 AD) and served the town of Kellis before it was abandoned (Fairgrieve and Molto, 2000).

From the selection of skeletal elements available at Western (from the DOP collection) vertebrae from burial 20, 265 and 280 were selected for analysis (table 3.1).

3.5: Actual Sectioned Sample Inventory

As it is not common to view disease or bone samples in cross-section in archaeology I will now present a summary of the final prepared samples selected for synchrotron XRF analysis.
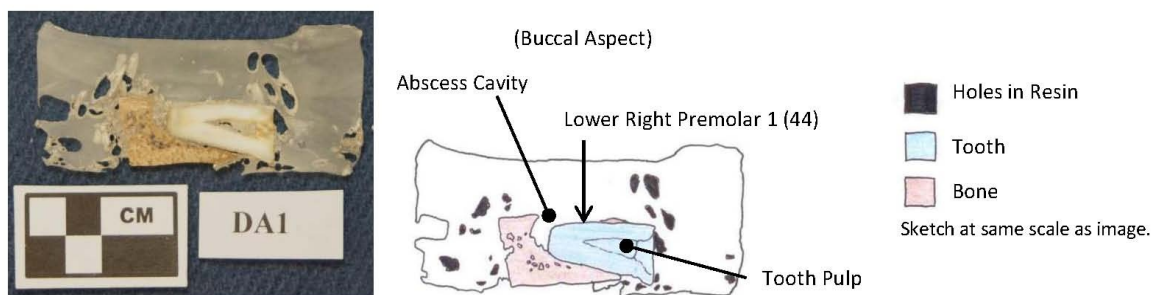
Figure 3.9. Image and sketch of sample DA1.

The first sample DA1, from Varden individual #6, displays the classic presentation of a dental abscess in cross-section.
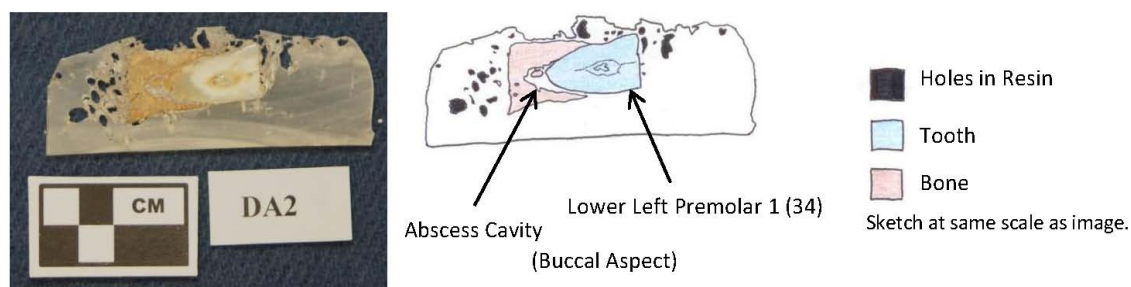
Figure 3.10. Image and sketch of sample DA2.

The second abscess sample, from Varden individual #6, was visibly 'healthy' from outside inspection and was intended to be the intra-skeletal control for the Varden samples. On cross-section there is a clear abscess (or granuloma) cavity around the apex of the tooth root. Thus this sample becomes another example of an abscess.

In sample DA3, from Varden individual #7, a small abscess cavity can be seen under the apex of the root towards the buccal side. Considering the size of the cloaca associated with this abscess (see figure 3.3) I re-assessed the sample and determined that the distal root was missed in sectioning. Sample DA3 is a section through the proximal root of the molar which was not the primary location of the abscess. Thus a second

section was cut from the remaining resin block through the distal root.

Table 3.1. List of samples selected along with demographic and other pertinent data from the literature.

Site	Cultural Affiliation	Time Period	Sample	Burial #	Diseased	Age	Sex	C/N Ratio	Collagen Yield	Crystallinity Index	C/P	aDNA TB test[c]
Varden[d]	Ontario Princess Point	500 - 1050 AD	DA1	6	Y			3.3				- -
			DA2	6	~~N~~Y[a]			3.3				- -
			DA3[b]	7	Y			3.2				- -
			DA3-2									
			DA4	3	N			3.2				- -
San Pedro	PostClassic Maya	1400 - 1650 AD	DA5[b]	11-3/1	Y	20 - 25	F	3.24	3.65	3.18	0.25	- -
			DA5-2									
			DA6	11-3/4	Y	40 +	F?	3.30	4.80	3.10	0.24	- -
			DA7	4	N	30 - 40	M	3.24	6.42	3.11	0.23	- -
			DA8[b]	11-3/1	N	20 - 25	F	3.24	3.65	3.18	0.25	- -
			DA8-2									
Varden	Princess Point	500 - 1050 AD	DA9	7	Y			3.2				- -
Kellis II[e]	Egyptian Christian	100 - 400 AD	TB1-L	265	Y	40 ± 5	M					✔
			TB1-O									
			TB2	280	Y	60 +	F					✔
			TB3	280	N	60 +	F					✔
			TB4	20	N	55 ± 5						✗
Le Vesconte	Ontario Point Peninsula	300 BC - 500 AD	R1	18	Y	30- 40	M					- -
			R2	8	N	40+	F					- -
			R3	8	Y	40+	F					- -
Kellis II	Egyptian Christian	100 - 400 AD	R4	280	N	60 +	F					✔

[a]This tooth was actually diseased when viewed in cross-section.

[b]Due to problems in sectioning this sample was re-cut.

[c]TB DNA analysis from Donoghue *et al.*, 2005.

[d]Varden C/N data from Katzenberg *et al.*, 1995.

[e]Kellis demographic data from personal communication Dr. E. Molto.
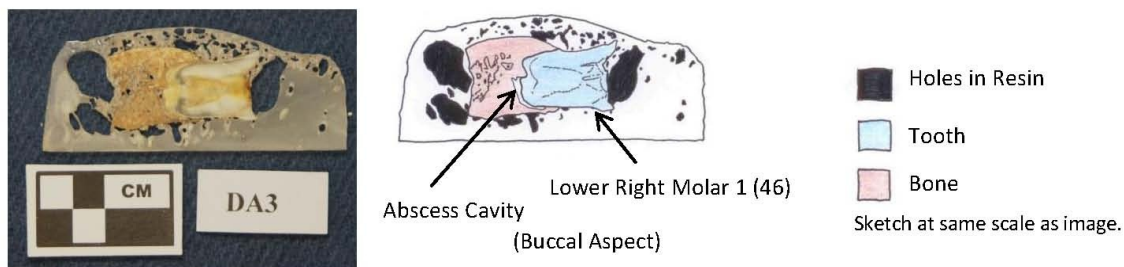
Figure 3.11. Image and sketch of sample DA3.
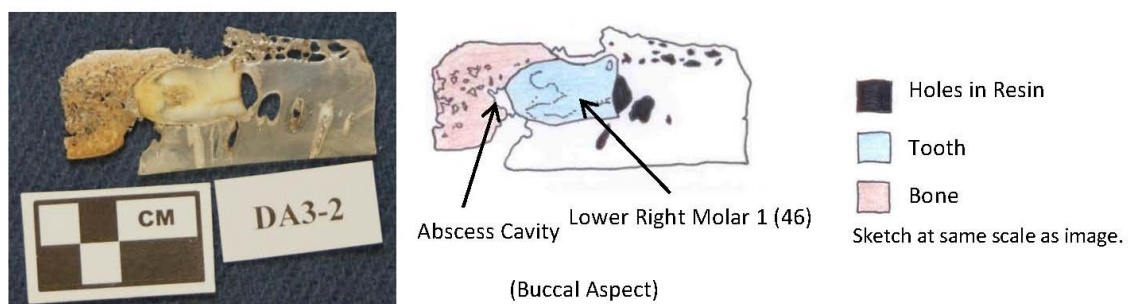
Figure 3.12. Image and sketch of sample DA3-2.

Sample DA3-2 is a cut through the distal root of the lower right molar of Varden individual #7. The abscess pocket is more clearly visible as is the drainage cloaca. This represents a second example of a dental abscess from this site.
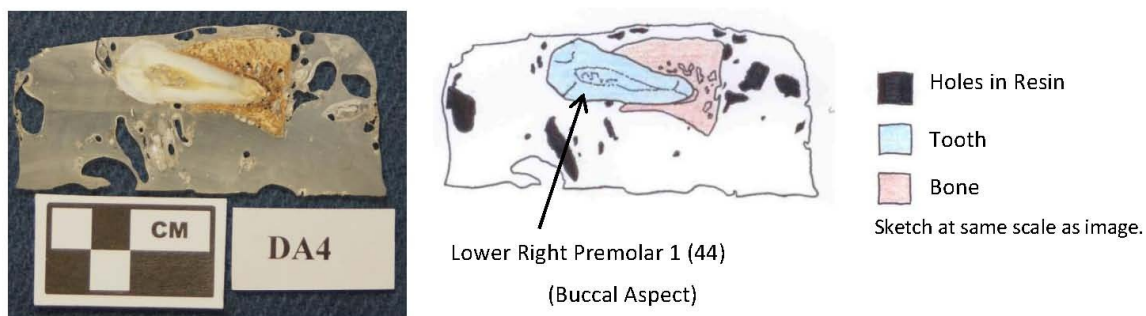
Figure 3.13. Image and sketch of sample DA4.

Cross-section DA4 is through the healthy lower right premolar 1 of Varden individual #3. This represents a healthy tooth in a healthy socket, the close contact between the tooth and the alveolar bone should be noted. This sample represents the intra-population unaffected comparison sample for the Varden site.

Figure 3.14 shows the sample DA5 which was taken from San Pedro, individual 11 3/1. This sample was identified as a diseased type sample, unfortunately the sample became too thin in polishing and could not hold up to handling. As a result a second cut from this lower left second incisor was taken for analysis, see figure 3.15.
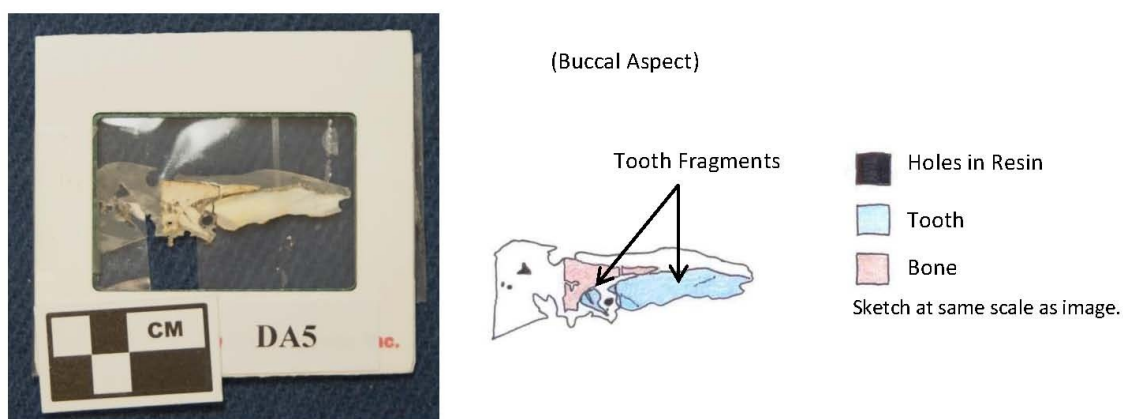
Figure 3.14. Image and sketch of sample DA5.
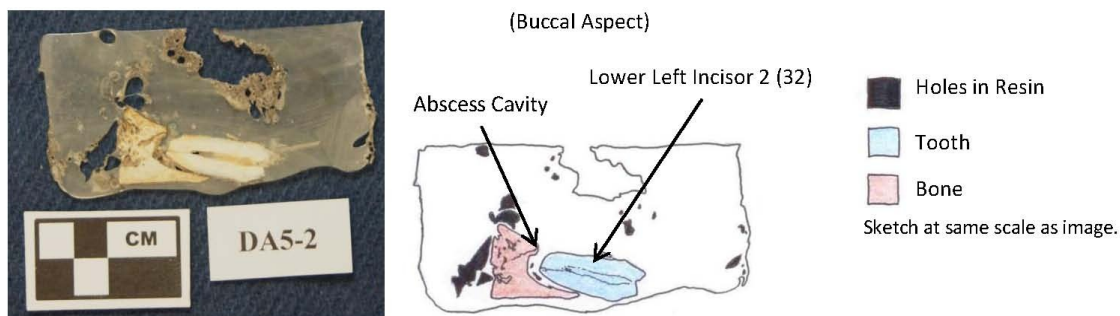
Figure 3.15. Image and sketch of sample DA5-2
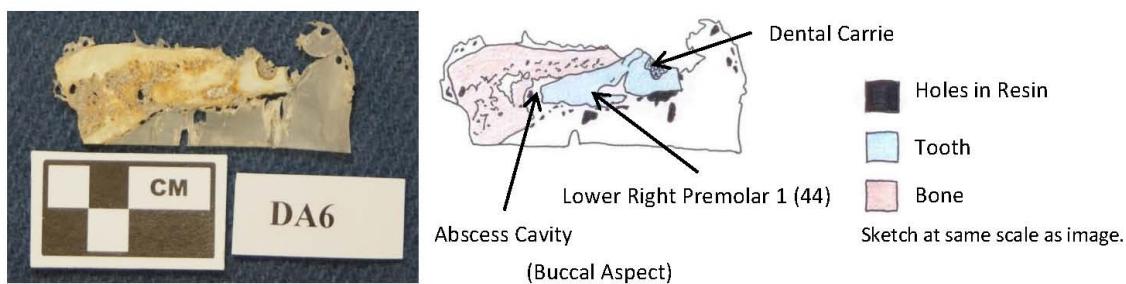
Figure 3.16. Image and sketch of sample DA6.

Sample DA6 represents an alternate diseased case from San Pedro. Taken from individual 11 3/4, this lower right first premolar displays a clear abscess pocket at the apex of the root. Also visible in the sample is a large dental carie (cavity) on the occlusal surface of the tooth.
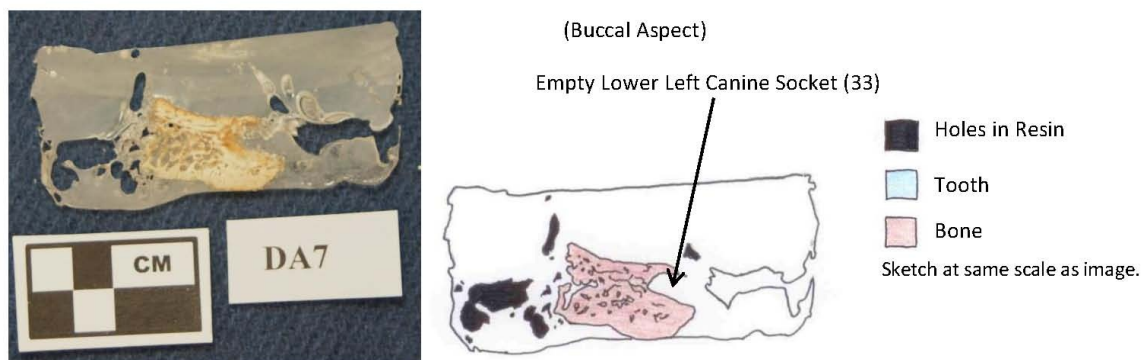
Figure 3.17. Image and sketch of sample DA7.

The intra-population unaffected sample for the San Pedro population comes from an empty socket of the lower left canine tooth from burial #4. Most of the teeth from this mandible were not present in their sockets. This particular tooth could not be found with the remains and it was assumed that the tooth was lost post mortem as no visible signs of healing (ie. absence of sclerotic thickening or shallowing of the socket depth) could be

seen within the empty socket.

The last sample from San Pedro is considered the intra-skeletal unaffected comparison. Taken from individual 11 3/1, it is the lower right first incisor from this individual. This particular tooth was only separated from the sample DA5 by one tooth. Again, there was a mis-cut of this sample and the original sample DA8 (figure 3.18) missed the centre of the tooth. This sample was re-cut to give sample DA8-2 which is shown in figure 3.19.
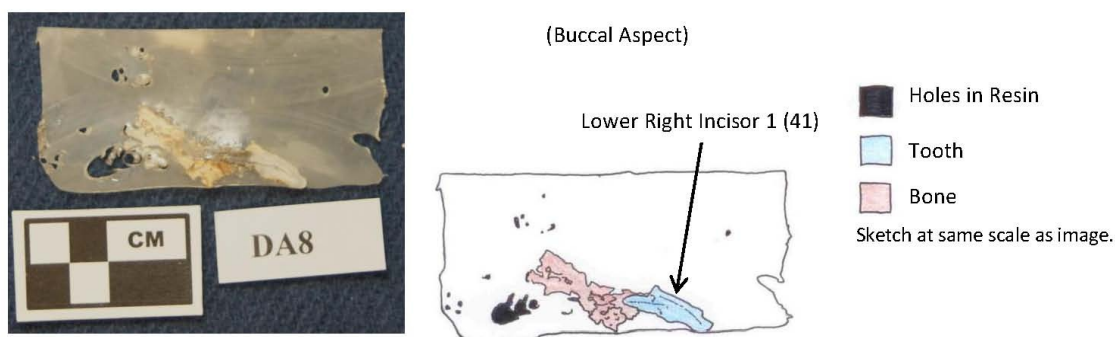
Figure 3.18. Image and sketch of sample DA8.
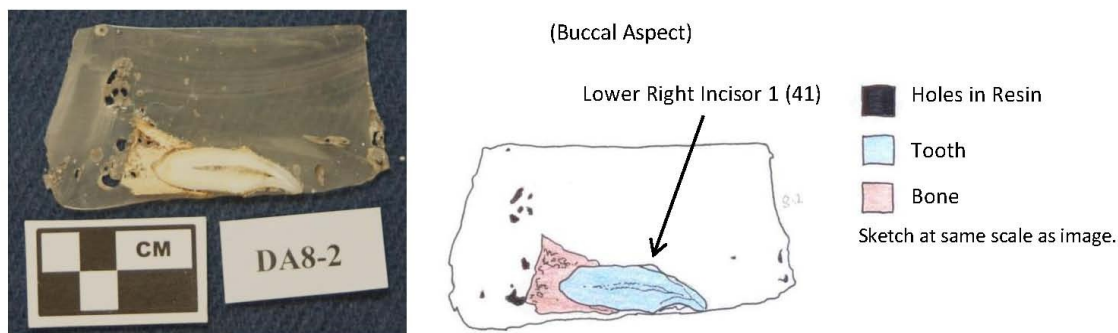
Figure 3.19. Image and sketch of sample DA8-2.

One other sample (DA9) was made, as mentioned above this was from a tooth which showed an uncovered root indicating an infection of the tooth root or neighbouring tooth root. The image below (figure 3.20) for this sample clearly shows no apical abscess cavity associated with this lesion. Time was not sufficient to include this sample in any

further analysis.
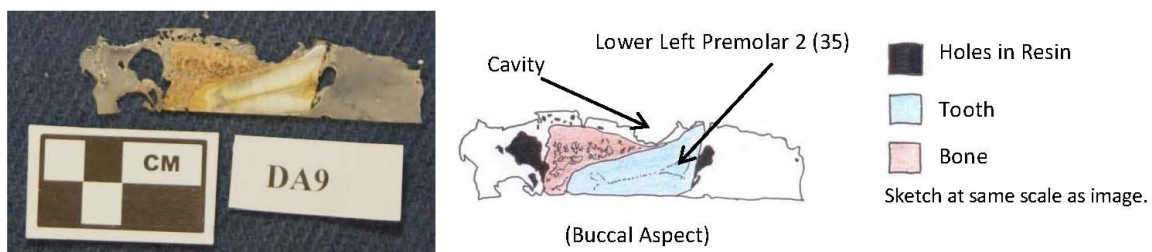
Figure 3.20. Image and sketch of sample DA9.

The above 8 samples comprise the comparison set for testing the null hypothesis for this project (there is no difference in elemental distribution between bone affected by dental abscesses and unaffected bone) in the case of dental abscesses. In figure 3.21, I have reproduced the comparison web from the beginning of the chapter indicating where each actual sample fits in the comparison set.
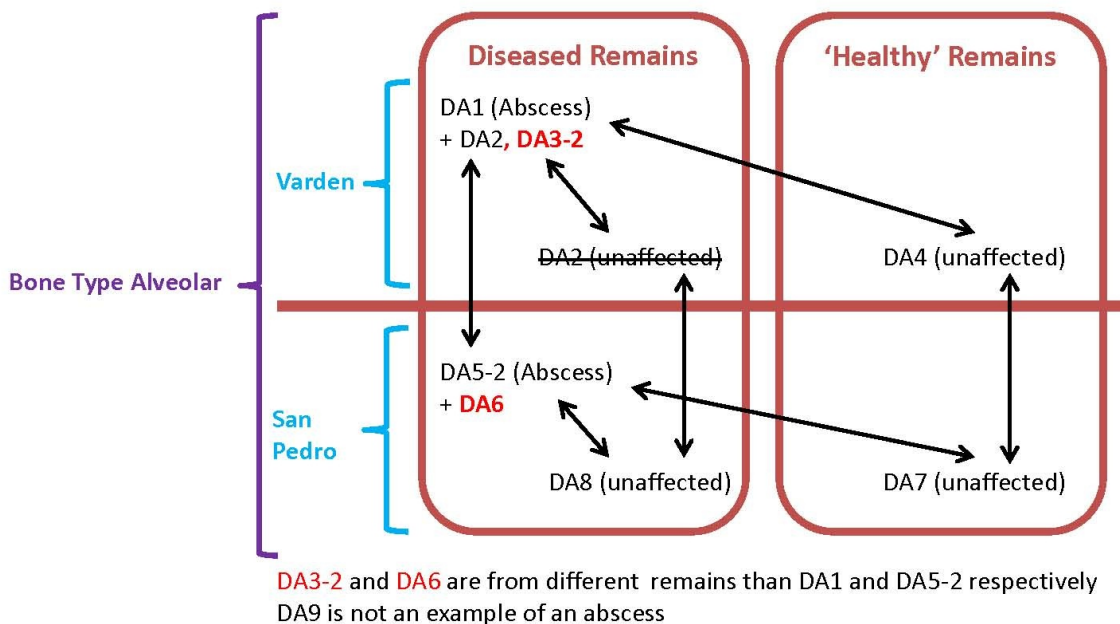
Figure 3.21. Actual comparison web for the Dental Abscess samples.

Now, for the Tuberculosis sample set, which was limited to only one sample site,

the first sample was TB1 which was split into: TB1-L comprising the lesion and associated trabecular bone of the vertebra body; and TB1-O which cross-sectioned a classic parrot beak osteophyte growing from the inferior margin of the body.

The size of the lesion cavity in relation to the body is clear in TB1-L, figure 3.22. In the image a small amount of sclerotic thickening can be seen to the anterior body margin above and below the opening of the lesion, it is important to note that no thickening is apparent along the interior wall of the lesion itself, which is consistent with the lytic nature of Tuberculosis lesions. These two samples were taken from a lumbar vertebra L2) of Kellis II individual 265.

Figure 3.23 shows a cross-section of the parrot beak osteophyte. Of interest are the extensions of sclerotic new bone up the anterior body wall and along the inferior body margin of the vertebra (Indicated by red arrows in the figure). Also the inferior tip of the osteophyte has a more trabecular appearance indicating the region of rapid new bone growth within the osteophyte.
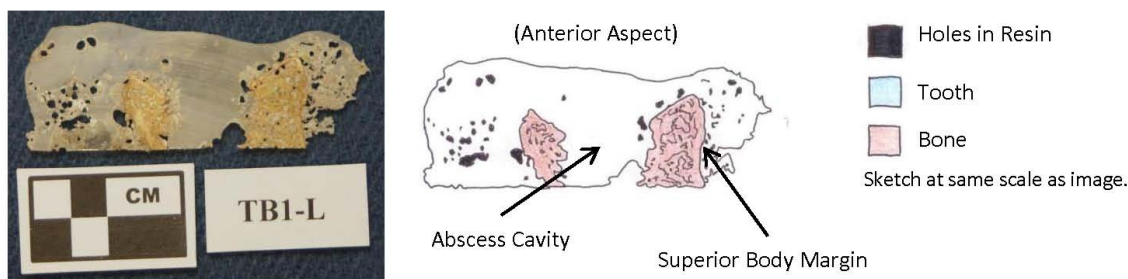
Figure 3.22. Image and sketch of sample TB1-L.
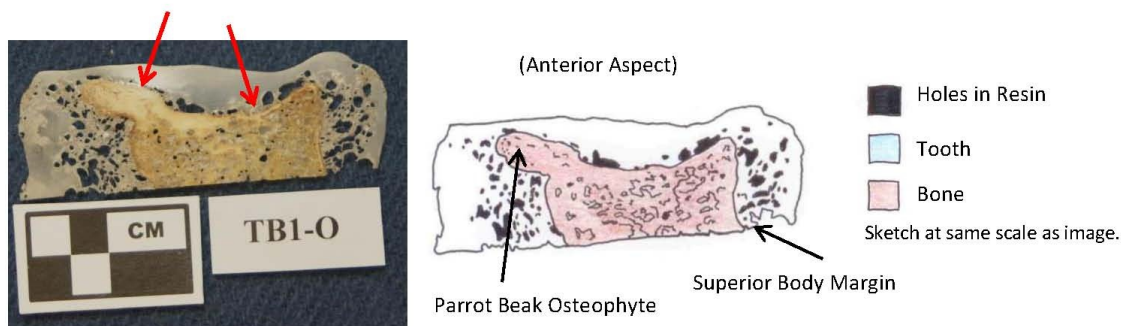
Figure 3.23. Image and sketch of sample TB1-O. (Arrows indicate areas of sclerotic bone).

The osteophyte does not have any direct bearing on the question of this thesis but it is interesting to investigate this example of pathological bone formation.

The next sample TB2, was extracted from a thoracic vertebra (T2) from Kellis II individual 280. This is another example of a Tuberculosis lesion. Unfortunately, during the cutting procedure some of the fragile trabecular bone broke away from the sample leaving me unsure as to the actual location of the lesion and body margins on this rather small sample. The indications in figure 3.24 are my best guess.
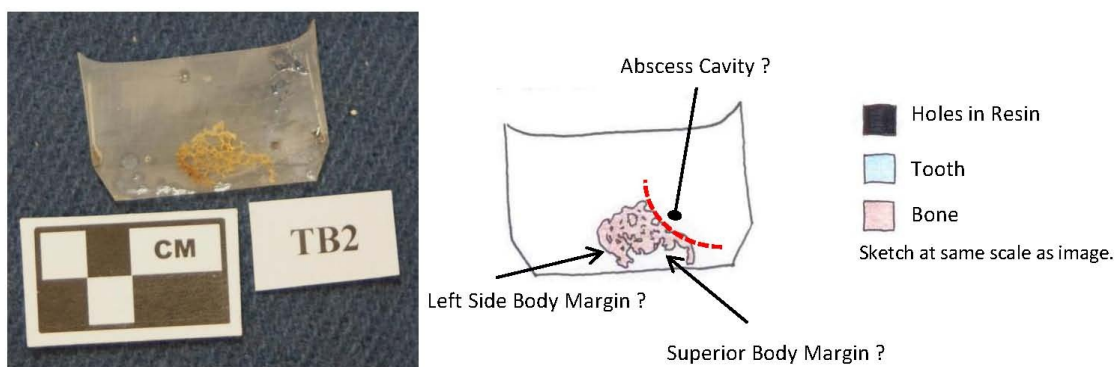
Figure 3.24. Image and sketch of sample TB2.

Sample TB3 represents the intra-skeletal unaffected comparison sample. It was drawn from a lumbar (L1) vertebra of individual 280 from Kellis II. It is good to note at this point that in the images of samples one can see parallel curved striations on the
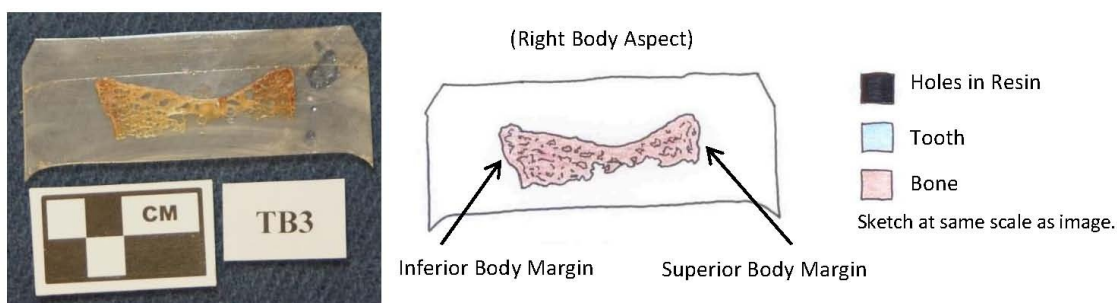
Figure 3.25. Image and sketch of sample TB3.
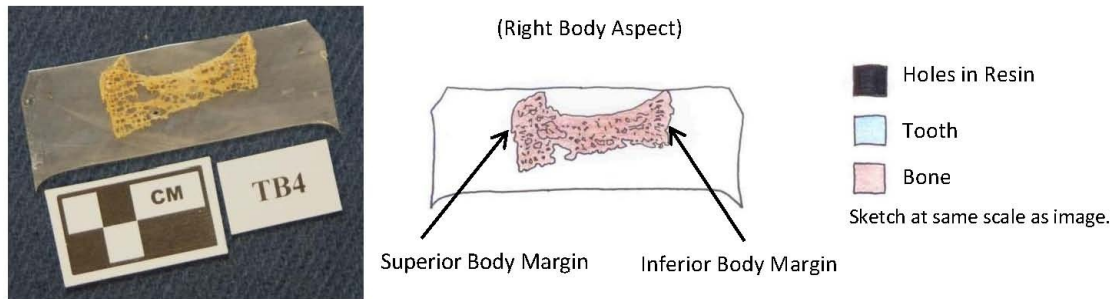
Figure 3.26. Image and sketch of sample TB4.

samples, a good example is seen in figure 3.25 just below the bone. These are cut marks left over from the sectioning of the sample. The marks are actually on the back side of the samples, the front surfaces are flat and polished, the reverse sides of the samples were not polished.

The final Tuberculosis sample in the comparison set (TB4, figure 3.26) was taken from a third individual from Kellis II. In is an unaffected lumbar (L5) vertebra from individual 20 and will function as the intra-population comparison sample. Again below, for your reference, I reproduce the comparison web for the Tuberculosis samples indicating where each sample fits.

This leaves the extra rib series of samples which do not fit into any comparison scheme. First, there is the rib cross-section of the Actinomycosis rib (R1) below. Both the proliferative and lytic nature of this pathology are clearly seen in the cross-section. The darker (black) regions are areas of soil contamination within the bone's porous structure which were not blown out during sample preparation. This rib sample was taken from a right rib of LeVesconte individual #18.
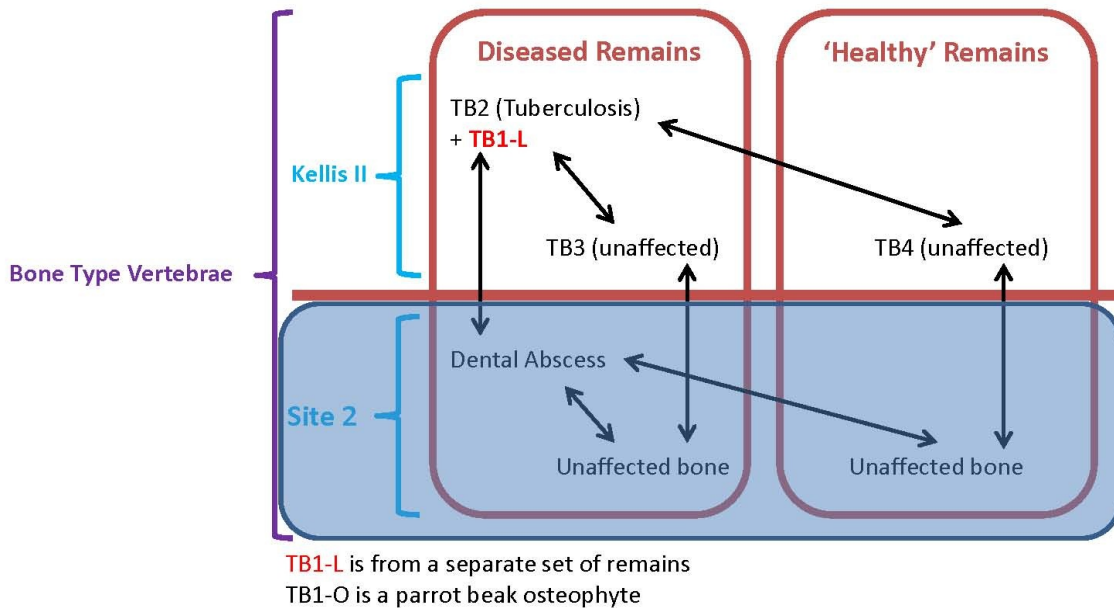
Figure 3.27. Actual comparison web for the Tuberculosis samples.
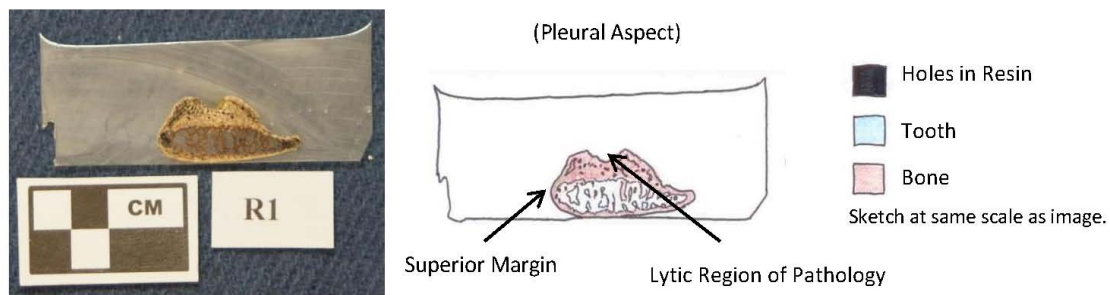
Figure 3.28. Image and sketch of sample R1.
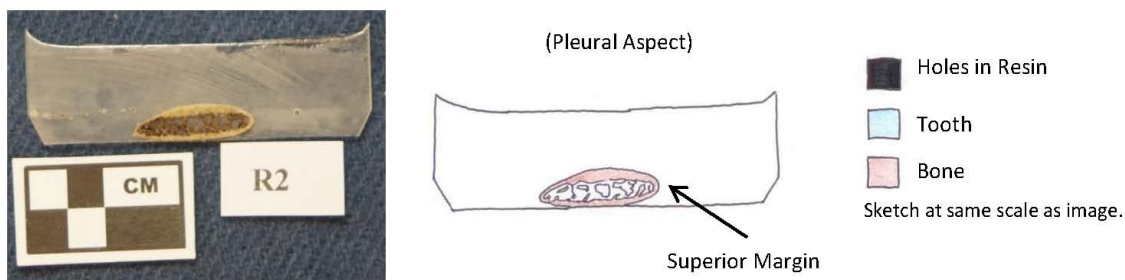
Figure 3.29. Image and sketch of sample R2.

Samples R2 and R3 are from either end of the same rib. This comes from LeVesconte individual #8. This individual is thought to have suffered from Leukemia. Sample R2 is from the healthy costal end of the rib and looks normal in appearance, a ring of thick cortical bone on the outside with trabecular bone in the interior. Sample R3 was taken from the sternal end which displayed small lytic punch-out type lesions. On close examination of this rib (figure 3.30) it can be seen that the outer walls are thinned
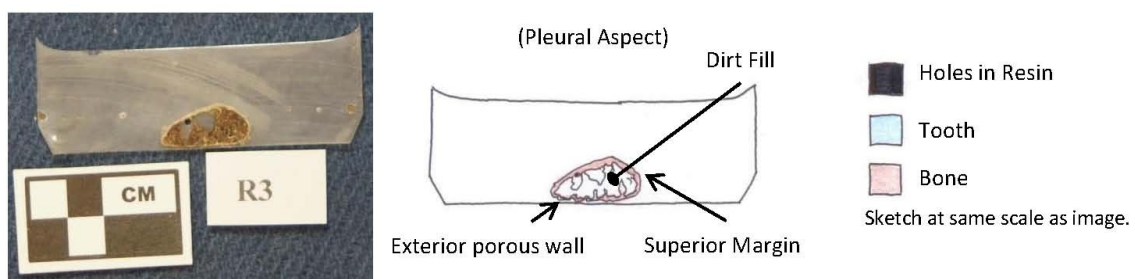
Figure 3.30. Image and sketch of sample R3.

with several areas missing on the exterior surface of the rib (corresponding to the lytic lesions). Also the interior space is almost devoid of trabeculae, the light brown material is actually compacted soil which was not removed in preparation.

The final sample prepared is a rib sample (R4, figure 3.31) from Kellis II burial 280, which as described above had some small sclerotic nodules on the superior border of the costal end of the rib, which may be normal but looked interesting to sample, none the less.
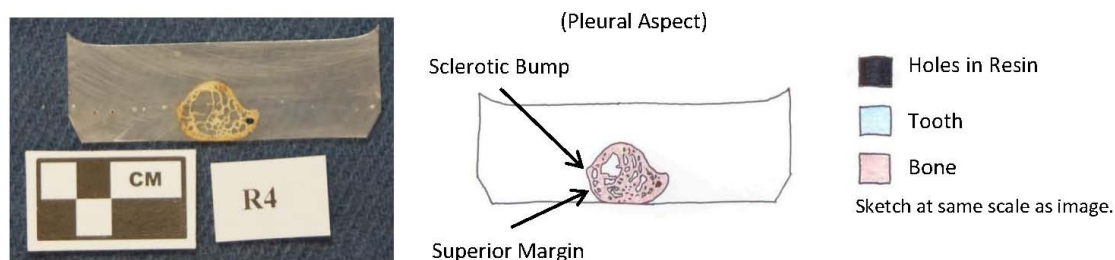
Figure 3.31. Image and sketch of sample R4.

Now I will turn to a description of the elemental analysis technique which was applied to the above samples in order to answer the hypothesis of this thesis, namely, Synchrotron Radiation X-ray Fluorescence Mapping.

CHAPTER 4: SYNCHROTRON EXPERIMENTS

In order to investigate the chosen lesions for elements at a micrometre length scale I have chosen to utilize Synchrotron Radiation X-ray Fluorescence Mapping (SR-XRF). Of the possible techniques which could be utilised for this study (Laser Ablation-Mass Spectrometry, PIXE, SEM, TEM) Synchrotron XRF offers the best spacial resolution and sensitivity at the current time. This situation may of course change in the future as technical advances continue in all fields. Synchrotron also allows the user to access several other experiments such as XANES, XRD or EXAFS without changing the sample preparation or experimental setup significantly.   In the next several sections I will provide a short primer on Synchrotron Radiation and XRF, if you are already familiar with these techniques of analysis feel free to skip to section 4.8 pg. 93. For those interested I would also recommend several excellent books that introduce SR to a general audience (Margaritondo, 1988; Winick, 1994; Willmott, 2011).

4.1: A Brief Synchrotron History

When charged particles (electrons, protons, positrons) travelling at close to the speed of light (termed: relativistic), are bent around a curve they emit electromagnetic radiation tangential to their path (see figure 4.1). This emitted light is termed synchrotron radiation (Margaritondo, 1988; Winick, 1994; Sham, 2002).

Electromagnetic Radiation refers to wave like oscillations of electronic and magnetic fields, better known (from its easily detectable range) as "Light". The electromagnetic spectrum incorporates all energies (colours) of electromagnetic oscillations. The regions that have been found to be useful and detectable, include; radio waves, micro waves, infrared, visible light, ultraviolet, soft X-rays, hard X-rays and gamma rays. These various types of light have wavelengths that range from longer than km's (radio) to smaller than pm's (gamma rays) and energies that range from less than μeV to MeV, respectively (Ohanian, 1985. p. 812).
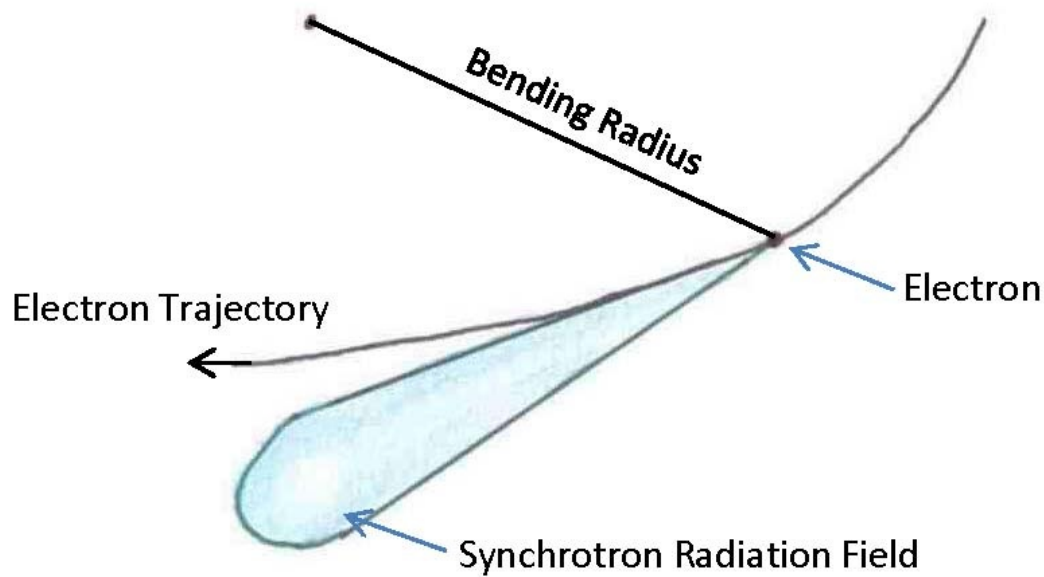
Figure 4.1. Schematic of the radiation field emitted by a relativistic electron.

Note: the Electron Volt (eV) is a unit of energy, commonly used to describe the energy of light **or** of a small particle in motion. It is equivalent to 1.6×10^{-19} J - which is the kinetic energy gained by one electron accelerated over 1 volt, hence the name. This is a very small quantity, obviously. To gain some perspective, visible light occurs in the range of 1.6 - 3.3 eV. X-rays typically have energies of several thousand eV's.

The description of light emitted by a moving particle can be traced back to the classical treatment of Joseph Larmor at the turn of the 20th century (Willmott, 2011). In the 1940's electron accelerators with closed orbits were developed, the synchrotron type being proposed in 1945 (McMillan, 1945; Veksler, 1945). At this point in time the phenomenon of emitted radiation revived in interest because the amount of light emitted by the charged particles in the accelerators limited the ultimate speeds that could be obtained. Theoretical descriptions of the basic properties of the radiation emitted from relativistic charged particles in accelerators appeared about the same time (Iwanenko and Pomeranchuk, 1944).

Synchrotron radiation was first observed in the laboratory by Elder *et al.* (1948) in April 1947 at the General Electric Research Laboratory in Schenectady, NY on their new synchrotron (hence the name). Because it limited the energy obtainable for an accelerated charged particle it was originally considered a nuisance. It was not until 1956 that the potential of this nuisance light as a powerful research tool was realized (Tomboulian and Hartman, 1956). Even so, it was not considered important enough to propose building an accelerator just for creating this radiation.

As a result the first generation of synchrotron sources were added on to existing particle physics accelerators. These parasitic facilities, making use of the throw away radiation of the accelerators were not ideally suited for use by researchers wanting to make use of the X-rays. As the usefulness of this source of X-rays was more fully realized the idea of building an accelerator strictly suited to providing synchrotron radiation was considered. In 1966 the first synchrotron used exclusively as a source of radiation was built at University of Wisconsin-Madison. The success of this early synchrotron source, named Tantalus (Sham, 2002; Willmott, 2011), and its successor at UW-Madison, Aladin, helped spur an international interest in building synchrotron sources. Significant technical improvements to the accelerators and associated equipment lead to new brighter sources of synchrotron light. Termed the second and third generation of sources, these facilities such as the ones used in this thesis (NSLS (2nd generation), APS, ALS, ESRF (3rd generation) and others worldwide) are the current facilities which are the most versatile. The facilities continue hosting a vast number of various experiments for an unprecedented number of research disciplines (Sham, 2002). The never ending quest for more spectral brightness from these sources has led to the proposal of fourth generation sources such as Free Electron Lasers and Energy Recovery Linear Accelerators which may be built in the near future (Winick, 1994; Sham, 2002).

To fully grasp the experiments that follow it is useful to present the fundamental features of a modern synchrotron storage ring.

4.2: The Synchrotron Storage Ring

A typical third generation synchrotron storage ring facility is shown schematically in figure 4.2. The synchrotron facility consists of two main components, the storage ring itself, which produces the light, and the beamlines, which direct, focus, and modify the light so that it is useful for a particular experiment. The storage ring itself keeps charged particles circulating under vacuum in a closed orbit at relativistic speeds and consists of several components (Winick, 1994; Sham, 2002; Willmott, 2011):

1) The injection system, which starts with a source of electrons, accelerates then injects them into the main ring vacuum chamber. Injection systems are small accelerators in their own right and can range from a simple linear accelerator to a small synchrotron.

2) The storage ring vacuum chamber. This is a metal tube through which the electrons circulate under ultrahigh vacuum (10^{-9} torr or less, atmospheric pressure is 760 torr). The vacuum is necessary to prevent the loss of electrons due to scattering off residual gas molecules.

3) The RF (radio frequency) cavity. This is the essential component of a storage ring which separates the accelerator from its physics counterparts. This device supplies a radio wave of appropriate frequency so that as the circulating electrons pass through the cavity they experience an electric field gradient which accelerates the electrons by a small amount. This has the effect of replenishing the energy lost by the electrons as they are bent around the ring giving off synchrotron radiation.

4) Other orbit control magnets, which are responsible for controlling the orbit of the electrons as well as the physical size of the electron beam.

5) The bending magnets (figure 4.3). These are the main magnetic elements responsible for directing the electrons around the closed orbit. They also produce synchrotron radiation which radiates along the tangent to the orbit as the electrons are steered around the corners.

6) Insertion devices. These are periodic arrays of magnets arranged so that the electrons describe a sinusoidal path along the direction of travel (see figure 4.4). These devices produce intense synchrotron radiation which is emitted along the straight section
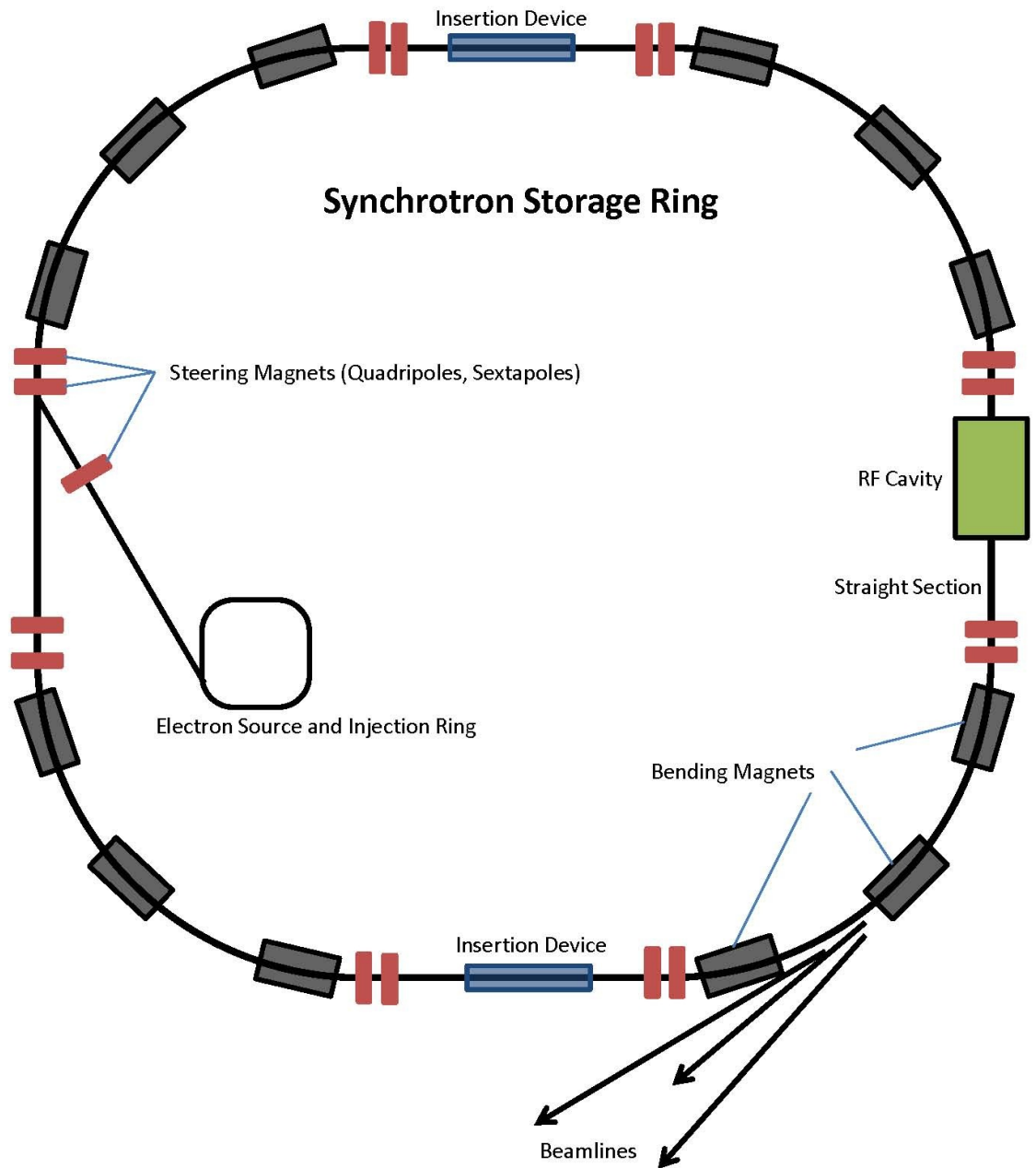
Figure 4.2. Schematic of a typical third generation synchrotron storage ring.

beam path. Because each wiggle produces radiation, the many oscillations along the length of the device add up, producing more radiation. These devices are the main

sources at third generation rings. If the physical size of the electron oscillations can be
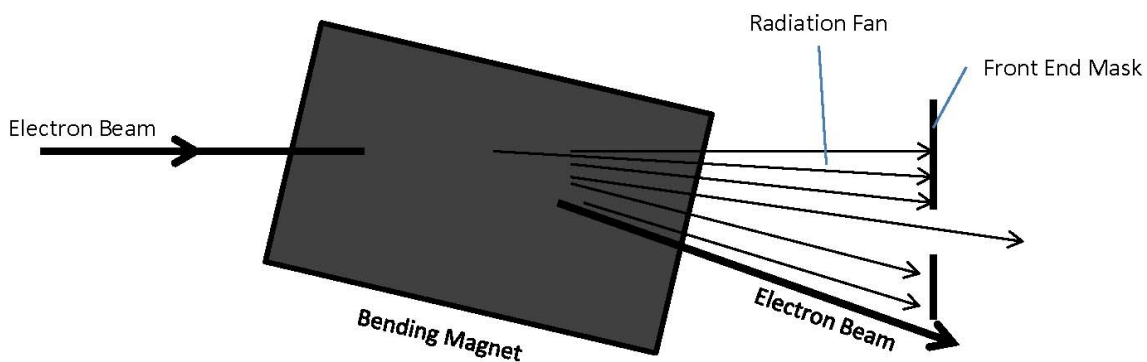
Figure 4.3. Schematic of a typical bending magnet producing synchrotron radiation.

matched to the wavelength of the light required then the light produced can approach laser like wavefront coherence.
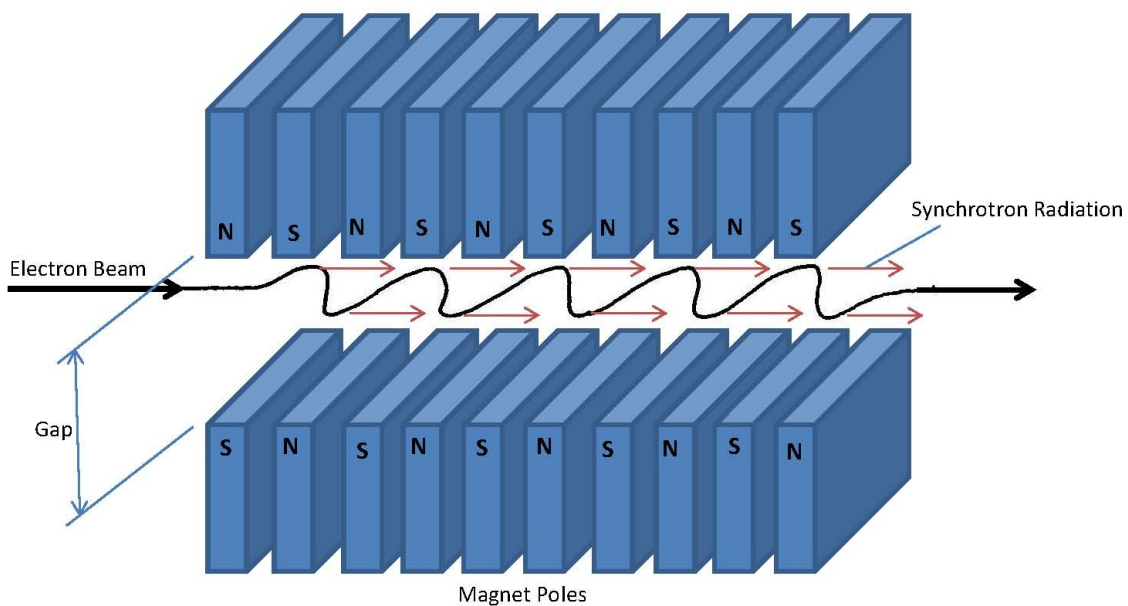
Figure 4.4. Schematic of a typical insertion device.

7) The beam ports, usually termed Front ends. This set of equipment allows the emitted light to travel down the beamlines to the experimental stations, while stopping any harmful radiation that might be produced and protecting the main ring vacuum.

The injection system produces charged particles, typically electrons, and accelerates them to some energy below that of the final operating energy. The electrons are then injected into the main ring. Due to the varying magnetic fields experienced by the electrons in the RF cavity the electrons form bunches which circulate around the closed orbit. Typically a ring current of 200 - 500 mA is injected into the ring. The magnetic fields in the main ring are then increased in the bending magnets to accelerate the electrons to relativistic speeds, energies of typically 1 - 10 GeV. After the operating energy and current have been reached the synchrotron can store the beam of electron bunches for several hours. Most third generation accelerators can operate in top-up mode, meaning that every several minutes a small current of new electrons are injected into the main ring at the operating speed in sync with the existing orbiting electrons. This allows the synchrotron to operate 24-7 with almost no decrease in intensity of the synchrotron light produced.

4.3: Synchrotron Radiation Characteristics: Why?

Obviously, the typical synchrotron facility is large and expensive. Even though over 60 independent experiments can be conducted simultaneously on various beamlines in many facilities, why all the trouble? The short answer is that synchrotrons are the most versatile sources of X-rays and Infrared radiation available today.

This arrises because of the specific characteristics of the emitted radiation. The first important characteristic is the spectral range of the emitted radiation. In conventional sources of X-rays a metal anode is bombarded by a stream of electrons producing X-rays. The radiation produced is emitted at a single energy (for Al - 1486.6 eV, Mg - 1253.6 eV) with only a modest intensity. Experiments using these sources are limited to those requiring the specific energy of the source and to long acquisition times. Synchrotrons produce light from the Infrared up to a maximum which depends on the

energy of the orbiting electrons (Margaritondo, 1988; Winick, 1994; Sham, 2002; Willmott, 2011).
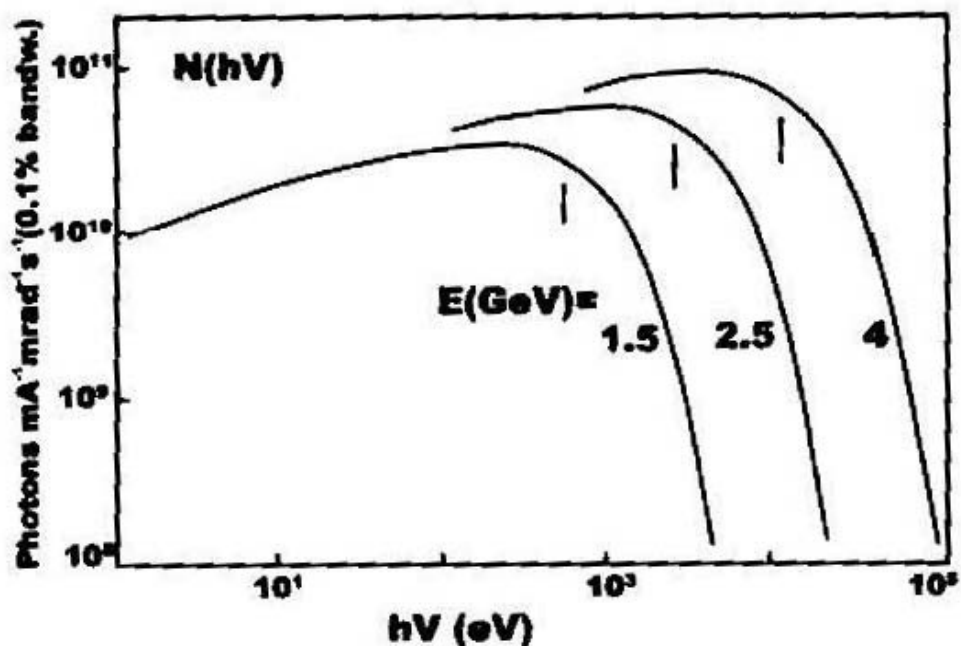
Figure 4.5. Bending magnet radiation from Stanford Synchrotron Radiation Laboratory showing the spectral distribution at electron beam energies of 1.5, 2.5 and 4 Gev.

Thus with appropriate beamline equipment any energy of X-ray, UV or Infrared radiation that is desired can be obtained.

The second characteristic of synchrotrons is their immense brightness. One of the driving forces for continued development of sources has been their brightness (Winick, 1988; Sham, 2002). At this point in time third generation sources are about 12 orders of magnitude brighter than a conventional X-ray tube source (figure 4.6). Why is this important? Each time an experiementer wants to increase the spatial resolution or the spectra resolution of the light they are using, some radiation is lost in the beamline. Thus a modern synchrotron can be focussed to high spacial precision and resolution yet still have enough brightness left to allow for very high experimental sensitivity (in the ppm range) with reasonable count times. A conventional tube source focussed to the same

size and spectral resolution would barely have enough brightness to allow for any useful experimental application.
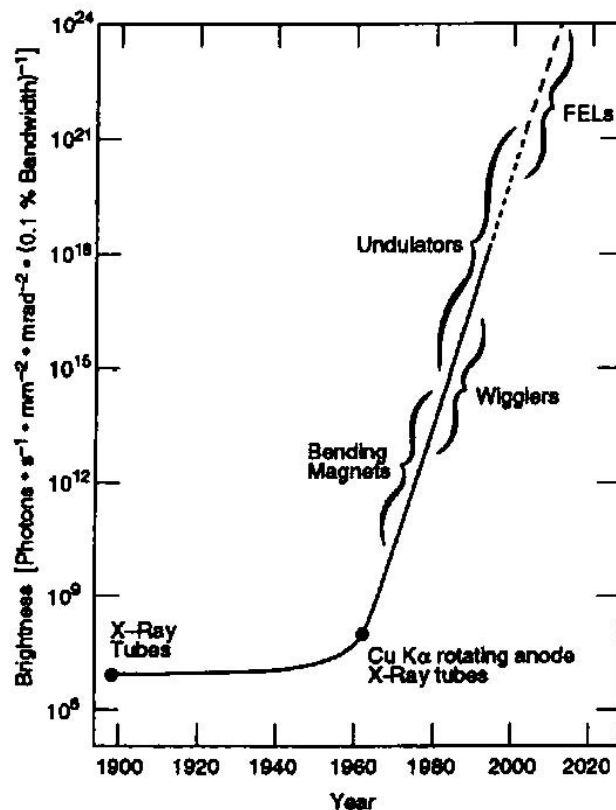
Figure 4.6. The evolution of spectral brightness of X-ray sources through time. (After Winick, 1994).

Other advantages of synchrotron radiation include: 1) the radiation is inherently collimated. This means that the light does not quickly diverge from the source, it is emitted over a small range of angles, producing an intense beam which is more easily focussed. Also, important in this regard is that the source of the X-rays is the beam of circulating electrons which is tightly confined creating a very small original source; 2) the electron beam in the ring in broken into bunches by the action of the RF cavity, this creates an inherent time structure to the emitted light. Synchrotron radiation is like a very fast strobe light, with nano-second pulses. In chemistry this allows the investigation of reactions as they are actually occurring, and 3) synchrotron radiation is inherently

polarized linearly in the plane of the ring. This property has been utilized to measure slight differences of molecular arrangements on surfaces, among other experiments.

4.4: Beamlines

Besides the focussing optics, the most important part of any beamline is the monochromator. This is a device used to select the exact energy of X-ray that the experimenter desires for an experiment. The monochromator limits the capabilities of the beamline to the energy range that it was designed for. There are many types of monochromators in synchrotron radiation work. In the present case a monochromator which functioned in the mid-range of X-ray energies (about 2 - 27 keV) was required in order to allow the excitation of a significant number of elements up to about Br (element 35, requires about 13 keV). Both beamlines used the same type of monochromator, which is the standard type used in much X-ray work.

In the X-ray region of energies, diffraction of the light from the crystal planes of a single crystal solid, is used to separate energies of light. The separation is based on Bragg diffraction [$n\lambda = 2d\sin\Theta$], where λ is the wavelength of light diffracted and Θ is the angle at which the light strikes the crystal surface and d refers to the distance between atomic planes in the crystal. In the most common type of crystal monochromator, two crystals are used in sequence creating better energy (wavelength) resolution (shown schematically in figure 4.7). The crystal chosen needs to have a d-spacing which closely matches the wavelengths one wants to use. Both beamlines used in this work, X-27A of the National Synchrotron Light Source (NSLS) located at Brookhaven National Laboratory in Upton, NY and beamline 20-ID-B of the Advanced Photon Source (APS) located at Argonne National Laboratory in Argonne, Il, utilized double crystal monochromators with Si(111) crystals, which operate best between about 4.3 - 27 keV.

After the wavelength of light has been selected a series of focussing mirrors is used to bring the light into the experimental equipment. In this case these mirrors included a pair of Kirkpatrick-Baez (K-B) mirrors (Willmott, 2011) which are thin mirrors which can be bent cylindrically to focus the light down to micro-metre size spots,

one mirror focuses in the horizontal direction and the other in the vertical direction. This arrangement has the advantage that the focal lengths are independent of the light's energy.

In addition to these basic components each beamline also includes beam position monitors, slits and intensity monitors all of which are controlled by the beamline workstation computers in concert with the monochromators and focussing mirrors.
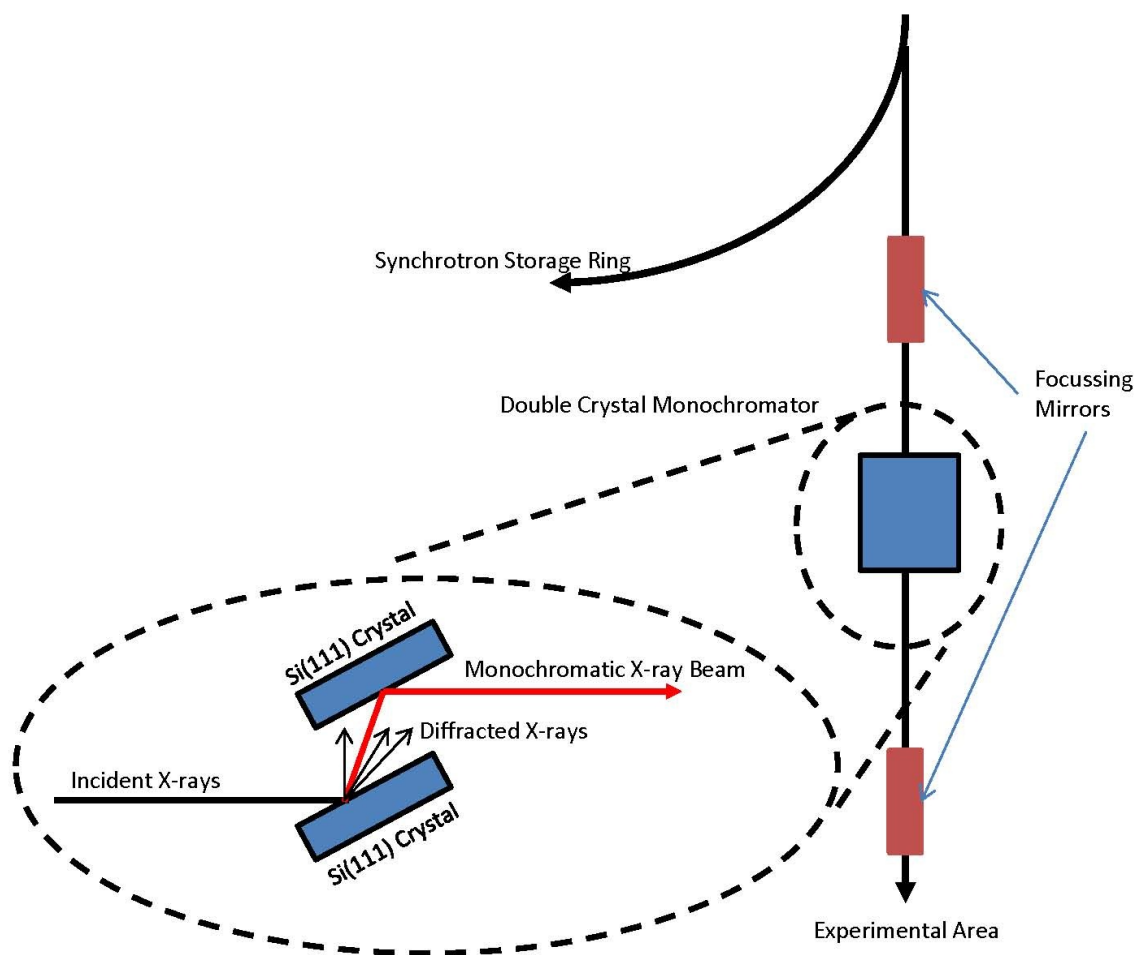
Figure 4.7. Schematic diagram of a Double Crystal Monochromator.

It may seem strange to talk of mirrors for X-rays, as generally we think of X-rays penetrating through materials. This is true, for X-rays to be reflected from a surface the angle of incidence of the light needs to be very small, about 1 - 2°. These grazing

incidence mirrors can be almost a metre long and are all slightly curved to provide some focussing not just reflection. It is also interesting that in a double crystal monochromator the energy selected depends on the angel of incidence of the light onto the crystals, however as the angle changes the position of the monochromatic beam produced moves
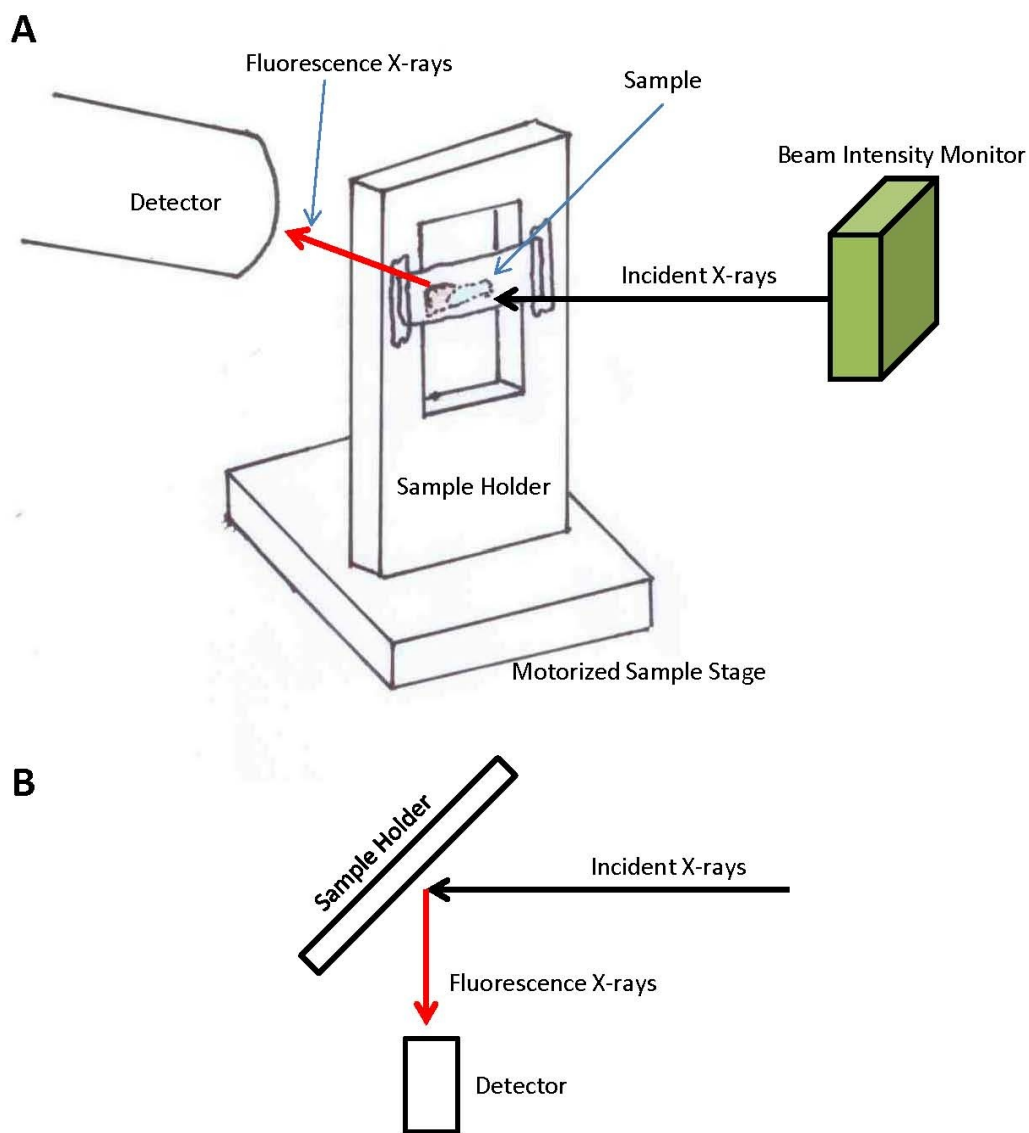
Figure 4.8. Schematic of the experimental set up for XRF. A) general view. B) overhead view showing actual geometry.

(usually vertically) as the angle changes. It is possible to prevent this translation of the beam but it is so technically challenging, that in most cases it is easier to have the whole experimental apparatus mounted on motors so it moves in concert with the beam.

4.5: Experimental Setup

The actual experimental set-up at the end of the beamline is very simple (figure 4.8). It consists of an acrylic sample holder mounted on a set of linear motion stepping motors. These motors allow the attached objects to be moved in steps of less than a micro-metre and computer controlled. The sample is set at a 45 deg. angle to the incident beam and the X-ray detector is placed at 90 deg. to the beam. The sample is simply taped on to the mounting plate with scotch tape, being careful not to cover over the sample. The experiment was run in ambient air and temperature. In order to choose sample regions to scan each beamline was equipped with a microscopic video camera.

The angle of incidence at the sample is chosen specifically as this angle reduces the intensity of the scattered incident X-rays at the detector, however, for this type of micro-mapping application this geometry presents a slight complication. To explain this we need to consider the interaction of the incident X-rays with the sample.

The X-rays are absorbed by the sample but not all at the surface they penetrate into the material gradually losing intensity as they go until the light disappears. How far they penetrate is governed by the density of the material and the energy of the X-rays. In table 4.1, I have calculated the $1/e$ absorption length (how far an X-ray can penetrate before it drops to $1/e$ of its initial intensity) which is a typical measure of the penetration depth of an X-ray.

It is important to realize that the fluorescent X-rays that will be detected are of different energies than the incident X-ray and thus have their own absorption profile in the sample. The distance an X-ray, once generated inside a material, can travel in the material and still be detectable (about the $1/e$ intensity limit) is commonly termed the escape depth. Clearly, each characteristic fluorescent X-ray produced, samples a unique volume of material, this is good to realize and is important if one wants to quantify the

amount of X-rays produced, but otherwise, does not present too much of a problem.

A problem develops because of the geometry of the experiment, a close up schematic of a sample is presented in (figure 4.9). The X-ray penetrates at a 45 deg. angle through the resin block, some distance from the actual sample, but it hits the base of the sample producing fluorescent X-rays. As a result a signal for the element being analysed will be detected. But physically the X-ray is not on the sample yet. This creates

Table 4.1. Penetration and Escape depths of characteristic X-rays in Hydroxyapatite.

Characteristic X-ray	Energy (eV)	Penetration or Escape Depth* (µm)
Incident X-rays at NSLS	13500	157.3
Incident X-rays at APS	16200	264.9
Ca K_α X-rays	3692	13.8
Ti K_α X-rays	4512	7.8
V K_α X-rays	4952	9.9
Cr K_α X-rays	5414	12.5
Mn K_α X-rays	5900	15.8
Fe K_α X-rays	6405	19.7
Ni K_α X-rays	7480	30.0
Cu K_α X-rays	8046	36.7
Zn K_α X-rays	8637	44.7
As K_α X-rays	10543	78.1
Se K_α X-rays	11224	93.1
Br K_α X-rays	11924	110.6
Pb L_β X-rays	12614	129.7
Sr K_α X-rays	14165	180.5

* Calculated using the freeware program Hephaestus © and the data compiled by (Elam *et al.*, 2002) for $Ca_5(PO_4)_3(OH)$ and a density of 3.16 g/cm^3 (crystal hydroxyapatite)

a blurring or skewing of the mapped image for this element but only in the horizontal plane of the experiment (see Martin *et al.*, 2004 for a good example of this effect). This

A) Side view of sample

Incident X-rays

Fluorescence X-rays

Sample Surface

~ 400 μm

Bone
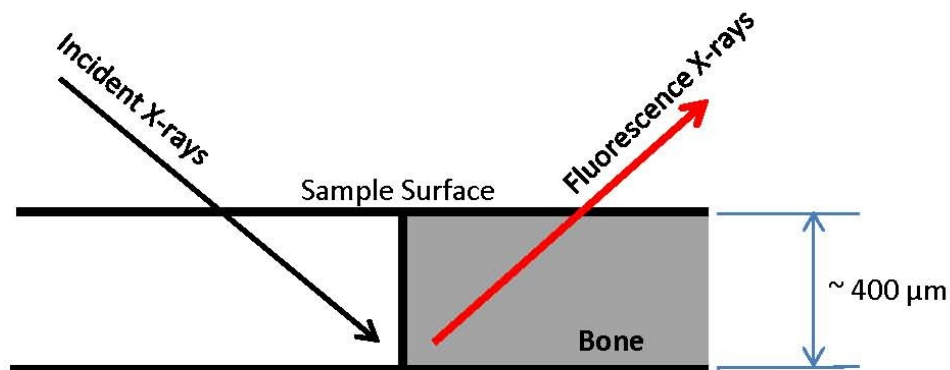
B) Appearance of X-ray Intensity Map

Apparent Sample Edge

Skewed Intensity Gradient

Actual Sample Edge
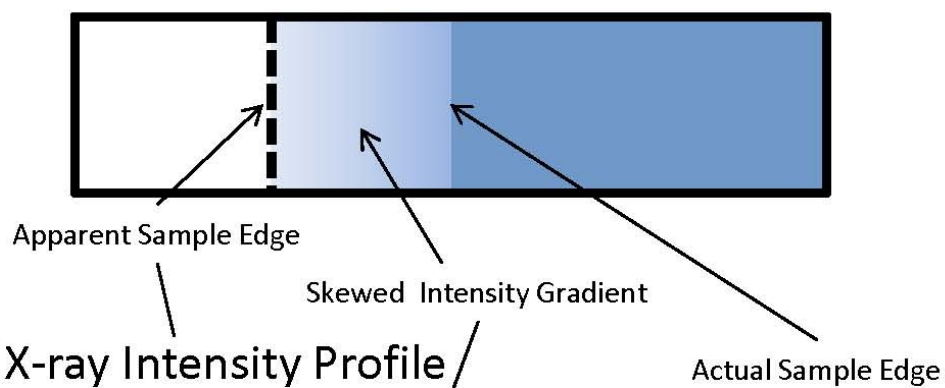
C) X-ray Intensity Profile

Fluorescence Intensity

Horizontal Position
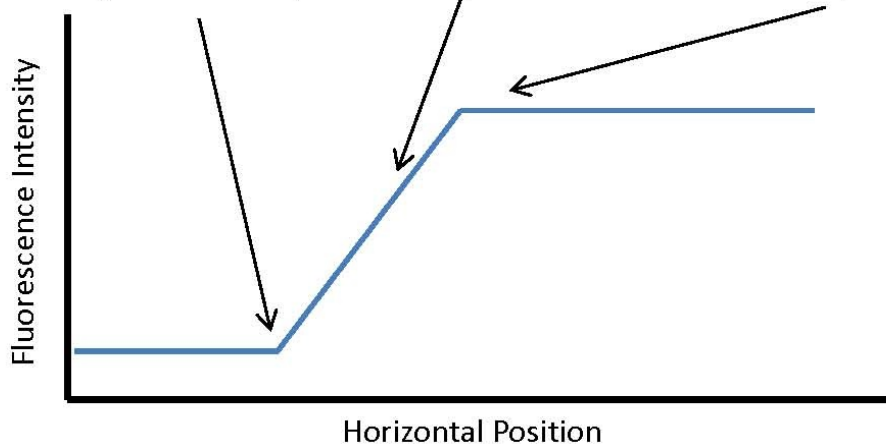
Figure 4.9. Schematic of the effect of detector geometry on the element map in XRF.

needs to be kept in mind when interpreting the images.

      I mention this complication as a recent innovation in micro-fluorescence mapping is to add a focussing optics (usually a micro-capillary) to the front of the detector. This gives the detector its own focus cone shown schematically in figure 4.10 In this situation only fluorescence X-rays from the overlap of the incident beam and focus cone of the detector are recorded. Thus, the sample depth is limited. This is termed confocal XRF and significantly reduces the geometrical blurring of the mapped image (Kanngieβer et al., 2003). This technique was available at the APS beamline.
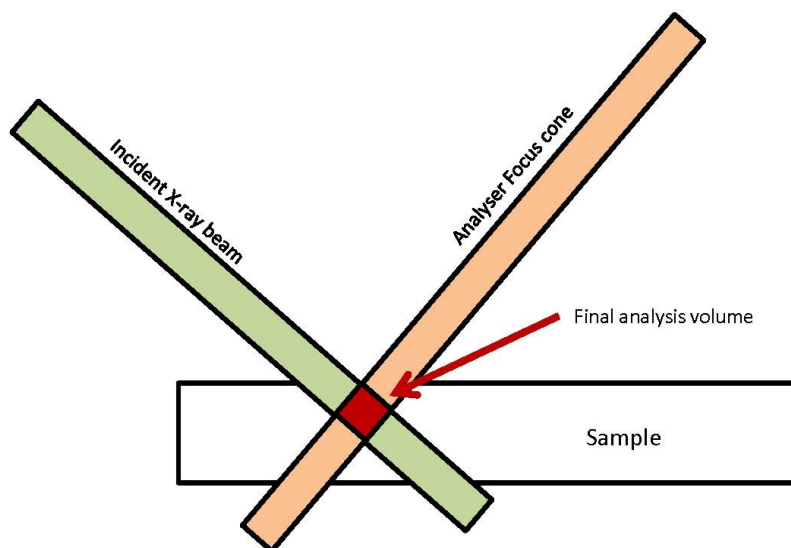
Figure 4.10. Schematic of the principle of confocal XRF.

4.6: X-ray Fluorescence

      When light strikes a substance it can do several things including (but not limited to) reflect (bounce off without changing energy), diffract (bounce off changing energy) or it can be absorbed. When light is absorbed, the wave disappears and the energy must be used to do something to the material. What effect the light has depends on the energy of the light. For example, low energy light, in the Infrared range makes molecules wiggle when absorbed. Light with energies from the visible and up are capable of knocking electrons out of the material. In general this is called the photoelectric effect.

      To see what is happening we need to take a look at where the electrons in a material are in terms of their <u>energy</u>. Here we use a short hand diagram (figure 4.11) where the vertical direction indicates energy and things are not drawn to any scale. The

horizontal lines in figure 4.11 indicate levels of energy where electrons can exist, according to quantum mechanics, the electrons can not exist at energies between levels. Also the levels are grouped together. These groups are called shells and have been labelled K, L, M etc. in increasing energy.

In the diagram (figure 4.11) two atoms are closely spaced together. The electrons with the highest energy around the atoms interact to form bonds between the atoms. These high energy electrons are termed the valence electrons and visible light has enough energy to knock these valence electrons out of the material. The electrons that have lower energy (down in the wells by the atoms) do not interact with each other and hence maintain their atomic 'flavour'. These are termed the core electrons.
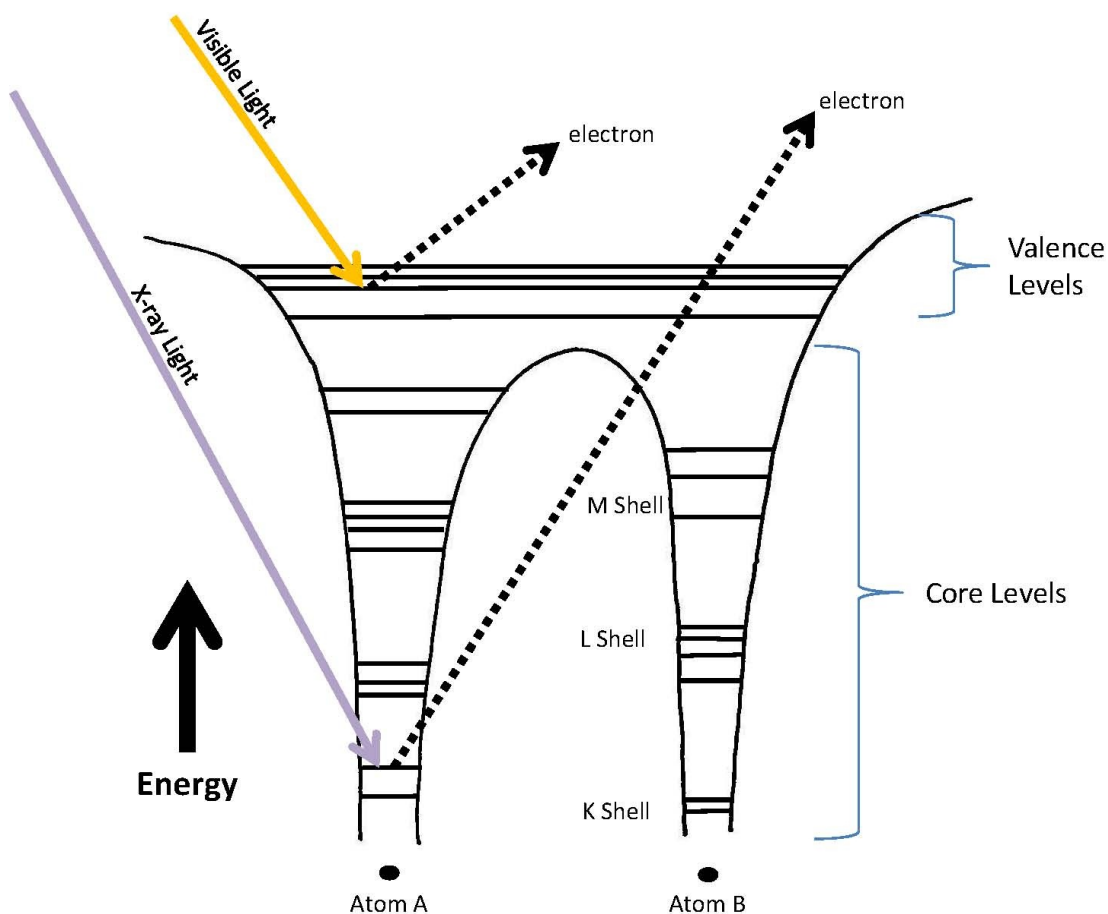
Figure 4.11. Schematic of the electron energy levels of a general diatomic molecule.

X-rays have the energy required to knock a core electron from the material when they are absorbed. For an atom or molecule to be in it's lowest energy state (which is where it will naturally want to be) all of the core energy levels need to be filled with electrons as well as the lowest valence levels. When an X-ray is absorbed a core electron is lost leaving a space, this arrangement represents what is called an excited state and is unstable. At this point the excited state has to be resolved (returned to its lowest energy state) or the molecule may fall apart. There are several ways in which the electrons can rearrange themselves to re-obtain the lowest energy state (termed relaxation).

Fluorescence emission is just one of these processes. In fluorescence an electron from a higher energy level in the atom drops down to take up position in the empty energy level. For this to be possible the electron must give up some of it's energy, which it does by emitting a new wave of light. The energy of this emitted light, termed fluorescence, depends on the difference between the two energy levels.

The energy levels of each atom are unique giving rise to specific X-ray energies which reflect the atom from which the original electron was ejected regardless of its molecular arrangement in the material. Thus the X-ray fluorescence (XRF) spectra (see figure 4.12) provides a fingerprint for determining the elemental composition of any material. The characteristic fluorescence X-rays are named after the energy level of the electron that was ejected in the original excitation process. Hence the name indicated in table 4.1 and figure 4.12 signify fluorescence X-rays produced by filling gaps in the lowest possible core levels in an atom (the K shell).

In XRF mapping a spectra is taken at each point then electronically a background is subtracted and the area of a selected peak is calculated. This area represents the intensity of the emitted fluorescence X-rays at that energy and is matched up with the position of the sample stage, the sample stage is then moved and another spectra is taken, and analysed to create a map (figure 4.12). This process can be done for any number of fluorescence peaks in the spectrum simultaneously.

A) Incident X-ray Ejects a Core Electron

Atom

Incident X-Ray

Allowed energies

E

Ejected core electron

Empty Space for Electron

electrons

E
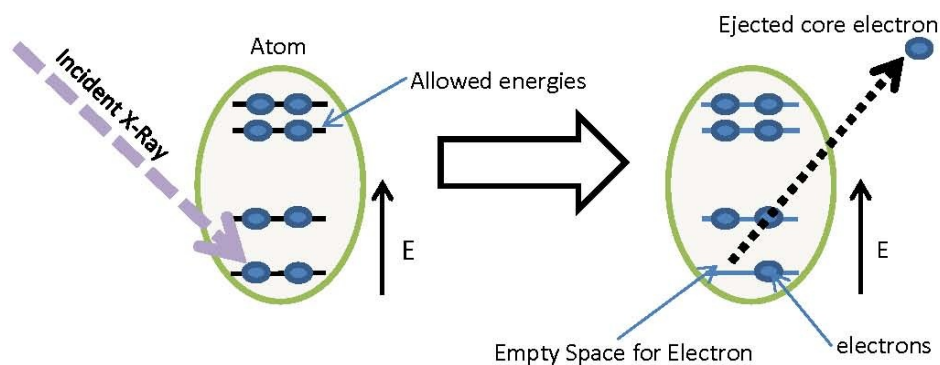
B) Excited Atom Relaxes producing a Fluorescence X-ray

Excited state
Requires continuous
energy input to exist

Emitted X-Ray

Higher Energy electron "relaxes"

Energy is dependent on
atomic energy spacing **thus**
it is characteristic of the
atom excited.

E
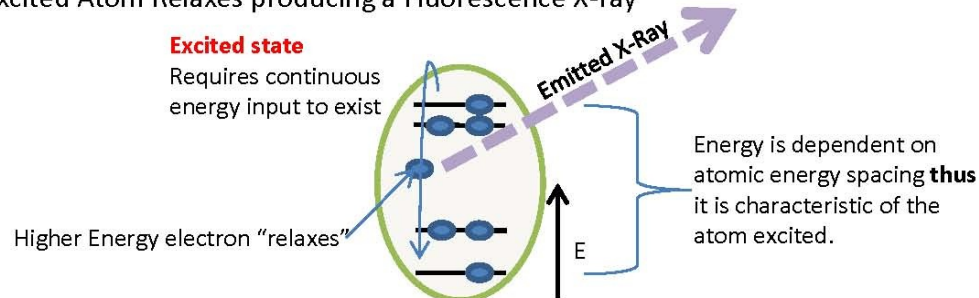
C) Energy Spectrum of Emitted X-rays

**Typical XRF Spectrum.
Four Characteristic
Fluorescence Lines are
Labeled.**

Zn Kα

Mn Kα

Fe Kα

Cu Kα

Counts

Fluorescence Energy (eV)

Background and
Area of Peaks
Calculated for
each Sample
Position
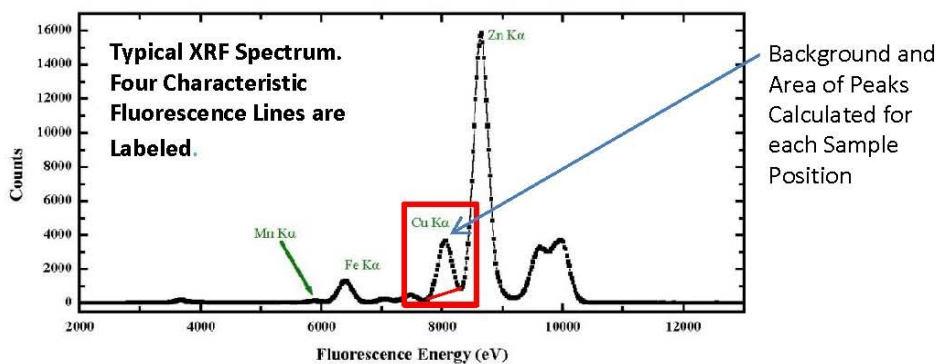
D) Raster Scanning of Sample produces an Element Map

10 x 10 μm Incident X-ray

Sample

Figure 4.12. Pictorial explanation of the acquiring of an XRF elemental map.

4.7: X-ray Detectors

I want to briefly mention how X-rays are detected in these experiments, mainly to highlight the several different detectors that were used in the experiments. The simplest form of X-ray detector is an ionization chamber. In this device a box is filled with a gas, usually Nitrogen or Argon. The box has windows which are transparent of X-rays and contains two electrodes. A high voltage is connected to one electrode and the other is grounded. When an X-rays pass through the gas a small fraction of them are absorbed by gas molecules, producing electrons which are attracted to the electrodes. The flow of electrons at the collector is measured and is proportional to the total amount of X-rays passing through the chamber (figure 4.13A). Such detectors are used to monitor the incident beam intensity (Willmott, 2011).
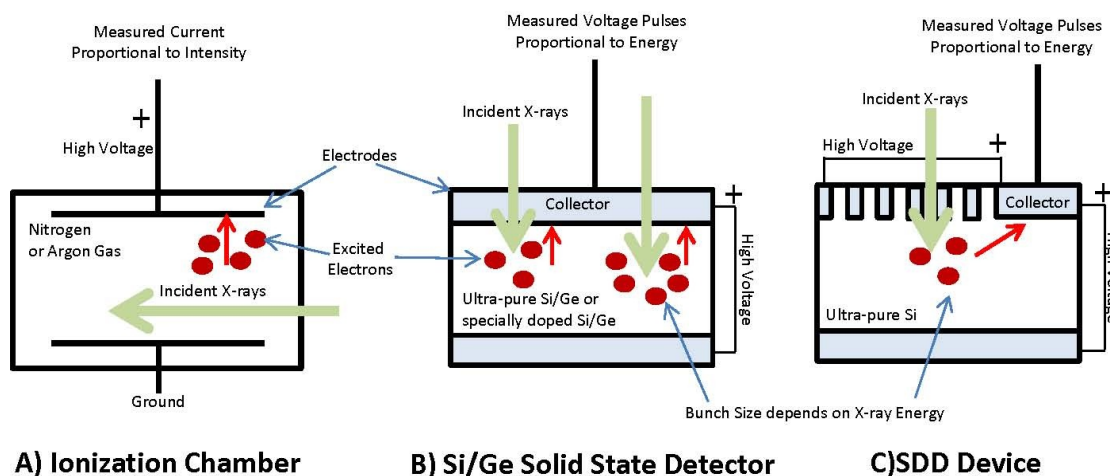
Figure 4.13. Simplified schematics of the operation of three types of X-ray detector.

The next type of detector is used to measure the emitted fluorescence X-rays. In a solid state energy dispersive (EDX) detector the ion chamber is replaced by a piece of high purity (or specially doped) Silicon or Germanium incorporated in a semiconductor chip. The high density Silicon or Germanium is ionized when struck by X-rays but now the number of electrons produced is proportional to the X-ray energy (higher energy light penetrates more deeply and strikes more atoms, thus more electrons). Again the electrons

are attracted to high voltage contacts on either side of the detector (figure 4.13B). At the collector the electron bunches register as voltage pulses of a height indicating the X-ray energy (Willmott, 2011). The number of pulses of a specific height are counted to indicate the amount of X-rays of that energy detected. Typically these detectors count individual absorption events at a rate of 100 000's of counts per second. There are many types of this kind of detector and many of them must be operated at Liquid Nitrogen temperature to reduce the background noise from the collector electrode. This requirement leads to a physically bulky detector, a significant drawback. At NSLS a 13 element Ge detector was used.

At APS another type of improved EDX detector was used. In this type, termed a Silicon Drift Detector (SDD) (figure 4.13C), the principle of operation is identical to the common EDX detector. In this case however a horizontal potential gradient is set up (using a series of patterned electrodes on the silicon chip) which draws the ejected electrons across the detector to a very small collector (Lechner *et al.*, 1996). When the pulses of electrons arrive at the collector they are analysed in the same way. The advantage of this type of detector is that the small collector reduces the noise level enough that cooling to Liquid Nitrogen temperatures is not required, while the area remains large allowing excellent sensitivity. SDD detectors are as a result much smaller allowing for easier set up and the possible incorporation of other devices around the experiment.

4.8: Synchrotron Experimental Conditions

The cross-sectioned bone samples were analysed using Synchrotron radiation induced X-ray fluoresce mapping in two groups. The first was done at beamline X27A in the National Synchrotron Light Source (NSLS) located at Brookhaven National Laboratory. This beamline was equipped with a Si(111) double crystal monochromator and a pair of K-B mirrors which provided a spot size of 7 μm horizontally by 14 μm vertically at the sample surface. An incident beam energy of 13500 eV was chosen. Element maps were taken in 10 μm steps both horizontally and vertically with a count

time of 0.2 sec per point. The fluorescence X-rays were collected using a 13 element Ge detector (Oxford Instruments). Maps of the Ca Kα, Ti Kα, V Kα, Cr Kα, Mn Kα, Fe Kα, Ni Kα, Cu Kα, Zn Kα, As Kα/Pb Lα and Br Kα characteristic fluorescent X-rays were recorded simultaneously. The data were collected and analysed using freely available X27A software package running on the IDL© platform.

The second group of samples were done on beamline 20-ID-B in the Advanced Photon Source (APS) located at Argonne National Laboratory. This beamline was equipped with a Si(111) Double Crystal monochromator and a pair of K-B mirrors which provided a spot size of 5 μm horizontally by 4 μm vertically at the sample surface. An incident energy of 16200 eV was chosen. The same fluorescent X-rays were collected as at NSLS with the addition of The Sr Kα, Se Kα and Pb Lβ lines using a Vortex© SDD detector equipped with a polycapillary focussing optics which restricted the analysis depth to 60 μm. Again the sample was mapped using 10 μm steps, both horizontally and vertically, with a counting time of 0.5 seconds per point. The data were collected and analysed using freely available PNC-CAT software packages.

The As Kα and Pb Lα characteristic fluorescent lines overlap. In order to determine which element is present one can reduce the incident X-ray energy below the energy where Pb core levels can be excited. If the fluorescent line is still present then at least some As must be present. Alternatively, using a high enough incident X-ray energy (>16000 eV), one could look for the As Kβ and Pb Lβ lines which occur at distinct energies.

Under the experimental conditions the typical multi-element map for this study (several mm square) was acquired over 5-8 hours. This allows two or three samples to be run per day of beamtime, depending on the set up time for each sample. If larger areas need to be scanned or other experiments are required to be done such as EXAFS, XANES or XRD then less samples can be run in a day.

There is one possible drawback to using Synchrotron XRF, that any experimenter should be made aware of. That is beam damage. The brightness of the incident beam is such that a significant heat load is applied to the sample and burning can occur. In the

present case the residence time of the beam at any one spot on the sample was short enough that no damage was seen to occur.

CHAPTER 5: RESULTS AND DISCUSSION

5.1: General XRF Spectra

I want to start looking at the data by first reviewing the X-ray Fluorescence Spectra which make up the elemental maps. Two typical XRF spectra, from the equipment at NSLS, are shown in figure 5.1. These are taken from a random spot on the bone in sample DA6 and from a spot just on the embedding resin. In figure 5.1 A the spectra are shown with a linear scale while a logarithmic scale was chosen for the same spectra in figure 5.1 B. The log scale accentuates the small peaks and is typically used in looking at XRF spectra.

The first thing to note is that even in the resin, which it is hoped, has very little or no elements besides C, N and O there are two large sets of peaks at about 13000 eV and 3700 eV. These are not element peaks but represent: 1) the scattered incident X-rays which make it to the detector at 13500 eV with a tail of lower energy X-rays which lost some energy to the sample before reaching the detector and 2) a significant portion of scattered X-rays which have lost 9800 eV in causing an electronic transition in the Ge which makes up the detector (termed the Ge loss peak) followed by its own lower energy tail.

Both of these peaks are present in every spectra and can obscure characteristic element peaks, so care must be taken to set the incident energy so that the Ge loss peak does not significantly influence the Ca emission lines while allowing as many elements as possible to be detected. Hence the choice of 13500 eV which allows the examination of the elements in the fourth row of the periodic table between Ca and Br. Below the Ca lines the spectra is obscured by the emission lines and scattering from the components of air (N_2, O_2, He, Ar) because the experiments are done under ambient conditions.

The next observation to note is that in figure 5.1 B the resin spectrum is not completely flat, there are a few very small peaks, these could be from several sources: impurities in the resin, scatter from beamline components intersecting the beam, or
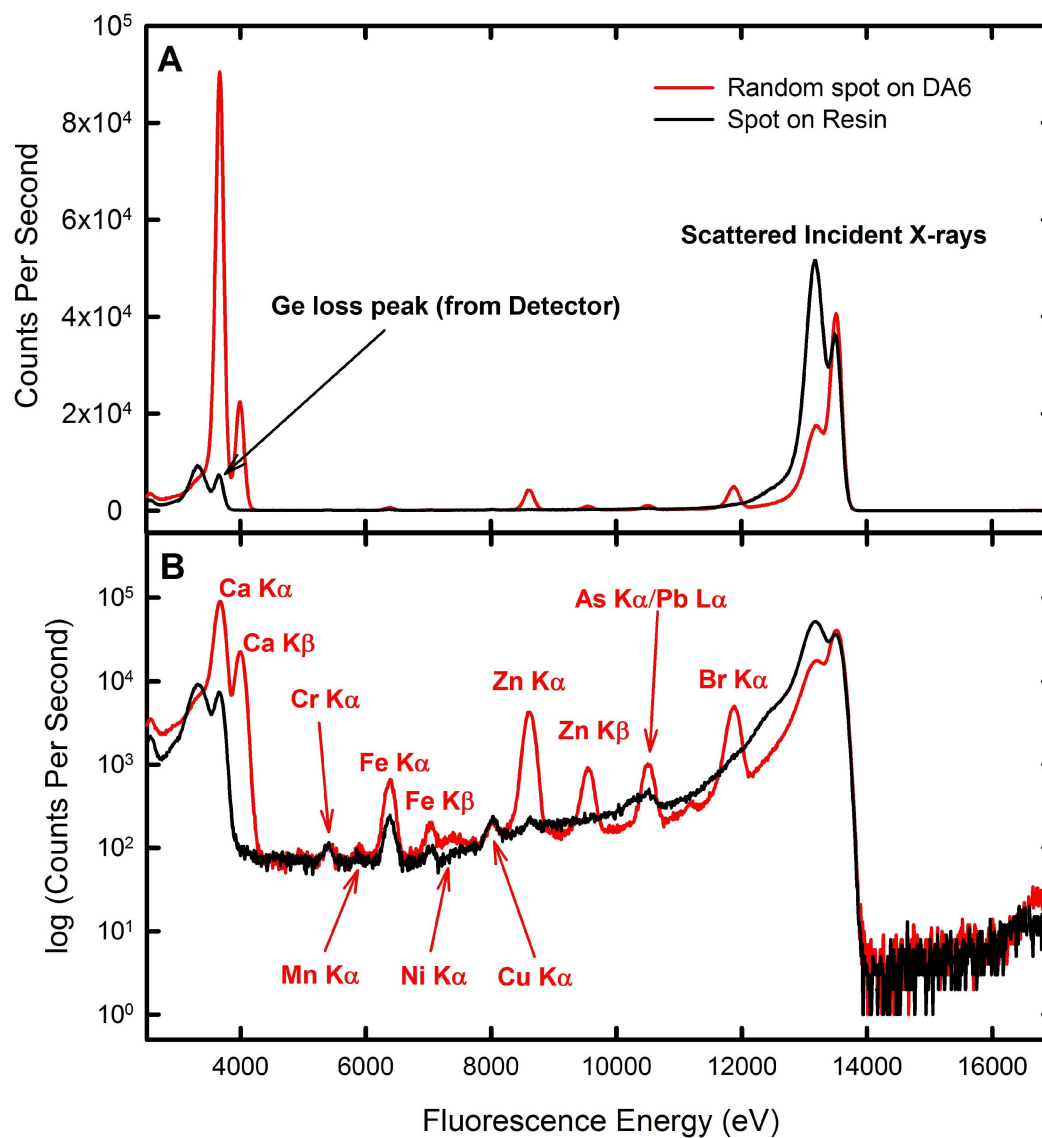
Figure 5.1. Representative XRF Spectra from NSLS shown on a A) linear scale and B) log scale.

contamination from the cutting and polishing process. Of course these peaks are very small and barely above the background of the spectrum so whatever their origin they can mostly be ignored provided the element lines are sufficiently intense. This should be kept in mind especially for the trace elements like Ni, Cu, Cr and Mn which seem to have similar intensities, at least at this point on the sample DA6.

Third, the characteristic fluorescence emission lines have been labelled. One
should note that the lines come in pairs (ie. Ca Kα and Ca Kβ) the higher energy emission
being less intense. In the case of weak emissions the β line is often not observed. Also,
as I mentioned earlier some lines overlap. The most important for this work is the As Kα,
which overlaps with the Pb Lα line. At NSLS lowering the incident X-ray energy to
about 13000 eV causes the As line to decrease in intensity but not disappear. This
indicates that the emission seen is caused by both As and Pb being present in the sample.
This is true of every sample run at NSLS regardless of site of origin or disease state. At
APS the As Kβ and Pb Lβ lines, which do not overlap, could both be seen in every
spectra.
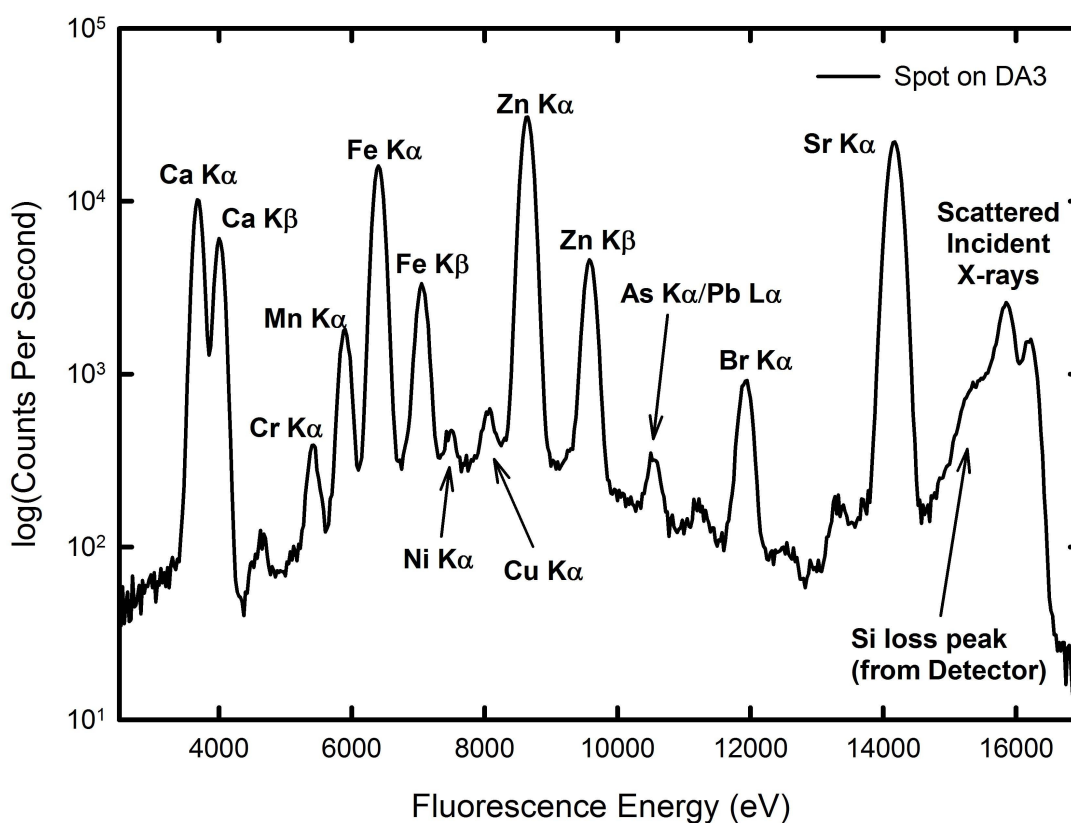
Figure 5.2. Representative XRF spectrum from APS.

Thus the first clear observation to make is that; all the samples examined

contained clear Ca, Zn, Fe, As, Pb and Br emission lines with much smaller lines arising from Cr, Mn, Ni and Cu. The same conclusion can be made from an examination of an XRF spectrum from APS (Figure 5.2) with the addition of a strong Sr emission line which can be seen because the incident energy at APS was 16200 eV.

Three quick points about the XRF from APS. 1) Because of the focusing optics used on the detector the scattered peak and background are greatly reduced. 2) In this case the detector chip was made from Si not Ge, the Si loss peak appears under the scattered peak (only separated by 1700 eV). 3) The APS synchrotron has greater X-ray flux and this along with a more sensitive detector helps resolve the weaker element emissions.

5.2: Introduction to the Elemental Maps (DA1 analysis)

Now, to turn our attention to the elemental maps. Firstly, I will lay out a detailed analysis of the first sample DA1, before I turn to comparisons between samples.
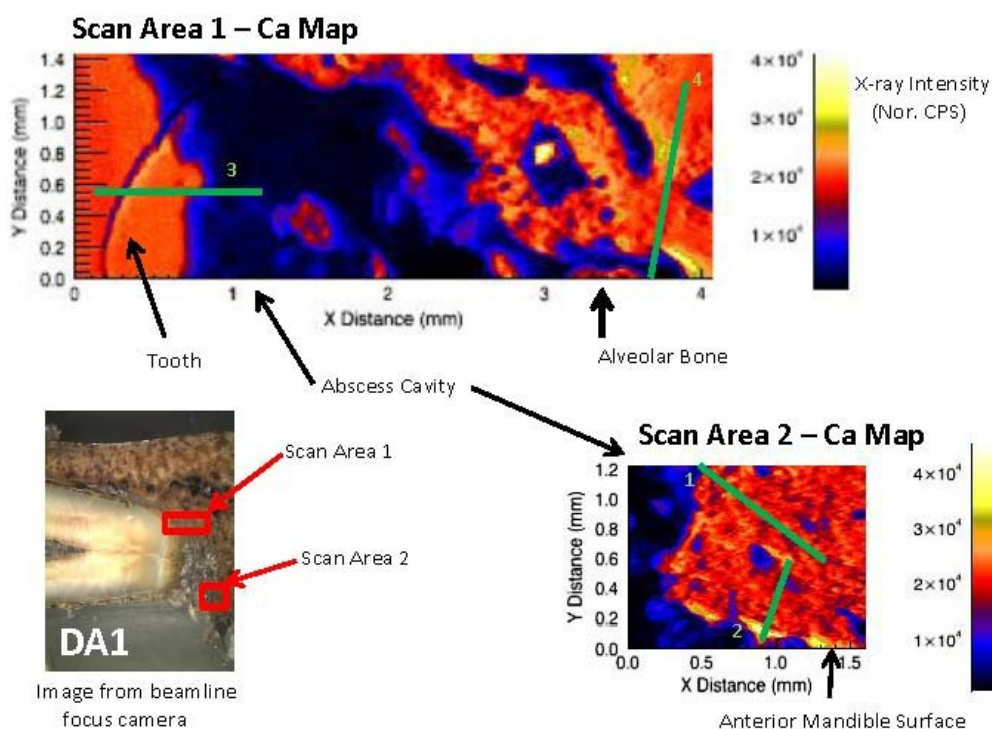
Figure 5.3. Ca Maps from two areas bordering the abscess cavity in sample DA1. (The numbered lines indicate the position of the extracted line profiles shown in figures 5.6 and 5.7)
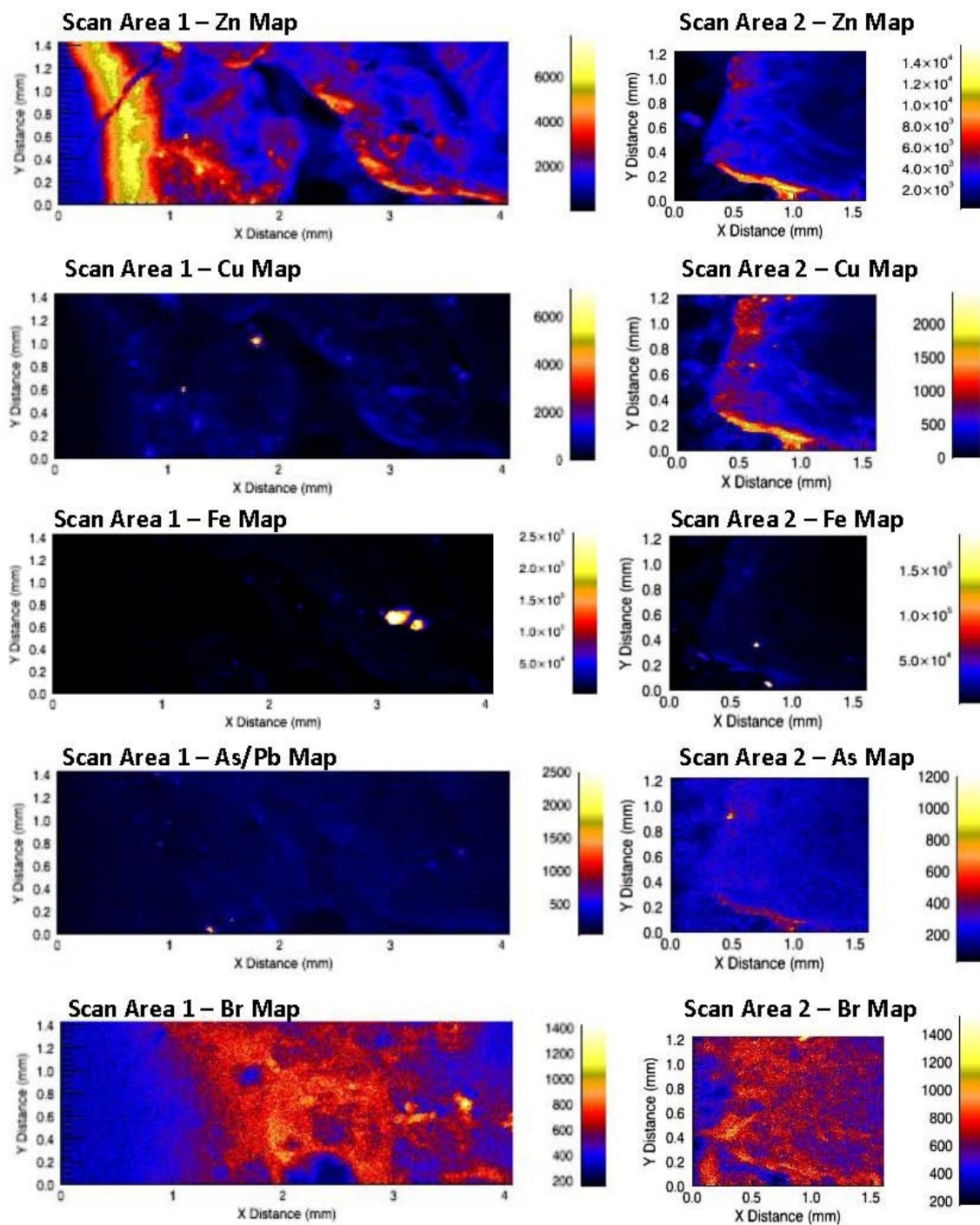
Figure 5.4. Zn, Cu, Fe, As/Pb and Br XRF intensity maps from sample DA1.
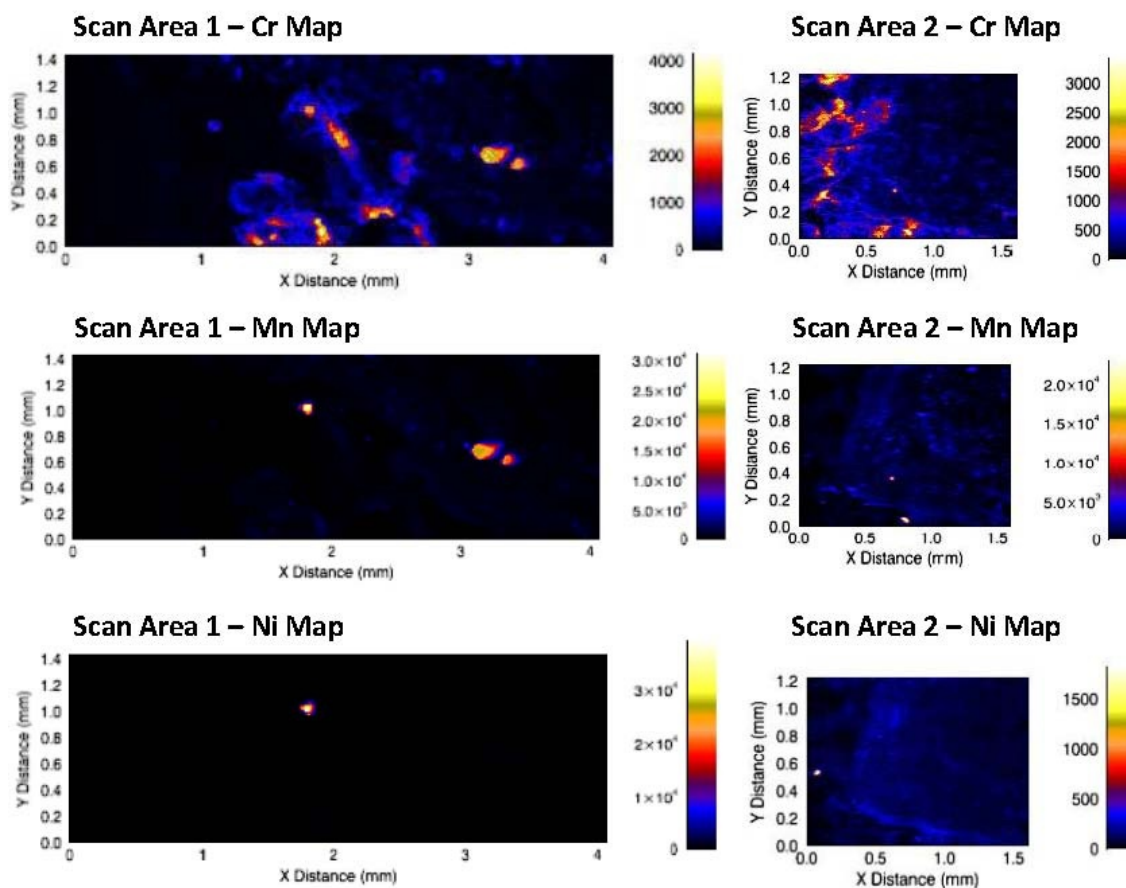
Figure 5.5. Cr, Mn and Ni XRF intensity maps from sample DA1.

The preceding three figures (Fig. 5.3 - Fig. 5.5) present the nine collected element maps for two regions from the first dental abscess sample. The data are bewildering, to say the least. First some technical points, as indicated in figure 5.3, the colour scale bars represent the XRF intensity in units of Normalized Counts Per Second (CPS). For simplicity of the figures I have not included the label or units for the colour bars in any subsequent figures. Normalized, in this instance, indicates that for each element the CPS recorded has been adjusted to a common incident X-ray intensity for all of the maps run at NSLS. This is not a calibration procedure, it simply accounts for any variation of signal arising from variation in the incident beam intensity, it is a necessary first step in

any spectroscopy experiment. The conversion of the XRF intensities in CPS to absolute concentration units, such as ppm, is not a simple calculation and I have not undertaken to convert the intensity values at this point. Such conversion requires knowledge of: sample density, sample thickness, distance between sample and detector, self-absorption, and fluorescence cross-sections to name some of the factors. These factors should not, however, be confused with 'Matrix effects' talked about in mass-spectroscopy, the fluorescence is not affected by the chemical composition of the sample it is an atomic spectroscopy. Note, X-ray intensity values allow comparison of the relative intensity of Fe in one image to Fe in another, for instance, **but** Fe can not be compared to Ni or any other element. The conversion from intensity to ppm is unique for each element. I should also note that the false colour scales for intensity are non-linear and enhance the lower values in a similar fashion to the log scale for an XRF spectrum.

Qualitatively, the Ca maps (figure 5.3) indicate the regions of tooth and bone surrounding the abscess lesion. At the right of area 1 is the tip of the tooth root, which has a crack running vertically through it. This crack is likely due to postmortem drying of the tooth. To the left of the image of area 1 are the trabeculae of the alveolar bone. The trabeculae are estimated at about 380 - 440 μm across. Note the yellow colour variation at the edge of some of the trabeculae which indicates a local increase in Ca density only about 50 μm wide.

A similar Ca increase is seen along the lower edge of the bone in area 2. This represents the anterior face of the mandible just below the abscess cloaca. Also in area 2 the bone has a less 'wormy' appearance, being generally even, with small round to oval openings, about 140 μm in diamater. This is the typical appearance of compact bone structure. The blue coloured edges appearing around the bone arise from two effects, 1) the blurring caused by the geometry of the experiment and the escape depth of the Ca X-rays and 2) the fact that the sample is three dimensional and the edges of the bone and tooth are not necessarily perpendicular to the surface of the cross-section being examined.

The shape of the bone and tooth edges through the depth of the sample is quite clear in the Zn map of area 1 (figure 5.4). Here the abscess gap seen in the Ca map

appears filled in. Remember that the Zn X-ray escape depth is 45 μm compared to only 14 μm for the Ca X-rays (table 4.1, pg 85). Thus the Zn image is picking up the sloping sides of the tooth and abscess cavity which is beyond the view of the Ca image.

On the left side of the Zn map of area 1 is the tooth root apex. The intense ½ mm wide band of increased Zn intensity indicates the cementum of the tooth (Martin *et al.*, 2004; 2007; 2010) as seen in our pervious work. The very left edge of the image is the dentine of the tooth. On the right side of the area 1 Zn image are again the trabecula of the bone: note the similar narrow bands of increased Zn intensity along the edges of some of the trabeculae. The Zn map of area 2 also has a narrow (~ 60 μm) band of increased Zn along the anterior mandible edge, corresponding to the area of increased Ca intensity. There is also some increased Zn intensity immediately adjacent to the abscess cavity at the top of the map in area 2. Also note, however, that the bone area which is blue in colour along the edges changes to black in the upper right of the map of area 2. This indicates a decrease of Zn concentration from the outer edge of the bone (both the abscess cavity and the anterior mandible surface) towards the middle of the bone. This band of increased Zn intensity is about 500 to 600 μm wide.

The wide band of increased Zn intensity which occurs around the outside of the bone in area 2, is reproduced in the Cu, Fe and Ni (and possibly a narrower band in Cr) maps in this sample. The band on the outside of the bone both inside the lesion and at the mandible surface may be indicative of the leaching of elements into the bone from the soil matrix (diagenesis). This is the type of band expected in the case of diffusion based leaching of elements into bone from an exposed surface. The DA1 sample is from the Varden site which was inundated with water for many years, an ideal situation for ion exchange diagnesis. Note, however that in area 1, the same obvious increase at the edge of the bone is not evident. This is puzzling, the bone in area 1 is trabecular bone, thus we could ask if the type of bone has an effect on diagenesis, or is the absence of a wide increased Zn band an experimental artifact (see later) relating to the thin tube nature of the bone material.

Regardless, the very intense narrow regions of increased Zn are not likely

diagenetic in origin. This is inferred from the fact that these regions do not occur all the way around the exposed bone surface. Such a regionalised and intense increase over and above the already existing Zn increase around the edge can not be explained by any diagenetic process which should affect all exposed bone in a similar fashion. Of course, I just noted above that the trabecular bone seems to behave differently. A different behaviour for unique bone types is, however, biogenic in origin. Thus, the intense narrow bands of Zn are suspected to be of biogenic origin, while the wider band of Zn, Fe and Cu increase are of possible diagenetic origin.

Looking at the Cu map of area 2 (figure 5.4) a similar wide band of Cu is seen decreasing towards the upper right or interior of the bone. Again Cu shows an additional increase in a narrow band at the anterior surface of the bone with a slightly wider increase along the edge of the abscess cavity. The area 1 map for Cu indicates a similar distribution as seen in Zn with the exception of the cementum of the tooth. This is difficult to see in the image as an intense Cu spike in the centre top of the map, only about 10 - 15 μm in diameter, has shifted the colour scale mostly into the blue range. This spot is likely a small particle inclusion of soil or polishing debris and more of these inclusions are visible in other maps.

The Fe map of area 1 (figure 5.4) is dominated by two similar inclusions which are clearly composed of mainly Fe, Cr and Mn (see figure 5.5). Even so the Fe distribution in area 2 also displays a decreasing concentration from the edges towards the upper right of the map, or towards the interior of the bone. The Fe map lacks a narrow increased band at the edges of the bone. The Fe concentration change can be more easily seen taking a line slice through the maps. These are shown in figure 5.6 and 5.7, and the locations of the line sections are indicated by the green lines in figure 5.3.

For completeness, the map of the As/Pb line is shown in Figure 5.4. There is a slight increase in the intensity along the mandible edge in area 2 along with an obvious inclusion spot. However, there is nothing in the distribution, which is mostly even throughout the bone, that can help elucidate a clear disposition between As and Pb or that might indicate a specific origin of either element. Thus, without being able to separate

the contributions from As and Pb we must conclude that in general they are both present in the sample. This statement is true for all the samples studied regardless of site origin. All As/Pb maps show a general evenly distributed signal of about the same intensity as the one in DA1. As a result I will not try to analyse this data further until follow up experiments can be done to specifically look at the separate distributions of As and Pb in the bone.

Of course the presence of As and Pb in all the samples is in itself an intriguing situation. Reviews of elements (Emsley, 2001) suggest that very small amounts of both these elements are present in the average diet and find their way into the bone at low concentrations (0.1 - 1.6 ppm for As, 3 - 30 ppm for Pb). Without separating the contributions of the two elements and calculating their absolute concentrations I cannot compare the current results with any expected concentrations of As and Pb form the literature. One thing is clear though, with all the maps having approximately the same intensity, no one site or sample sticks out as being unique.

The Br images (in figure 5.4) show that Br is more concentrated in the bone than in dental tissues, as seen before (Martin *et al.*, 2013). The distribution within the bone is generally even throughout with no obvious intense regions. This is true for all the Br maps seen and thus, in the case of Br the average intensity of the XRF within the bone is the most important factor to examine.

Cr, Mn, and Ni are very weak peaks in the XRF spectra in all the samples. Typically they reach significant levels only in inclusions within the bone. A good example is the Cr map in figure 5.5. The distribution of the intense Cr nodules occurs outside the bone or within gaps in the bone structure. The Cr images are often a good indication of the distribution of the various particle inclusions within the samples. A comparison of the inclusion particles seen in the maps for DA1, illustrates the inherent variability of the elemental composition of the included particles, whether soil or of other origin.

The low concentrations of Cr, Mn and Ni within the bone in DA1 and all the other samples, leads me to exclude these elements from further analysis. Trying to interpret

element distributions and origins based on very weak signals would be problematic. In order to err on the side of caution I will not speculate about these elements or As/Pb without further follow up experiments specifically directed at those particular elements.

In the above I suggested that looking at line sections from the images is perhaps more useful. In figure 5.6 below, such line sections are shown for the three most intense lines observed, namely Ca, Fe and Zn. The bone edges are marked, and the vertical blue lines indicate approximate boundaries of regions that can be identified within the bone interior, namely, lesion edge bone, deep bone (term chosen to represent the typical unaffected bone well away from any elemental changes occurring around the edges), peak
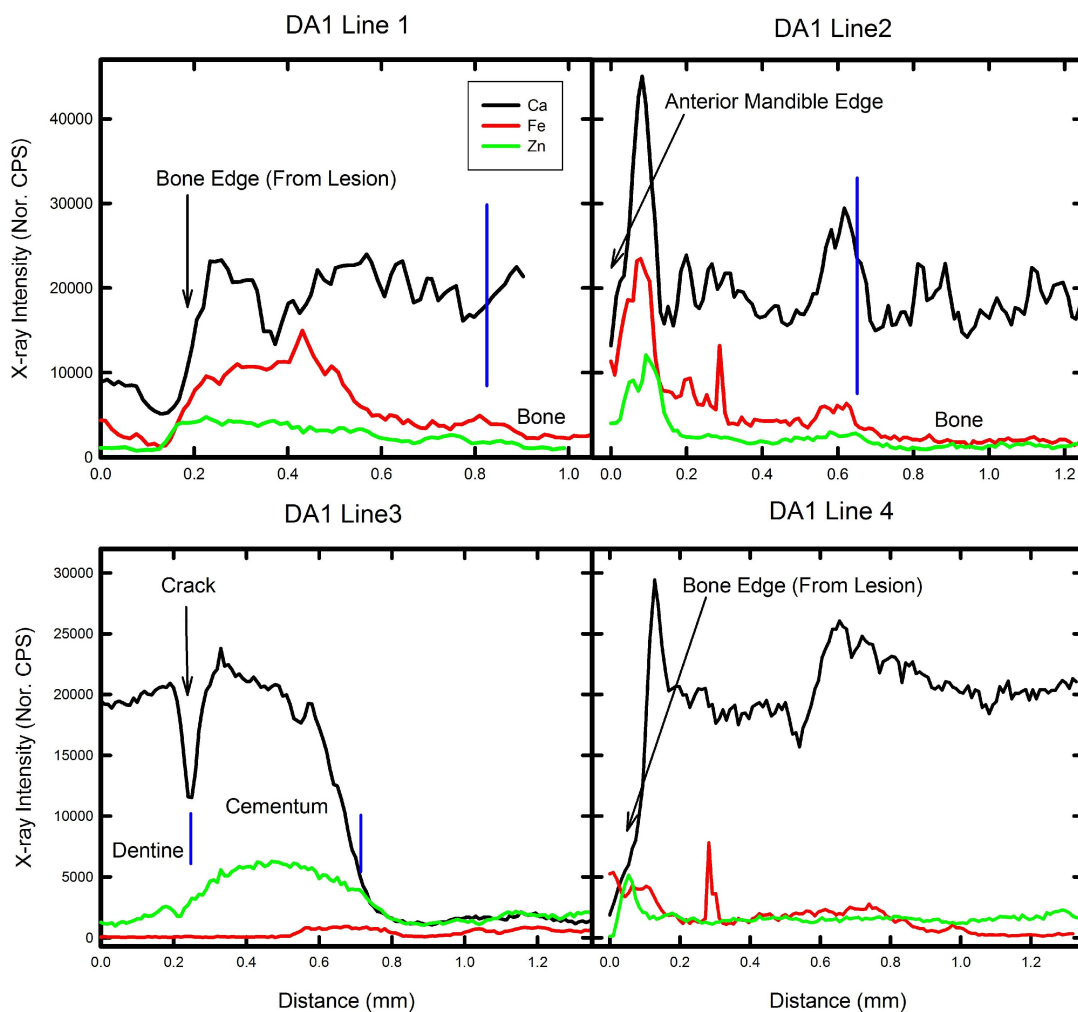
Figure 5.6. Line sections for Ca, Fe and Zn taken along the four lines shown in figure 5.3.

values and the cementum and dentine. The intense Zn, Ca and Fe areas at the edges of
the bone can be clearly identified as can the more modest increase of Fe and Zn around
the edge of the bone samples.

In order to summarise the data further, I have calculated an average XRF intensity
for each element in each identified region of bone or tooth. These averages were
calculated by averaging the individual data points along each of the line sections within
an identified region of bone. As an example to calculate the average Zn intensity within
the cementum I extracted the part of the line section along line 3 between the two blue
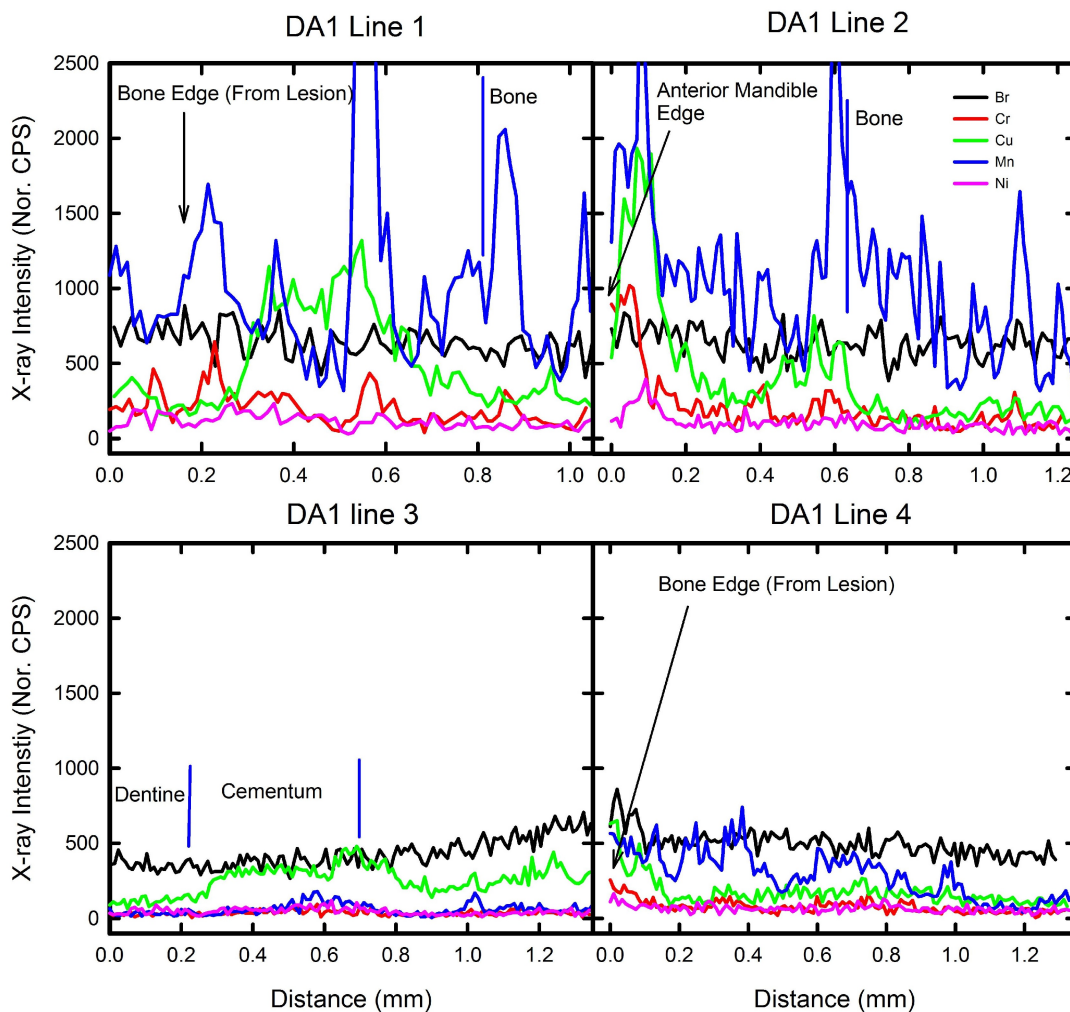
Figure 5.7. Line sections for Br, Cr, Cu, Mn and Ni taken along the four lines shown in figure 5.3.

lines. The data points were then averaged. Such averages can be used as a crude indication of the relative concentrations of elements in the identified bone regions. These values are seen in table 5.1, along with the standard deviation for the values averaged, for sample DA1.

A couple of things to note about the calculated XRF intensity values shown below. First, the standard deviations of the sampled points are often quite large. There are many holes (lacuna, Haversian canals, cracks) in the bone structure. Thus the values reflect the heterogeneity and density variation of the material. Second, in a couple of instances the standard deviation is comparable to the average value (Fe in cementum, for instance). A large standard deviation renders the value meaningless for comparison purposes, and in this instance reflects a poor choice of area to average, one that does not reflect the obvious elemental patterning.

Table 5.1. Average XRF Intensity data in Normalized CPS (σ) for sample DA1.

Element	Dentine	Cementum	Deep Bone	Lesion Edge	Width (mm)	Peak*	Width (mm)
Ca	19811 (620)	18030 (4339)	18068 (2254)	19805 (3055)	0.6	45050	0.15
						29430	0.1
Zn	1651 (492)	5186 (885)	1309 (211)	2787 (859)	0.6	12092	0.15
						5130	0.15
Fe	65 (18)	346 (345)	2027 (301)	6755 (3053)	0.6	23482	0.15
						5355	0.15
Br	352 (40)	371 (52)	621 (90)	638 (95)	- -	- -	- -
Cr	27 (8)	44 (18)	115 (50)	201 (103)	- -	1030	0.1
Cu	113 (22)	315 (72)	174 (52)	559 (290)	0.6	1934	0.15
Mn	33 (14)	77 (44)	833 (362)	1087 (783)	0.6	3251	0.15
Ni	46 (20)	61 (22)	73 (29)	113 (42)	- -	394	0.15

* Single highest value from line 2 and line 4.

Nevertheless, these XRF intensity values illustrate the conclusions reached so far; there is an increased rim of Zn, Fe, Cu and possibly Mn around the edges of the bone, and there

are also <u>separated overlapping localised areas of significantly increased element concentrations, including Zn and Ca localizations</u>.

5.3: Analysis of Zn Distributions

Diseased Samples
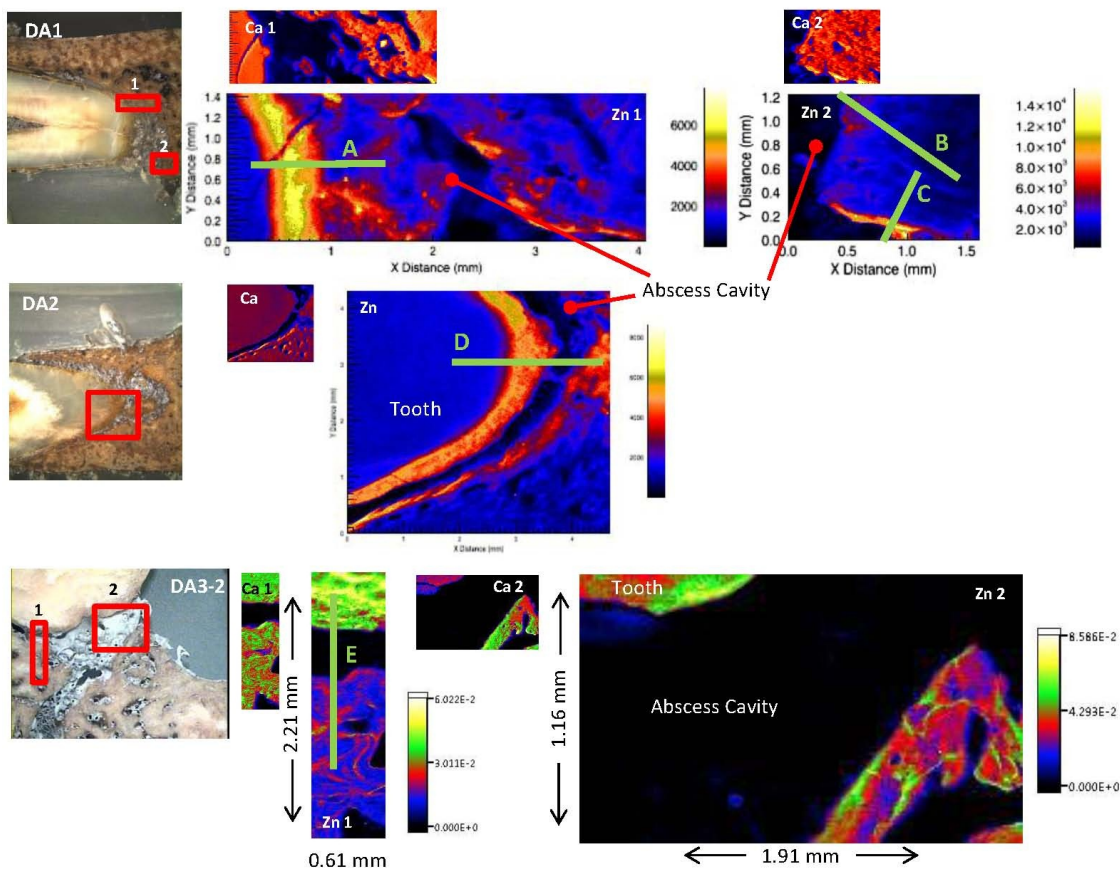
Unaffected Samples
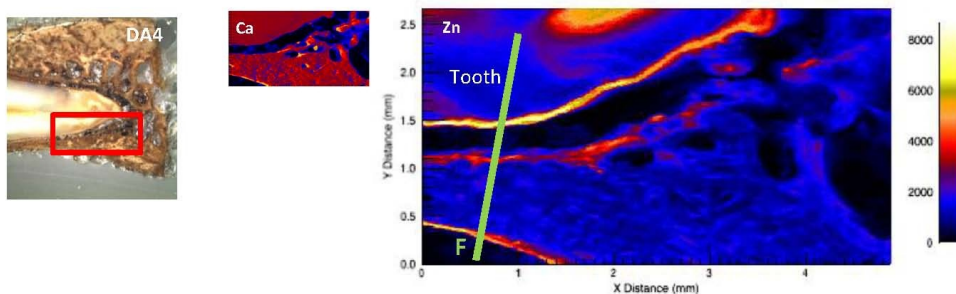
Figure 5.8. Zn maps of the dental abscess samples from the Varden Site. (Lines indicate the positions of the cross-sections seen in figure 5.11).

Figure 5.8 shows a comparison of the various Zn maps from the Varden dental abscess samples. Each Zn map is accompanied by the corresponding Ca map for comparison and the beamline camera view indicating the scanned area(s) in red. Also on each Zn map are green lines, labelled alphabetically which refer to extracted line sections. Also here I introduce some maps from APS experiments, so note, the colour scale is different, the X-ray intensity at APS can not be compared to that at NSLS directly and the overall size of the map images are indicated.
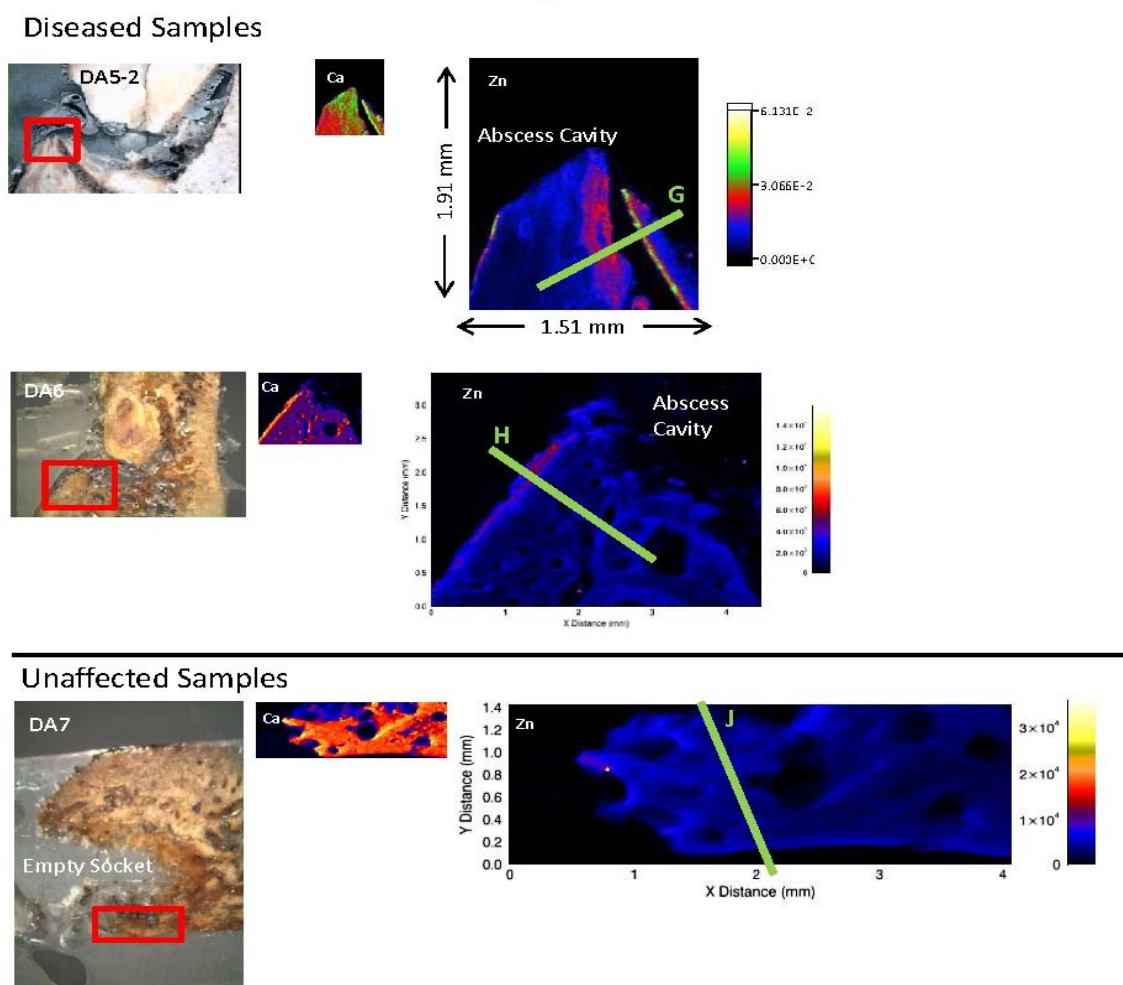
Figure 5.9. Zn maps of the dental abscess samples from San Pedro. (Lines indicate the positions of the cross-sections seen in figure 5.11).

In sample DA2 (from the Varden Site), the Zn band in the cementum at the tooth root is clear. Opposite this is a narrow band of intense Zn long the alveolar margin of the tooth socket which widens towards the bottom of the socket. The space between the tooth and bone widens at the bottom of the socket towards an abscess cavity visible at the top of the Zn map. There is no evidence in this map of a wider band of increased Zn around the edge of the tooth socket, although the area of the map is restrictive.

In the Zn maps of sample DA3-2, also from Varden, the abscess cavity is clear in area 2. The cementum of the tooth is also clear at the top of both maps. The Zn in the bone across the abscess cavity from the tooth has numerous very narrow intense bands of Zn throughout the alveolar bone. The patchy banding of the Zn is clearly seen across the triangular section of bone seen in area 2. The patches are less than one tenth of a millimetre in width.

The unaffected sample DA4 from the Varden site has intense bands of Zn around the cementum of the tooth, across the socket gap and on the anterior edge of the mandible. There is no indication of a wider band of intense Zn around the edge of the bone in this image as well.

In figure 5.9, the Zn maps from the San Pedro dental abscess samples are shown, again with the Ca maps and beamline camera images for reference. The distribution of Zn within the triangular region of bone scanned for sample DA5-2 is unique in its having a gap, about 0.3 wide, along the inner edge, opening into the abscess cavity. This gap of unknown origin creates an interesting Zn pattern with both very intense and less intense bands along either side of the gap. The Zn in this instance also seems to have a broad region of increased Zn which decreases towards the interior of the bone.

In the image from sample DA6 there is an intense narrow band of Zn along the anterior mandible surface. The edge of the abscess cavity does appear to have a wide area of slightly increased Zn concentration, this is made difficult to see due to the significant large holes in this area of the bone.

The unaffected bone sample from San Pedro, DA7, represents the anterior ridge of bone from an empty socket. Here there are no obvious narrow intense Zn bands. A slight

increase of Zn intensity around all the edges of the bone appears to be present. Comparing the unaffected bone maps for Zn from DA4 and DA7, the distribution of Zn appears different within the non-diseased socket. The distribution of Zn around the area of the abscess cavity in DA1, DA2, DA3-2, DA5-2 and DA6 are not consistent in terms of the location of any narrow intense Zn bands or any wide less intense bands like those seen in the DA1 analysis. So initially, the maps appear to indicate that no clear pattern emerges which means that the null hypothesis needs to be accepted in the case of Zn and dental abscesses, that being that there is no difference between disease affected bone and normal bone. Just to confirm this conclusion I will look briefly at the XRF intensity line sections indicated in figures 5.8 and 5.9.

Before I turn to the extracted lines and average Zn intensity values calculated for the dental abscess samples, I want to take a look at the tuberculosis samples. The Zn maps are shown in figure 5.10. In the map of sample TB1-L there is a clear wide (about ½ mm) band of intense Zn. This band is located on the anterior edge of the vertebra sectioned. The very open trabeclular structure of the vertebral bone is evident in the map, and again, it is difficult to determine if there is any variation of Zn within the trabecula close to the lesion edge (top of the map image).

The difficulty in determining Zn gradients within trabecular bone is even more evident in the map from sample TB2. Taken at APS, with the confocal arrangement which limited the depth of analysis to 60 μm, the thin tubular nature of the trabeculae is evident. Blobs of Zn appear in the map as the trabeculae undulate through the focal plane of the experiment. Without a clear dense area of bone wider than about 0.4 mm, it is not possible to establish any trends even at the edge of the abscess cavity (the upper right corner of the map).

The unaffected sample TB3, is similar to TB1-L in that at least some area of agglomerated bone is evident at the edge of the vertebral body (right side of image). Still there is not a great amount of bone to see. Although there are areas of intense localized Zn intensity at the top right edge of the map.

Diseased Samples
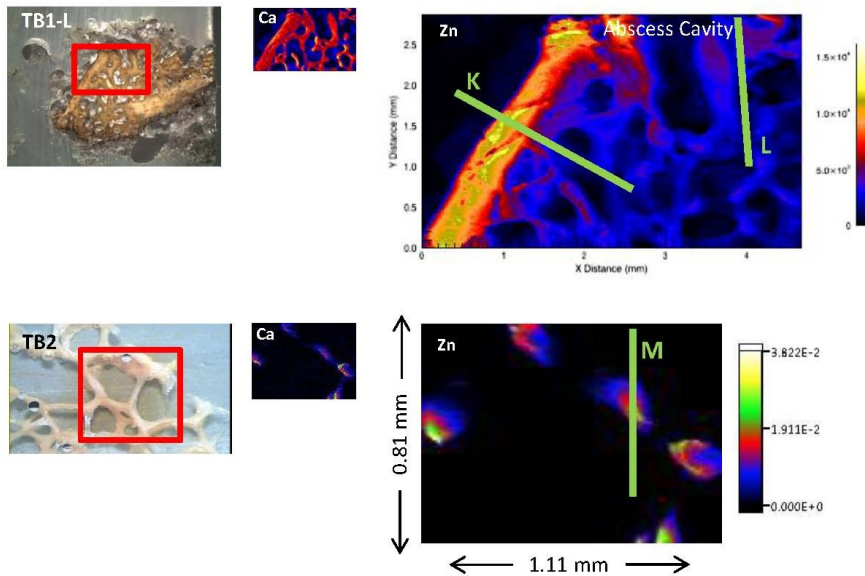
Unaffected Samples
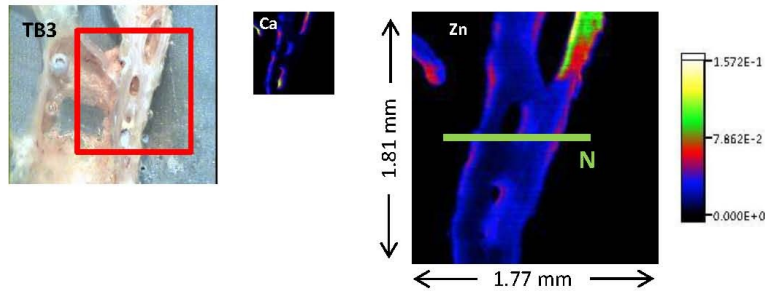
Figure 5.10. Zn maps of the tuberculosis vertabrae samples scanned from Kellis II. (Lines indicate the position of the cross-sections seen in figure 5.11).

In comparing these images the affected and unaffected sample maps have a similar appearance. It is hard to gauge anything from the map for TB2, indeed the Ca map and all other elements maps appear identical for this sample. Clearly examining the elemental composition of trabecular bone at the micrometre scale is not the best fit experimentally, creating significant interpretive problems. As a result, and not wanting to base any conclusions on just two analysable maps I will refrain from making any conclusions in the case of bone affected by tuberculosis, and I will not mention the TB

samples further for any element unless obvious anomalies need pointing out.

Turning to the extracted line sections for the Zn dental abscess samples. These sections are shown in figure 5.11 for each sample. The maps from APS where the
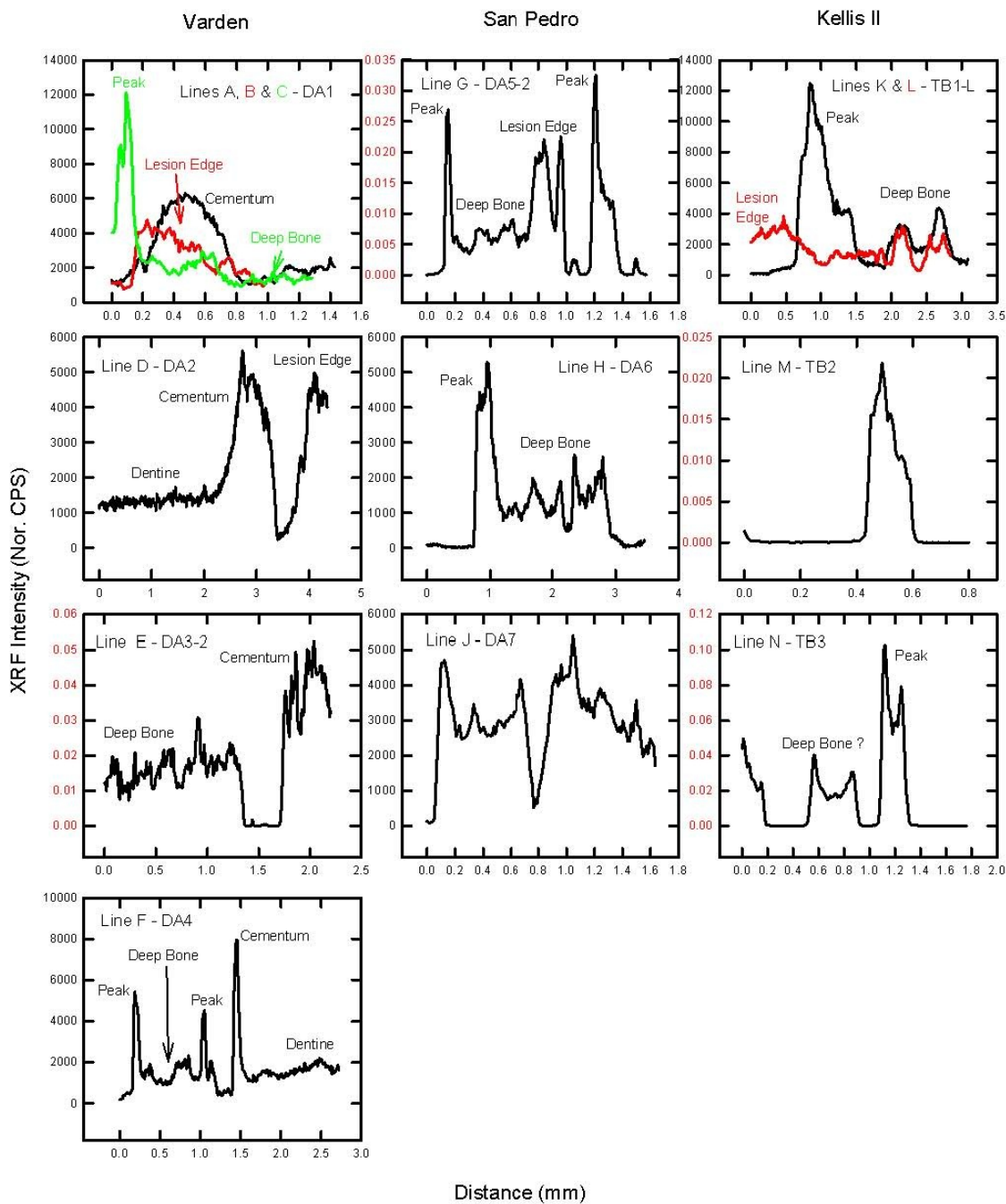
Figure 5.11. Zn intensity line sections from the dental abscess and tuberculosis samples run.

normalization is different have the intensity values given in red as a reminder that they can not be compared directly to the NSLS values, although they can be compared to each other. I have labelled areas of the sections which can be identified. It is clear from scanning down the Varden column in figure 5.11 that not all the maps have areas that can be identified with an increase in Zn intensity at the lesion edge. Although the cementum region is clear where present there are also sharp peaks in the profiles not related to the cementum but only in DA1 and DA4, a diseased and unaffected sample respectively. The lesion edge region for Line D could also be identified as a peak region from the map of DA2, even if this is done Line E from sample DA3-2 does not display a peak of Zn intensity at the bone edge.

The San Pedro column is similarly inconsistent showing no lesion edge increase of Zn intensity in Line H of DA6 which appears in the other diseased sample in the set from DA5-2, Line G. The unaffected sample DA7, Line J appears to have Zn evenly distributed in the image but in section the variation across the bone is remarkable.

The Zn intensity cross-sections from the tuberculosis samples (Kellis II) column can be considered interesting but difficult to interpret as with the images. In TB1-L, the intense Zn band along the anterior edge of the vertebra is clear, the intensity quickly drops to a value which appears consistent across any trabeculae crossed by the beam in the interior of the bone. From Line L, there does not appear to be an increase in Zn intensity at the lesion edge. Line M, TB2, just indicates an area of Zn, and not much more can be said. Line N, TB3, is similar to Line M, except it crosses several trabecula, does have some interesting structure. First the right most area is significantly more intense than the middle bone area. This area is to the outside of the vertebra. Second, the two-horned appearance of both these peaks typically indicates a distribution which is enriched at the surface of a cylindrical-shaped object (Martin *et al.*, 2005).

Again a table of Zn intensity values extracted from the line sections in figure 5.11 is presented in table 5.2. Examining these Zn intensity values, the inherent variability is clear in the large standard deviations. However, there does seem to be a grouping of values around 1) the dentine and deep bone, which are clearly significantly separated

Table 5.2. Average Zn XRF Intensity data in Normalized CPS (σ) for the dental abscess and TB samples.

Sample	Dentine	Cementum	Deep Bone	Lesion Edge	Width (mm)	Peak*	Width (mm)
DA1	1651 (492)	5186 (885)	1309 (211)	2787 (859)	0.6	12092	0.15
DA2	1344 (119)	4384 (588)	- -	3814 (895)	?	- -	- -
DA3-2	- -	0.039 (0.007)†	0.016 (0.004)	- -	- -	- -	- -
DA4	1575 (278)	5854 (1815)	1420 (363)	- -	- -	5415	0.07
DA5-2	- -	- -	0.006 (0.0001)	0.015 (0.005)	0.26	0.033	0.05
DA6	- -	- -	1346 (453)	- -	- -	5292	0.2
DA7	- -	- -	3235 (739)	- -	- -	- -	- -
TB1-L	- -	- -	2463 (550)	2779 (344)	?	12474	0.43
TB2	- -	- -	0.014 (0.004)	- -	- -	- -	- -
TB3	- -	- -	0.022 (0.007)	- -	- -	0.103	0.22

* Single highest value from line.

† APS run samples.

from 2) the cementum and peak values. Where present there is an increase in Zn intensity at the lesion edge but this increase is often too small to be significant with the background variability of the bone concentrations.

After all this we can conclude that: 1) no clear pattern related to the presence of a dental abscess lesion emerges from an analysis of either the Zn element maps or the extracted line sections. This means that the null hypothesis can not be rejected in the case of Zn and dental abscesses, that being that there is no difference between disease affected bone and normal bone. 2) due to the nature of the trabecular bone, any analysis of the TB samples will be unfruitful. 3) there are intense patterns of increased Zn concentration throughout very small regions of bone and teeth. Although not related to the presence of a dental abscess lesion, an explanation for the observed patterning needs to be sought.

5.4: Analysis of Fe Distributions around Dental Abscesses

An overview of the Fe element maps from the dental abscess samples, shown in figure 5.12, indicates that the Fe seen is predominantly located in nodules outside of the
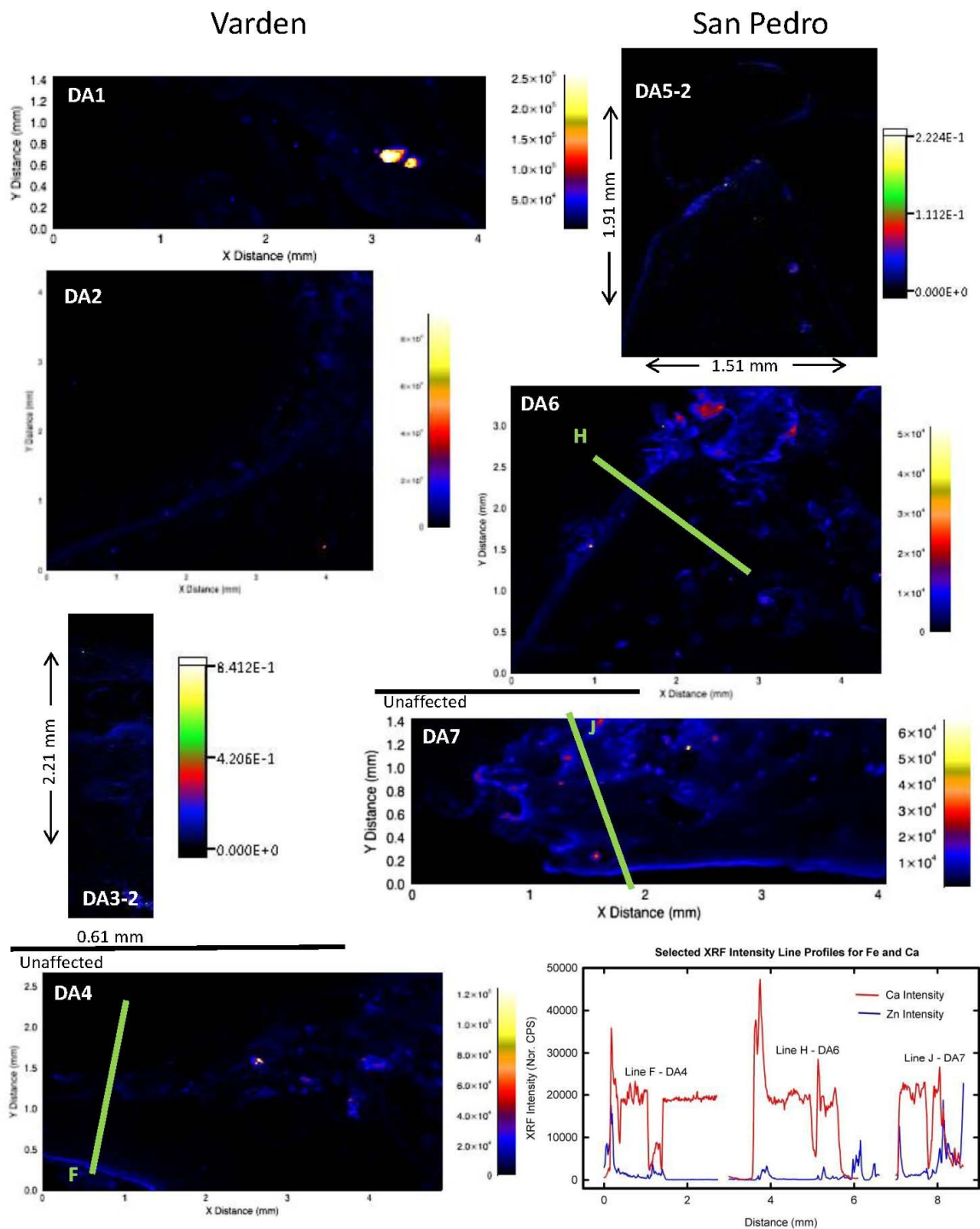
Figure 5.12. Fe elemental maps for the dental abscess sample set.

bone (DA1, DA4, DA6, DA7). In several instances, notably DA3-2, DA4, DA5-2 and

DA7 there is some Fe increase at the exposed outside edge of the bone but not as concentrated as in the nodules. This can be clearly seen in the extracted sections shown at the lower right of figure 5.12.

The presence of Fe in localized nodules, which are most likely soil particles, is hardly unexpected as Fe is a major elemental component in most soils being the fourth most abundant element (Emsley, 2001). The increased concentration of Fe around exposed bone areas, decreasing toward the interior of the bone suggests that this Fe is of diagenetic origin, leaching in from the soils. It is interesting to note that in each sample that displays this Fe pattern the area of bone affected is approximately ½ mm or less. The scale of the leaching is similar in all samples, even in the Varden samples where the inundation conditions were ideal for diagenetic ion transfer, but not all samples from a site show leaching behaviour. Also of note, again, is the extremely localized patterning of the elements in the soil and in the bone.

Occasionally there are increased Fe areas within the deeper bone, which are likely of biogenic origin, but these areas show no correlation to disease status, which means that we must conclude that the presence of a dental abscess has no effect on the Fe content of impacted bone.

5.5: Analysis of Cu Distributions around Dental Abscesses

The compilation of Cu XRF intensity maps for the dental abscess samples is shown in figure 5.13. The Cu signal is one of the less intense lines in the XRF spectra, generally. Still, looking at the images one can identify localized areas of increased Cu intensity around the edges of the bone in DA1, DA2, DA3-2, DA4 and DA5. DA2, DA3-2 and DA4 show an increased Cu content in the cementum of the teeth. Also evident is the presence of Cu in the soil inclusions notably, DA1, DA4, DA6 and DA7.

Comparing these images to the ones for Zn in figure 5.8 and figure 5.9, the distribution is similar, this suggests that the biological function of Cu may be related to that of Zn if the presence of these elements in the bone is of biogenic origin. Again, as in the case of Zn there is no consistent correlation between the distribution patterns seen and
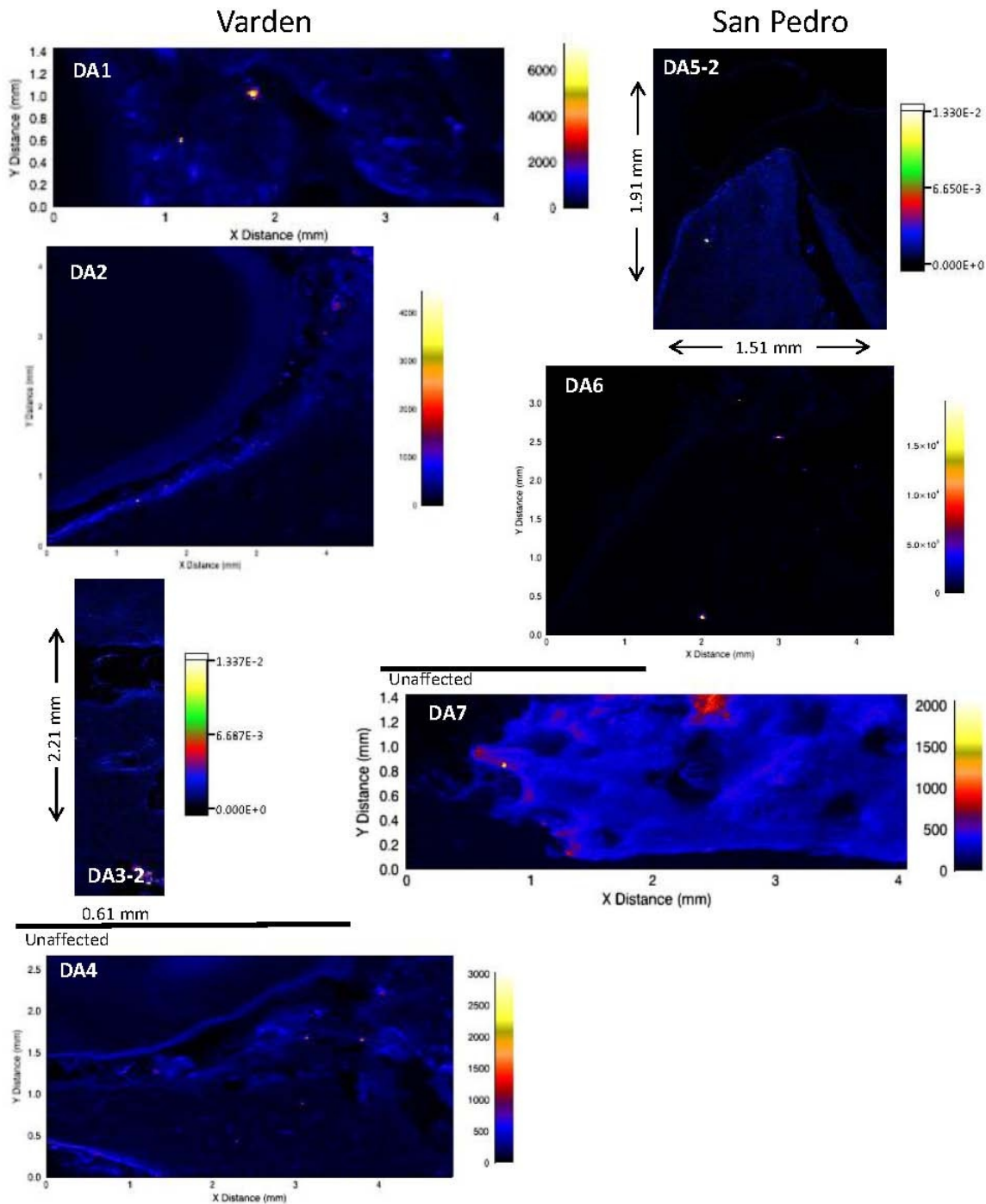
Figure 5.13. Cu XRF intensity maps from the dental abscess samples.

the presence of a dental abscess lesion. Thus, we must conclude that <u>dental abscesses do not affect the Cu concentrations in neighbouring bone</u>.

5.6: Analysis of Br Distributions around Dental Abscesses
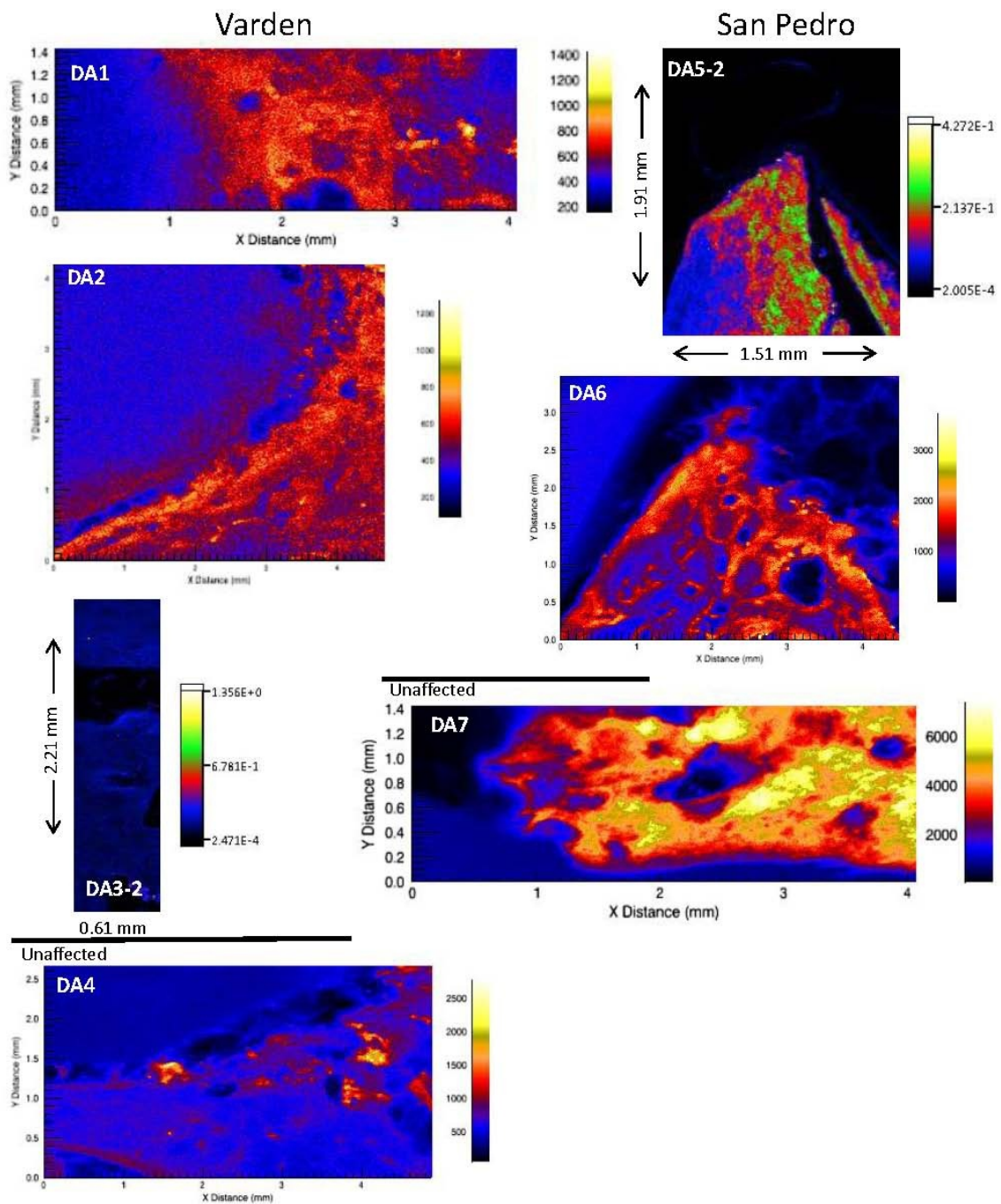
Figure 5.14. Br XRF intensity maps from the dental abscess samples.

The Br XRF peak is of significant height, and looking at the elemental maps

generated in figure 5.14, the distributions of Br in the bone are different from those examined so far. Firstly, in DA1, DA2 and DA4, the concentration of Br in the teeth is less than that in the bone in all cases, this has been reported before (Dolphin *et al.*, 2013). Second, in each of the elemental maps the concentration of Br in the bone appears evenly distributed throughout. The notable exception is DA5-2 where the left portion of the bone appears to be lower in intensity, but an examination of the scale shows that the difference is not pronounced and just an artifact of the scale of the image. Also notable is the rather intense localized areas of Br seen in DA4. These occur within voids in the bone structure, the origin of this single anomaly is unclear at this time.

In table 5.3, below, I have calculated the average Br intensities within the bone from along the line sections. I have colour coded the samples from the various sites, Varden-blue, San Pedro-red, LeVesconte-green and Kellis-white. Although tentative, the samples appear to fall into groups based on site with San Pedro having significantly larger Br intensity than Varden and Kellis. The LeVesconte Mound samples are variable but fall generally lower than Varden and San Pedro. In reference to my previous work in the literature, Br concentration can be related to high Br sources in the diet, either marine or some nuts (Dolphin *et al.*, 2013). As a result it can be tentatively concluded that those at San Pedro, had a marine component of their diet. This is not surprising as San Pedro is situated on an island off the coast of Belize. Such a result needs more study for confirmation and the conversion of the intensity values into absolute concentrations.

Table 5.3. Average Br XRF intensities from within the bones studied. (Colours indicate sample site: Blue - Varden; Red - San Pedro; Green - LeVesconte).

NSLS Sample	DA1	DA2	DA4	DA6	DA7	TB1-L
Br Intensity (Nor. CPS) (σ)	641 (97)	625 (66)	656 (68)	1404 (204)	3773 (996)	706 (125)
APS Samples	DA3-2	DA5-2	R1	R2	R3	R4
Br Intensity (Nor. CPS) (σ)	0.092 (0.018)	0.155 (0.052)	0.017 (0.005)	0.031 (0.002)	0.074 (0.008)	0.066 (0.020)

5.7: The Rib Samples and the Parrot Beak Osteophyte
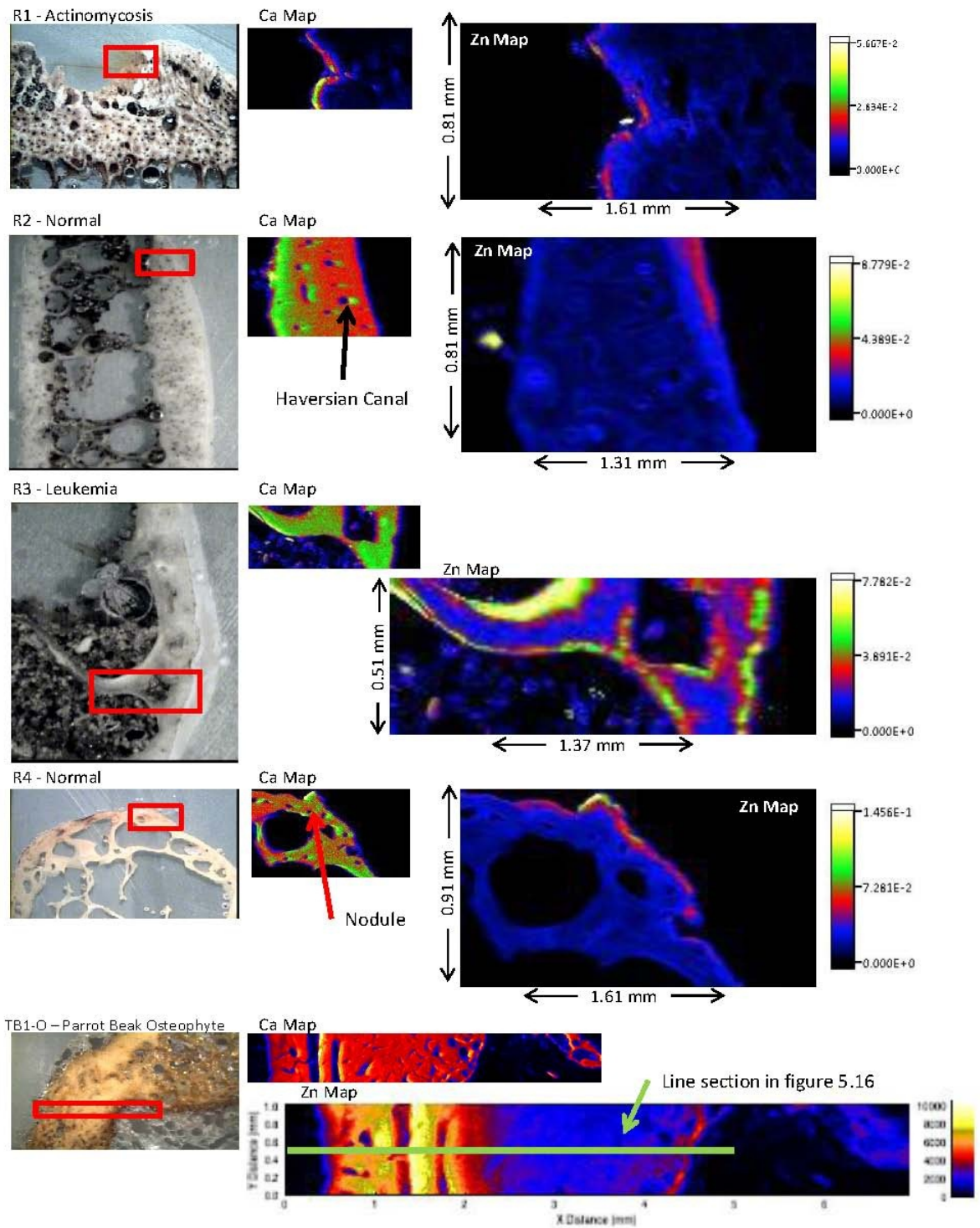
Figure 5.15. Ca and Zn XRF intensity maps for the four Rib samples and the Parrot Beak osteophyte from sample TB1.

Figure 5.15 shows the beamline camera images, Ca maps and Zn maps for each of the four Rib samples looked at and a section through the Parrot Beak osteophyte from sample TB1.

The region chosen for imaging on the Actinomycosis affected sample was from the area of new bone built on the rib surface which was also undergoing lytic attack. The area shows a band of increased Ca along the edge which corresponds to an intense Zn band. The second rib sample was normal. This sample is one to note particularily, as it displays the classic lamellar bone structures seen in XRF mapping (Swanston *et al.*, 2012). The Ca map clearly shows several circular Haversian canals which can also be identified in the Zn map. In this, disease unaffected, sample there is some increase of Zn along the outer edge of the bone, but localized to the top right of the image.

The third rib sample was taken from the opposite end of the rib from R2. This end had the classic appearance of Leukemia. The region scanned was from the opposite rib face as the lytic lesions. The dirt inclusions in these rib samples are clearly visible in the beamline images. Even on the apparently unaffected rib face the Zn image of this rib shows a patchwork of intense Zn areas.

The fourth rib section was taken as normal, however, there was a small nodule on the rib face. The nodule can clearly be seen in the element maps and in the Zn image and has a rim of increased Zn intensity on its outer surface.

The section taken through the osteophyte (TB1-O) is interesting in several respects. First, the sclerotic new bone growth appears to have occurred in layers, visible at the left of the Ca map and the Zn map. Second, the most intense Zn area is seen at the edge of the middle layer, not at the outermost layer. Thirdly, as shown in figure 5.16 the osteophyte also has very intense concentrations of Mn as well as increased Ni intensity at the outer

(anterior) edge of the osteophyte. The presence of Mn and Ni in the sclerotic bone can also be seen in the sclerotic anterior face of the vertebra seen in section TB1-L. Again the question arises, What are Mn and Ni doing in these regions of bone? At this point no answer can be advanced, but the presence of Mn and Ni in the osteophyte, presents a clear
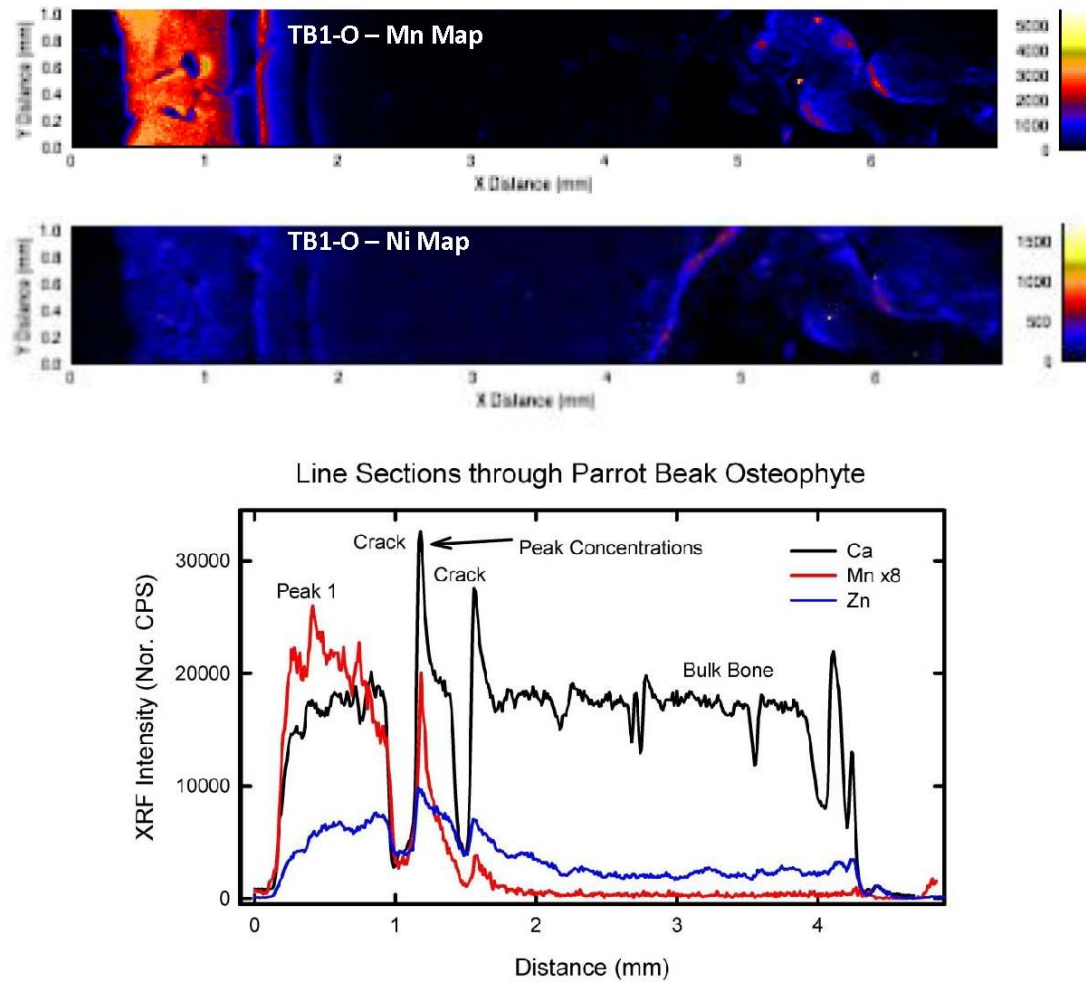
Figure 5.16. Parrot Beak Osteophyte element maps for Mn and Ni and selected line sections.

area for future study, Can the presence of Mn and Ni be related to processes of osteophyte growth or to the physiology of TB? Note: I ask about the physiology of TB here because the person in question had TB infection confirmed by aDNA work, however, TB is usually lytic in nature with sclerotic areas occurring mostly in cases of vertebral collapse. Also the Parrot Beak osteophyte structure is more commonly seen in cases of *Brucellosis* infection, thus in searching for the cause of the Mn and Ni distributions other infectious agents need to be considered.

The line sections shown in figure 5.16, show that the highest XRF intensities for

Ca, Zn and Mn all occur at the right edge of the left most crack. The XRF intensities occurring in the anterior region are also elevated over the bulk bone values and I have chosen to label these 'Peak 1' values. From these observations it is clear that there is a more complicated mechanism behind the production of an osterophyte than layers of bone layed down under the periosteum. It would be very interesting to study other pathological bone growths such as those in DISH or enthesophytes (which occur in muscle tissue). Would similar divided structures and element concentrations be evident?

5.8: Zn Distributions Revisited

The correspondence in location between the Zn, and Mn XRF intensities and the Ca intensity peaks seen in figure 5.16, suggests an alternate analysis for the Zn XRF intensities. Looking back at all the images of Ca and Zn presented so far, there does seem to be a correspondence between intense areas of Zn and those of Ca. Table 5.4 looks more closely at this relationship. Also included are the peak Zn intensities from the cementum regions identified in the images.

The peak XRF intensities of Ca are indicative of an increase in bone density, this is most likely evidence of localized bone formation. Add to this supposition, the intense Zn values found in the cementum (the cementum is an active calcified tissue forming region) as opposed to the dentine (Martin *et al.*, 2004; 2010) and the presence of elevated levels of Zn located at the mineralization front in cartilage (Zoeger *et al.*, 2008). Together then the accumulated evidence indicates that the presence of increased Zn levels in bone is related to bone formation. It is important to note that this correlation happens not at the level of the tissue but occurs in micro-regions within the bone tissue where bone formation is occurring.

The implications of this conclusion are profound. Three immediately occur: 1) Zn is thus implicated in the bone formation process; 2) the concentration of Zn in areas of bone formation is significantly higher than normally occurs in surrounding bone tissues; 3) Zn appears to be moved into regions of bone formation and out of non-forming bone regions otherwise the concentration of Zn in the bone would remain at its elevated levels

throughout the bone.

Table 5.4. The correspondence between Zn and Ca peak positions (Nor. CPS (σ)).

Sample	Deep Bone Zn	Peak Zn	Corresponding Ca Peak	Peak Ca	Deep Ca
DA1	1309 (211)	12092	✔	45050	18068 (2254)
		5130	✔	29430	
		6285	Cementum		
DA2		4968	✔	22246	- -
		5603	Cementum		
DA4	1420 (363)	5415	✔	35862	19302 (2852)
		7931	Cementum		
DA6	1346 (453)	5292	✔	47319	16099 (6336)
DA7	3225 (739)	- -	- -	- -	14712 (7584)
TB1-L	2463 (550)	12474	✔	26377	17307 (3586)
TB1-O	2274 (358)	9859	✔	32570	15526 (5350)
		7604		- -	- -
DA3-2*	0.016 (0.004)	0.031	✔	0.015	- -
		0.05	Cementum		
DA5-2	0.006 (0001)	0.033	✔	0.016	0.0098 (0.002)
R1	0.004 (0.002)	0.017	✔	0.008	0.00041 (0.0003)
R2	0.010 (0.006)	0.032	✔	0.013	0.0075 (0.0026)
R3	0.019 (0.005)	0.075	✔	0.011	0.0089 (0.0009)
R4	0.023 (0.01)	0.12	✔	0.011	0.0057 (0.0018)

* APS Samples

The involvement of Zn in bone formation is not surprising, Zinc is known to play an important role in the growth, development and maintenance of bone (Tang *et al.*, 2006; Hie *et al.*, 2011). Zn deficiency is known to decrease the function of osteoblasts and osteoclasts (Hie *et al.*, 2011) leading to osteopenia and osteoporosis.

Bone structure and function are maintained by a delicate homeostasis between the osteoblasts and osteoclasts and Zn has been shown to affect both cell types (Tang *et al.*, 2006). Still, despite the long known relation of Zn to bone formation researchers have

not yet documented the mechanisms behind the expression and regulation of Zn uptake in bone cells (Tang *et al.*, 2006). So it is not surprising then that nutritional researchers report both positive correlations (Sazawal *et al.*, 1998) between dietary Zn levels and improved clinical outcomes and no correlations (Caulfield *et al.*, 1999; Heinig *et al.*, 2006). Obviously much more needs to be learned about the physiology and control of Zn especially within bone.

In this case the concentration of Zn in bone obtained by common methods involving bulk analysis and digestion will have very little relevance to the concentration of Zn in bone that is involved in bone formation. The concentration of Zn is often a factor of five to ten times higher in localized areas of bone formation, than within the rest of the tissue.

The elevated levels of Zn in the cementum of teeth remain high relative to the dentine even though only the outer layers of cementum are the ones actively being deposited. This fact suggests that the control of Zn is handled by cellular components, as active cells occur in bone but not in the cementum. The mobile Zn could also be the result of the chemical composition of the Zn, is it bound to the crystals, or in cells, enzymes? Is the Zn chemically distinct in the cementum/active bone/deep bone? These questions can be approached by examining the X-ray Absorption Spectra of Zn which can be done with the same synchrotron equipment as the present study at the same micro-scale.

Of course the actual high concentration of Zn in live bone required to cause bone growth, which is suggested by this study of dry archaeological bone, is difficult to relate to the Zn intensities found. An attempt to quantify the absolute Zn concentration in the areas of bone growth based on this study will be an important next step, although it may not relate directly to the in vitro Zn concentrations involved.

In bioarchaeology and forensics, one interesting question arrises, how fast does the Zn enter the bone to promote bone growth? and could this, if discovered, <u>allow for finer determinations of the timing of fractures relative to time of death in forensic cases</u>? Could the peri-mortem timing of tooth loss be determined from an analysis of Zn in the

empty socket?

Medically, could the introduction of Zn to localized areas of bone around fractures promote healing? Or, could the incorporation of Zn into the Ca cements used in bone implants promote osteointegration? In the area of physiology, does the enhanced concentration of Zn imply new avenues for the elucidation of the mechanisms of Zn use and uptake in bone and other tissues?

CHAPTER 6: CONCLUSIONS

In this thesis I set out to investigate the elemental distributions in bone surrounding areas of bacterial infection. This question and the techniques used to investigate it were suggested based on observations of anomalous micron scale distributions of elements seen in the literature and my own previous work on teeth. Bacterial diseases were chosen because it was thought that the presence cells having unique and distinct metabolic requirements from the surrounding tissues could have led to unique elemental distributions in the bone affected.

After much work this turned out to be not the case. It was found that in the case of Zinc, Copper, Iron, and Bromine that the distribution of elements, although patterned, at a micron scale, as expected, could not be related to the presence of a dental abscess lesion. As a result I have failed to reject the null hypothesis, that being; <u>There is no difference in the elemental distribution between normal bone and bone affected by a dental abscess, at least in the case of these four elements</u>. I should note, that due to the limited range of elements accessible experimentally, a conclusion for only these four elements can be reached. For that matter, a conclusion cannot be reached for any other factor that could be affected by disease such as the bone crystal structure. It is hoped that due to anaerobic bacteria's use of sulphur the distribution of S around a dental abscess may be unique, but that could not be investigated in this study.

The analysis of tuberculosis lesions was not possible due to complications arising from the nature of trabecular bone which need to be addressed on future work. As a result I can not conclude one way or the other on the null hypothesis regarding the distribution of elements around TB lesions. Nor can I make any comparisons between aerobic and anaerobic bacteria at this time. Appropriate experimental methods to assess the element distributions in regions of trabecular bone is an important area to be addressed in future element studies.

The findings were not all negative, however, it was found that the Br concentrations appear to correlate with the site of origin of the samples and thus with the

dietary intake of Br at each site. It would be premature to conclude what the dietary source of the Br was at the study sites.

In some instances it was possible to clearly see the effect of element diagenesis on the samples. This took the form of soil inclusions as well as leaching of some elements into exposed bone. The diagenetic signal could be differentiated from the biogenic signal with careful analysis. The diagenetic leaching of elements like the biogenetic signal could not be correlated to any site or disease state but was extremely localized in extent.

Another important result was the correlation of localized areas of increased Zn concentration with areas of bone formation. This result demonstrates very clearly the variability of elemental concentrations at scales smaller than the bone tissue, and the necessity of micro-scale analysis rather than bulk analysis in elemental studies. The importance of Zn distribution correlating with bone formation and the enhanced concentration that is evident in these areas, is clear. Zn distribution in bones needs more intense study in the future, the possibility of timing fracture healing is just one exciting direction for continued research.

In terms of pathology, the growth of Parrot Beak osteophytes presents several areas for fruitful future research. For example: What function, if any, do Mn and Ni have in the process? Are Mn and Ni involved in any other pathological bone formation processes such as Carries Sicca? Another interesting area for future investigation is the physical structure of the osteophyte. The intense Zn in the middle of the structure suggests that the active bone growth is not at the outer edge of the osteophyte but within its structure.

The current work clearly answers few questions but opens up many interesting avenues for future research in many academic areas.

REFERENCES CITED

Alomary, A., IF. Al-Momani and AM. Massadeh, 2006. Lead and cadmium in human teeth from Jordan by atomic absorption spectrometry: Some factors influencing their concentrations. *Science of the Total Environment* **369**, 69-75.

Ambrose, SH., 1993. Isotopic analysis of paleodiets: methodological and interpretive considerations. In: MK. Sandford, Ed*. Investigations of Ancient Human Tissue: Chemical Analyses in Anthropology*. Gordon and Breach Science Publishers, Langhorne.

Aufderheide, AC. and C. Rodríguez-Martín, 1998. The Cambridge Encyclopaedia of Human Paleopathology. Cambridge University Press, Cambridge.

Bazhanova, VV., LF. Guljaeva, SE. Krasilnikov, VS. Titova, AD. Shaporenko and Y. Shulga, 2007. Using XRF SR for the study of changes in elemental composition of healthy and pathological tissues of human organism. *Nuclear Instruments and Methods in Physics Research A* **575**, 206-209.

Berdanier, CD. and J. Zempleni, 2009. *Advanced Nutrition: Macronutrients, Nicronutrients and Metabolism*. CRC Press, Boca Raton.

Berna, F., A. Matthews and S. Weiner, 2004. Solubilities of bone mineral from archaeological sites: the recrystallization window. *Journal of Archaeological Science* **31**, 867-882.

Bigi, A., G. Cojazzi, S. Panzavolta, A. Ripamonti, N. Roveri, M. Romanello, K. Noris Suarez and L. Moro, 1997. Chemical and Structural Characterization of the Mineral Phase from Cortical and Trabecular Bone. *Journal of Inorganic Biochemistry* **68**, 45-51.

Bonar, LC., AH. Roufosse, WK. Sabine, MD. Grynpas and MJ. Glimcher, 1983. X-ray diffraction studies of the crystallinity of bone mineral in newly synthesized and density fractionalted bone. *Calcified Tissue International* **35**, 202-209.

Brenn, R., Ch. Haug, U. Klar, S. Zander, KW. Alt, DN. Jamieson, KK. Lee and H. Schutkowski, 1999. Post-mortem intake of lead in 11th century human bones and teeth studied by milli- and microbeam PIXE and RBS. *Nuclear Instruments and Methods in Physics Research B* **158**, 270-274.

Brothwell, DR., 1981. *Digging up Bones. Third Ed.* Cornell University Press, Ithaca.

Buikstra, JE. and DH. Ubelaker, Eds., 1994. *Standards for data collection from human skeletal remains: proceedings of a seminar at the Field Museum of Natural History.* Arkansas Archaeological Survey, Fayetteville.

Burton, J., 2008. Bone chemistry and trace metal analysis. In: MA. Katzenberg and SR. Saunders, Eds., *Biological Anthropology of the Human Skeleton, Second Ed.* Wiley-Liss, Hoboken.

Burton, JH. and TD. Price, 2000. The Use and Abuse of Trace Elements for Paleodietary Research. In: SH. Ambrose and MA. Katzenberg, Eds., *Biogeochemical Approaches to Paleodietary Analysis*. Kluwer Academic/Plenum, New York.

Carvalho, ML., C. Casaca, T. Pinheiro, JP. Marques, P. Chevallier and AS. Cunha, 2000. Analysis of human teeth and bones from the chalcolithic period by X-ray spectrometry. *Nuclear Instruments and Methods in Physics Research B* **168**, 559-565.

Carvalho, ML., JP. Marques, AF. Marques and C. Casaca, 2004. Synchrotron microprobe determination of the elemental distribution in human teeth of the Neolithic period. *X-Ray Spectrometry* **33**, 55-60.

Carvalho, ML., T. Magalhães, M. Becker and A. von Bohlen, 2007. Trace elements in human cancerous and healthy tissues: A comparative study by EDXRF, TXRF, synchrotron radiation and PIXE. *Spectrochimica Acta B* **62**, 1004-1011.

Carvalho, ML., AF. Marques, JP. Marques and C. Casaca, 2007a. Evaluation of the diffusion of Mn, Fe, Ba and Pb in Middle Ages human teeth by synchrotron microprobe X-ray fluorescence. *Spectrochimica Acta B* **62**, 702-706.

Caulfield, LE., N. Zavaleta, A. Figueroa and Z. Leon, 1999. Maternal zinc supplementation does not affect size at birth or pregnancy duration in Peru. *Journal of Nutrition* **129**, 1563-1568.

Chang, LLY., RA. Howie and J. Zussman, 1996. *Rock-Forming Minerals, Volume 5B, Non-silicates: Sulphates, Carbonates, Phosphates, Halides*. Second Edition. Longman Group Limited, Harlow. Pg. 297.

Collins, MJ., MS. Riley, AM. Child, and G. Turner-Walker, 1995. A basic mathematical simulation of the chemical degradation of ancient collagen. *Journal of Archaeological Science* **22**, 75-183.

Collins, MJ., CM. Nielsen-Marsh, J. Hiller, CI. Smith, JP. Roberts, RV. Prigodich, TJ. Wess, J. Csapò, AR. Millard and G. Turner-Walker, 2002. The Survival of Organic Matter in Bone: A Review. *Archaeometry* **44**, 383-394.

Curzon, MEJ. and DC. Crocke, 1978. Relationships of trace elements in human tooth enamel to dental caries. *Archives of Oral Biology* **23**, 647-653.

Curzon, MEJ., FL. Losse and A. Macalister, 1975. Trace Elements in the enamel of teeth from New Zealand and the USA. *New Zealand Dental Journal* **71**, 80-83.

DeNiro, MJ., 1985. Postmortem preservation and alteration of in vivo bone collagen isotope ratios in relation to paleodietary reconstruction. *Nature* **317**, 806-809.

Dolphin, AE., and AH. Goodman, 2009. Maternal Diets, Nutritional Status, and Zinc in Contemporary Mexican Infants' Teeth: Implications for Reconstructing Paleodiets. *American Journal of Physical Anthropology* **140**, 399-409.

Dolphin, AE., AH. Goodman and DD. Amarasiriwardena, 2005. Variation in Elemental Intensities Among Teeth and Between Pre- and Postnatal Regions of Enamel. *American Journal of Physical Anthropology* **128**, 878-888.

Dolphin, AE., SJ. Naftel, AJ. Nelson, RR. Martin and CD. White, 2013. Bromine in teeth and bone as an indicator of marine diet. *Journal of Archaeological Science* **40**, 1778-1786.

Donoghue, HD., M. Spigelman, CL. Greenblatt, G. Lev-Maor, GK. Bar-Gal, C. Matheson, K. Vernon, AG. Nerlich and AR. Zink, 2004. Tuberculosis: from prehistory to Robert Koch, as revealed by ancient DNA. *The Lancet: Infectious Diseases* **4**, 584-592.

Donoghue, HD., A. Marcsik, C. Matheson, K. Vernon, E. Nuorala, JE. Molto, CL. Greenblatt and M. Spigelman, 2005. Co-infection of *Mycobacterium tuberculosis* and *Mycobacterium leprae* in human archaeological samples: a possible explanation for the historical decline of leprosy. *Proceedings of the Royal Society B* **272**, 389-394.

Dorozhkin, SV. and M. Epple, 2002. Biological and Medical Significance of Calcium Phosphates. *Angewandte Chemie International Edition* **41**, 3130-3146.

Durham, TR. and ET. Snow, 2006. Metal ions and carcinogenesis. In: LP. Bignold, Ed., *Cancer: Cell Structures, Carcinogens and Genomic Instability*. Birkhäuser Verlag, Berlin.

Elam, WT., B. Ravel and JR. Sieber, 2002. A new atomic database for X-ray spectroscopic calculations. *Radiation Physics and Chemistry* **63**, 121-128.

Elder, FR., RV. Langmuir and HC. Pollock, 1948. Radiation from electrons accelerated in a synchrotron. *Physical Review* **74**, 52-56.

Emsley, J., 2001. *Nature's Building Blocks: An A-Z Guide to the Elements*. Oxford University Press, Oxford.

Ezzo, JA., 1994. Putting the "Chemistry" Back into Archaeological Bone Chemistry Analysis: Modeling Potential Paleodietary Indicators. *Journal of Anthropological Archaeology* **13**, 1-34.

Fairgrieve, SI. and JE. Molto, 2000. Cribra Orbitalia in two temporally disjunct population samples from the Dakhleh Oasis, Egypt. *American Journal of Physical Anthropology* **111**, 319-331.

Fernández-Jalvo, Y., B. Sánchez-Chillón, P. Andrews, S. Fernández-López and L. Alcalá Martínez, 2002. Morphological Taphanomic Transformations of Fossil Bones in Continental Environments, and Repercussions on their Chemical Composition. *Archaeometry* **44**, 353-361.

Finegold, SM., 1977. *Anaerobic Bacteria in Human Disease*. Academic Press, New York. (mainly chapter 4: Oral and Dental Infections)

Foreman, LJ. and E. Molto, 2008-2009. Who Was Buried at the Varden Site (AdHa-1)? Osteological Insights into the Time of Interment and the Cultural Group Association of the Mortuary Component of a Long Point Fishing Station. *Ontario Archaeology* **85-88**, 157-177.

Geraki, K., MJ. Farquharson, DA. Bradley, O. Gundogdu and G. Falkenberg, 2008. The localisation of biologically important metals in soft and calcified tissues using a synchrotron x-ray fluorescence technique. *X-Ray Spectrometry* **37**, 12-20.

Grattan, J., L. Abu Karaki, D. Hine, H. Toland, D. Gilbertson, Z. Al-Saad and B. Pyatt, 2005. Analyses of patterns of copper and lead mineralization in human skeletons excavated from an ancient mining and smelting centre in the Jordanian desert: a reconnaissance study. *Mineralogical Magazine* **69**, 653-666.

Guo, H., and AS. Barnard, 2013. Naturally occurring iron oxide nanoparticles: morphology, surface chemistry and environmental stability. *Journal of Materials Chemistry A* **1**, 27-42.

Hackett, CJ., 1981. Microscopical focal destruction (tunnels) in excavated human bones. *Medicine, Science and the Law* **21**, 243-265.

Hancock, RGV., MD. Grynpas and KPH. Pritzker, 1989. The Abuse of Bone Analyses for Archaeological Dietary Studies. *Archaeometry* **31**, 169-179.

Hardwick, JL. and CJ. Martin, 1967. A pilot study using mass spectrometry for estimation of trace element content of dental tissues. *Helvetical Odontologica Acta* **11**, 62.

Hedges, REM., AP. Millard and AWG. Pike, 1995. Measurements and relationships of diagenetic alteration of bone from three archaeological sites. *Journal of Archaeological Science* **22**, 201-209.

Hedges, REM., 2002. Bone Diagenesis: An Overview of Processes. *Archaeometry* **44**, 319-328.

Heinig, MJ., KH. Brown, B. Lönnerdal and KG. Dewey, 2006. Zinc supplementation does not affect the growth, morbidity, or motor development of US term breastfed infants at 4-10 mo of age. *American Journal of Clinical Nutrition* **84**, 594-601.

Hie, M., N. Iitsuka, T. Otsuka, A. Nakanishi and I. Tsukamoto, 2011. Zinc deficiency decreases osteoblasts and osteoclasts associated with the reduced expression of Runx2 and RANK. *Bone* **49**, 1152-1159.

Hillson, S., 1996. *Dental Anthropology*. Cambridge University Press, Cambridge.

Hillson, S., 2005. *Teeth, Second Edition*. Cambridge University Press, Cambridge.

Iwanenko, D. and I. Pomeranchuk, 1944. On the maximum energy attainable in a Betatron. *Physical Review* **65**, 343.

Jans, MME., H. Kars, CM. Nielsen-Marsh, CI. Smith, AG. Nord, P. Arthur and N. Earl, 2002. *In Situ* preservation of archaeological bone: A histological study within a multidisciplinary approach. *Archaeometry* **44**, 343-352.

Jaouen, K., V. Balter, E. Herrscher, A. Lamboux, P. Telouk and F. Albarède, 2012. Fe and Cu Stable Isotopes in Archaeological Human Bones and Their Relationship to Sex. *American Journal of Physical Anthropology* **148**, 334-340.

Johnson, R., 1988. *Elementary Statistics, Fifth Edition*. PWS-Kent Publishing, Boston.

Katzenberg, MA., HP. Schwarcz, M. Knyf and FJ. Melbye, 1995. Stable Isotope evidence for Maize Horticulture and Paleodiet in Southern Ontario, Canada. American Antiquity 60, 335-350.

Katzenberg, MA., 2008. Stable Isotope Analysis; A Tool for Studying Past Diet, Demography, and Life History. In: MA. Katzenberg and SR. Saunders, Eds., *Biological Anthropology of the Human Skeleton, Second Ed.* Wiley-Liss, Hoboken.

Knudson, KJ. and TD. Price, 2007. Utility of Multiple Chemical Techniques in Archaeological Residential Mobility Studies: Case Studies From Tiwanaku- and Chiribaya-Affiliated Sites in the Andes. *American Journal of Physical Anthropology* **132**, 25-39.

Kotz, JC. and KF. Purcell, 1991. *Chemistry and Chemical Reactivity*, *Second Edition*. Saunders College Publishing, Philadelphia. pp. 485.

Larsen, CS., 1997. *Bioarchaeology: Interpreting behavior from the human skeleton*. Cambridge University Press, Cambridge.

Lee-Thorp, J., and M. Sponheimer, 2006. Contributions of Biogeochemistry to Understanding Hominin Ecology. *Yearbook of Physical Anthropology* **49**, 131-148.

Losee, F., TW. Cutress and R. Brown, 1974. Natural elements of periodic table in human dental enamel. *Caries Research* **8**, 123-124.

Kanngieβer, B., W. Malzer and I. Reiche, 2003. A new 3D micro X-ray fluorescence analysis set-up - First archaeometric applications. *Nuclear Instruments and Methods in Physics Research B* **211**, 259-264.

Kumar, V., AK. Abbas, N. Fausto and RN. Mitchell, 2007. *Robbins Basic Pathology, 8th Edition*. Saunders Elsevier, Philadelphia.

Lechner, P., S. Eckbauer, R. Hartmann, S. Krisch, D. Hauff, R. Richter, H. Soltau, L. Strüder, C. Fiorini, E. Gatti, A. Longoni and M. Sampietro, 1996. Silicon drift detectors for high resolution room temperature X-ray spectroscopy. *Nuclear Instruments and Methods in Physics Research A* **377**, 346-351.

Madigan, DJ., Z. Baumann, OE. Snodgrass, HA. Ergül, H. Dewar and NS. Fisher, 2013. Radiocesium in Pacific Bluefin Tuna *Thunnus orientalis* in 2012 Validate New Tracer Technique. *Environmental Science and Technology* **47**, 2287-2294.

Margaritondo, G., 1988. *Introduction to Synchrotron Radiation*. Oxford University Press, New York.

Martin, RR., IM. Kempson, SJ. Naftel and WM. Skinner, 2005. Preliminary synchrotron analysis of lead in hair from a lead smelter worker. *Chemosphere* **58**, 1385-1390.

Martin, RR., SJ. Naftel, S. Macfie, K. Jones and A. Nelson, 2013. Pb distribution in bones from the Franklin expedition: synchrotron X-ray fluorescence and laser ablation/mass spectroscopy. *Applied Physics A* **111**, 23-29.

Martin, RR., SJ. Naftel, AJ. Nelson, M. Edwards, H. Mithoowani and J. Stakiw, 2010. Synchrotron radiation analysis of possible correlations between metal status in human cementum and periodontal disease. *Journal of Synchrotron Radiation* **17**, 263-267.

Martin, RR., SJ. Naftel, AJ. Nelson, AB. Feilen and A. Narvaez, 2004. Synchrotron X-ray fluorescence and trace metals in the cementum rings of human teeth. *Journal of Environmental Monitoring* **6**, 783-786.

Martin, RR., SJ. Naftel, AJ. Nelson, AB. Feilen and A. Narvaez, 2007. Metal distributions in the cementum rings of human teeth: Possible depositional chronologies and diagenesis. *Journal of Archaeological Science* **34**, 936-945.

Mays, S., GM. Taylor, AJ. Legge, DB. Young and G. Turner-Walker, 2001. Paleopathological and Biomolecular Study of Tuberculosis in a Medieval Skeletal Collection from England. *American Journal of Physical Anthropology* **114**, 298-311.

McInerney, MJ. and LM. Gieg, 2004. An overview of Anaerobic Metabolism. In: MM. Nakano and P. Zuber, Eds., *Strict and Facultative Anaerobes: Medical and Environmental Aspects*. Horizon Bioscience, Wymondham.

McMillan, EM., 1945. The Synchrotron - A Proposed High Energy Particle Accelerator. *Physical Review B* **68**, 143-144.

Molokhia, A. And GS. Nixon, 1984. Determination of bromine in the hard tissues by epithermal neutron activation analysis. *Caries Research* **18**, 362-366.

Molto, JE., 1990. Differential Diagnosis of Rib Lesions: A Case Study From Middle Woodland Southern Ontario Circa 230 A.D. *American Journal of Physical Anthropology* **83**, 439-447.

Monro, A., As quoted in: M. Kakutani, *Master of the Intricacies of the Human Heart.* International New York Times, Oct. 10, 2013. (http://www.nytimes.com/ 2013/10/11/books/alice-munro-mining-the-inner-lives-of-girls-and-women.html?)

Murray, RK., DK. Granner, PA. Mayes and VW. Rodwell, 2000. *Harper's Biochemistry, 25th Edition*. Appleton and Lange, Stamford. Chap. 2.

Naftel, SJ., I. Coulthard, TK. Sham, D.-X. Xu, L. Erickson and SR. Das, 1999. Electronic structure of nickel silicide in subhalf-micron lines and blanket films: An x-ray absorption fine structures study at the Ni and Si $L_{3,2}$ edge. *Applied Physics Letters* **74**, 2893-2895.

Nielsen-Marsh, CM. and REM. Hedges, 1999. Bone Porosity and the use of Mercury Intrusion Porosimetry in Bone Diagenesis Studies. *Archaeometry* **41**, 165-174.

Nielsen-Marsh, CM., and REM. Hedges, 2000. Patterns of Diagenesis in Bone I: The effects of site environments. *Journal of Archaeological Science* **27**, 1139-1150.

Ochiai, El-Ichiro, 1977. *Bioinorganic Chemistry: An Introduction*. Allyn and Bacon, Inc., Boston.

Ohanian, HC., 1985. *Physics*. W. W. Norton and Company, New York.

Olsen, KC., CD. White, FJ. Longstaffe, K. von Heyking, G. McGlynn and G. Grupe, 2008. The Effects of Pathology on Inter- and Intra-Individual Nitrogen-Isotope Compositions of Bone Collagen from a Medieval Poorhouse: A Preliminary Study. *Paleopathology Newsletter* **143**, 23-27.

Olsen, KC., CD. White, FJ. Longstaffe, K. von Heyking, G. McGlynn, G. Grupe and FJ. Rühli, 2014. Intraskeletal Isotopic Compositions ($\delta\,^{13}C$, $\delta\,^{15}N$) of Bone Collagen: Nonpathological and Pathological Variation. *American Journal of Physical Anthropology* **153**, 598-604.

Pinheiro, T., ML. Carvalho, C. Casaca, MA. Barreiros, AS. Cunha and P. Chevallier, 1999. Microprobe analysis of teeth by synchrotron radiation: environmental contamination. *Nuclear Instruments and Methods in Physics Research B* **158**, 393-398.

Price, TD., J. Blitz, J. Burton and JA. Ezzo, 1992. Diagenesis in Prehistoric Bone: Problems and Solutions. *Journal of Archaeological Science* **19**, 513-529.

Pyatt, FB., AJ. Pyatt, C. Walker, T. Sheen and JP. Grattan, 2005. The heavy metal content of skeletons from an ancient metalliferous polluted area in southern Jordan with particular reference to bioaccumulation and human health. *Ecotoxicology and Environmental Safety* **60**, 295-300.

Qu, Y., C. Jin, Y. Zhang, Y. Hu, X. Shang and C. Wang, 2013. Distribution patterns of elements in dental enamel of *G. Blacki*: a preliminary dietary investigation using SRXRF. *Applied Physics A* **111**, 75-82.

Radosevich, SC., 1993. The Six Deadly Sins of Trace Element Analysis: A Case of Wishful Thinking in Science. In: MK. Sandford, Ed*. Investigations of Ancient Human Tissue: Chemical Analyses in Anthropology*. Gordon and Breach Science Publishers, Langhorne.

Rasmussen, EG., 1974. Antimony, arsenic, bromine and mercury in enamel from human teeth. *Scandinavian Journal of Dental Research* **82**, 562-565.

Reddy, SB., MJ. Charles, GJN. Raju, BS. Reddy, TS. Reddy, PVBR. Lakshmi and V. Vijayan, 2004. Trace Elemental Analysis of Cancer-Afflicted Intestine by PIXE Technique. *Biological Trace Metal Research* **102**, 265-281.

Reiche, I., C. Vignaud and M. Menu, 2002. The Crystallinity of Ancient Bone and Dentine: New Insights by Transmission Electron Microscopy. *Archaeometry* **44**, 447-459.

Retief, DH., PE. Cleaton-Jones, J. Turkstra and WJ. De Wet, 1971. The quantitative analysis of sixteen elements in normal human enamel and dentine by neutron activation analysis and high-resolution gamma-spectrometry. *Archives of Oral Biology* **16**, 1257-1267.

Roberts, C. and K. Manchester, 2007. *The Archaeology of Disease, Third Edition*. Cornell University Press, Ithaca.

Sandford, MK., 1993. Understanding the Biogenic-Diagenetic Continuum: Interpreting Elemental Concentrations of Archaeological Bone. In: MK. Sandford, Ed*. Investigations of Ancient Human Tissue: Chemical Analyses in Anthropology*. Gordon and Breach Science Publishers, Langhorne.

Sazawal, S., RE. Black, S. Jalla, S. Mazumdar, A. Sinha and M. Bhan, 1998. Zinc supplementation reduces the incidence of acute lower respiratory infections in infants and preschool children. *Pediatrics* **102**, 1-5.

Schutkowski, H., B. Herrmann, F. Wiedemann, H. Bocherens and G. Grupe, 1999. Diet, Status and Decomposition at Weingarten: Trace Element and Isotope Analyses of Early Mediaeval Skeletal Material. *Journal of Archaeological Science* **26**, 675-685.

Schwartz, JH., 2007. *Skeleton Keys: An Introduction to Human Skeletal Morphology, Development, and Analysis.* Oxford University Press, New York.

Sham, TK., 2002. Synchrotron Radiation: An Overview. In: GS. Henderson and DR. Baker, Eds., *Synchrotron Radiation: Earth, Environmental and Material Applications*. Mineralogical Association of Canada, Ottawa.

Sillen, A., 1989. Diagenesis of the inorganic phase of cortical bone. In: TD. Price, Ed. *The Chemistry of Prehistoric Human Bone*. Cambridge University Press, Cambridge.

Sillen, A., JC. Sealy and NJ. van der Merwe, 1989. Chemistry and Paleodietary Research: No More Easy Answers. *American Antiquity* **54**, 504-512.

Soremark, R. and K. Samsahl, 1961. Gamma-ray spectrometric analysis of elements in normal human enamel. *Archives of Oral Biology* **6**, 275-283.

Soremark, R. and K. Samsahl, 1962. Gamma-ray spectrometric analysis of elements in normal human dentine. *Journal of Dental Research* **41**, 603-606.

Swanston, T., T. Varney, I. Coulthard, R. Feng, B. Bewer, R. Murphy, C. Hennig and D. Cooper, 2012. Element localization in archaeological bone using synchrotron radiation X-ray fluorescence: identification of biogenic uptake. *Journal of Archaeological Science* **39**, 2409-2413.

Tang, Z., SN. Sahu, MA. Khadeer, G. Bai, RB. Franklin and A. Gupta, 2006. Overexpression of the ZIP1 zinc transporter induces an osteogenic phenotype in mesenchymal stem cells. *Bone* **38**, 181-198.

Tomboulian, DH. and PL. Hartman, 1956. Spectral and Angular Distribution of Ultraviolet Radiation from the 300-MeV Cornell Synchrotron. *Physical Review* **102**, 1423-1447.

Trueman, CN. and DM. Martill, 2002. The Long-Term Survival of Bone: The Role of Bioerosion. *Archaeometry* **44**, 371-382.

Ulian, G., G. Valdrè, M. Corno and P. Ugliengo, 2013. Periodic ab initio bulk investigation of hydroxylapatite and type A carbonated apatite with both pseudopotential and all-electron basis sets for calcium atoms. *American Mineralogist* **98**, 410-416.

Underwood, EJ. and W. Mertz, 1987. In: W. Mertz, ed., *Trace Elements in Human and Animal Nutrition*, Fifth Edition. Academic Press, Inc., London. Chap. 1.

van Klinken, GJ., 1999. Bone Collagen Quality Indicators for Paleodietary and Radiocarbon Measurements. *Journal of Archaeological Science* **26**, 687-695.

Veksler, V., 1945. A New Method of Acceleration of Relativistic Particles. *Journal of Physics (USSR)* **9,** 153-157.

Vuorinen, HS., S. Pihlman, H. Mussalo-Rauhamaa, U. Tapper and T. Varrela, 1996. Trace and heavy metal analyses of a skeletal population representing the town people in Turku (Åbo), Finland in the 16th-17th centuries: with special reference to gender, age and social background. *Science of the Total Environment* **177**, 145-160.

Waldron, T., 2009. *Paleopathology*. Cambridge University Press, Cambridge.

Weiner, S., 2010. *Microarchaeology: Beyond the Visible Archaeological Record.* Cambridge University Press, Cambridge. Chap. 5.

Weiner, S., I. Sagi and L. Addadi, 2005. Choosing the Crystallization Path Less Traveled. *Science* **309**, 1027-1028.

Weiner, S. and H. D. Wagner, 1998. The material Bone: Structure-Mechanical Function Relations. *Annual Review of Materials Science* **28**, 271-298.

White, CD. and GJ. Armelagos, 1997. Osteopenia and Stable Isotope Ratios in Bone Collagen of Nubian Female Mummies. *American Journal of Physical Anthropology* **103**, 185-199.

White, TD., MT. Black and PA. Folkens, 2012. *Human Osteology, Third Edition*. Academic Press, Amsterdam. Chap. 3.

Williams, JS., CD. White and FJ. Longstaffe, 2005. Trophic Level and Macronutrient Shift Effects Associated With the Weaning Process in the Postclassic Maya. *American Journal of Physical Anthropology* **128**, 781-790.

Willmott, P., 2011. *An Introduction to Synchrotron Radiation: Techniques and Applications*. Wiley, Chichester.

Winick, H., Ed., 1994. *Synchrotron Radiation Sources, a Primer*. World Scientific, Singapore.

Wittmers Jr., LE., AC. Aufderheide, JG. Pounds, KW. Jones and JL. Angel, 2008. Problems in Determination of Skeletal Lead Burden in Archaeological Samples: An Example From the First African Baptist Church Population. *American Journal of Physical Anthropology* **136**, 379-386.

Wood, JW., GR. Milner, HC. Harpending and KM. Weiss, 1992. The Osteological Paradox: Problems of Inferring Prehistoric Health from Skeletal Samples. *Current Anthropology* **33**, 343-370.

Wright, LE. and HP. Schwarcz, 1996. Infrared and Isotopic Evidence for Daigenesis of Bone Apatite as Dos Pilas, Guatemala: Palaeodietary Implications. *Journal of Archaeological Science* **23**, 933-944.

Wrobel, G., 2007. Issues related to determining burial chronology by Fluorine analysis of bone from the Maya archaeological site of Chau Hiix, Belize. *Archaeometry* **49**, 699-711.

Zaichick, S., and V. Zaichick, 2010. Method and portable facility for energy-dispersive X-ray fluorescent analysis of zinc content in needle-biopsy specimens of prostate. *X-ray Spectrometry* **39**, 83-89.

Zapata, J., C. Pérez-Sirvent, MJ. Martínez-Sánchez and P. Tovar, 2006. Diagenesis, not biogenesis: Two late Roman skeletal examples. *Science of the Total Environment* **369**, 357-368.

Zoeger, N., C. Streli, P. Wobrauschek, C. Jokubonis, G. Pepponi, P. Roschger, J. Hofstaetter, A. Berzlanovich, D. Wegrzynek, E. Chinea-Cano, A. Markowicz, R. Simon and G. Falkenberg, 2008. Determination of the elemental distribution in human joint bones by SR micro XRF. *X-ray Spectrometry* **37**, 3-11.

APPENDIX A: SOME USEFUL INFORMATION FOR NON-SCIENTISTS

Table A.1. SI prefixes and some notes on scales using length as an example.

Unit Name	Abbreviation	Multiplier	Decimal	Fraction	Notes
Terametre	Tm	10^{12}	1 000 000 000 000	trillion	
Gigametre	Gm	10^9	1 000 000 000	billion	
Megametre	Mm	10^6	1 000 000	million	
Kilometre	km	10^3	1 000	thousand	
meter	m	1	1	-	
centimetre	cm	10^{-2}	0.01	hundredth	~ width of index finger
millimetre	mm	10^{-3}	0.001	thousandth	
micrometre	μm	10^{-6}	0.000 001	millionth	~ the size of a cell or bacteria
nanometre	nm	10^{-9}	0.000 000 001	billionth	a ribosome is ~ 20 nm in diameter, typically used to measure the wavelength of light
Angstrom	Å	10^{-10}	0.000 000 000 1	-	used mainly by chemists to measure bond lengths, which range from 2-5 Å
picometre	pm	10^{-12}	0.000 000 000 001	trillionth	atoms average several hundred pm in diameter

Other useful notes:

1) 1 amu = 1.66 x 10^{-24} g - approximate mass of one proton or neutron.

2) Parts Per Million = ppm = mg/kg = μg/g = μL/L (also if 1mL has a mass of 1g = μg/mL)

3) ‰ (permille) - used in stable isotope analysis is actually equivalent to parts per thousand

4) eV (electron volt) = 1.6 x 10^{-19} J = kinetic energy of a single electron accelerated across 1 Volt.   For light λ(nm) = 1239.84/E(eV)

Table A.2. List of elements and molecular ions mentioned in the thesis arranged alphabetically by symbol.

Element Symbol	Name	Atomic #	Main ion
As	Arsenic	33	3+*
Ba	Barium	56	2+
Br	Bromine	35	1-*
C	Carbon	6	4+*
Ca	Calcium	20	2+
Cd	Cadmium	48	2+
Co	Cobalt	27	2+*
Cr	Chromium	24	2+*
Cu	Copper	29	2+*
F	Fluorine	9	1-
Fe	Iron	26	3+*
H	Hydrogen	1	1+
I	Iodine	53	1-*
K	Potassium	19	1+
Li	Lithium	3	1+
Mg	Magnesium	12	2+
Mn	Manganese	25	2+*
Mo	Molybdenum	42	6+*
N	Nitrogen	7	3+*
Ni	Nickel	28	2+*
O	Oxygen	8	2-
P	Phosphorus	15	5+*
Sb	Antimony	51	3+*
Se	Selenium	34	4+*
Si	Silicon	14	4+
Sr	Strontium	38	2+
V	Vanadium	23	5+*
Zn	Zinc	30	2+

Molecular Ions		
Ion	Name	Ion Charge
CO_3	Carbonate	2-
OH	Hydroxide	1-
PO_4	Phosphate	3-

* Element is capable of having several ionic charges, only the most common is listed.

APPENDIX B: DETAILED OSTEOLOGIES OF SAMPLES

A note on osteometrics:

In the calculation of numerical means of osteological measurements I have followed the suggestion of White *et al.* (2012) and presented the mean values as:

$$\text{Mean} \pm \sigma_M$$

where σ_M is the **standard error of the mean** and is given by the **standard deviation** (σ) of the individual measurements divided by the square root of the number of measurements.

$$\sigma_M = \sigma/N^{1/2}$$

Why?   Basically, the standard deviation of the sample set is a measure of the difference between any individual measurement and the sample mean.   The standard error is a measure of the difference between the **sample mean and the theoretic true mean** which the sample mean is supposed to represent.   Thus, σ_M is a better estimate of the error of the measurement assuming of course that the correct measurement was done and done correctly. (In that case the theoretical distribution is represented in part by the actual distribution of measurements.) The magnitude of the error decreases with an increase in the number of values measured even if the standard deviation of the measurements remains the same, or put another way, as the sample size increases we have more confidence that the mean is an accurate representation of the true value.

Numeric ranges of error can then be calculated based on the confidence limits required, as such (Johnson, 1988):

Confidence Limit	± numeric range
68 %	$\pm \sigma_M$
95 %	$\pm 1.96 \sigma_M$
98 %	$\pm 2.33 \sigma_M$

Note: The standard deviation and the standard error only relate to a single group or distribution of measurements (one measurement), they do not have any bearing on comparing one measurement with another.   I state this explicitly as I have found a confusing plethora of uses of statistical terms, symbols and uses in the literature, even in

elementary statistical texts.

Within the osteometric tables in the appendix values in brackets were those which were roughly estimated because of partial destruction of the element being measured. Where a value is missing the measurement could not even be estimated because of significant destruction of the bone.

B-1: Samples DA1 and DA2

For Section #: DA1, DA2   Master's Thesis Bone Form / Mandible

Recorded By: Steven Naftel   **Date Completed:** Dec. 23, 2011
Site Name: Varden (AdHa-1)   **Skeleton #:** 6

Description:

Right Condylar Head and posterior portion of right Ramus up to the Mandibular fossa are fractured and missing post-mortem, otherwise the mandible is in excellent condition. There is a small amount of osteophytic lipping on the anterior edge of the remaining condyl. The left second molar and left 1st incisor are missing post-mortem. All other teeth show significant wear and alveolar resorption. Tooth 47 has large chip of enamel broken off from distal-lingual quadrant, sharp edge with no rounding suggests post-mortem damage.

Pathologies:

1 apical abscess surrounding root of right premolar 1 with labial drainage and sharp edges, suggestive of active infection. Oval shaped opening measuring 6.2 X 7.6 mm. All incisors have had their crowns completely worn away. Tooth 44 has small chips of remaining enamel broken off on both the lingual and buccal sides. Tooth 36 displays cracking of tooth crown and slight chipping of enamel on the lingual edge.

Non-Metrics:

Mandibular Torus (A, P, T, -) . . . . A
Accessory Mental Foramen (A, P, #) . . . . . A
Accessory Mandibular Foraman (A, P, #) . . A
Mylo-hyoid Bridge (A, P, -) . . . . A
3rd Molar Agenesis (A, P, -) . . . . A
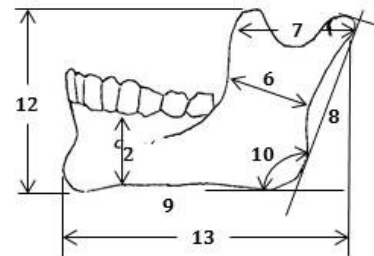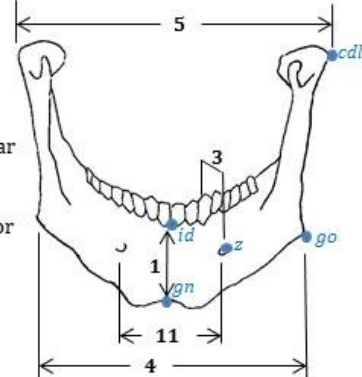
Metrics: Compilation from: Brothwell 1981; Buikstra and Ubelaker 1994; Schwartz 2007 (From left side) ($\sigma_M = \sigma/N^{\frac{1}{2}}$)

Measurement (mm)	Trial 1	Trial 2	Trial 3	Trial 4	Trial 5	Mean ± σ_M
1) Symphyseal Height (Chin Height) id-gn (H_1)	30.90	32.08	30.50	30.62	31.22	31.06 ± 0.283
2) Height of Mandibular Body (at Mentale)	28.80	29.00	29.12	28.78	29.00	28.94 ± 0.065
3) Breadth of Mandibular Body (at Mentale)	10.62	10.32	10.42	10.22	10.72	10.46 ± 0.093
4) Bigonial Width go-go	(108.10)	(111.14)	(111.16)	(110.88)	(111.82)	(110.62)
5) Bicondylar Breadth cdl-cdl (BCB, W_1)	(128.80)	(125.48)	(129.32)	(125.60)	(129.72)	(127.78)
6) Minimum Ramus Breadth (RB')	33.00	33.00	33.00	33.00	32.60	32.92 ± 0.080
7) Maximum Ramus Breadth	43.30	42.42	42.70	43.10	43.00	42.90 ± 0.155
8) Maximum Ramus Height go-cdl	52.38	52.60	51.42	51.12	50.50	51.60 ± 0.392
9) Mandibular Body Length (Maximum Projection Length) gn-go	77.90	80.06	75.08	79.70	80.60	78.67 ± 1.005
10) Mandibular Angle	130.0	129.0	130.5	128.5	126.0	128.8 ± 0.78
11) Foramen Mentalia Breadth z-z	48.38	49.40	48.30	48.60	47.50	48.44 ± 0.304
12) Coronoid Process Height (CrH)	53.42	54.10	54.38	54.22	55.20	54.26 ± 0.285
13) Mandibular Length (ML, MBL)	106.00	107.62	107.80	106.12	109.38	107.38 ± 0.621

For Section #: DA1, DA2 Master's Thesis Bone Form / Mandible

Recorded By: Steven Naftel   **Date Completed:** Dec. 23, 2011
Site Name: Varden (AdHa-1)   **Skeleton #: 6**

Tooth	FDI	48	47	46	45	44	43	42	41	31	32	33	34	35	36	37	38
	Mühlreiter	$_3$M	$_2$M	$_1$M	$_2$P	$_1$P	$_1$C	$_2$I	$_1$I	I$_1$	I$_2$	C$_1$	P$_1$	P$_2$	M$_1$	M$_2$	M$_3$
# LEH		0	0	0	0	0	0	na	na	X	na	0	0	0	0	X	0
# Caries/Type		0	0	0	0	0	0	0	0	X	0	0	0	0	0	X	0
# Abscess/Drain		N	n	n	n	1-1	n	n	n	X	n	n	n	n	n	X	n
Wear Score		2	2	2	2	3	3	3	3	X	3	3	3	2	2	X	2
Calculus Score		1	2	1	1	na	1	na	na	X	na	1	1	1	1	X	1
Alveolar Res. Level		1	1	1	1	1	1	1	1	X	1	1	1	1	1	X	1

Missing Antemortem: ▮
Missing Postmortem: XX
Caries Type: 1-occlusal, 2-interproximal, 3-buccal/lingual, 4-cervical, 5-root, 6-too large to assess site (Buikstra and Ubelakere 1994)
Abscess Drainage: 1-buccal/linbial, 2-lingual
Wear Score: 0 – no attrition, 1 - attrition to enamel 2- attrition to dentine, 3 – attrition to pulp
Calculus Score: 1 – slight, 2 – moderate, 3 – considerable (Brothwell 1981)
Alveolar Resorption Level: 0 – CEJ, 1 – reduction, 2 – Attachment lower half of root 3 – attachment lower 2/3 of root
   For Missing Teeth: N – Not healed, H - Healed

Wear Pattern
Caries Location
Abscess Location
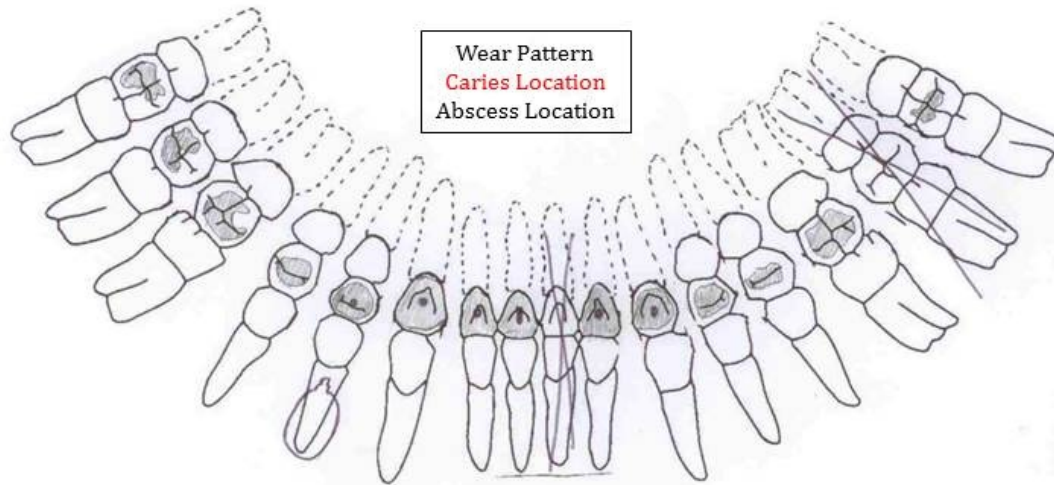
Notes:

Master's Thesis Bone Form / Mandible: Pictures

For Section #: DA1, DA2

Recorded By:
   Steven Naftel
Site Name:
   Varden (AdHa-1)

Skeleton #: 6

Date Completed:
   Dec. 23, 2011

Top View

Front View

Right Side

Left Side

Master's Thesis Bone Form / Mandible: Pictures

For Section #: DA1, DA2

Recorded By:
Steven Naftel
Site Name:
Varden (AdHa-1)

Skeleton #: 6

Date Completed:
Dec. 23, 2011

Rear View

Bottom View

Pathology:

Sampling Procedure

1) Remove neighbouring teeth from the mandible
2) Cut abcess to either side through empty sockets
3) Tooth 44 and 34 will be retained (and destroyed) as part of the samples.
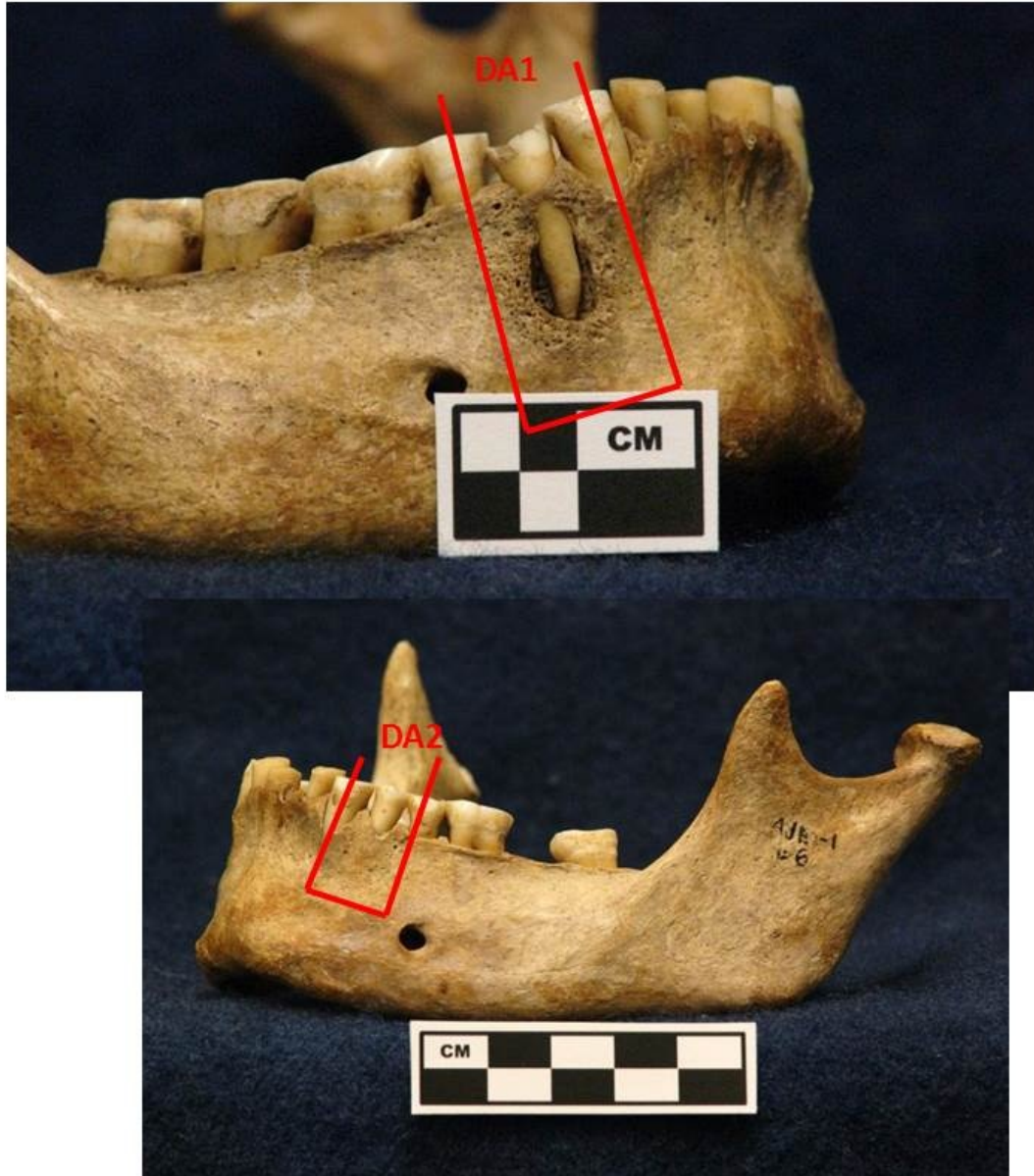
B-2: Samples DA3 and DA9

For Section #: DA3, DA9   Master's Thesis Bone Form / Mandible

Recorded By: Steven Naftel   **Date Completed:** Jan. 5, 2012
**Site Name:** Varden (AdHa-1)   **Skeleton #: 7**

Description: Right ramus is broken off just behind second molar with some weathering to the exposed interior of the body. The labial surface of the right body is broken away up to the level of the first molar. It is difficult to determine if the 3rd molar was present at the time of death.

The inferior posterior edge of the left body is also broken off along with the left condyle. The left coronoid process was broken but has been refitted. The teeth show significant wear and periodontal resorption particularly around the molars.

There are significant fenestrations along the front teeth roots, 44, 43, 33, 34, 35. Tooth 31 is missing post mortem.

Pathologies: The Left 3rd molar (38) is impacted at about a 15° angle to the second molar. The site of impaction on the second molar is damaged but it is difficult to determine if it is carious. The 3rd molar also appears to be broken in two from the mid-crown through the posterior root (see diagram). The surface is smooth with rounded edges suggesting an ante mortem condition.

Much of the left first molar (36) crown (lingual side) has been broken off post mortem. The incisor and canine crowns are completely worn away. The tooth wear is significant and uneven.

(-continued on next page-)

Non-Metrics:

Mandibular Torus (A, P, T, -) . . . . .A
Accessory Mental Foramen (A, P, #) . . . . . A
Accessory Mandibular Foraman (A, P, #) . . A
Mylo-hyoid Bridge (A, P, -) . . . . P, complete, centre
3rd Molar Agenesis (A, P, -) . . . . A
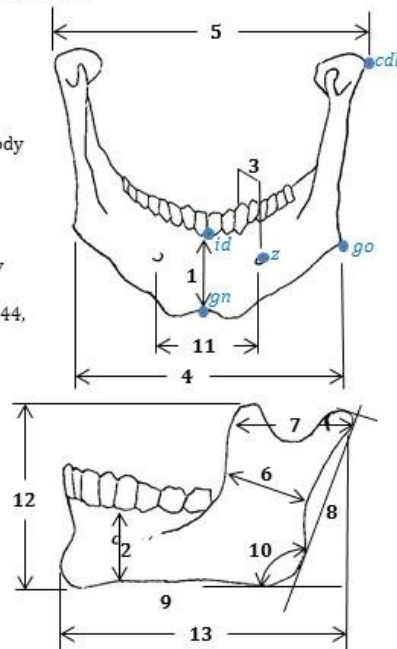
Metrics: Compilation from: Brothwell 1981; Buikstra and Ubelaker 1994; Schwartz 2007 (From left side) ($\sigma_M = \sigma/N^{\frac{1}{2}}$)

Measurement (mm)	Trial 1	Trial 2	Trial 3	Trial 4	Trial 5	Mean ± σ_M
1) Symphyseal Height (Chin Height) *id-gn* (H_1)	31.92	31.70	31.38	31.60	31.68	31.66 ± 0.087
2) Height of Mandibular Body (at Mentale)	35.00	34.32	34.42	34.92	34.30	34.59 ± 0.152
3) Breadth of Mandibular Body (at Mentale)	13.62	13.62	13.40	13.30	12.84	13.36 ± 0.143
4) Bigonial Width *go-go*	-	-	-	-	-	-
5) Bicondylar Breadth *cdl-cdl* (BCB, W_1)	-	-	-	-	-	-
6) Minimum Ramus Breadth (RB')	38.20	37.94	38.20	39.06	38.10	38.30 ± 0.196
7) Maximum Ramus Breadth	-	-	-	-	-	-
8) Maximum Ramus Height *go-cdl*	-	-	-	-	-	-
9) Mandibular Body Length (Maximum Projection Length) *gn-go*	(81.84)	(77.52)	(86.90)	(90.90)	(86.10)	(84.65)
10) Mandibular Angle	114.5	116.0	112.5	113.0	113.5	113.9 ± 0.62
11) Foramen Mentalia Breadth *z-z*	46.22	45.72	46.08	46.08	45.92	46.00 ± 0.085
12) Coronoid Process Height (CrH)	70.40	70.00	70.30	72.06	69.94	70.54 ± 0.390
13) Mandibular Length (ML, MBL)	-	-	-	-	-	-

For Section #: DA3, DA9   Master's Thesis Bone Form / Mandible

Recorded By: Steven Naftel   **Date Completed**: Jan. 5, 2012
Site Name: Varden (AdHa-1)   **Skeleton #: 7**

Pathologies: Continued

35 has significant lingual chip ante mortem, 44 has a labial chip post mortem. 45 has a lingual chip ante mortem.

37 has an interproximal carries. 47 has an interproximal carries which could be from the impaction of 48.

Apical abscess surrounding the distal root of 46 but also encompasses the mesial root, possibly two sites of infection grown together judging by the dumbbell shape of the space. The abscess has buccal drainage and appears to be active at time of death. The drainage opening is 9mm x 6mm.   There is a rounded pocket between the roots of 34 and 35 which may be evidence of another healed abscess on 35.

For Section #: DA3, DA9   Master's Thesis Bone Form / Mandible

Recorded By: Steven Naftel   **Date Completed:** Jan. 5, 2012
Site Name: Varden (AdHa-1)   **Skeleton #:** 7

Tooth	FDI	48	47	46	45	44	43	42	41	31	32	33	34	35	36	37	38
	Mühlreiter	$_3$M	$_2$M	$_1$M	$_2$P	$_1$P	$_1$C	$_2$I	$_1$I	I$_1$	I$_2$	C$_1$	P$_1$	P$_2$	M$_1$	M$_2$	M$_3$
# LEH		X	0	0	0	0	na	na	na	X	na	0	na	na	0	0	0
# Caries/Type		X	1-2	0	0	0	0	0	0	X	0	0	0	0	0	1-2	0
# Abscess/Drain		X	0	1-1	0	0	0	0	0	X	0	0	0	?-1	0	0	0
Wear Score		X	3	3	3	3	3	3	3	X	3	3	3	3	3	3	3
Calculus Score		X	1	1	1	1	1	1	1	X	1	1	1	1	1	1	1
Alveolar Res. Level		X	3	2	1	1	1	1	1	X	1	1	1	1	2	2	3

Missing Antemortem: ▮
Missing Postmortem: XX
Caries Type: 1-occlusal, 2-interproximal, 3-buccal/lingual, 4-cervical, 5-root, 6-too large to assess site (Buikstra and Ubelakere 1994)
**Abscess Drainage:** 1-buccal/labial, 2-lingual
Wear Score: 0 – no attrition, 1 - attrition to enamel 2- attrition to dentine, 3 – attrition to pulp
Calculus Score: 1 – slight, 2 – moderate, 3 – considerable (Brothwell 1981)
Alveolar Resorption Level: 0 – CEJ, 1 – reduction, 2 – Attachment lower half of root, 3 – attachment lower 2/3 of root
  For Missing Teeth: N – Not healed, H - Healed

Wear Pattern
Caries Location
Abscess Location

Notes:

Master's Thesis Bone Form / Mandible: Pictures

For Section #: DA3, DA9

Recorded By:
Steven Naftel

Site Name:
Varden (AdHa-1)

Skeleton #: 7

Date Completed:
Jan. 5, 2012

Top View

Front View

Right Side

Left Side

Master's Thesis Bone Form / Mandible: Pictures

For Section #: DA3, DA9

Recorded By:
Steven Naftel

Site Name:
Varden (AdHa-1)

Skeleton #: 7

Date Completed:
Jan. 5, 2012

Rear View

Bottom View


Pathology:

Sampling Procedure

1) Remove neighbouring teeth from the mandible
2) Cut abcess to either side through empty sockets
3) Tooth 46 and possibly 35 will be retained (and destroyed) as part of the samples.

B-3: Sample DA4

For Section #: DA4   Master's Thesis Bone Form / Mandible

Recorded By: Steven Naftel   **Date Completed:** Dec. 29, 2011
Site Name: Varden (AdHa-1)   **Skeleton #:** 3

Description: Mandible of younger individual, in excellent condition although there is some enamel cracking evident. Lateral knob of right condyle is broken off post-mortem. Mandible is broken in two along the symphyseal line but has been refitted. Teeth 41, 42, 43, 32, and 33 missing post-mortem.

Pathologies: Teeth 38 (buccal), 36 (lingual) and 46 (lingual) have enamel chips with sharp edges showing no wear, suggesting post-mortem.
Tooth 38 has 1 buccal carries. Tooth 47 has one occlusal carries. Overall minor wear and calculus on all teeth with minor alveolar resorption.

Non-Metrics:

Mandibular Torus (A, P, T, -) . . . . A
Accessory Mental Foramen (A, P, #) . . . . . A
Accessory Mandibular Foraman (A, P, #) . . A
Mylo-hyoid Bridge (A, P, -) . . . . A
3rd Molar Agenesis (A, P, -) . . . . A
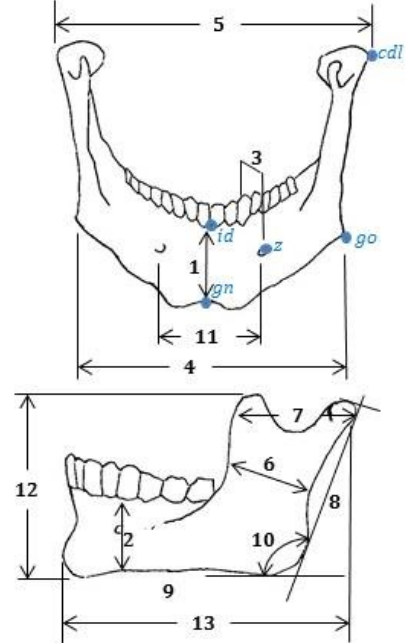
Metrics: Compilation from: Brothwell 1981; Buikstra and Ubelaker 1994; Schwartz 2007 (From left side) ($\sigma_M = \sigma/N^{\frac{1}{2}}$)

Measurement (mm)	Trial 1	Trial 2	Trial 3	Trial 4	Trial 5	Mean ± σ_M
1) Symphyseal Height (Chin Height) id-gn (H_1)	30.74	30.78	31.00	30.90	30.58	30.80 ± 0.072
2) Height of Mandibular Body (at Mentale)	28.60	28.50	28.94	28.44	28.58	28.61 ± 0.087
3) Breadth of Mandibular Body (at Mentale)	12.28	13.18	12.42	12.66	12.32	12.57 ± 0.166
4) Bigonial Width go-go	100.16	99.40	99.60	100.24	100.24	99.93 ± 0.178
5) Bicondylar Breadth cdl-cdl (BCB, W_1)	(126.56)	(125.10)	(126.12)	(125.98)	(126.32)	(126.02)
6) Minimum Ramus Breadth (RB')	34.78	35.00	34.72	34.82	34.56	34.78 ± 0.071
7) Maximum Ramus Breadth	41.70	42.48	42.42	42.48	41.60	42.14 ± 0.199
8) Maximum Ramus Height go-cdl	60.46	60.18	60.88	60.88	61.00	60.68 ± 0.155
9) Mandibular Body Length (Maximum Projection Length) gn-go	77.80	74.18	75.40	73.18	76.10	75.33 ± 0.795
10) Mandibular Angle	114.5	115.0	114.0	113.0	114.0	114.1 ± 0.33
11) Foramen Mentalia Breadth z-z	47.38	47.28	47.82	47.18	47.22	47.38 ± 0.116
12) Coronoid Process Height (CrH)	63.60	63.30	63.72	63.90	63.78	63.66 ± 0.102
13) Mandibular Length (ML, MBL)	97.22	98.72	97.06	99.82	99.62	98.49 ± 0.581

For Section #: DA4   Master's Thesis Bone Form / Mandible

Recorded By: Steven Naftel   **Date Completed:** Dec. 29, 2011
Site Name: Varden (AdHa-1)   **Skeleton #:** 3

Tooth	FDI	48	47	46	45	44	43	42	41	31	32	33	34	35	36	37	38
	Mühlreiter	$_3M$	$_2M$	$_1M$	$_2P$	$_1P$	$_1C$	$_2I$	$_1I$	I_1	I_2	C_1	P_1	P_2	M_1	M_2	M_3
# LEH		0	0	0	0	0	X	X	X	0	X	X	0	0	0	0	0
# Caries/Type		0	1-1	0	0	0	X	X	X	0	X	X	0	0	0	0	1-3
# Abscess/Drain		0	0	0	0	0	X	X	X	0	X	X	0	0	0	0	0
Wear Score		1	1	2	2	2	X	X	X	2	X	X	2	1	2	2	1
Calculus Score		1	1	1	1	1	X	X	X	1	X	X	1	1	1	1	1
Alveolar Res. Level		0	0	1	0	1	X	X	X	1	X	X	1	0	1	0	0

Missing Antemortem: ▮
Missing Postmortem: XX
Caries Type: 1-occlusal, 2-interproximal, 3-buccal/lingual, 4-cervical, 5-root, 6-too large to assess site (Buikstra and Ubelakere 1994)
Abscess Drainage: 1-buccal/labial, 2-lingual
Wear Score: 0 – no attrition, 1 - attrition to enamel 2- attrition to dentine, 3 – attrition to pulp
Calculus Score: 1 – slight, 2 – moderate, 3 – considerable (Brothwell 1981)
Alveolar Resorption Level: 0 – CEJ, 1 – reduction, 2 – Attachment lower half of root, 3 – attachment lower 2/3 of root
   For Missing Teeth: N – Not healed, H - Healed

Wear Pattern
Caries Location
Abscess Location

Notes:

Master's Thesis Bone Form / Mandible: Pictures

For Section #: DA4

Recorded By:
  Steven Naftel
Site Name:
  Varden (AdHa-1)
Skeleton #: 3

Date Completed:
  Dec. 29, 2011

Top View

Front View

Right Side

Left Side

Master's Thesis Bone Form / Mandible: Pictures

For Section #: DA4

Recorded By:
    Steven Naftel
Site Name:
    Varden (AdHa-1)
Skeleton #: 3
Date Completed:
    Dec. 29, 2011

Rear View

Bottom View

Pathology:

Sampling Procedure

1) Remove neighbouring teeth from the mandible
2) Cut either side of tooth through empty sockets
3) Tooth 44 will be retained (and destroyed) as part of the samples.

B-4: Samples DA5 and DA8

### For Section #: DA5, DA8   Master's Thesis Bone Form / Mandible

Recorded By: Steven Naftel   **Date Completed**: Dec. 30, 2011
Site Name: San Pedro   **Skeleton #**: 11 -3/1

Description: Mandible of a younger individual, 3rd molars not fully erupted. There is a crack running through the left body from the left third molar (38) posteriorly and inferiorly which has been refitted. The right condyle mesial side of the knob has been broken off post-mortem. All teeth are present with minimal wear. Teeth 42, 43, 44, 33 have fenestrations exposing the anterior of the teeth roots.

Pathologies: The left 2nd incisor (32) crown has been chipped post-mortem with only about ¼ of the crown left. The left 2nd incisor also has an apical abscess at the base of the root, about 3.5 mm in diameter, which has spread to encompass the 1st incisor. The abscess opens labialy and superiorly between the incisors (having a total opening of 7.5 mm). The abscess has rounded edges indicative of being inactive at the time of death. Both left and right, 1st premolars and canines show enamel hypoplasias. The right 1st premolar is cracked through the crown.

Non-Metrics:

Mandibular Torus (A, P, T, -) . . . . A
Accessory Mental Foramen (A, P, #) . . . . . A
Accessory Mandibular Foraman (A, P, #) . . A
Mylo-hyoid Bridge (A, P, -) . . . . A
3rd Molar Agenesis (A, P, -) . . . . A
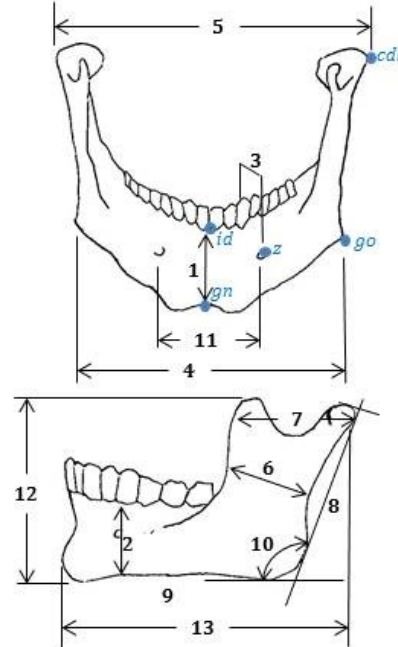
Metrics: Compilation from: Brothwell 1981; Buikstra and Ubelaker 1994; Schwartz 2007 (From left side) ($\sigma_M = \sigma/N^{\frac{1}{2}}$)

Measurement (mm)	Trial 1	Trial 2	Trial 3	Trial 4	Trial 5	Mean ± σ_M
1) Symphyseal Height (Chin Height) *id-gn* (H_1)	29.64	28.40	28.58	29.12	28.60	28.87 ± 0.227
2) Height of Mandibular Body (at Mentale)	28.60	27.10	28.56	28.20	28.88	28.27 ± 0.311
3) Breadth of Mandibular Body (at Mentale)	13.82	13.86	13.62	13.44	13.42	13.63 ± 0.092
4) Bigonial Width *go-go*	86.84	86.88	87.00	87.00	86.90	86.92 ± 0.032
5) Bicondylar Breadth *cdl-cdl* (BCB, W_1)	122.10	122.12	122.16	122.10	122.42	122.18 ± 0.061
6) Minimum Ramus Breadth (RB')	30.00	29.50	30.10	30.10	30.00	29.94 ± 0.112
7) Maximum Ramus Breadth	37.18	37.48	37.00	36.22	37.58	37.09 ± 0.241
8) Maximum Ramus Height *go-cdl*	57.74	57.86	57.48	57.96	57.32	57.67 ± 0.119
9) Mandibular Body Length (Maximum Projection Length) *gn-go*	69.92	69.00	69.70	67.60	68.10	68.86 ± 0.448
10) Mandibular Angle	116.5	115.5	117.0	117.5	117.0	116.6 ± 0.35
11) Foramen Mentalia Breadth *z-z*	44.00	44.08	44.44	44.00	38.96	43.10 ± 1.037
12) Coronoid Process Height (CrH)	53.02	53.08	53.00	53.00	53.10	53.04 ± 0.021
13) Mandibular Length (ML, MBL)	92.88	96.72	93.10	91.62	93.00	93.46 ± 0.857

For Section #: DA5, DA8   Master's Thesis Bone Form / Mandible

Recorded By: Steven Naftel   **Date Completed:** Dec. 30, 2011
Site Name: San Pedro   **Skeleton #:** 11-3/1

Tooth	FDI	48	47	46	45	44	43	42	41	31	32	33	34	35	36	37	38
	Mühlreiter	$_3M$	$_2M$	$_1M$	$_2P$	$_1P$	$_1C$	$_2I$	$_1I$	I_1	I_2	C_1	P_1	P_2	M_1	M_2	M_3
# LEH		0	0	0	0	1	2	0	0	0	0	2	1	0	0	0	0
# Caries/Type		0	0	0	0	0	0	0	0	0	0	0	0	0	0	0	0
# Abscess/Drain		0	0	0	0	0	0	0	0	0	1-1	0	0	0	0	0	0
Wear Score		0	1	1	1	1	1	1	1	1	1	1	1	1	1	1	0
Calculus Score		1	1	1	1	1	1	1	1	1	1	1	1	1	1	1	1
Alveolar Res. Level		0	0	1	0	0	0	0	1	na	na	0	0	0	0	0	0

Missing Antemortem: █████
Missing Postmortem: XX
Caries Type: 1-occlusal, 2-interproximal, 3-buccal/lingual, 4-cervical, 5-root, 6-too large to assess site (Buikstra and Ubelakere 1994)
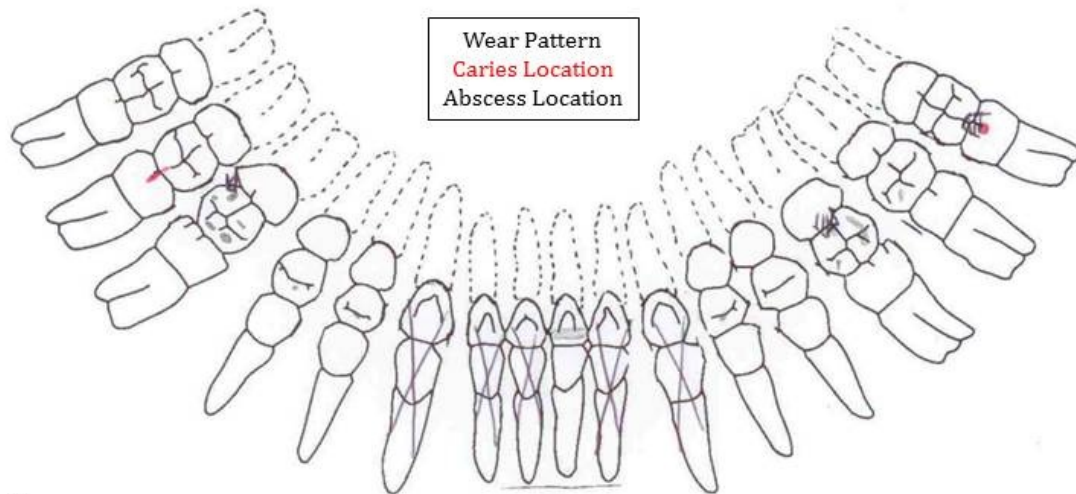**Abscess Drainage:** 1-buccal/labial, 2-lingual
Wear Score: 0 – no attrition, 1 - attrition to enamel 2- attrition to dentine, 3 – attrition to pulp
Calculus Score: 1 – slight, 2 – moderate, 3 – considerable (Brothwell 1981)
Alveolar Resorption Level: 0 – CEJ, 1 – reduction, 2 – Attachment lower half of root, 3 – attachment lower 2/3 of root
    For Missing Teeth: N – Not healed, H - Healed

Wear Pattern
Caries Location
Abscess Location

Notes:

Master's Thesis Bone Form / Mandible: Pictures

For Section #: DA5, DA8

Recorded By:
  Steven Naftel
Site Name:
  San Pedro
Skeleton #: 11-3/1

Date Completed:
  Dec. 30, 2011

Top View

Front View

Right Side

Left Side

**Master's Thesis Bone
Form / Mandible:
Pictures**

For Section #: DA5, DA8

Recorded By:
    Steven Naftel
Site Name:
    San Pedro
Skeleton #: 11-3/1
Date Completed:
    Dec. 30, 2011

Rear View

Bottom View

Pathology:

Sampling Procedure

1) Remove neighbouring teeth from the mandible
2) Cut abcess to either side through empty sockets
3) Tooth 41, 31 and 32 will be retained (and destroyed) as part of the samples.

B-5: Sample DA6

**For Section #: DA6**   **Master's Thesis Bone Form / Mandible**

Recorded By: Steven Naftel   **Date Completed**: Dec. 30, 2011
Site Name: San Pedro   **Skeleton #**: 11-3/4

Description:
Mandible is in good condition except missing left condyle post-mortem.

Pathologies: All right molars are missing ante-mortem and the alveolus is fully resorbed. On the left side the 2nd and 3rd molars are missing ante-mortem but the alveolus has not completely resorbed, but is well healed showing no evidence of sockets. Both right incisors and the left 1st incisor were lost ante-mortem. The left 2nd incisor was lost post-mortem.

The remaining teeth, with the exception of the left 2nd premolar (35) are severely worn unevenly. The distal half of the right 2nd premolar (45) crown has chipped off ante-mortem. There is a interproximal carries on the right 1st premolar along with an apical abscess, draining labialy with a 3.5 x 5 mm opening. The left canine is unevenly worn or chipped distally. The left 1st premolar crown is completely missing. The left 2nd premolar was also chipped ante-mortem in the distal labial quadrant. The left 1st molar is only partially represented by the mesial root which is slanted lingually and protruding from the labial alveolar surface.

Teeth 43, 33, and 34 show fenestrations revealing the roots.

Non-Metrics:
Mandibular Torus (A, P, T, -) . . . . A
Accessory Mental Foramen (A, P, #) . . . . . A
Accessory Mandibular Foraman (A, P, #) . . A
Mylo-hyoid Bridge (A, P, -) . . . . A
3rd Molar Agenesis (A, P, -) . . . . na
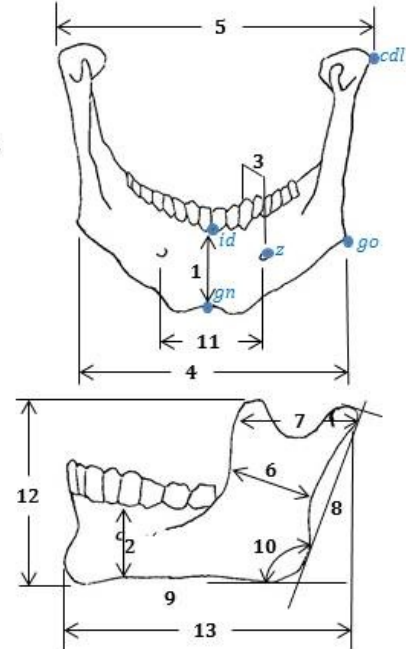
Metrics: Compilation from: Brothwell 1981; Buikstra and Ubelaker 1994; Schwartz 2007 (From left side) ($\sigma_M = \sigma/N^{1/2}$)

Measurement (mm)	Trial 1	Trial 2	Trial 3	Trial 4	Trial 5	Mean ± σ_M
1) Symphyseal Height (Chin Height) *id-gn* (H_1)	29.40	28.92	28.30	28.16	28.24	28.60 ± 0.240
2) Height of Mandibular Body (at Mentale)	31.42	31.84	30.36	30.80	30.74	31.03 ± 0.264
3) Breadth of Mandibular Body (at Mentale)	11.30	12.06	12.10	11.40	12.00	11.77 ± 0.174
4) Bigonial Width *go-go*	84.30	84.62	83.72	83.46	84.00	84.02 ± 0.205
5) Bicondylar Breadth *cdl-cdl* (BCB, W_1)	(125.60)	(122.60)	(125.00)	(124.16)	(124.76)	(124.42)
6) Minimum Ramus Breadth (RB')	33.62	33.76	34.16	34.14	33.80	33.90 ± 0.108
7) Maximum Ramus Breadth	45.50	45.50	46.10	46.08	45.62	45.76 ± 0.136
8) Maximum Ramus Height *go-cdl*	60.72	62.60	60.82	62.00	60.54	61.34 ± 0.407
9) Mandibular Body Length (Maximum Projection Length) *gn-go*	74.90	75.96	75.20	73.50	70.88	74.09 ± 0.895
10) Mandibular Angle	114.0	112.0	116.5	115.0	113.0	114.1 ± 0.78
11) Foramen Mentalia Breadth *z-z*	46.92	47.20	47.20	47.16	47.60	47.22 ± 0.109
12) Coronoid Process Height (CrH)	59.54	60.42	60.32	59.78	60.14	60.04 ± 0.166
13) Mandibular Length (ML, MBL)	100.40	106.00	105.74	107.38	105.82	105.07 ± 1.205

For Section #: DA6   **Master's Thesis Bone Form / Mandible**

Recorded By: Steven Naftel   **Date Completed:** Dec, 30, 2011
Site Name: San Pedro   **Skeleton #:** 11-3/4

Tooth	FDI	48	47	46	45	44	43	42	41	31	32	33	34	35	36	37	38
	Mühlreiter	$_3M$	$_2M$	$_1M$	$_2P$	$_1P$	$_1C$	$_2I$	$_1I$	I_1	I_2	C_1	P_1	P_2	M_1	M_2	M_3
# LEH					0	1	1				X	na	na	0	na		
# Caries/Type					0	1-2	0				X	0	0	0	0		
# Abscess/Drain					0	1-1	0				X	0	0	0	0		
Wear Score					3	3	2				X	3	3	1	3		
Calculus Score					1	1	1				X	1	1	1	1		
Alveolar Res. Level		H	H	H	3	1	1	H	H	N	X	1	1	2	3	N	N

Missing Antemortem: ▮
Missing Postmortem: XX
Caries Type: 1-occlusal, 2-interproximal, 3-buccal/lingual, 4-cervical, 5-root, 6-too large to assess site (Buikstra and Ubelakere 1994)
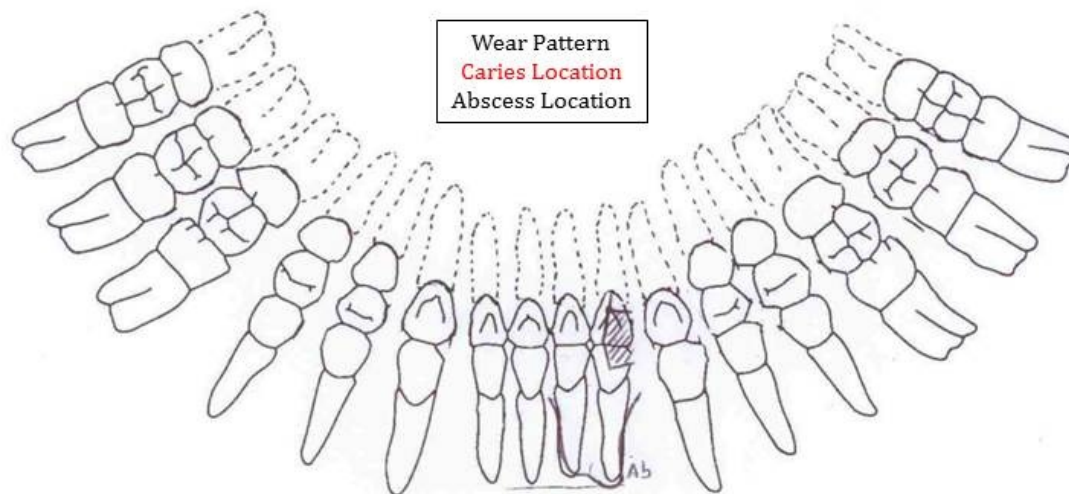**Abscess Drainage:** 1-buccal/labial, 2-lingual
Wear Score: 0 – no attrition, 1 - attrition to enamel 2- attrition to dentine, 3 – attrition to pulp
Calculus Score: 1 – slight, 2 – moderate, 3 – considerable (Brothwell 1981)
Alveolar Resorption Level: 0 – CEJ, 1 – reduction, 2 – Attachment lower half of root, 3 – attachment lower 2/3 of root
   For Missing Teeth: N – Not healed, H - Healed

Wear Pattern
Caries Location
Abscess Location

Notes:

Master's Thesis Bone Form / Mandible: Pictures

For Section #: DA6

Recorded By:
   Steven Naftel
Site Name:
   San Pedro

Skeleton #: 11-3/4

Date Completed:
   Dec. 30, 2011

Top View

Front View

Right Side

Left Side

Master's Thesis Bone Form / Mandible: Pictures

For Section #: DA6

Recorded By:
  Steven Naftel
Site Name:
  San Pedro
Skeleton #: 11-3/4
Date Completed:
  Dec. 30, 2011

Rear View

Bottom View

Pathology:

Sampling Procedure

1) Remove neighbouring teeth from the mandible
2) Cut absess to either side through empty sockets
3) Tooth 44 will be retained (and destroyed) as part of the samples.

B-6: Sample DA7

For Section #: DA7   **Master's Thesis Bone Form / Mandible**

Recorded By: Steven Naftel   **Date Completed**: Jan. 6, 2012
Site Name: San Pedro   **Skeleton #**: 4

Description: Mandible is in excellent condition except the right condyl is broken off even with the notch in the ramus. The left ramus has several cracks that have been refitted. Many of the teeth are missing post-mortem (37, 33, 32, 31, 41, 42, 44, 45, 47, 48). The remaining teeth are worn and have significant periodontal resorption.
        The right canine (43) crown is badly cracked and missing post-mortem. The left canine (33) is broken off at the level of the alveolus post-mortem.

Pathologies: The right 1st molar (46) is chipped in the distal lingual quadrant ante-mortem. The left 2nd premolar (35) is chipped in the mesial labial quadrant ante-mortem. There is a cervical carries on the buccal side of the left 3rd molar (38).

Non-Metrics:

Mandibular Torus (A, P, T, -) . . . . .A
Accessory Mental Foramen (A, P, #) . . . . . A
Accessory Mandibular Foraman (A, P, #) . . A
Mylo-hyoid Bridge (A, P, -) . . . . P, central, right
3rd Molar Agenesis (A, P, -) . . . . A
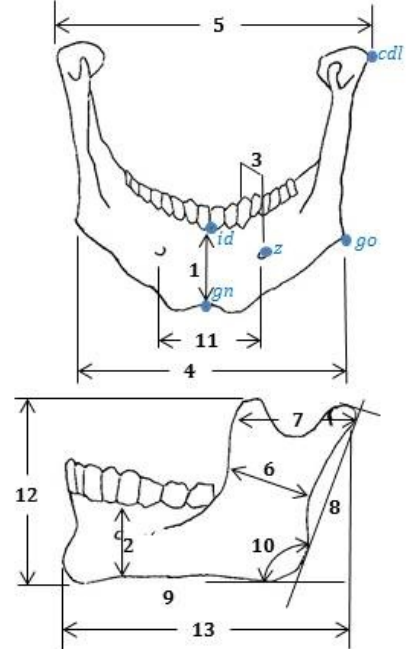
Metrics: Compilation from: Brothwell 1981; Buikstra and Ubelaker 1994; Schwartz 2007 (From left side) ($\sigma_M = \sigma/N^{\frac{1}{2}}$)

Measurement (mm)	Trial 1	Trial 2	Trial 3	Trial 4	Trial 5	Mean ± σ_M
1) Symphyseal Height (Chin Height) *id-gn* (H_1)	32.84	33.26	32.88	33.20	33.10	33.06 ± 0.084
2) Height of Mandibular Body (at Mentale)	36.00	33.00	35.70	35.40	36.40	35.30 ± 0.598
3) Breadth of Mandibular Body (at Mentale)	11.70	11.10	11.20	11.20	11.16	11.27 ± 0.108
4) Bigonial Width *go-go*	96.62	96.90	96.32	97.10	95.70	96.53 ± 0.245
5) Bicondylar Breadth *cdl-cdl* (BCB, W_1)	(125.62)	(125.60)	(124.20)	(126.10)	(125.20)	(125.34)
6) Minimum Ramus Breadth (RB')	41.70	37.00	36.70	36.70	36.68	37.76 ± 0.988
7) Maximum Ramus Breadth	48.90	48.80	47.92	48.22	48.34	48.44 ± 0.183
8) Maximum Ramus Height *go-cdl*	68.50	69.00	70.10	69.70	69.00	69.26 ± 0.284
9) Mandibular Body Length (Maximum Projection Length) *gn-go*	76.60	73.42	76.64	77.40	76.94	76.20 ± 0.709
10) Mandibular Angle	104.5	105.0	104.5	103.0	105.0	104.4 ± 0.37
11) Foramen Mentalia Breadth *z-z*	43.80	43.60	44.00	43.70	43.68	43.76 ± 0.069
12) Coronoid Process Height (CrH)	69.72	68.20	68.26	68.20	69.16	68.71 ± 0.312
13) Mandibular Length (ML, MBL)	100.00	97.30	100.30	100.86	100.66	99.82 ± 0.648

For Section #: DA7   Master's Thesis Bone Form / Mandible

Recorded By: Steven Naftel   **Date Completed:** Jan. 6, 2012
Site Name: San Pedro   **Skeleton #:** 4

Tooth	FDI	48	47	46	45	44	43	42	41	31	32	33	34	35	36	37	38
	Mühlreiter	$_3M$	$_2M$	$_1M$	$_2P$	$_1P$	$_1C$	$_2I$	$_1I$	I_1	I_2	C_1	P_1	P_2	M_1	M_2	M_3
# LEH		X	X	0	X	X	na	X	X	X	X	X	na	0	0	X	0
# Caries/Type		X	X	0	X	X	na	X	X	X	X	X	na	0	0	X	1-4
# Abscess/Drain		X	X	0	X	X	0	X	X	X	X	X	0	0	0	X	0
Wear Score		X	X	2	X	X	na	X	X	X	X	X	na	1	2	X	2
Calculus Score		X	X	1	X	X	1	X	X	X	X	X	na	1	1	X	1
Alveolar Res. Level		X	X	3	X	X	1	X	X	X	X	X	na	2	3	X	2

Missing Antemortem: ▮
Missing Postmortem: XX
Caries Type: 1-occlusal, 2-interproximal, 3-buccal/lingual, 4-cervical, 5-root, 6-too large to assess site (Buikstra and Ubelakere 1994)
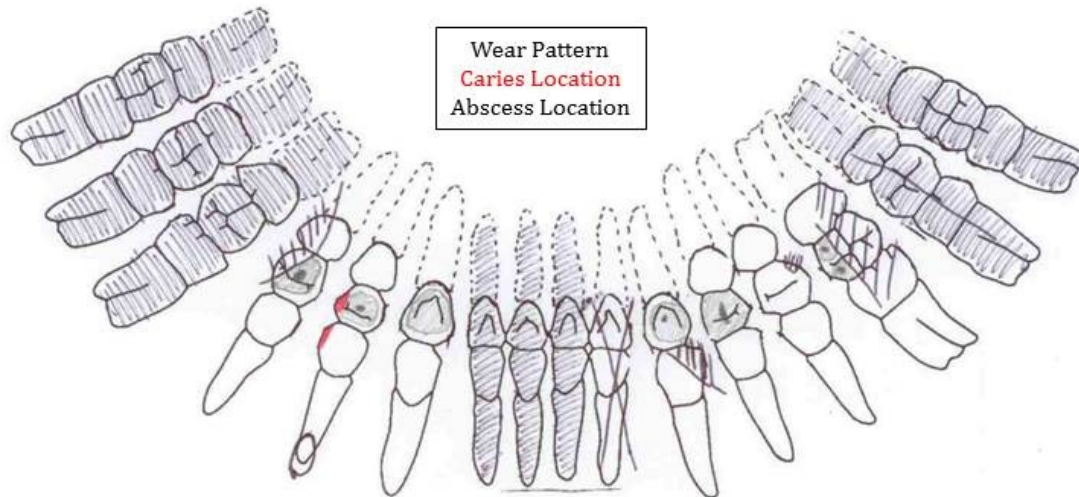**Abscess Drainage:** 1-buccal/labial, 2-lingual
Wear Score: 0 – no attrition, 1 - attrition to enamel 2- attrition to dentine, 3 – attrition to pulp
Calculus Score: 1 – slight, 2 – moderate, 3 – considerable (Brothwell 1981)
Alveolar Resorption Level: 0 – CEJ, 1 – reduction, 2 – Attachment lower half of root, 3 – attachment lower 2/3 of root
   For Missing Teeth: N – Not healed, H - Healed

Wear Pattern
Caries Location
Abscess Location

Notes:

Master's Thesis Bone Form / Mandible: Pictures

For Section #: DA7

Recorded By:
  Steven Naftel
Site Name:
  San Pedro
Skeleton #: 4

Date Completed:
  Jan. 6, 2012

Top View

Front View

Right Side

Left Side

Master's Thesis Bone Form / Mandible: Pictures

For Section #: DA7

Recorded By:
Steven Naftel

Site Name:
San Pedro

Skeleton #: 4

Date Completed:
Jan. 6, 2012

Rear View

Bottom View

Pathology:

Sampling Procedure

1) Remove neighbouring teeth from the mandible
2) Cut either side of socket 33 through empty sockets
.

B-7: Samples TB1-L and TB1-O

For Section #: TB1-L / Master's Thesis Bone Form / Vertebra
TB1-O

Recorded By: Steven Naftel   **Date Completed: Jan. 16, 2012**

Site Name: Kellis II   **Skeleton #: 265**

Description:

Lumbar Vertebra (L2), generally in excellent condition. There is a small amount of ostoephytic lipping on the articular surfaces.

Pathologies:

There is a large (17 x 8 mm) Cloaca opening on the anterior face of the body. This opening reveals a multi-chambered lytic focus penetrating deep into the body. There is also a cloaca opening on the central dorsal side of the body (5 x 8 mm) covered by a remnant of ligament within the vertebral canal.

Inferior and to the left of the cloaca is a parrot beak osteophyte, 14 mm in length.

The interior trabecula around the edge of the lesion appear sharp.

There is some new bone formation superior to the cloaca and along the inferior body margin to either side of the parrot beak.
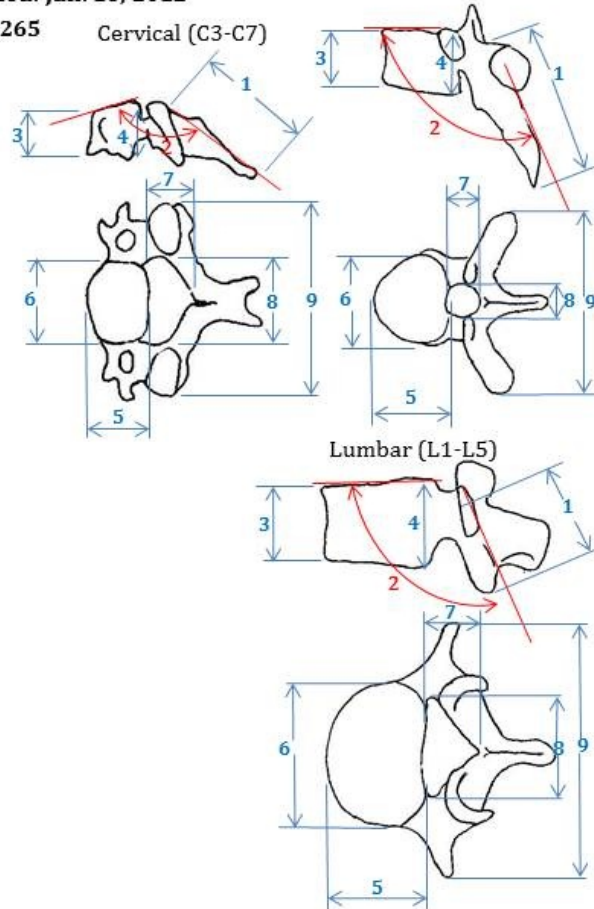
Cervical (C3-C7)

Thoracic (T1-T12)

Lumbar (L1-L5)

Non-Metrics:

Accessory transverse foramen (C3-C7) (A, P) . . . . .
Cervical Rib (C7) (A, P) . . . .

Metrics: Compilation from: Schwartz 2007; White, Black and Folkens 2012 $(\sigma_M = \sigma/N^{\frac{1}{2}})$

Measurement (mm)	Trial 1	Trial 2	Trial 3	Trial 4	Trial 5	Mean ± σ_M
1) Spinous Process Length	37.14	37.40	36.00	36.70	36.96	36.84 ± 0.239
2) Spinous Process Angle	3.5	3.5	4.0	5.0	5.0	4.2 ± 0.34
3) Ventral Body Height	24.74	24.62	24.68	24.62	25.08	24.75 ± 0.086
4) Dorsal Body Height	27.10	25.80	26.42	26.50	27.80	26.72 ± 0.339
5) Sup. Dorso-ventral Diameter	34.86	33.50	34.12	33.84	35.58	34.38 ± 0.374
6) Sup. Transverse Diameter	48.00	47.96	47.82	48.00	47.22	47.80 ± 0.149
7) Vertebral Canal Length	12.88	13.16	13.24	13.12	13.14	13.11 ± 0.060
8) Vertebral Canal Breadth	19.62	19.68	19.70	19.56	19.66	19.64 ± 0.025
9) Maximum Breadth	69.80	69.50	70.00	69.82	69.84	69.79 ± 0.081

-180-

Master's Thesis Bone Form / Vertebra

Pictures:

For Section #: TB1-L / TB1-O

Recorded By: Steven Naftel   **Date Completed:** Jan. 16, 2012
Site Name: Kellis II   **Skeleton #:** 265

Front View

Back View

Right Side View

Left Side View

Master's Thesis Bone Form / Vertebra:

Pictures:

For Section #: TB1-L / TB1-O

Recorded By:
  Steven Naftel
Site Name:
  Kellis II
Skeleton #: 265
Date Completed:
  Jan. 16, 2012

Top View

Bottom View

Pathology:

Sampling Procedure

Cut on either side of cloaca to about center or vertebra, including parrot beak osteophyte – creating two sections, TB1-L will include top and bottom of lesion, TB1-O will be a slice through the osteophyte.

B-8: Sample TB2

For Section #: TB2   **Master's Thesis Bone Form / Vertebra**

Recorded By: Steven Naftel   **Date Completed: May 29, 2012**
Site Name: Kellis II   **Skeleton #: 280**

Description:

Thoracic Vertebra (T2), generally in good condition with several areas of retained cartilage, on the superior body face and right transverse process.

Pathologies:

There is a large lytic lesion (cloaca) opening on the anterior face of the body, approximately circular and 9 mm in diameter. The internal cavity traverses the entire body length including an obvious widening of the posterior foramen. The interior of the lesion does not display any thickening of the trabecula.

There is a small circular opening, 2 mm, in the superior body surface opening on the interior of the lesion.

The anterior surface of the body is flat in profile and not concave. The customary sclerotic outer surface of the body is worn away to reveal the trabecula, indeed a 7 mm section of the inferior hemi ring is missing.

The body shape is also not symmetrical, the right superior demi-facet appears to be pushed in towards the center line while the right inferior demi-facet is more built up away from the center line of the body with evidence of new bone formation around the facet.

The edges of the transverse costal facets are sharp and display minor osteophytes. The right inferior articular facet is larger in area than the left, including an area of the inferior pedicle . There are marginal osteophytes around the right facet, especially there is a prominent ~ 5 mm osteophyte emanating from the superior edge of the facet projecting into the vertebral canal.

Non-Metrics:

Accessory transverse foramen (C3-C7) (A, P) . . . . .
Cervical Rib (C7) (A, P) . . . .
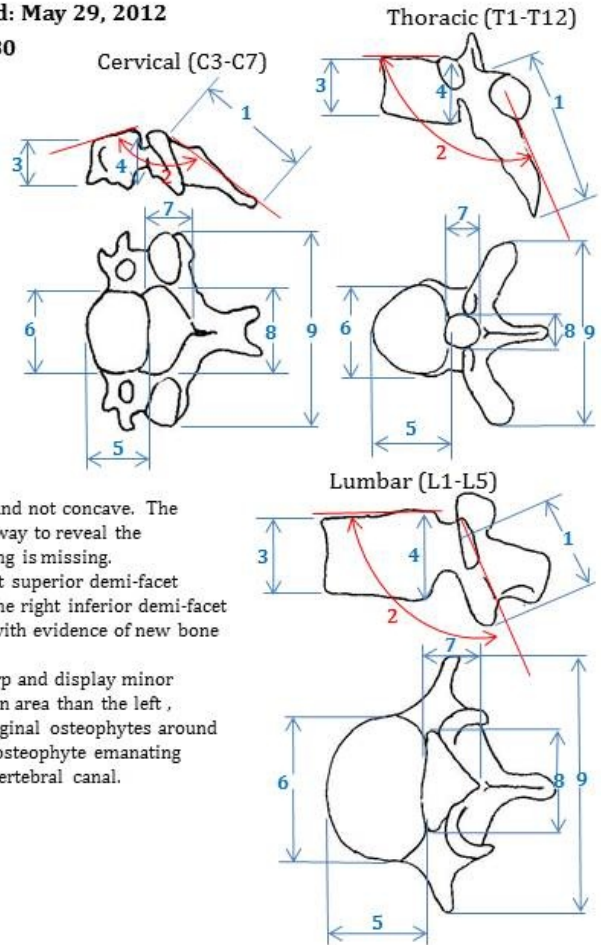
Cervical (C3-C7)

Thoracic (T1-T12)

Lumbar (L1-L5)

Metrics: Compilation from: Schwartz 2007; White, Black and Folkens 2012 $(\sigma_M = \sigma/N^{1/2})$

Measurement (mm)	Trial 1	Trial 2	Trial 3	Trial 4	Trial 5	Mean ± σ_M
1) Spinous Process Length	35.48	35.28	35.04	35.20	35.20	35.22 ± 0.059
2) Spinous Process Angle	42.5	41.5	42.0	44.5	46.0	43.3 ± 0.85
3) Ventral Body Height	13.96	14.50	14.10	13.92	14.00	14.10 ± 0.105
4) Dorsal Body Height	15.22	15.12	15.20	15.52	15.02	15.22 ± 0.084
5) Sup. Dorso-ventral Diameter	18.42	16.92	16.40	16.62	16.00	16.87 ± 0.415
6) Sup. Transverse Diameter	23.22	24.68	24.80	24.10	24.40	24.24 ± 0.282
7) Vertebral Canal Length	14.38	14.02	14.10	14.02	14.00	14.10 ± 0.071
8) Vertebral Canal Breadth	17.70	17.42	17.64	17.70	17.50	17.59 ± 0.056
9) Maximum Breadth	67.72	67.94	67.90	67.54	68.10	67.84 ± 0.096

Master's Thesis Bone Form / Vertebra

Pictures:

For Section #: TB2

Recorded By: Steven Naftel   **Date Completed: May 29, 2012**
Site Name: Kellis II   **Skeleton #: 280**

Front View

Rear View

Right Side View

Left Side View

Master's Thesis Bone Form / Vertebra

Pictures:

For Section #: TB2

Recorded By: Steven Naftel   **Date Completed: May 29, 2012**
Site Name: Kellis II   **Skeleton #: 280**

Top View

Bottom View

Pathology:

Sampling Procedure

Take a thin section to the left of the cloaca into the center of the body, attempting to leave the cloaca opening intact.

B-9: Sample TB3

For Section #: TB3   **Master's Thesis Bone Form / Vertebra**

Recorded By: Steven Naftel   **Date Completed:**
Site Name: Kellis II   **Skeleton #: 280**

Description:

Lumbar vertebra (L1) in excellent preservation.

Note: The vertebra has been x-rayed and Micro-CT scanned. No large internal voids were found but the CT scan shows some unusual small transverse voids.
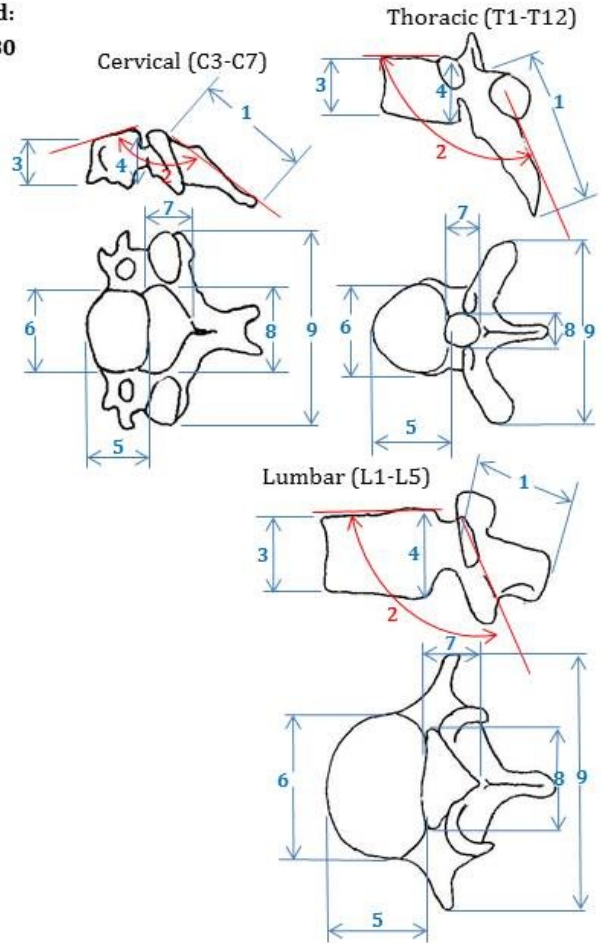
Pathologies:

Non-Metrics:

Accessory transverse foramen (C3-C7) (A, P) . . . . .
Cervical Rib (C7) (A, P) . . . .

Cervical (C3-C7)

Thoracic (T1-T12)

Lumbar (L1-L5)

Metrics: Compilation from: Schwartz 2007; White, Black and Folkens 2012   ($\sigma_M = \sigma/N^{\frac{1}{2}}$)

Measurement (mm)	Trial 1	Trial 2	Trial 3	Trial 4	Trial 5	Mean ± σ_M
1) Spinous Process Length	34.00	32.46	32.70	32.70	33.60	33.09 ± 0.299
2) Spinous Process Angle	13.0	10.0	11.0	12.0	12.0	11.6 ± 0.51
3) Ventral Body Height	24.60	25.58	24.96	25.20	25.36	25.14 ± 0.169
4) Dorsal Body Height	27.60	27.08	27.40	27.42	27.56	27.41 ± 0.092
5) Sup. Dorso-ventral Diameter	29.96	30.10	30.10	30.00	30.04	30.04 ± 0.028
6) Sup. Transverse Diameter	46.32	46.32	46.20	46.08	46.22	46.23 ± 0.044
7) Vertebral Canal Length	15.10	15.18	15.22	15.42	14.78	15.14 ± 0.104
8) Vertebral Canal Breadth	21.36	21.40	21.42	21.40	21.32	21.38 ± 0.018
9) Maximum Breadth	70.62	70.70	70.72	70.64	70.48	70.63 ± 0.042

Master's Thesis Bone Form / Vertebra

Pictures:

For Section #: TB3

Recorded By: Steven Naftel   **Date Completed:**
Site Name: Kellis II   **Skeleton #: 280**

Front View

Rear View

Right Side View

Left Side View

Master's Thesis Bone Form / Vertebra

Pictures:

For Section #: TB3

Recorded By: Steven Naftel   **Date Completed:**
Site Name: Kellis II   **Skeleton #: 280**

Top View

Bottom View

Sampling Procedure

Cut an ~ 7mm slice from the right side of the body in towards the centre..

B-10: Sample TB4

**For Section #: TB4**   **Master's Thesis Bone Form / Vertebra**

Recorded By: Steven Naftel   **Date Completed: June 5, 2012**
Site Name: Kellis 2   **Skeleton #: 20**

Description:

Lumbar Vertebra (L5) in excellent condition. The right half of the neural arch is missing. The right lamina is broken off from just below the superior articular facet to the centre point of the spinous process. The right portion of the lamina is well healed but lumpy in appearance. This is an occurence of partial spondylolysis. trauma.

The left portion of the spinous process presents an oval slightly concave appearance resembling a syphysis type joint (accessory articulation). This surface angles laterally away from the center line of the vertebra, this suggests that the spinous process was congenitally unfused (Spina Bifita of L5).

Two other similar accessory articular areas appear, one on the inferior surface of the left transverse process and one on the inferior surface of the right transverse process. The left area is oval/bean shaped 18 mm at the longest dimension with some slight sclerotic lipping. The right area is oval about 8 mm diameter. These areas would have articulated with the superior aspect of the ala of the sacrum. This indicates partial sacralization of L5.

Pathologies:

Beyond the congenital conditions and trauma mentioned above the body margins display some minor osteophytuic lipping. As well the superior anterior edge of the body is rounded over.

Non-Metrics:

Accessory transverse foramen (C3-C7) (A, P) . . . . .
Cervical Rib (C7) (A, P) . . . .
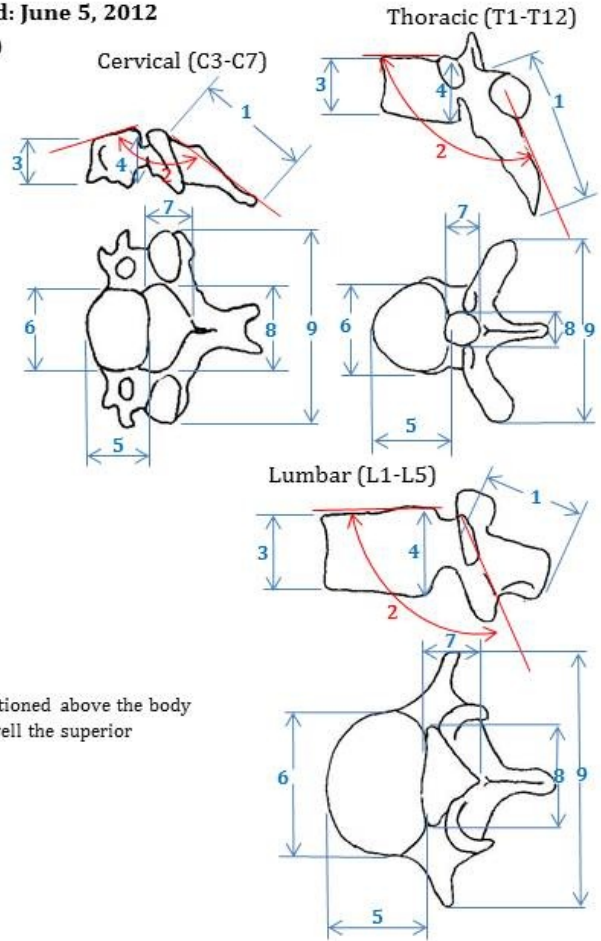
Metrics: Compilation from: Schwartz 2007; White, Black and Folkens 2012   ($\sigma_M = \sigma/N^{\frac{1}{2}}$)

Measurement (mm)	Trial 1	Trial 2	Trial 3	Trial 4	Trial 5	Mean ± σ_M
1) Spinous Process Length						
2) Spinous Process Angle	(41.0)	(41.5)	(42.5)	(43.0)	(41.5)	(41.9)
3) Ventral Body Height	24.14	24.08	24.22	23.94	24.38	24.15 ± 0.073
4) Dorsal Body Height	17.94	17.98	17.62	17.90	17.78	17.84 ± 0.065
5) Sup. Dorso-ventral Diameter	28.10	27.62	27.20	27.42	29.20	27.91 ± 0.356
6) Sup. Transverse Diameter	46.28	44.78	44.44	45.00	45.10	45.12 ± 0.311
7) Vertebral Canal Length						
8) Vertebral Canal Breadth	28.46	28.40	28.54	28.64	28.70	28.55 ± 0.055
9) Maximum Breadth	89.70	90.00	89.66	89.60	90.30	89.85 ± 0.131

Master's Thesis Bone Form / Vertebra

Front View

Rear View

Right Side View

Left Side View

Master's Thesis Bone Form / Vertebra

Pictures:

For Section #: TB4

Recorded By: Steven Naftel   **Date Completed:** June 5, 2012
Site Name: Kellis II   **Skeleton #: 20**

Top View

Bottom View

Pathology:

Sampling Procedure

Sample through right side of body about 1 cm towards the centre.

B-11: Sample R1

For Section #: R1 **Master's Thesis Bone Form / Rib**

Recorded By: Steven Naftel **Date Completed:** May 30, 2012
Site Name: La Vesconte **Skeleton #:** 18

Description:

Portions of right rib, unknown #, head and sternal end missing however good preservation otherwise.

Pathologies:

Lateral surface smooth and normal except for some small < 1 mm punched out lytic lesions with rounded edges around the sternal end.

Pleural surface shows extensive new bone formation with a porous texture. The new bone is healing and the rib cross section is thickened more towards the middle creating a triangular profile for the rib.

There are also multiple large coalescing lytic lesions revealing the interior trabecula of the rib, these are concentrated toward the sternal end of the rib. There are small oval lytic lesions present along both the inferior and superior margins of the rib.

Non-Metrics:

Bifid Rib (A, P) . . . . A

Metrics: From: White, Black and Folkens 2012 $(\sigma_M = \sigma/N^{\frac{1}{2}})$

Measurement (mm)	Trial 1	Trial 2	Trial 3	Trial 4	Trial 5	Mean ± σ_M
1) Total Rib Length						
2) External Arc of Rib						
3) Tubercle-Ventral Arc						
4) Tubercle-Ventral Chord						
5) Tubercle-Ventral Subtense						
6) Sternal End Max. Diameter						
7) Sternal End Min. Diameter						

Master's Thesis Bone Form / Rib

Pictures:

For Section #: R1

Recorded By: Steven Naftel   **Date Completed: May 30, 2012**
Site Name: La Vesconte   **Skeleton #: 18**

Lateral View

Pleural View

Master's Thesis Bone Form / Rib

Pictures:

For Section #: R1

Recorded By: Steven Naftel **Date Completed: May 30, 2012**
Site Name: La Vesconte **Skeleton #: 18**

Pathology:

Sampling Procedure

Take a thin section near the sternal end of the rib.

B-12: Samples R2 and R3

For Section #: R2/R3   Master's Thesis Bone Form / Rib

Recorded By: Steven Naftel   **Date Completed:** May 30, 2012
Site Name: La Vesconte   **Skeleton #:** 8

Description:

Portions of right rib with sternal end in good condition. The body of the rib appears normal along most of its length.

Pathologies:

The sternal end has a concentration of small lytic lesions on the lateral surface. The pleural surface has many less lesions of the same type and size. The lesions also extend along the inferior and superior margins of the rib for about 42 mm from the sternal end. The lesions are all small < 1 mm circular or oval with rounded edges.

Non-Metrics:

Bifid Rib (A, P) . . . . A

Metrics: From: White, Black and Folkens 2012 $(\sigma_M = \sigma/N^{\frac{1}{2}})$

Measurement (mm)	Trial 1	Trial 2	Trial 3	Trial 4	Trial 5	Mean ± σ_M
1) Total Rib Length						
2) External Arc of Rib						
3) Tubercle-Ventral Arc						
4) Tubercle-Ventral Chord						
5) Tubercle-Ventral Subtense						
6) Sternal End Max. Diameter	10.92	13.10	12.48	12.36	12.92	12.36 ± 0.384
7) Sternal End Min. Diameter	8.00	8.40	8.30	8.10	8.10	8.18 ± 0.073

Master's Thesis Bone Form / Rib

Pictures:

For Section #: R2/R3

Recorded By: Steven Naftel   **Date Completed: May 30, 2012**
Site Name: La Vesconte   **Skeleton #: 8**

Lateral View

Pleural View

Master's Thesis Bone Form / Rib

Pictures:

For Section #: R2/R3

Recorded By: Steven Naftel **Date Completed:** May 30, 2012
Site Name: La Vesconte **Skeleton #:** 8

Pathology:

Sampling Procedure

Two sections to be cut one from the "healthy" end of the section, the other from the sternal end with the multiple lytic lesions.

B-13: Sample R4

For Section #: R4   **Master's Thesis Bone Form / Rib**

Recorded By: Steven Naftel   **Date Completed:** June 5, 2012
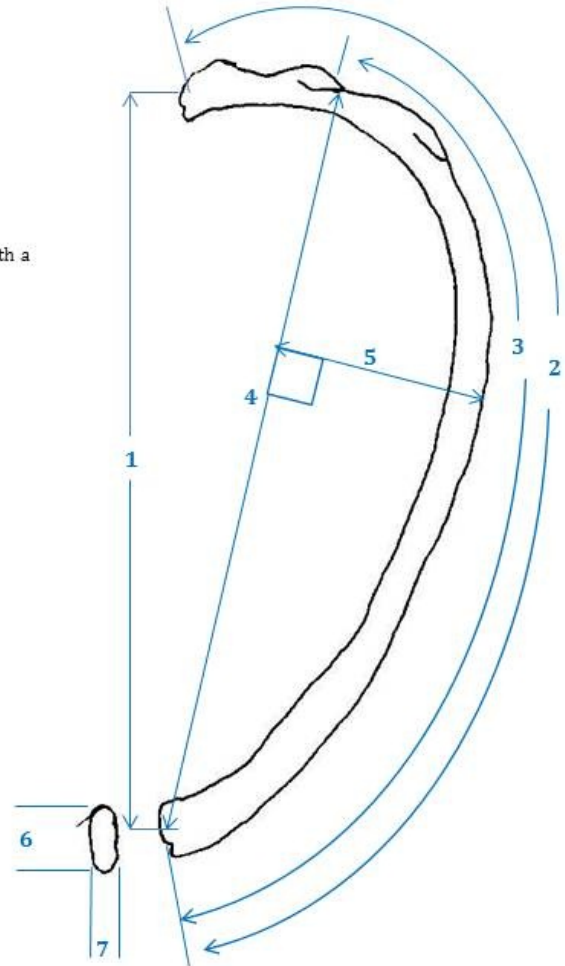**Site Name:** Kellis II   **Skeleton #:** 280

Description:

Vertebral portion of left rib (unknown #). Preservation is good with some retained soft tissue scales. The sternal end is missing.

Pathologies:

The rib appears normal except for a series of small nodules of new bone spread along the superior margin, for about 5 cm, from the tubercle towards the sternal end of the rib.

Non-Metrics:

Bifid Rib (A, P) . . . . A

Metrics: From: White, Black and Folkens 2012 $(\sigma_M = \sigma/N^{\frac{1}{2}})$

Measurement (mm)	Trial 1	Trial 2	Trial 3	Trial 4	Trial 5	Mean ± σ_M
1) Total Rib Length						
2) External Arc of Rib						
3) Tubercle-Ventral Arc						
4) Tubercle-Ventral Chord						
5) Tubercle-Ventral Subtense						
6) Sternal End Max. Diameter						
7) Sternal End Min. Diameter						

Master's Thesis Bone Form / Rib

Pictures:

For Section #: R4

Recorded By: Steven Naftel   **Date Completed:** June 5, 2012
Site Name: Kellis II   **Skeleton #:** 280

Lateral View

Pleural View

Master's Thesis Bone Form / Rib

Pictures:

For Section #: R4

Recorded By: Steven Naftel   **Date Completed: June 5, 2012**
Site Name: Kellis II   **Skeleton #: 280**

Pathology:

Sampling Procedure

Take an ~ 7 mm cross-section of the rib incorporating one of the nodules.

APPENDIX C: ETHICS APPROVALS

C-1: General Ethics Statement

Project Title: Trace Elements in Bone Diseases

Principal Investigator: Steven Naftel

Address: Department of Anthropology, University of Western Ontario, London, Ontario, CANADA, N6A 5C2

Telephone: ███████ **E-Mail:** ████████ **FAX:**

Funding Source: SSHRC

Summary of Project: Please indicate how samples were obtained

The project involves examining the trace element distribution within areas of bone disease to determine if distinct elements or patterns of element distributions are present within the diseased areas (lesion). The samples are all derived from archaeological collections displaying examples of Dental Abcesses and/or Tuberculosis. Once identified in the skeletal remains each lesion will be removed, embedded in resin and finally cross-sectioned to create the samples to be analyzed. These cross-sections will be analyzed primarily using Synchrotron Radiation X-ray Fluorescence Mapping, X-ray Diffraction, and X-ray Absorption Spectroscopy to determine the elemental distribution patterns, structural and chemical compositions.

The samples will be drawn from the following collections which have been obtained legally and exported with all applicable permits:

Name	Date	Place of Origin	Curator
Stirrup Court	1828-1896 AD	Ontario	Dr. Andrew Nelson, UWO
Marco Gonzales	100 BC-1350 AD	Belize	Dr. Christine White, UWO
San Pedro	1400-1650 AD	Belize	Dr. Christine White, UWO
Kellis II	100-400 AD	Egypt	Dr. Eldon Molto, UWO
Varden	500-1050 AD	Ontario	Dr. Eldon Molto, UWO

All the samples are anonymous and identified only by numeric codes. For this project new codes will be assigned to the samples created for analysis. Typical demographic data (age, sex) will be obtained for each burial from previously published reports on each site.

The data collected will be stored as computer files. Access to all computers and backups of data will be restricted by password and available only to the researchers involved in the project.

C-2: Letter of Approval from Research Western

Research
Western

January 10, 2012

Steven Naftel, Department of Anthropology
C/O Dr. Eldon Molto, Department of Anthropology
Social Science Centre 3433
University of Western Ontario

Dear Mr. Naftel,

RE: Trace Elements in Bone Diseases

Thank you for your email regarding the use of human remains from several different collections at The University of Western Ontario for your Master's thesis in Osteology. You have indicated that these remains are anonymous and identified only by numeric code. In your project you wish to examine the trace element distribution within areas of bone disease to determine if distinct elements or patterns of element distributions are present within the diseased area.

Based on the Office of Research Ethics guideline 2-G-026 this project does not require the approval of a research ethics board as you have indicated that you will only be using the remains obtained through several collections held at The University of Western Ontario, which are anonymous, for research purposes. Therefore, it is my opinion that this activity does not require approval of the University of Western Ontario Health Sciences Research Ethics Board.

Thank you for bringing this project to our attention and the best of luck with your project and publication.

The University of Western Ontario
Office of Research Ethics
Support Services Building Room 5150 • London, Ontario • CANADA – N6G 1G9
PH: 519-661-3036 • F: 519-850-2466 • ethics@uwo.ca • www.uwo.ca/research/ethics

C-3: Brookhaven National Laboratory Human Subjects Exemption

BROOKHAVEN NATIONAL LABORATORY
EXEMPT HUMAN SUBJECTS RESEARCH APPLICATION
45 CFR 46.101(b)

To qualify as exempt from the federal policy for the protection of human subjects, proposed research must be limited to one or more of the following categories. Please check the most accurate category.

☐ **(1)** Research conducted in established or commonly accepted educational settings, involving normal educational practices, such as
(i) research on regular and special education instructional strategies, or
(ii) research on the effectiveness of or the comparison among instructional techniques, curricula, or classroom management methods
as long as the research does not involve prisoners as subjects and the research is not FDA-regulated.

☐ **(2)** Research involving the use of educational tests (cognitive, diagnostic, aptitude, achievement), survey procedures, interview procedures or observation of public behavior, **unless:**
(i) Information obtained is recorded in such a manner that human subjects can be identified, directly or through identifiers linked to the subjects; **and**
(ii) any disclosure of the human subjects' responses outside the research could reasonably place the subjects at risk of criminal or civil liability or be damaging to the subjects' financial standing, employability, or reputation
as long as if the research involves children, the procedures are limited to observation of public behavior when the investigators do not participate in the activities being observed and educational tests; The research does not involve prisoners as subjects; and the research is not FDA-regulated

☐ **(3)** Research involving the use of educational tests (cognitive, diagnostic, aptitude, achievement), survey procedures, interview procedures, or observation of public behavior that is not exempt under item (2) of this section, if:
(i) The human subjects are elected or appointed public officials or candidates for public office; or
(ii) federal statute(s) require(s) without exception that the confidentiality of the personally identifiable information will be maintained throughout the research and thereafter
as long as the research does not involve prisoners as subjects and the research is not FDA-regulated.

☒ **(4)** Research, involving the collection or study of existing data, documents, records, pathological specimens, or diagnostic specimens, if these sources are publicly available or if the information is recorded by the investigator in such a manner that subjects cannot be identified, directly or through identifiers linked to the subjects
as long as "existing" means that the reviewed materials exist at the time; the research is proposed the research does not involve prisoners as subjects and the research is not FDA-regulated.

☐ **(5)** Research and demonstration projects which are conducted by or subject to the approval of department or agency heads, and which are designed to study, evaluate, or otherwise examine:
(i) Public benefit or service programs;
(ii) procedures for obtaining benefits or services under those programs;
(iii) possible changes in or alternatives to those programs or procedures; or
(iv) possible changes in methods or levels of payment for benefits or services under those programs.
as long as the research does not involve prisoners as subjects and the research is not FDA-regulated.

☐ **(6)** Taste and food quality evaluation and consumer acceptance studies,
(i) if wholesome foods without additives are consumed or
(ii) if a food is consumed that contains a food ingredient at or below the level and for a use found to be safe, or agricultural chemical or environmental contaminant at or below the level found to be safe, by the Food and Drug Administration or approved by the Environmental Protection Agency or the Food Safety and Inspection Service of the U.S. Department of Agriculture.
as long as the research does not involve prisoners as subjects.

CURRICULUM VITAE

Name:	Steven James Naftel
Place of Birth:	Des Moines, Iowa, USA
Date of Birth:	November 18, 1967
Post-Secondary Education and Degrees:	Western University London, Ontario 1986 - 1991 Honours B.Sc. Chemistry Western University London, Ontario 1991 - 1999 Ph.D. (Physical Chemistry) Western University London, Ontario 2010 - 2014 M.A. (Applied Archaeology)
Selected Honours and Awards:	Queen's University, Department of Biology Kingston, Ontario 2004 - 2005 Good Family Visiting Research Fellowship
Area of Study:	Synchrotron Radiation Techniques in Physical Anthropology
Main Experimental Techniques:	Soft and Hard X-ray Absorption Spectroscopy Micro- X-ray Fluorescence Elemental Mapping
Publications Summary:	49 Articles, 3 Book Chapters, 2 Theses 10 Talks, 31 Posters 19 Technical Reports, 2 Instruction Pamphlets

Related Work Experience: Reviewer - J. of Synchrotron Radiation (1 article)
                                 - Nucl. Inst. Meth. Phys. Res. B (2 articles)
                                 - Totem (2 articles)

Tutorial Assistant
Western University
2010 - 1012

Archaeological Crew Member
Davidson Site (AhHk-54)
2009

Publications:

54.   **S. J. Naftel**, *Elemental Distribution in Bone Impacted by Bacterial Diseases* (M.A. Thesis, Western University, London, Canada, 2014).

53.   R. R. Martin, **S. J. Naftel**, S. M. Doucet, D. Hanley and C. Weisener, "Synchrotron Radiation Analysis in the Study of Pollution in the Ring Billed Gull (*Larus delawarensis*): A novel application of the technique", X-ray Spectrometry **42**, 437 (2013).

52.   R. R. Martin, **S. J. Naftel**, S. Macfie, K. Jones and A. Nelson, "Pb distribution in bones from the Franklin expedition: synchrotron X-ray fluorescence and laser ablation/mass spectroscopy", Applied Physics A **111**, 23 (2013).

51.   A. E. Dolphin, **S. J. Naftel**, A. J. Nelson, R. R. Martin and C. D. White, "Bromine in teeth and bone as an indicator of marine diet", Journal of Archaeological Science **40**, 1778 (2013).

50.   R. R. Martin, W. S. Shotyk, **S. J. Naftel**, J. M. Ablett and P. Northrup, "Speciation of Antimony in Polyethylene Terephthalate (PET) Bottles", X-ray Spectrometry **39**, 257 (2010).

49.   R. R. Martin, **S. J. Naftel**, A. J. Nelson, M. Edwards, H. Mithoowani and J. Stakiw, "Synchrotron radiation analysis of possible correlations between metal status in human cementum and periodontal disease.", Journal of Synchrotron Radiation **17**, 263 (2010).

48.   A. R. Gerson, C. Anastasio, S. Crowe, D. Fowle, G. Guo, I. Kennedy, E. Lombi, P. S. Nico, M. A. Marcus, R. R. Martin, **S. J. Naftel**, A. J. Nelson, D. Paktunc, J. A. Roberts, C. G. Weisener and M. L. Werner, "Frontiers in assessing the role of chemical speciation and natural attenuation on the bioavailability of contaminants in the terrestrial environment", in R. Naidu, ed., "*Chemical Bioavailability in terrestrial environments*", Elsevier, New York, 2008. ch. 7.

47.   R. R. Martin, **S. J. Naftel**, A. J. Nelson and W. D. Sapp III, "Comparison of the distribution of bromine, lead and zinc in tooth and bone from an ancient Peruvian burial site by X-ray fluorescence", Can. J. Chem. **85**, 831 (2007).

46.   R. R. Martin, **S. J. Naftel**, A. J., Nelson, A. B. Feilen and A. Narvaez, "Metal distributions in the cementum rings of human teeth: Possible depositional chronologies and diagenesis", J. Arch. Sci. **34**, 936 (2007).

45.   **S. J. Naftel**, R. R. Martin, S. M. Macfie, F. Courchesne and V. Séguin, "An investigation of metals at the soil/root interface using synchrotron radiation analysis", Can. J. Anal. Sci. Spectrosc. **52**, 18 (2007).

44.   R. R. Martin, **S. J. Naftel**, S. M. Macfie, K. W. Jones, H. Feng and C. Trembley, "High variability of the metal content of tree growth rings as measured by synchrotron micro X-ray fluorescence", X-ray Spectrometry, **35**, 57 (2006).

43.   P.-S. G. Kim, **S. J. Naftel**, <u>T. K. Sham</u>, I. Coulthard, Y.-F. Hu, A. Moewes and J. W. Freeland, "Photon-in photon-out studies of Alq$_3$ (tris-aluminum-8-hydroxyquinolinate): Synchrotron light excited optical luminescence and X-ray emission", J. Elec. Spec. Rel. Phen. **144-147**, 901 (2005). *From the poster presented at: VUV-XIV, Cairns, Australia, Jul. 19-23 2004*.

42.   R. R. Martin, I. M. Kempson, **S. J. Naftel** and W. M. Skinner, "Preliminary Synchrotron Analysis of Lead in Hair from a Lead Smelter Worker", Chemosphere, **58**, 1385 (2005).

41.   V. Séguin, F. Courchesne, C. Gagnon, R. R. Martin, **S. J. Naftel** and W. Skinner, "Mineral Weathering in the Rhizosphere of Forested Soils", in P. M. Huang and G. R. Gobran, eds., "*Biogeochemistry of Trace Elements in the Rhizosphere*", Elsevier, New York, 2005. pp. 29-55.

40.   R. R. Martin, **S. J. Naftel**, A. J. Nelson, A. B. Feilen and A. Narvaez, "Synchrotron X-ray Fluorescence and Trace Metals in the Cementum Rings of Human Teeth", J. Environ. Monit. **6**, 783 (2004).

39.   T. K. Sham, **S. J. Naftel**, P.-S. G. Kim, R. Sammynaiken, Y. H. Tang, I. Coulthard, A. Moewes, J. W. Freeland, Y.-F. Hu and S. T. Lee, "The electronic structure and optical properties of silicon nanowires: a study using x-ray excited optical luminescence and x-ray emission spectroscopy", Phys. Rev. B **70**, 045313 (2004).

38.   R. R. Martin, **S. J. Naftel**, S. Macfie, W. Skinner, F. Courchesne and V. Séguin, "Time of Flight Secondary Ion Mass Spectrometry Studies of the Distribution of Metals Between the Soil, Rhizosphere and Roots of *Populus tremuloides Minchx* Growing in Forest Soil", Chemosphere **54**, 1121 (2004).

37.   R. R. Martin, **S. J. Naftel**, W. Skinner, K. W. Jones and H. Feng, "Micro-Synchrotron X-ray Fluorescence of the Metal Distribution in A Black Spruce Tree Stem: Evidence for Radial Mobility", X-ray Spectrometry **32**, 402 (2003).

36. **S. J. Naftel**, P.-S. G. Kim, T. K. Sham, R. Sammynaiken, B. W. Yates and Y.-F. Hu, "Soft X-ray Excited Optical Luminescence from Poly (N-vinylcarbazole)", J. Appl. Phys. **93**, 5191 (2003).

35. R. R. Martin, **S. J. Naftel**, T. K. Sham, B. Hart and M. A. Powell, "XANES of Chromium in Sludges Used as Soil Ameliorants", Can. J. Chem. **81**, 193 (2003).

34. R. Sammynaiken, **S. J. Naftel**, T. K. Sham, K. W. Cheah, B. Averboukh, R. Huber, Y. R. Shen, G. G. Qin, Z. C. Ma and W. H. Zong, "Structure and Electronic properties of SiO_2/Si multilayer superlattices: Si K edge and $L_{3,2}$ edge X-Ray Absorption Fine Structure Study", J. Appl. Phys. **92**, 3000 (2002).

33. <u>**S. J. Naftel**</u>, R. R. Martin, F. Courchesne, V. Séguin and R. Protz, "Studies of the Effect of Soil Biota on Metal Bioavailability", Can. J. Anal. Sci. Spectrosc. **47**, 36 (2002). *From the talk presented at: 47th ICASS, Toronto, Canada, Aug. 19-21 2001.*

32. X.-H. Sun, R. Sammynaiken, **S. J. Naftel**, Y. H. Tang, P. Zhang, P.-S. Kim, T. K. Sham, X. H. Fan, Y.-F. Zhang, C. S. Lee, N. B. Wong, Y.-F. Hu and K. H. Tan, "Ag nanostructures on a silicon nanowire template: Preparation and X-ray absorption fine structure study at the Si K-edge and Ag $L_{3,2}$-edge", Chem. Mater. **14**, 2519 (2002).

31. T. K. Sham, **S. J. Naftel** and I. Coulthard, "Multicore Multichannel-Detection (MCMD) X-Ray absorption fine structures (XAFS) studies of thin films", in T. K. Sham, ed., "*Chemical Applications of Synchrotron Radiation*", World Scientific, Singapore, 2002. p. 1154.

30. Y. F. Hu, K. H. Tan, P. S. Kim, P. Zhang, **S. J. Naftel**, <u>T. K. Sham</u>, I. Coulthard and B. W. Yates, "Soft X-Ray excited optical luminescence: Some recent applications", Rev. Sci. Instr. **73**, 1379 (2002). *From the talk presented at: SRI Conference*

29. **S. J. Naftel**, <u>R. R. Martin</u>, K. W. Jones, H. Feng, M. M. Savard and C. Bégin, "Synchrotron Radiation Analysis of a Smelter Impacted Tree-Ring Sample", Can. J. Anal. Sci. Spectrosc. **46**, 118 (2001). *From the talk presented at: 47th ICASS, Toronto, Canada, Aug. 19-21 2001.*

28. X.-H. Sun, T.-H. Tang, P. Zhang, **S. J. Naftel**, R. Sammynaiken, T. K. Sham, H. Y. Peng, Y.-F. Zhang, N. B. Wong and S. T. Lee, "X-ray absorption fine structure and electron energy loss spectroscopy study of silicon nanowires at the Si $L_{3,2}$ edge", J. Appl. Phys. **90**, 6379 (2001).

27. P. Zhang, **S. J. Naftel** and T. K. Sham, "Multichannel detection x-ray absorption near edge study on the structural characteristics of dendrimer-stabilized CdS quantum dots", J. Appl. Phys. **90**, 2755 (2001).

26. I. Coulthard, T. K. Sham, Y.-F. Hu, **S. J. Naftel**, P.-S. Kim and J. W. Freeland, "Threshold Behavior of the Cu $L_3M_{4,5}M_{4,5}$ Auger effect of Cu Metal at the L_3 edge", Phys. Rev. B **64**, 115101 (2001).

25. **S. J. Naftel**, R. R. Martin, T. K. Sham, S. M. Macfie and K. W. Jones, "Micro-Synchrotron X-ray Fluorescence of Cadmium-Challenged Corn Roots", J. Elec. Spec. Rel. Phen. **119**, 235 (2001). *From the poster presented at: PacifiChem, Hawaii, December 14-16 2000.*

24. **S. J. Naftel**, Y. M. Yiu, T. K. Sham and B. W. Yates, "X-ray Excited Optical Luminescence (XEOL) Studies of CaF_2 at the Ca $L_{3,2}$-edge", J. Elec. Spec. Rel. Phen. **119**, 215 (2001). *From the poster presented at: PacifiChem, Hawaii, December 14-16 2000.*

23. **S. J. Naftel**, P. Zhang, P.-S. Kim, T. K. Sham, I. Coulthard, W. J. Antel, Jr., J. W. Freeland, S. P. Frigo, M.-K. Fung, S. T. Lee, Y. F. Hu and B. W. Yates, "Soft X-ray-Excited Luminescence and Optical X-ray Absorption Fine Structures of tris (8-hydroxyquinoline) aluminum", Appl. Phys. Lett. **78**, 1847 (2001).

22 **S. J. Naftel**, T. K. Sham, Y. M. Yiu and B. W. Yates, "Calcium L-edge XANES Study of some Calcium Compounds", Journal of Synchrotron Radiation **8**, 255 (2001). *From the poster presented at: XAFS XI, Ako, Japan, July 26-31 2000.*

21. I. Coulthard, R. Sammynaiken, **S. J. Naftel**, P. Zhang and T. K. Sham, "Porous Silicon: A Template for the Preparation of Nanophase Metals and Bimetallic Aggregates", Physica Status Solidi A **182**, 157 (2000). *From the poster presented at: PSST-2000, International Conference on Porous Semiconductors - Science and Technology, Madrid, Spain, Mar. 12-17 2000.*

20. **S. J. Naftel**, I. Coulthard, D. T. Jiang, T. K. Sham, B. W. Yates and K. H. Tan, "The Role of Oxygen in the Photoluminescence of Porous Silicon: Some Recent Observations", Physica Status Solidi A **182**, 373 (2000). *From the poster presented at: PSST-2000, International Conference on Porous Semiconductors - Science and Technology, Madrid, Spain, Mar. 12-17 2000.*

19. I. Coulthard, W. J. Antel Jr., S. P. Frigo, J. W. Freeland, J. Moore, W. S. Calaway, M. J. Pellin, M. Mendelsohn, T. K. Sham, **S. J. Naftel** and A. P. J. Stampfl, "Resonant Auger Studies of Metallic Systems", J. Vac. Sci. Tech. A **18**, 1955 (2000). *From the talk presented at: 46th AVS Meeting, Seattle WA, Oct. 25-29 1999.*

18. I. Coulthard, W. J. Antel Jr., J. W. Freeland, T. K. Sham, **S. J. Naftel** and P. Zhang, "Influence of Sample Oxidation on the Nature of Optical Luminescence from Porous Silicon.", Appl. Phys. Lett. **77**, 498 (2000).

17. T. K. Sham, R. Sammynaiken, Y. J. Zhu, P. Zhang, I. Coulthard and **S. J. Naftel**, "X-ray Excited Optical Luminescence (XEOL): A Potential Tool for OLED Studies", Thin Solid Films **363**, 318 (2000). *From the talk presented at: APOELMD-99, Hong Kong, June 8-11 1999.*

16.   **S. J. Naftel**, *Interactions of Transition Metals with Si(100): The Ni-Si, Co-Si and Au/Si(100) Systems* (Ph.D. Thesis, University of Western Ontario, London, Canada, 1999).

15.   **S. J. Naftel** and T. K. Sham, "Co $L_{3,2}$-edge and multi-detection channel XAFS studies of Co-Si interactions.", J. Synchrotron Rad. **6**, 526 (1999). *From the poster presented at: XAFS X, Chicago IL, Aug. 10-14 1998.*

14.   **S. J. Naftel**, I. Coulthard, T. K. Sham, D.-X. Xu, L. Erickson and S. R. Das, "Electronic structure of nickel silicide in sub-half-micron lines and blanket films: An X-ray absorption fine structures study at the Ni and Si $L_{3,2}$-edge.", Appl. Phys. Lett. **74**, 2893 (1999).

13.   **S. J. Naftel**, A. Bzowski and T. K. Sham, "A study of the electronic structure of Au-V bimetallics using X-ray photoelectron spectroscopy (XPS) and X-ray absorption near-edge structure (XANES).", J. Alloys and Compounds **283**, 5 (1999).

12.   I. Coulthard, **S. J. Naftel** and T. K. Sham, "Synchrotron X-Ray Absorption Spectroscopy Studies of Pt/Si Systems.", Mat. Res. Soc. Symp. Proc. **524**, 291 (1998). *From the poster presented at: MRS '98 Spring Meeting, San Francisco CA, April 13-17 1998.*

11.   **S. J. Naftel**, I. Coulthard, Y. Hu, T. K. Sham and M. Zinke-Allmang, "X-Ray Absorption Fine Structure (XAFS) Studies of Cobalt Silicide Thin Films.", Mat. Res. Soc. Symp. Proc. **524**, 273 (1998). *From the talk presented at: MRS '98 Spring Meeting, San Francisco CA, April 13-17 1998.*

10.   H. H. Hsieh, Y. K. Chang, W. F. Pong, J. Y. Pieh, P. K. Tseng, T. K. Sham, I. Coulthard, **S. J. Naftel**, J. F. Lee, S. C. Chung and K. L. Tsang, "Electronic Structure of Ni-Cu Alloys: The *d*-electron Charge Distribution.", Phys. Rev. B **57**, 15204 (1998).

9.   **S. J. Naftel**, I. Coulthard, T. K. Sham, S. R. Das and D.-X. Xu, "Structural and Electronic Property Evolution of Nickel and Nickel Silicide Thin Films on Si(100) from Multi-Core X-Ray Absorption Fine Structures Studies.", Phys. Rev. B **57**, 9179 (1998).

8.   **S. J. Naftel**, T. K. Sham, S. R. Das and D.-X. Xu, "Silicon $L_{2,3}$-Edge XANES Study of Platinum Silicide Thin Films.", Mat. Res. Soc. Symp. Proc. **441**, 175 (1997). *From the poster presented at: MRS '96 Fall Meeting, Boston MA, Dec. 2-6 1996.*

7.   T. K. Sham, I. Coulthard and **S. J. Naftel**, "$M_{3,2}$-Edge X-Ray Absorption Near Edge Structure of 5d Metals.", J. Phys. IV France **7**, C2-477 (1997). *From the poster presented at: XAFS 9, Grenoble, France, Aug. 26-30 1996.*

6.   **S. J. Naftel**, A. Bzowski, T. K. Sham, D.-X. Xu and S. R. Das, "XAFS Studies of Self-Aligned Platinum Silicide Thin Films at the Pt $M_{3,2}$ Edge and the Si K-Edge.", J. Phys. IV France **7**, C2-1131 (1997). *From the poster presented at: XAFS 9, Grenoble, France, Aug. 26-30 1996.*

5.   **S. J. Naftel**, T. K. Sham, V. I. Smelyansky, J. S. Tse and J. D. Garrett, "Angular Dependent XAFS Studies of a MoSi$_2$ Single Crystal.", J. Phys. IV France **7**, C2-495 (1997). *From the poster presented at: XAFS 9, Grenoble, France, Aug. 26-30 1996.*

4.   **S. J. Naftel**, I. Coulthard, <u>T. K. Sham</u>, D.-X. Xu and S. R. Das, "Synchrotron Radiation Characterization of Metal Silicide Thin Films: Some Observations.", Thin Solid Films 308-309, 580 (1997). *From the talk presented at: ICMCTF 97, San Diego, April 1997.*

3.   T. K. Sham, **S. J. Naftel**, A. Bzowski, S. R. Das, D.-X. Xu, S. M. Heald, D. Brewe and M. Kuhn, "Synchrotron Radiation Studies of Platinum Silicide Thin Films.", Mat. Res. Soc. Symp. Proc. **402**, 587 (1996). *From the poster presented at: MRS '95 Fall Meeting, Boston MA, Nov. 27 - Dec. 1 1995.*

2.   T. K. Sham, **S. J. Naftel** and I. Coulthard, "M$_{3,2}$-edge x-ray absorption near-edge structure spectroscopy: An alternative probe to the L$_{3,2}$-edge near-edge structure for the unoccupied densities of *d* states of 5*d* metals", J. Appl. Phys. **79**, 7134 (1996).

1.   Zheng Yuan, Detong Jiang, **S. J. Naftel**, T. K. Sham and Richard J. Puddephatt, "Dimethylpalladium(II) Complexes as Precursors for Chemical Vapor Deposition of Palladium", Chem. Mater. **6**, 2151 (1994).